

THE EFFECTS OF SHOT PEENING ON LOW  
CYCLE FATIGUE LIFE OF 7075-T6 ALUMINIUM  
ALLOY ROUND BAR

By

DMD Peters

Submitted in fulfilment of the requirements for the  
degree of:

Magister Technologiae: Engineering: Mechanical

at the Nelson Mandela Metropolitan University

December 2014

Supervisor: Prof PJ McGrath

## **COPYRIGHT STATEMENT**

The copy of this dissertation has been supplied on condition that anyone who consults it is understood to recognize that its copyright rests with the Nelson Mandela Metropolitan University and that no quotation from the dissertation and no information derived from it may be published without the prior consent of the University.

Copyright © 2014 Nelson Mandela Metropolitan University

*All rights reserved*

Declaration

**DECLARATION**

I, the undersigned hereby declare that the work contained in this dissertation is my own and that I have not previously, in its entirety or in part, submitted it at any university for a degree.

Signature:

*DMD Peters*

DMD Peters

## **ABSTRACT**

The aim in this dissertation was to improve our understanding of the effectiveness of shot peening in prolonging fatigue life, of 7075-T6 Aluminium Alloy round bar, taking into consideration surface residual stress, microstructural and micro-hardness parameters.

Three point bending, high stress, moderately low cycle, fatigue tests were conducted to study the effects of shot peening and associated surface residual compressive stresses on fatigue life. The influence of shot peening on the microstructure was explored, including the application of mechanical small plastic straining and surface skimming, to vary the surface residual compressive stresses and induce strain hardening.

Tests were performed to measure residual stress-depth distribution, plastic straining, micro-hardness, and the microstructure analysed on scanning electron microscopy (SEM) fractographs.

The Juvinall and Marshek life prediction model was used in conjunction with the Gerber equation for non-zero mean stress applications to generate a proposed life prediction model for this material which is user-friendly. The proposed life prediction model has a linear equation format with the flexibility to conservatively accommodate most of the various types, and combinations, of treatments applied in this research by the use of customised constants.

The results show that there was good correlation between actual and predicted fatigue life as well as useful insights into the role of the microstructure in explaining fatigue life behaviour.

## **ACKNOWLEDGEMENTS**

When recalling the degree of help and input I have received for spiritual, familial, fraternal, supervisory, and institutional support, one feels a humbled and hopeless bankrupt in attempting to articulate the debt owed by me in the acknowledgements below.

Firstly, I would like to express my deepest thankfulness to my Lord God and saviour Who has sustained and strengthened me through the joys of discovery and the trials of research, about (metal) fatigue, a word all too familiar to many who have followed this arduous path.

I would like to express my unqualified appreciation to those people who have played such a vital role in supporting and assisting me in so many ways:

My wife Brenda and children, Jeremy, Andrew and Kyle, who have been so resolute and loving in their continuous and irreplaceable support for me through this time.

Mr TAP van der Schyff from CPUT, my first research supervisor, who was the epitome of support in important administration, including arranging the acquisition of the material required for this research, the shot peening at CPUT, the fatigue testing and supervision at UCT, and demonstrating such kindness in the granting of permission to use the test results obtained through my time of study in Cape Town.

Prof RB Tait, my supervisor at UCT, with such high-level expertise in the field of metal fatigue, who guided and opened this eager novice to his world of research. He was a true mentor and excellent lecturer, generously entrusting me to the intricacies of the all-important fatigue testing machine which had to work for many long hours to achieve the essential requirements for this research.

My colleagues and friends at my previous workplace, WSU, especially Dr Carlo van Zyl.

Finally, to Prof PJ McGrath, my supervisor, who kindly re-opened the door for me to continue my studies through NMMU and provided essential redirection for this research, helping me believe in the benefits of second chances, for which I am so grateful. Also, to Prof Hannalie Lombard, HOD, who provided essential assistance to complete this dissertation.

## DEDICATIONS

This work is dedicated to my family who have played an essential role and contribution in my life.

To my wife, Brenda, who has been my one and only “bride” and “helpmeet” for 39 years, and who has shown unconditional love and dedication to myself and our children.

She has endured the extensive demands with me through long days and nights, turning her into a “grass widow” at times especially during my research year at Cape Town and the final throes of this dissertation. I will forever be in her debt for the price she so willingly paid.

To our children, their wives and grandchildren, Jeremy, Andrew and Taryn with our grandchildren Ashton and Michaela, Kyle and Sophie, thank you for your love and support, and at times, occasionally cheekily, pushing their “Pops” to complete this research.

To my late parents, Colin and Florence, who endured the early part of their marriage with his absence, during the 2<sup>nd</sup> world war, taught me about faithfulness and honesty in spite of circumstances. Her zest for life was something to behold! I am sure they would have been proud of their son for completing this research and I hope that I have honoured their parental sacrifices.

## CONTENTS

<b>COPYRIGHT STATEMENT.....</b>	<b>II</b>
<b>DECLARATION .....</b>	<b>III</b>
<b>ABSTRACT.....</b>	<b>IV</b>
<b>ACKNOWLEDGEMENTS .....</b>	<b>V</b>
<b>DEDICATIONS.....</b>	<b>VI</b>
<b>CONTENTS.....</b>	<b>VII</b>
<b>TABLE OF FIGURES.....</b>	<b>XII</b>
<b>LIST OF TABLES .....</b>	<b>XVIII</b>
<b>LIST OF EQUATIONS.....</b>	<b>XX</b>
<b>LIST OF ABBREVIATIONS .....</b>	<b>XXIII</b>
<b>NOMENCLATURE .....</b>	<b>XXIV</b>
<b>CHAPTER 1. INTRODUCTION .....</b>	<b>1</b>
<b>1.1 ACKNOWLEDGEMENT OF PRIOR TESTING.....</b>	<b>1</b>
<b>1.2 INTRODUCTION .....</b>	<b>1</b>
<b>1.3 APPLICATIONS .....</b>	<b>2</b>
<b>1.4 PROBLEM STATEMENT .....</b>	<b>3</b>

Contents

<b>1.5</b>	<b>SUB-PROBLEMS</b> .....	<b>3</b>
<b>1.6</b>	<b>HYPOTHESIS</b> .....	<b>4</b>
<b>1.7</b>	<b>DELIMITATIONS</b> .....	<b>5</b>
<b>1.8</b>	<b>RESEARCH METHODS</b> .....	<b>7</b>
1.8.1	Literature Review .....	7
1.8.2	Development and Implementation of Tests.....	7
1.8.3	Analysis of Test Results .....	8
<b>CHAPTER 2. LITERATURE REVIEW</b> .....		<b>9</b>
<b>2.1</b>	<b>METAL FATIGUE</b> .....	<b>9</b>
2.1.1	Crack Initiation .....	9
2.1.2	Crack Propagation.....	10
2.1.3	Fatigue Crack Analysis.....	13
2.1.4	Factors Affecting Fatigue.....	15
2.1.5	Designing Against Fatigue.....	15
<b>2.2</b>	<b>SURFACE TREATMENTS TO SLOW DOWN FATIGUE CRACK INITIATION</b> .....	<b>16</b>
2.2.1	Introduction .....	16
2.2.2	Rolling .....	16
2.2.3	Hammer Peening .....	17
2.2.4	Shot Peening.....	17
2.2.5	Laser Peening .....	18
2.2.6	Other Varieties of Peening .....	19
2.2.7	Summary.....	19
<b>2.3</b>	<b>PHYSICAL CHARACTERISTICS OF 7075–T6 ALUMINIUM ALLOY</b> .....	<b>20</b>
<b>2.4</b>	<b>SHOT PEENING</b> .....	<b>20</b>
2.4.1	Introduction .....	20
2.4.2	Types and Sizes of Shot.....	21
2.4.3	Equipment.....	22
2.4.4	Almen Test System .....	26
2.4.5	Control of Process Variables .....	30

Contents

2.4.6	Applications.....	32
2.4.7	Geometry .....	36
2.4.8	Limitations.....	36
2.4.9	Process After Peening.....	36
2.4.10	Summary.....	37
<b>2.5</b>	<b>RESIDUAL STRESSES INDUCED BY SHOT PEENING .....</b>	<b>37</b>
2.5.1	Distribution of Residual Stresses.....	37
2.5.2	Magnitude of Residual Stresses .....	43
2.5.3	Depth of Residual Stresses .....	46
2.5.4	Relaxation of Residual Stresses .....	49
2.5.5	Effect on Fatigue Life by Residual Stresses .....	50
2.5.6	Residual Stress Measurement: Centre Hole Drilling Method .....	52
2.5.7	Summary.....	53
<b>2.6</b>	<b>MICROSTRUCTURE .....</b>	<b>54</b>
2.6.1	Surface and Sub-Surface Deformation .....	54
2.6.2	Effects of Small Plastic Strain.....	56
2.6.3	Effects on Fatigue Life.....	59
2.6.4	Summary.....	60
<b>2.7</b>	<b>MICROHARDNESS .....</b>	<b>61</b>
<b>2.8</b>	<b>FRACTOGRAPHY .....</b>	<b>63</b>
<b>2.9</b>	<b>LIFE PREDICTION MODELS .....</b>	<b>70</b>
2.9.1	Mean Stress Correction with Constant Amplitude Loading .....	70
2.9.2	Effects of the Stress and Fatigue Ratios.....	70
2.9.3	Application of the Gerber Equation .....	72
2.9.4	Application of the Juvinal and Marshek Life Prediction Method.....	74
2.9.5	Approach to Combining the Gerber with Juvinal and Marshek Methods .....	78
2.9.6	Summary.....	81
<b>CHAPTER 3.</b>	<b>EXPERIMENTAL DETAILS .....</b>	<b>82</b>
<b>3.1</b>	<b>INTRODUCTION .....</b>	<b>82</b>

Contents

<b>3.2</b>	<b>FATIGUE TESTING</b> .....	<b>82</b>
3.2.1	Specimen Details .....	82
3.2.2	Specimen Fatigue Testing.....	86
<b>3.3</b>	<b>RESIDUAL STRESS TESTING</b> .....	<b>90</b>
3.3.1	Residual Stress Drilling Assembly .....	90
3.3.2	Residual Stress Measurement.....	91
3.3.3	Magnitude and Calibration of Residual Stresses .....	94
<b>3.4</b>	<b>SHOT PEENING AT CPUT</b> .....	<b>97</b>
<b>3.5</b>	<b>MICROSTRUCTURAL TESTING</b> .....	<b>101</b>
3.5.1	Plastic Straining .....	101
3.5.2	Diametral Skimming .....	104
3.5.3	Microhardness Tests .....	105
3.5.4	Scanning Electron Microscope (SEM) Tests.....	107
<b>3.6</b>	<b>SUMMARY</b> .....	<b>111</b>
<b>CHAPTER 4. ANALYSIS OF RESULTS</b> .....		<b>114</b>
<b>4.1</b>	<b>INTRODUCTION</b> .....	<b>114</b>
<b>4.2</b>	<b>FATIGUE ANALYSIS PROFILES</b> .....	<b>114</b>
4.2.1	General Test Specimen List and Groupings .....	114
4.2.2	Fatigue Tests: Groupwise.....	116
4.2.3	Residual Stress-Depth Tests.....	121
4.2.4	Microstructural Effects.....	146
<b>4.3</b>	<b>LIFE PREDICTION MODELLING</b> .....	<b>166</b>
4.3.1	S-N Curve Selection.....	166
4.3.2	Groupwise Life Prediction Modelling .....	176
<b>4.4</b>	<b>SUMMARY</b> .....	<b>189</b>
4.4.1	Fatigue Analysis Profiles .....	189
4.4.2	Microstructural Effects.....	194
4.4.3	Life Prediction Modelling .....	196

Contents

**CHAPTER 5. CONCLUSION ..... 199**

**5.1 SUMMARY ..... 199**

**5.2 RECOMMENDATIONS FOR FUTURE WORK..... 205**

**APPENDICES ..... 210**

**APPENDIX A: THREE MODES OF CRACK PROPAGATION BY APPLIED FORCES.. 210**

**APPENDIX B: PROPERTIES OF 7075-T6 ALUMINIUM ALLOY ..... 211**

**APPENDIX C: CRACK LENGTH VS CYCLES TO FAILURE DP 5 ..... 214**

**APPENDIX D: FRACTOGRAPH OF DP 27 SHOT PEENED LAYER AFTER SKIM..... 215**

**TABLE OF FIGURES**

Figure 1 Illustration of slip during fatigue and monotonic loading <sup>[9]</sup>.....9

Figure 2 Schematic of microstructural features in metallic materials <sup>[9]</sup> ..... 10

Figure 3 Typical beach markings <sup>[6,9]</sup>..... 12

Figure 4 Characteristics of the fatigue crack growth rate curve  $da/dn - \Delta K$  <sup>[9]</sup>..... 14

Figure 5 Schematic of shot peening machine <sup>[6]</sup>.....23

Figure 6 Shot separator for use with a shot peening machine <sup>[16]</sup>.....24

Figure 7 Photo of shot peening in progress <sup>[14]</sup>.....25

Figure 8 The Almen strip system employs standardized strips of spring steel that become curved when peened on one side only. The degree of curvature is proportional to the absorbed kinetic energy <sup>[3]</sup> .....27

Figure 9 Saturation curve, developed by exposing individual Almen strips at increasing time increments until there is less than a 10 % increase in curvature when the time is doubled. The Almen strips are said to be “saturated” at time T <sup>[3]</sup>.....27

Figure 10 Depth of compression vs Almen arc height. Depth is proportional to the intensity and hardness of the material being peened <sup>[3]</sup> .....28

Figure 11 Geometry of residual stress fields due to direct and bending type relaxation <sup>[3]</sup> .....29

Figure 12 Expected curvature of Almen test strip for full coverage shot peening vs normalised Almen strip thickness <sup>[3]</sup> .....30

Figure 13 Reversed bending fatigue of flat bars of varying Rockwell hardness showing improved fatigue limit C45 <sup>[14]</sup>..... 33

Figure 14 Example of residual compressive stress profile imparted by shot peening <sup>[3,14]</sup>37

Figure 15 Combined residual and applied bending loading <sup>[3]</sup> .....38

Figure 16 1st process on the left shows elastic-plastic elongation of surface layer with max residual stress at or near surface. The 2nd process on the right shows the maximum resultant shear stress at 0.47a below surface <sup>[17]</sup> .....39

Figure 17 Magnitude and distribution of residual stress induced by different shot peening parameters on 7075–T6 Aluminium Alloy <sup>[19]</sup>..... 45

Figure 18 Depth of compression vs Almen arc height. Depth is proportional to the intensity and hardness of the material being peened <sup>[14]</sup> ..... 46

## Table of Figures

Figure 19	Effects of shot peening dimple depression on the magnitude and distribution of residual stress <sup>[3]</sup> .....	47
Figure 20	Residual stress vs depth using S230 and S660 shot <sup>[14]</sup> .....	48
Figure 21	Relaxation of Residual Stress after One Cycle of Fatigue at 3 Levels of Alternating Stress (Rotating Bending) in Shot Peened Specimens <sup>[3]</sup> .....	49
Figure 22	Results of reversed bending fatigue tests on unpeened and shot peened specimens of 7075-T6 Aluminium Alloy <sup>[3]</sup> .....	50
Figure 23	Effect of re-peening on the total fatigue life of 0.4C steel and 7075-T6 aluminium alloy <sup>[3]</sup> .....	51
Figure 24	Distortion factor variation with cycles of fatigue for shot peened 2024-T351 aluminium alloy up to (a) 20 cycles and (b) 20000 cycles <sup>[3]</sup> .....	55
Figure 25	Dislocation density (solid line) and residual stress (dashed line) profile of shot peened 2024-T351 aluminium alloy <sup>[3]</sup> .....	55
Figure 26	Residual stress profiles of shot peened copper after plastic straining <sup>[3]</sup> .....	57
Figure 27	Indenter impression of Vickers microhardness tester <sup>[5,39]</sup> .....	61
Figure 28	Tensile strength vs surface hardness for various aluminium alloys <sup>[25]</sup> .....	62
Figure 29	Microhardness profile of a 2024 aluminium alloy shot peened specimen <sup>[26]</sup> ..	63
Figure 30	Principle of the SEM process <sup>[27]</sup> .....	64
Figure 31	SEM incident electron beam showing ejected electrons and X-rays <sup>[27]</sup> .....	65
Figure 32	Brittle transgranular fracture of an unknown metal with flat cleavage planes and sharp edges along the atomic steps <sup>[37]</sup> .....	66
Figure 33	Surface of voids on the surface of an aluminium casting x 1000 <sup>[38]</sup> .....	66
Figure 34	Equiaxed dimples from ductile overload of unknown metal <sup>[38]</sup> .....	67
Figure 35	Ductile fracture of an unknown metal with clear ductile dimples (microvoids) with significant plastic deformation of the material between dimples. Many of the dimples show a defect in the centre of the dimple which may have been responsible for the dimple formation <sup>[37]</sup> .....	68
Figure 36	Brittle fracture surface of an aluminium casting x 1000. The angular silicon particles at the surface contribute to the brittleness <sup>[38]</sup> .....	68
Figure 37	Microvoid coalescence in 8090-T8511 aluminium alloy formed by a combining of voids, some seen with precipitate particles at their centres <sup>[28]</sup> .....	69
Figure 38	Low cycle fatigue of aluminium alloy 5383-H21 showing ductile striations causing transgranular fracture <sup>[28]</sup> .....	69
Figure 39	Fatigue cycle diagrams with typical variations of stress ratio R (adapted) <sup>[31]</sup> ..	71

## Table of Figures

Figure 40	Various fluctuating uniaxial stresses corresponding to equal fatigue life <sup>[31]</sup> ....	72
Figure 41	Graphical representation of the parabolic Gerber mean stress correction for fatigue life analysis. Also shown are the Morrow, Goodman and Soderberg lines <sup>[40]</sup> .	73
Figure 42	Graphical representation of the Juvinall and Marshek life prediction model <sup>[5,31]</sup> .....	75
Figure 43	S-N Curves for axially loaded 7075-T6 aluminium alloy at various stress ratios. The lowest curve is for fully reversed cyclic stress amplitude where $R = -1$ <sup>[32]</sup> .....	76
Figure 44	S-N graph showing 7075-T6 aluminium alloy under fully reversible cyclic bending fatigue <sup>[33]</sup> .....	77
Figure 45	Haigh diagram showing Gerber lines of constant fatigue life (adapted) <sup>[40]</sup> .....	78
Figure 46	Surface factor vs tensile strength and hardness for steel <sup>[31]</sup> .....	80
Figure 47	Specimen diagram showing 14 mm testing diameter. The 12 mm and 10 mm test diameter specimens were to the same profile. ....	83
Figure 48	Tensile Tester Datasheet for DP 31 & 32.....	85
Figure 49	Tensile tester load-extension graphs for DP 31 & DP 32 .....	85
Figure 50	The ESH fatigue testing machine at UCT .....	87
Figure 51	Specimen mounted on two supports with the cross-head supplying the cyclic load.....	88
Figure 52	The complete setup showing the cross-head, load cell, mounted specimen, and optical microscope .....	89
Figure 53	Air turbine hole drilling machine at NMMU .....	90
Figure 54	Air turbine hole drilling assembly showing the main components.....	91
Figure 55	Specimen with strain gauge rosette attached showing the wire connections...	92
Figure 56	Data sheet for strain gauge rosette EA-06-031RE-120 .....	93
Figure 57	Raw residual stress analysis data sheet showing parameters and principal stresses .....	94
Figure 58	Example of stress-depth diagrams for DP15 specimen.....	96
Figure 59	Data for strain gauge used for plastic straining at CPUT .....	102
Figure 60	Vickers hardness vs diametral cross-section for 3 specimens.....	106
Figure 61	DP 19 showing the crack initiation site and next frame .....	107
Figure 63	DP 19 showing the whole shot peened depth .....	108
Figure 62	DP 19 clearly showing the sub-surface crack initiation site on the right, the shot peened layer and unpeened region.....	108

## Table of Figures

Figure 65	DP 20. Commonly seen ductile dimples with significant plastic deformation between dimples. White coloured defects can be seen at the centres of some dimples which may have contributed to the dimple formation.....	109
Figure 64	DP 19 showing magnification of the shot peened region and the typical shear cleavage with high atomic steps of ductile materials .....	109
Figure 67	DP 27. Fast fracture site at the specimen centre. Multiple cracks can be seen in the ductile dimpled region .....	110
Figure 66	Crack initiation site of DP 27. Transgranular cracking shown at the centre with small intergranular cracking branching off on the right end of the crack .....	110
Figure 68	DP 27. Magnification of centre- right hand crack in figure 61 showing the crack extension through the centres of the dimples where probable defect elements are embedded, as seen on the dimple to the left of the crack .....	111
Figure 69	Fatigue test 1: comparison for groups 1, 2 and 9 .....	117
Figure 70	Fatigue test 2: comparison for group 3.....	118
Figure 71	Fatigue test 3: comparison for group 4.....	119
Figure 72	Fatigue test 4: comparison for groups 4a and 5 .....	120
Figure 73	Fatigue test 5: comparison for groups 6, 7 and 8 .....	121
Figure 74	DP 1: unpeened: residual stress vs depth.....	123
Figure 75	DP 1: unpeened: total bending and residual stress vs depth.....	123
Figure 76	DP 15: unpeened, prefatigued to 20000 cycles, shot peened at SAA: residual stress vs depth.....	125
Figure 77	DP 15: unpeened, prefatigued to 20000 cycles and shot peened at SAA: total bending (525 MPa) and residual stress vs depth .....	125
Figure 78	DP 14, 17: estimated residual stress and total bending & residual stress distribution vs depth .....	126
Figure 79	DP 13: shot peened at SAA with 0.4103 % plastic strain: residual stress vs depth .....	128
Figure 80	DP 5: shot peened at SAA with 0.5 % plastic strain: residual stress vs depth.....	128
Figure 81	DP 5: shot peened at SAA with 0.5 % plastic strain: total bending (maximum 480 MPa) and residual stress vs depth .....	129
Figure 82	DP 13: shot peened at SAA with 0.4103 % plastic strain: total bending (maximum 525 MPa) and residual stress vs depth.....	129
Figure 83	DP 5 & 13: Trendlines of residual stress vs depth and bending and residual stress vs depth.....	131

## Table of Figures

Figure 84	DP 19: shot peened at SAA with 0.1703 % plastic strain: residual stress vs depth .....	133
Figure 85	DP 19: shot peened at SAA with 0.1703 % plastic strain: total bending and residual stress vs depth .....	133
Figure 86	DP 35: shot peened at SAA with 0.2815 % plastic strain: residual stress vs depth .....	135
Figure 87	DP 35: shot peened at SAA with 0.2815 % plastic strain: total bending and residual stress vs depth .....	136
Figure 88	DP 25: shot peened at CPUT with 1.0072 % plastic strain and 200 $\mu\text{m}$ skim: residual stress vs depth .....	138
Figure 89	DP 25: shot peened at CPUT with 1.0072 % plastic strain and 200 $\mu\text{m}$ skim: total bending and residual stress vs depth .....	138
Figure 90	DP 38: shot peened at CPUT: residual stress vs depth.....	141
Figure 91	DP 38: shot peened at CPUT: total bending and residual stress vs depth ...	142
Figure 92	DP 50: estimated residual stress vs depth .....	143
Figure 93	DP 50: shot peened at SAA, estimated total bending and residual stress vs depth .....	144
Figure 94	DP 4: Shot peened at SAA, not fatigued: residual stress vs depth .....	145
Figure 95	Graph showing all groups and relevant trendlines with gradients.....	149
Figure 96	Plastic strain vs depth of residual compressive stress .....	152
Figure 97	Average residual stress between 200-300 $\mu\text{m}$ depth vs plastic strain .....	155
Figure 98	Graph showing conversion between Vickers and Rockwell B hardness .....	157
Figure 99	Vickers hardness vs Stress derived from figure 28 .....	158
Figure 100	Diametral depth vs estimated proof stress derived from Vickers hardness values .....	158
Figure 101	DP 19 and 20 fractographs of the crack initiation sites showing similar fracture surface features .....	160
Figure 102	Close up views of the crack initiation sites of DP 19 and 20 showing the shot peened layers close to the surface and cleavage fracture on the planes of maximum shear .....	161
Figure 103	Magnification of Figure 101 showing shot peened region with flat cleavage planes (left) and fracture trough at crack initiation (right).....	161
Figure 104	Further magnification of Figure 102 showing shear cleavage and high atomic steps of the ductile region .....	162

Table of Figures

Figure 105 DP 20 showing ductile dimpled microvoids due to tensile overload with high plastic deformation between the dimples and white coloured precipitate particle defects at their centres. Intergranular microvoid coalescence is also shown. .... 162

Figure 106 DP 37 and 45 at crack initiation sites showing the much smaller shot peened depth due to skimming. Notice the much darker compacted surface from the heavier shot peening ..... 163

Figure 107 DP 37 and 45. Magnifications near the surface of Figure 105 of the top centre ..... 164

Figure 108 DP 27 and 36 showing shot peened surfaces and shear cleavage with atomic steps and ductile striations..... 164

Figure 109 DP 27 and 36 showing magnifications of figure 107 at the top surface near the centre ..... 165

Figure 110 DP 27 with two images of the fast fracture region showing intergranular microvoid coalescence cracking, typical of ductile materials ..... 165

Figure 111 Generalised S-N curves for polished 7.6 mm diameter steel specimens <sup>[31]</sup> 167

Figure 112 Axial to bending conversion line for S-N diagram..... 168

Figure 113 S-N diagram showing axial and bending lines for R = -1 ..... 170

Figure 114 Log S-Log N diagram for axial and bending lines for R = -1 ..... 170

Figure 115 Log S-Log N showing the MIL-HDBK-5J diagram of Group 1 for unpeened specimens for R = -1 ..... 172

Figure 116 S-N diagram showing the Atlas of Fatigue Curves line for R = -1 ..... 174

Figure 117 Log S-Log N diagram of Group 1 showing the Atlas of Fatigue Curves line for R = -1..... 175

Figure 118 Log S-Log N of Group 9 for shot peened specimens at CPUT and SAA for R = -1 ..... 181

Figure 119 Log S-Log N of Group 6 for shot peening at CT and plastic strain for R = -1 ..... 185

Figure 120 Log S-Log N of Group 8 for shot peening at CPUT, plastic strain and skim for R = -1..... 188

## LIST OF TABLES

Table 1	Physical characteristics of 7075-T6 aluminium alloy. Excerpt from Appendix B .	20
Table 2	Critical Strain and Maximum Tensile Residual Stress Values <sup>[3]</sup> .....	57
Table 3	Spreadsheet sample of stress calculations for DP 15 specimen .....	96
Table 4	Shot peening machine test settings record at CPUT .....	98
Table 5	Program used in automatic peening mode at CPUT .....	99
Table 6	Specifications for various types of shot at CPUT. S230 steel shot was used ...	100
Table 7	Specimens that were plastically strained.....	103
Table 8	Fatigue life of shot peened specimens with various plastic straining and a 200 µm surface skim .....	104
Table 9	Vickers hardness - diametral depth experimental values .....	106
Table 10	Research specimen control list with groupwise test details .....	115
Table 11	DP 1: unpeened specimen.....	122
Table 12	DP 15: unpeened, prefatigued to 20000 cycles and shot peened at SAA.....	124
Table 13	DP 14, 17: estimated unpeened, prefatigued to 20000 cycles, and shot peened at SAA .....	126
Table 14	DP 5: shot peened at SAA with 0.5 % plastic strain and a maximum bending stress of 480 MPa .....	127
Table 15	DP 13: shot peened at SAA with 0.4103 % plastic strain and a maximum bending stress of 525 MPa .....	127
Table 16	DP 5 & 13: residual stress vs depth and total bending & residual stress vs depth values, showing their variances .....	131
Table 17	DP 19: shot peened at SAA with 0.1703 % plastic strain.....	132
Table 18	DP 35: shot peened at SAA with 0.2815 % plastic strain.....	135
Table 19	DP 25: shot peened at CPUT with 1.0072 % plastic strain and 200 µm skim .	137
Table 20	DP 38: shot peened at CPUT.....	141
Table 21	DP 50: shot peened at UCT estimated residual stress vs depth.....	143
Table 22	DP 4: Shot peened at SAA, not fatigued: residual stress vs depth .....	144
Table 23	Portion of Table 10 to highlight surface treatment, plastic strain, skim and fatigue life .....	148
Table 24	Plastic strain vs depth of residual compressive stress.....	152
Table 25	Conversion from Rockwell hardness B to Vickers hardness and stress against incremental depth .....	157

List of Tables

Table 26 Axial to bending conversions for unpeened specimens for R = -1 ..... 169

Table 27 S-N and log-log values calculated from the Atlas of Fatigue Curves <sup>[33]</sup>..... 173

Table 28 S-N and log-log values for group 9: shot peening ..... 180

Table 29 S-N and log-log values for group 6: shot peening CT and plastic strain ..... 185

Table 30 S-N and log-log values for group 8: shot peening CPUT, plastic strain and skim  
..... 187

Table 31 Life prediction model equation constants per process..... 198

**LIST OF EQUATIONS**

Equation 2.1	$K = \sigma(\pi a Q)^{\frac{1}{2}}$ .....	13
Equation 2.2	$K = Y\left(\frac{a}{W}\right) \cdot \sigma(\pi a Q)^{\frac{1}{2}}$ .....	13
Equation 2.3	$\frac{da}{dn} = C(\Delta K)^m$ .....	13
Equation 2.4	$\frac{da}{dn} = \frac{C(\Delta K)^m}{[(1-R)K_c - \Delta K]}$ .....	14
Equation 2.5	$K = \frac{8 \times \text{Almen Number}}{d^2}$ .....	28
Equation 2.6	$M = \int_{z_2}^{z_1} \sigma_r(z^*) \cdot \left[ z - \left( \frac{t}{2} \right) \right] dz$ .....	28
Equation 2.7	$K = \frac{12M_o(1-\nu^2)}{Et^3}$ .....	29
Equation 2.8	$K = \frac{(5.966c - 5.53)k}{Ec^3 a}$ .....	29
Equation 2.9	$z_{\Gamma, \max} = 0.47a$ .....	39
Equation 2.10	$p_o = \frac{3}{2} \times \text{mean contact pressure} = \frac{3}{2\pi} \cdot \frac{F}{a^2}$ .....	39
Equation 2.11	$\tau_{\max} = 0.31 \cdot \frac{3}{2\pi} \cdot \frac{F}{a^2}$ .....	39
Equation 2.12	$a = \sqrt{2hr - h^2}$ .....	40
Equation 2.13	$\text{mass}_{\text{shot}} \times \text{acceleration}_{\text{shot}} = \text{area}_{\text{contact circle}} \times \text{pressure}_{\text{average}}$ ....	41

List of Equations

Equation 2.14  $\frac{4\pi}{3} \rho R^3 \frac{dv}{dt} = -\pi a^2 \bar{p} \dots\dots\dots 41$

Equation 2.15  $\frac{\bar{p}}{Y} = 0.6 + \frac{2}{3} \ln\left(\frac{Ea}{YR}\right) \dots\dots\dots 41$

Equation 2.16  $\frac{\bar{z}}{R} = \left(\frac{2}{3}\right)^{\frac{1}{2}} \left(\frac{\rho v_o^2}{\bar{p}}\right)^{\frac{1}{2}} Q \dots\dots\dots 42$

Equation 2.17  $\frac{\bar{z}}{R} = \left(\frac{2}{3}\right)^{\frac{1}{2}} \left(\frac{\rho v_o^2}{\bar{p}}\right)^{\frac{1}{2}} \dots\dots\dots 42$

Equation 2.18  $\lambda = 3 \left(\frac{2}{3}\right)^{\frac{1}{4}} \frac{R}{h} \left(\frac{\rho v_o^2}{\bar{p}}\right)^{\frac{1}{4}} \dots\dots\dots 42$

Equation 2.19  $K = f\left(\frac{a}{W}\right) \cdot \sigma(\pi a Q)^{\frac{1}{2}} \dots\dots\dots 52$

Equation 2.20  $\frac{da}{dn} = C(\Delta K)^m \dots\dots\dots 52$

Equation 2.21  $HV = \frac{F}{A_s} = \frac{2F \sin\left[\frac{\alpha}{2}\right]}{d^2} = \frac{1.8544F}{d^2} \dots\dots\dots 62$

Equation 2.22  $\sigma_n = \frac{\sigma_a}{1 - \left[\frac{\sigma_m}{\sigma_u}\right]^2} \dots\dots\dots 74$

Equation 2.23  $\sigma_m = \left[\frac{\sigma_{\max} + \sigma_{\min}}{2}\right] + \sigma_{\text{residual}} \dots\dots\dots 74$

Equation 2.24  $\sigma_a = \left[\frac{\sigma_{\max} - \sigma_{\min}}{2}\right] \dots\dots\dots 74$

List of Equations

Equation 2.25	$S_n = S'_n \cdot C_L \cdot C_G \cdot C_S \cdot C_T \cdot C_R$ .....	79
Equation 4.1	$m = \frac{\Delta N_f}{\Delta(\% \text{ Microstrain})}$ .....	147
Equation 4.2	$S_n = -0.9477 (\text{Log } N_f)^3 + 26.717 (\text{Log } N_f)^2 - 276.05 \text{ Log } N_f$ + 1137.4 .....	168
Equation 4.3	$\text{Log } S_n = -0.1074 \text{ Log } N_f + 3.032$ .....	169
Equation 4.4	$\text{Log } S_n = -0.1128 \text{ Log } N_f + 2.9514$ .....	173
Equation 4.5	$S_n = -0.6411 (\text{Log } N_f)^3 + 22.461 (\text{Log } N_f)^2 - 246.99 \text{ Log } N_f$ + 996.63 .....	174
Equation 4.6	$\text{Log } S_n = -0.1128 \text{ Log } N_f + 2.9514$ .....	175
Equation 4.7	$\text{Log } S_n = -0.1128 \text{ Log } N_f + 3.128$ .....	178
Equation 4.8	$\text{Log } S_n = -0.1128 \text{ Log } N_f + 3.1035$ .....	179
Equation 4.9	$\text{Log } S_n = -0.1128 \text{ Log } N_f + 3.0412$ .....	184
Equation 4.10	$\text{Log } S_n = -0.1128 \text{ Log } N_f + 3.0396$ .....	186
Equation 4.11	$N_f = 29752 (\%PS) + 25060$ .....	187
Equation 4.12	$\text{Log } S_n - -0.0028 \text{ Log } N_f + C$ .....	198

## LIST OF ABBREVIATIONS

- **CPUT:** Cape Peninsular University of Technology
- **HCF:** High Cycle Fatigue
- **$K_{1c}$  or  $K_c$ :** Fracture Toughness
- **LCF:** Low Cycle Fatigue
- **LEFM:** Linear Elastic Fracture Mechanics
- **MSSC:** Microstructural Short Crack
- **PSBs:** Persistent Slip Bands
- **R:** Stress Ratio
- **SAA:** refers to shot peening performed at South African Airways
- **SEM:** Scanning Electron Microscope
- **UTS:** Ultimate Tensile Stress

## NOMENCLATURE

- **Almen Intensity:** the height of arc, measured in mm, produced by compressive stresses induced in the surface of a steel test strip by shot peening
- **Aspect Ratio:** the ratio between the length (or large diameter) and the width (or small diameter) of an object
- **Cleavage Planes:** the fracture along crystallographic planes and are generally flat in nature
- **Cold Working:** the strengthening of metals by plastic deformation. Also called strain hardening or work hardening
- **Dislocation Density:** a measure of the amount of crystallographic defects within a crystal structure
- **Dislocation Pile-Up:** an accumulation of dislocations along a slip plane when hindered from continuing along the plane due to a barrier-like a grain boundary
- **Dislocations:** a crystallographic defect in a crystalline structure
- **Ductility:** The ability of a solid material to deform under tensile stress
- **Electron Microscope:** a microscope that uses accelerated electrons as a source of illumination (see par 2.8)
- **Endurance Limit:** the maximum cyclic stress amplitude applied to a material without causing fatigue failure
- **Fatigue Life:** the number of fluctuating load cycles a component can withstand prior to fatigue failure
- **Fatigue Striations:** the increment of growth of a ridge or marking which occurs in one load cycle by the operation of slip planes at a crack tip, causing blunting and sharpening, as seen in “beach markings”
- **Fractographs:** magnified images of fracture surfaces produced by an electron microscope in this research
- **Fracture Toughness ( $K_{Ic}$  or  $K_c$ ):** the property which describes the ability of a material to resist fracture
- **Generalised Fatigue Strength Factors:** conversion factors, greater than 0 and less or equal to 1, depending on types of fatigue loading, diameter size, surface conditions, temperature, reliability, and other relevant conditions, to be multiplied with the Moore endurance stress limit to find an endurance limit related to actual test conditions. It can also apply to the  $10^3$  cycle strength

- **High Cycle Fatigue (HCF):** fatigue testing where failure occurs from and above  $10^6$  cycles, caused by low fluctuating stress amplitudes
- **Inclusions:** an impurity or particle which are normally detrimental to the mechanical properties of the host metal
- **Intergranular:** between the crystalline grain boundaries
- **Life Prediction Model:** a normally empirical mathematical equation or formula with the cyclic stress amplitude and fatigue life as functions. The purpose is to find the stress amplitude at a designated number of cycles, or vice versa
- **Linear Elastic Fracture Mechanics (LEFM):** the method of determining crack growth in materials under the basic assumption that material conditions are predominantly linear elastic during the fatigue process
- **Low Cycle Fatigue (LCF):** fatigue testing where failure occurs up to approximately  $10^5$ , caused by high fluctuating stress amplitudes
- **Microhardness:** the measurement of the resistance of a material to plastic deformation by applying low loads to a diamond square-based pyramid shaped indenter
- **Microstrain:** is the strain  $\times 10^{-6}$
- **Microstructure:** the structure of a prepared surface of metal as revealed by a microscope at a magnification exceeding 25 times
- **Microvoid Coalescence:** the nucleation, growth and coalescence of microvoids caused by high local plastic deformation
- **Persistent Slip Bands (PSBs):** areas of intensive cyclic plastic strain of lamina-like shape arising from cyclic straining of crystalline materials, which normally slide to the surface of the metal (see Figure 1)
- **Plastic Strain:** is the straining of a material beyond the elastic limit so that it permanently deforms, or elongated for the purposes of this research
- **Residual Stress:** the internal stress remaining in a material after the force causing it has been removed
- **Shot:** Spherically shaped metal, glass or ceramic particles projected at high speed, to cause indentations and local plastic deformations, resulting in surface compressive residual stresses.
- **Shot Peening Intensity:** see Almen intensity
- **Skimming:** the removal of a small amount of surface metal by using a machining lathe
- **Slip Planes:** symmetrically identical crystalline planes along which dislocations can easily occur leading to plastic deformation

## Nomenclature

- **Strain Strengthening:** similar to cold working where a material is placed under a tensile load to extend or strain it beyond the elastic limit to increase its yield or proof stress
- **Stress Concentrations:** (or stress raisers) the location in a material where stress is concentrated at a particular area, often caused by a crack, instead of being evenly distributed throughout the whole area under load
- **Stress Ratio (R):** in cyclic fatigue testing. The ratio of the minimum bending stress to the maximum bending stress
- **Striations:** a series of ridges or edges forming a pattern at a fatigue fracture surface caused by each cycle of fatigue
- **Surface Coverage:** the percentage of surface area indented by shot peening to the total target area
- **Surface Roughness:** is the measure of “waviness” or lack of smoothness of a surface comprising of small local deviations
- **Transgranular:** refers to cracks that penetrate through the metallic grains (see Figure 1)
- **Ultimate Tensile Stress (UTS):** of a material which is the highest stress a material can withstand

## **CHAPTER 1. INTRODUCTION**

### **1.1 ACKNOWLEDGEMENT OF PRIOR TESTING**

Primary testing for this dissertation was done when the current researcher was previously registered for the same degree at Cape Peninsular University of Technology (CPUT).

Acknowledgement needs to be given for all the fatigue testing and shot peening of specimens (at SAA) at the University of Cape Town under Prof RB Tait (through CPUT), and the shot peening of specimens as well as all plastic straining at CPUT under Mr TAP van der Schyff, who both served as supervisors.

The current researcher performed a significant amount of information gathering at these two institutions, as well as writing a large part of the dissertation.

It is worth noting that none of the work was submitted for evaluation as the current researcher had to withdraw from continuing due to personal, logistical and financial reasons.

However, CPUT has generously permitted the current researcher to use all the test results obtained there for the continuation of his present studies at NMMU. Some changes to the topic have been made for the research at NMMU but still using most of the test data gained through CPUT. All the testing and associated data obtained through CPUT, however, still remains to be their property.

When being a registered student with CPUT the specimens were outsourced by the researcher at that time to NMMU, by arrangement, for residual stress-depth tests for the same degree, which can be used again here.

The researcher is especially grateful to CPUT for the use of their test data and sincerely thanks them for their generosity.

### **1.2 INTRODUCTION**

Metal fatigue may be regarded as the cumulative damage from structural deterioration caused by repeated cyclic application of often normal loading. Changes, such as design or manufacturing detail, high stress interfaces (e.g. keyways) and surface defects (e.g. inclusions, scoring), may be deleterious to fatigue life. In addition, for smooth polished surfaces, fatigue is associated with micro-plastic deformation processes, such as dislocation pile-up, producing surface intrusions and extrusions by means of slip on planes of atoms <sup>[1]</sup>. Fatigue strength and fatigue life are consequently very dependent on surface conditions such

as finish, local hardness and the presence of surface residual stresses which may be regarded as those stresses which would exist in an elastic solid body if all the external loads were removed <sup>[2]</sup>. Efforts are frequently made to inhibit surface fatigue crack initiation which can markedly enhance fatigue life. One such technique is shot peening, which is the process of cold-working the surface by means of a driven stream of hard shot <sup>[2]</sup>. The shot indents the surface causing plastic deformation including local compressive stresses in the surface which counteract the applied cyclic tensile stresses causing crack initiation <sup>[2]</sup>. In addition, shot peening substantially alters the surface microstructure of the material which can have fatigue inhibiting characteristics. The exact extent of the influence of shot peening and microstructure on fatigue improvement, however, is not yet fully understood.

This project is concerned with an experimental study of the effect of controlled shot peening on 7075-T6 aluminium alloy. In particular, account will be taken of surface roughness, microhardness, peening intensity, surface microstructure and residual stress.

An investigation is to be made to discriminate between the relative importance of residual stress, hardness and microstructural parameters of shot peening on fatigue life, and to develop a fundamental understanding of the relative importance of the mechanistic contribution to inhibition of fatigue initiation, particularly residual stress and localised microstructural effects.

### **1.3 APPLICATIONS**

Aluminium alloys are used substantially for engineering applications where material is required to be both light and strong, such as in the aircraft industry, mining skips, and even Porsche and BMW sports car connecting rods. The lifetime of many components or structures under service conditions in these fields is often limited by time-dependent processes such as corrosion, wear and fatigue. Since failure by these processes can result in significant economic loss, through loss of productivity and damage to machinery, often constituting safety hazards, much effort has been directed towards understanding their occurrence and minimising their effects. In the field of fatigue in particular, considerable advances have been made in recent years in both the understanding of the mechanisms of fatigue initiation and propagation processes <sup>[3]</sup>.

There are various ways of inhibiting, or at least slowing down, fatigue crack initiation in Aluminium, namely, rolling, hammer peening, laser peening, shot peening, and other varieties of techniques.

In the context of this research, shot peening may be considered as the indenting and plastic deformation of the surface layer by air (or water) blasting hard shot at a high velocity. Surface compressive stresses and some work hardening is produced both of which are beneficial, as long as surface roughness is not impaired. Shot peening has shown great success in enhancing the fatigue life in components and structural materials. The fatigue life and corresponding shot peening treatments need to be properly understood and documented for the varieties of metals.

One of the stalwart metals used for structural components of aircraft is 7075-T6 aluminium alloy due to its lightness and high tensile strength, which was developed by the Japanese company Sumitomo Metal Industries in 1936 and used for the Zero fighter aircraft during the 2nd World War <sup>[4]</sup>. The kind of applications required for this alloy subject it to a substantial amount of cyclic loading and fatigue, affecting safety levels involving people and expensive equipment, so techniques to enhance fatigue life characteristics are employed to assist designers and maintenance engineers in their areas of responsibility. It is hoped that this study of 7075-T6 aluminium alloy fatigue characteristics will be of assistance in putting the effects of shot peening into a useful perspective.

#### 1.4 PROBLEM STATEMENT

Shot peening is used to extend fatigue life in many industrial applications where metals are subject to cyclically fluctuating bending stresses. The primary issue in this dissertation is to improve our understanding of the effectiveness of shot peening in inhibiting fatigue crack initiation, and therefore the fatigue life, of 7075-T6 Aluminium Alloy round bar, taking into consideration surface residual stress, microstructural and micro-hardness parameters.

#### 1.5 SUB-PROBLEMS

Assessments of the following parameters, viewed as intrinsic to the analysis, need to be made to establish the extent of their validity.

**1.5.1** It is expected that the **residual compressive stresses** imposed by shot peening will be reasonably consistent with norms found in the shot peening community. To find the role of this residual stress to fatigue life, techniques of varying the stress will need to be implemented, and the limitations of these techniques recognised.

- 1.5.2 Microstructural parameters** are important but the least understood and probably the most difficult to identify and assess. An attempt will be made to judiciously choose microscopic parameters from those commonly identified in fatigue analysis.
- 1.5.3 Plastic straining** has been used as an effective way to reduce residual compressive stresses. It also includes microstructural altering with strain hardening as a sub-problem and becomes one of its parameters. The influence of plastic straining on the microstructure affecting fatigue life needs to be better understood.
- 1.5.4 Micro-hardness** can play a role in fatigue life analysis. It has been used to estimate residual stresses in steels but there is a level of doubt whether it will apply to aluminium alloys. Its degree of importance to this research will need to be analysed for this alloy.
- 1.5.5 Electron microscope fractographs** are important to visually analyse the properties of the fractured surfaces. Microstructural features like deformations, the shot peened layer, crack initiation, cleavage and final fracture, are some significant symptoms that assist in analysing the reaction of this metal under fatigue.

## **1.6 HYPOTHESIS**

It is hoped that the effects of shot peening on extending low cycle (high bending stress) fatigue life may be demonstrated through induced residual compressive stress, microstructural and micro-hardness effects. It is expected that residual compressive stresses will compensate for tensile bending stresses normally causing fatigue cracks. The changes in microstructure due to shot peening are also expected to cause resistance to crack initiation as well as hardness on the surface of the 7075–T6 Aluminium alloy.

A relationship between these parameters is expected to be identified and demonstrate their relative importance, hopefully assisting in designing more instructively against fatigue for this metal.

## 1.7 DELIMITATIONS

**1.7.1 Test specimens** are dog-bone shaped round bar 120 mm long, with 50 mm effective testing length and diameters of 10, 12 and predominantly 14 mm.

**1.7.2 Shot peening** was performed applying the Almen metric scale using cast steel S230 shot, with a 150% covering. The shot peening was performed at the SAA Denel and CPUT laboratories set to the 8 to 14 and 20 to 36 Almen ranges respectively.

**1.7.3 Fatigue testing** on all specimens was done on the University of Cape Town ESH universal servo hydraulic testing machine using a stress ratio of +0.1 with a tensile bending stress range from 48 to 480 MPa initially on the first six specimens, and then changed to 52.5 to 525 MPa at the request of the supervisor. Three point bending was performed in all fatigue tests.

**1.7.4 Residual stress–depth tests** on selected specimens were done on the NMMU residual stress analyser (RESTAN) air turbine hole drilling machine using the Integral Analysis Method. Only residual stresses up to a depth of 0.5 mm were considered. Specimen selection was based on the types of treatment, i.e. unpeened, prefatigued to 20000 cycles and then shot peened, shot peened and then plastically strained, shot peened and radially skimmed by 200  $\mu\text{m}$ , and shot peened only. Three specimens, one unpeened, one shot peened and the third shot peened and plastically strained, were fatigue tested before the residual stress-depth testing and the remaining six specimens afterwards. Precautions were taken with the three specimens fatigued beforehand to place the strain gauges at remote positions from the fracture sites, so as not to detrimentally affect their residual stress-depth results. One set of three specimens was tested at UCT on their Air Abrasive Centre Hole Drilling (AACHD) machine by a final year BSc student who co-exchanged some work with the author. The effects of the combination of bending and residual stresses at their particular depths will be analysed with the hope that their profiles will reveal useful information on the depth of crack initiation and fatigue life.

**1.7.5 Plastic straining** was performed on selected unpeened and shot peened specimens, intended to mechanically vary the residual compressive stresses, range between 0%

to 1% microstrain. Radial surface skims of about 200  $\mu\text{m}$  were machined off the shot peened surface of some of these specimens selected to eliminate distorted material in an attempt to simulate an “unpeened” surface, while still retaining some residual compressive stresses. It is uncertain whether these results will be sufficiently conclusive for all variables as published data is limited on this approach and therefore may need to be viewed as investigative.

**1.7.6 Microhardness** testing will be through the diameter cross-section of selected specimens by using the Vickers numbering method.

**1.7.7 Electron microscope fractograph** magnifications will range from 14 to 1200 times the original size. This is expected to offer sufficient visual inspection capabilities for analysing the required fractured surface characteristics.

**1.7.8** This research will be limited to the analysis of **final fatigue cycle failure** and fatigue life when applied to preparations and treatments of specimens.

The **fatigue life of untreated unpeened specimens** will serve as the point of reference **benchmark** for this research.

A fatigue life prediction model will be sought by using the Juvinall and Marshek as well as the Gerber mean stress equation methods to evaluate their relevance for this material <sup>[5]</sup>.

**Fatigue crack analysis** will be introductory and for relevant background purposes only. Quantitative analysis of **crack growth rates** will not be considered for this research except on a few relevant occasions in the analysis of results when a specific crack depth is compared to the residual stress at the same depth.

**1.7.9** It is well known that **fatigue results** can have fairly high variances and can often only be taken as trends rather than wished-for absolutes.

This will need to be taken into consideration when analysing conclusions.

## 1.8 RESEARCH METHODS

### 1.8.1 Literature Review

- Fatigue crack initiation, propagation and analysis
- Surface treatments to slow down fatigue crack initiation and failure
- Physical characteristics of 7075-T6 Aluminium Alloy
- Shot peening procedures and process variables
- Residual stresses induced by shot peening and their effects on fatigue life
- Microstructural and deformation effects on fatigue
- Microhardness-depth tests throughout the diameter cross-section
- Scanning electron microscope fractography of the fractured surfaces
- Life prediction models using mean stress and stress amplitude parameters

### 1.8.2 Development and Implementation of Tests

- Machine material to make test specimens according to specifications
- Select and send away specimens to be shot peened
- Prepare the specimens to be fatigue tested as follows:
  - Unpeened and fatigued to failure
  - Unpeened, prefatigued to 20000 cycles, shot peened, and fatigued to failure
  - Unpeened, plastically strained between 0% and 0.6% microstrain, and fatigued to failure
  - Shot peened and fatigued to failure
  - Shot peened, plastically strained between 0% and 1% microstrain, and fatigued to failure
  - Shot peened, plastically strained between 0% and 1% microstrain, skimming 200  $\mu\text{m}$  to simulate an “unpeened” specimen with residual compressive stress, and fatigued to failure
  - Tensile test two unpeened specimens to compare results with published data
- Select specimens representing the different preparations listed in the third main bullet above, before and after fatigue testing, for residual stress-depth testing

- Select specimens representing the different preparations listed in the third main bullet above for diametral microhardness-depth tests
- Select specimens representing the different preparations listed in the third main bullet above for SEM scanning of fractured cross-sections

### **1.8.3 Analysis of Test Results**

The test results indicating fatigue life, residual stress-depth distribution, plastic straining effects, microstructure and micro-hardness characteristics, and SEM fractography, will be analysed to determine their significance and relative importance in developing a prediction model for fatigue life.

The Juvinall and Marshek life prediction model in conjunction with the Gerber equation for mean stress will be used to determine a life prediction model for the 7075-T6 aluminium alloy bars in this research.

Conclusions will be drawn from the analysis in the hope that they will offer guidelines for the engineering fraternity.

**CHAPTER 2.****LITERATURE REVIEW****2.1 METAL FATIGUE****2.1.1 Crack Initiation**

Crack initiation may be split up into two stages, i.e. crystal deformation and the microstructural short crack (MSSC), which is so small ( $< 100 \mu\text{m}$ ) that it may be considered part of the transition to crack propagation <sup>[2,6,7,8]</sup>. Crystal deformation, through residual and applied stresses, may produce sliding of atoms along adjacent crystallographic shear planes which may be intensified by dislocations, voids, and inclusions. Under fatigue loading the surface material tends to deform by cyclic slip concentrated in persistent slip bands (PSBs) consisting of extrusions and intrusions. See Figure 1.

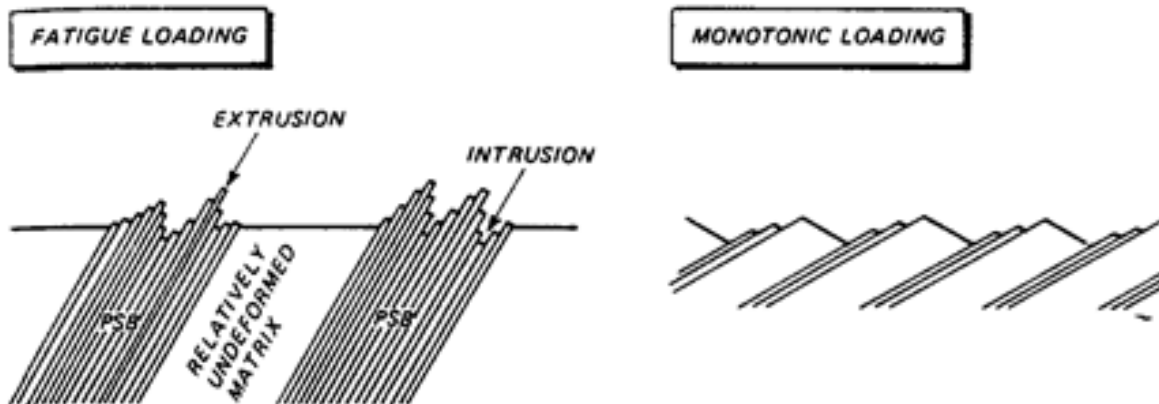


Figure 1 Illustration of slip during fatigue and monotonic loading <sup>[9]</sup>

Continuing cyclic slip leads to deepening of the intrusions and eventually the formation of a crack along the slip plane. This slip plane cracking may extend a few propagation. Slip bands may be accompanied by strain strengthening, which may resist slip <sup>[2,9]</sup>. With repeated loading the crystals may fragment due to deformation until a MSSC forms associated with the slip band <sup>[2]</sup>.

The MSSC is almost of the order of the microstructural unit size and the Linear Elastic Fracture Mechanics (LEFM) approach is not applicable because of continuum mechanics limitations <sup>[7]</sup>. The grain size for 7075-T6 aluminium alloy in analysing MSSC growth

behaviour is measured in the normal direction because grain boundaries in the normal direction are strongly affected by surface crack growth rates. MSSCs show a complicated growth behaviour, depending on the microstructure of the material.

Experiments on 7075-T6 aluminium alloy have shown that the growth of MSSCs depend strongly on the stress ratio,  $R$ , with cracks initiating at the inclusions [7].

### 2.1.2 Crack Propagation

Crack propagation takes over from the MSSC in the formation of mechanically small cracks, which experience low crack closure levels and exhibit little influence of the microstructure. Physically small cracks develop which have the same crack closure levels and growth behaviour as large cracks when LEFM is applied to characterise their growth rates. At this stage coalescence of these small cracks may become evident until large cracks are formed, normally along transgranular or intergranular paths [7]. Figure 2 shows a schematic of microstructural features in metallic materials.

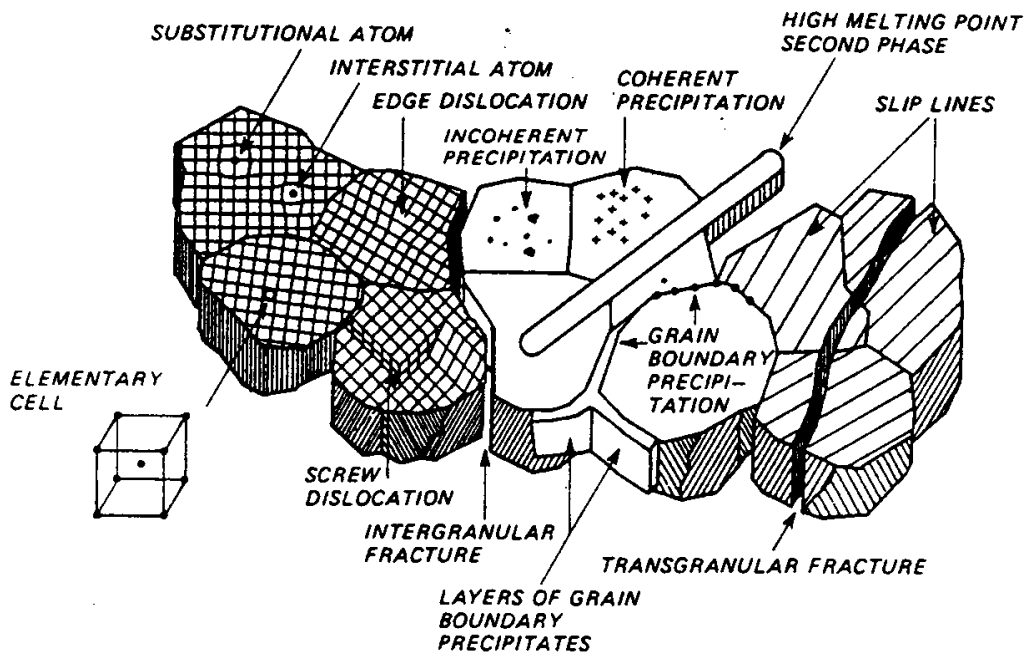


Figure 2 Schematic of microstructural features in metallic materials [9]

Ductile transgranular fracture by microvoid coalescence is caused by overload displaying a typical dimpled appearance of the fractured surface, the dimpled shape characterising the

type of loading. The microvoids that form dimples nucleate at various internal discontinuities, especially intermetallic particles, precipitates and grain boundaries. The microvoids grow and coalesce with increasing local stress and eventually form a continuous fracture surface [9].

Brittle transgranular fracture is caused by cleavage. Typical polycrystalline materials with more or less randomly oriented grains cause cleavage that propagates through one grain and probably changing direction as it crosses another grain or sub-grain boundary. These directional changes result in faceted fracture surfaces. Particles, precipitates and other imperfections complicate the fracture path even further. These orientation changes typically produce river or feather patterns, which are steps between cleavages on parallel planes. The apex of the feather markings point back to the fracture origin.

Transgranular fatigue fracture surfaces are macroscopically flat and smooth, and will often show “beach markings” which vary depending on the load history. See Figure 3 for typical beach markings. The area of the final fracture gives an indication of the magnitude of the loads. A large final fracture area indicates that the fracture toughness,  $K_{1c}$  or  $K_c$ , is exceeded at a relatively short crack length, which means that either the maximum load is too high or the fracture toughness low, or both.

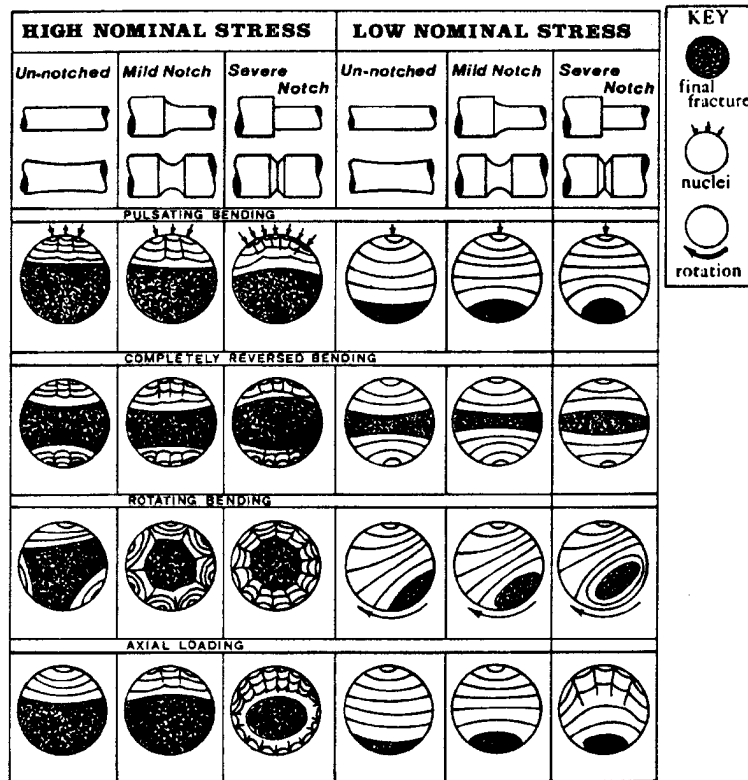


Figure 3 Typical beach markings <sup>[6,9]</sup>

Micromechanistic modelling is a subject of considerable interest and speculation, especially concerning fatigue striations. Striations represent successive positions of the crack front. Aluminium alloys generally give well-defined regular striations, but steels do not. Striations are perpendicular to the local direction of crack growth, a property which may be used in tracing backwards to the initiation site.

Each striation is formed during one load cycle and the spacing between them is an indication of local crack growth rates, especially with constant amplitude loading <sup>[9]</sup>.

Various models of fatigue striation have been proposed. Most only consider plastic flow at the crack tip <sup>[9]</sup>.

Intergranular fractures are typically the result of sustained load fracture, and precipitates to grain boundaries. Two main types of intergranular appearance are grain boundary separation with or without microvoid coalescence and are not readily identifiable without the aid of an electron microscope <sup>[9]</sup>.

Cracks can also have three types of separation modes [see Appendix A].

Mode I cracks are opening modes where the applied tensile stress is normal to the plane of the crack.

Mode II cracks are sliding modes where the applied shear stress acts parallel to the plane of the crack and perpendicular to the crack front.

Mode III cracks are tearing modes where the applied shear stress acts parallel to the plane of the crack and parallel to the crack front.

### 2.1.3 Fatigue Crack Analysis

Crack growth is often given in terms of the stress intensity factor, K:

$$K = \sigma(\pi a Q)^{\frac{1}{2}} \quad \text{Equation 2.1}$$

where: a = crack length

$\sigma$  = gross stress

Q = geometry correction factor

Other versions introduce a shape function,  $Y\left(\frac{a}{W}\right)$ , to find K:

$$K = Y\left(\frac{a}{W}\right) \cdot \sigma(\pi a Q)^{\frac{1}{2}} \quad \text{Equation 2.2}$$

Where W is the specimen width <sup>[10]</sup>

The crack growth rate,  $\frac{da}{dn}$ , for a given material is a function of the range of the stress intensity factor,  $\Delta K$ . Paris and Forman formulae are frequently used to express this function.

Paris' formula is:

$$\frac{da}{dn} = C(\Delta K)^m \quad \text{Equation 2.3}$$

Where:  $\Delta K = \Delta\sigma(\pi a Q)^{\frac{1}{2}}$

$\Delta\sigma = \sigma_{\max} - \sigma_{\min} = 2\sigma_{\text{amplitude}} = \text{gross stress range}$

n = number of applied stress cycles

m and C = empirical material parameters.

Forman's equation included the effect of the stress ratio,  $R = \sigma_{\min} / \sigma_{\max}$ , which allowed for greater acceleration of the crack growth rate before failure. Forman's equation is:

$$\frac{da}{dn} = \frac{C(\Delta K)^m}{[(1-R)K_c - \Delta K]} \quad \text{Equation 2.4}$$

where  $K_c$  is the fracture toughness of the material

In Figure 4 the 3 regions of curve shapes are shown on  $\log da/dn$  and  $\log \Delta K$  axes.

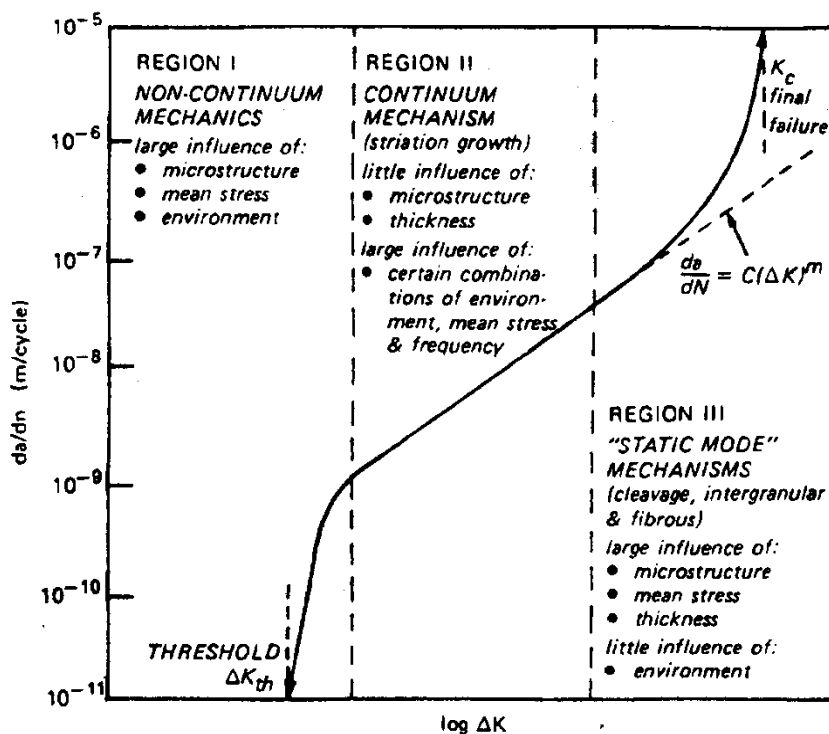


Figure 4 Characteristics of the fatigue crack growth rate curve  $da/dn - \Delta K$  [9]

In region 1 is a threshold value,  $\Delta K_{th}$ , below which cracks do not propagate. Above  $\Delta K_{th}$  the crack growth rate increases rapidly until it enters region 2 where there is a linear relation between the  $\log da/dn$  and  $\log \Delta K$  values, in which the Paris equation is most applicable. In region 3, suitable for Forman equation applications (large  $\Delta K$ ), the curve rises to an asymptote where the maximum stress intensity factor,  $K_{\max}$ , in the fatigue stress cycle becomes equal to the critical stress intensity factor,  $K_c$ .

Other equations like the inverse hyperbolic relationship, derived by Jaske et al, attempt to minimise the errors found in the Paris and Forman equations, and comply with variable shapes and bending conditions <sup>[6,9]</sup>.

#### **2.1.4 Factors Affecting Fatigue**

Account must be taken of the specimen condition and external factors when assessing the fatigue properties of a material. The microstructure, affected by the conditions of manufacture of the material and part, plays an intrinsic role in how the specimen reacts to fatigue. The size and arrangement of the grains, condition of the precipitates and matrix due to their production treatment, the inherent flaws and their geometry, all indicate as to the manner in which fracture may occur, because they affect the degree of difficulty of slip <sup>[11]</sup>.

One of the key factors is the surface condition in which the roughness, surface residual stress, stress concentrations and surface treatments must be taken into account. Rough surfaces may have protruding inclusions and extrusions, machining burrs and scores, incompletely removed dimples, etc., which, when combined with tensile residual stresses or stress concentrations, have the right recipe for fracture to occur, especially under cyclic loading or corrosive conditions <sup>[3]</sup>. The geometry of the specimen, especially if it includes sharp edges or too-small radii and notches, may provide sites for fatigue cracks to initiate.

Fatigue loading conditions including the mean stress, stress amplitude and ratio, frequency and degree of random loading, will, depending on the type of material, affect fatigue characteristics.

#### **2.1.5 Designing Against Fatigue**

In early designs engineers attempted to combat fatigue by tending to over-design, hoping that the excess material would easily cope with any expected loading, resulting in heavy and expensive products, but today's economic demands and more demanding designs force the designer to seek other effective means. The minimum affordable material must be used amidst the implementation of more complex design geometries and performance requirements. Factors affecting fatigue need to be taken into account in design to minimise

their effect as well as planned preventative maintenance programmes by utilisation of effective fatigue inhibiting treatments.

There are two main approaches to design against fatigue. In the first approach the S-N properties of the material are used to determine a safe, or expected replacement, life based as a factor of fatigue life estimations. Some problems in selecting a safety factor have led to the second approach which requires damage tolerant, or fail safe, estimations so that if fatigue cracks do develop they will not be catastrophic. Designers effectively accept that they can live with these defects and allow for the operationally loaded part to survive should an element fail. They use crack propagation rates, residual strength, cumulative damage estimates, critical defect sizes based on fracture mechanics estimations, appropriate non-destructive inspection procedures, and design details, which act as crack propagation barriers <sup>[12]</sup>. Unfortunately, damage tolerant designs have not always been quite as damage tolerant in service as their proponents expected, which could lead designers to be more inclined to utilise fatigue life enhancement techniques like shot peening <sup>[13]</sup>.

## **2.2 SURFACE TREATMENTS TO SLOW DOWN FATIGUE CRACK INITIATION**

### **2.2.1 Introduction**

The mechanical treatments listed for aluminium in par 1.3, which are elaborated on below, create surface residual compressive stresses to combat crack initiation and therefore the fatigue life-reducing effects of residual and applied tensile stresses discussed in par 1.2.

### **2.2.2 Rolling**

Rolling is a form of cold-working and is also suitable for metals other than aluminium such as steels, titanium and copper alloys, although the effect is usually greater for harder steels. Cold-working is preferable when surface heat treatments result in dimensional distortion or when a high surface hardness is not required. A strongly beneficial effect of local rolling can be obtained for components with high stress concentrations.

Surface rolling can be used for cylindrical or flat parts. Cylindrical parts are revolved on a lathe while suitably contoured rollers revolving in the opposite direction are pressed against

the treated surface. For flat parts the rollers revolve as they are pressed on to the part. Rolling can produce a thick cold-worked layer with quite a smooth surface, if the radius of the roller is sufficiently large. The thickness of the layer on shafts is related to its diameter ( $d$ ), recommended to be between  $0.025d$  to  $0.15d$ .

Important applications of surface rolling include large railway axles, shafts with fillets, press-fit joints, torsional bars, bolts, parts to be subsequently chrome-plated, etc. [6].

### 2.2.3 Hammer Peening

Hammer peening may be applied by hand or air driven methods and produces a rough surface. Deep cold-working by repeated hammering can result in comparatively higher fatigue strengths. A 75mm diameter steel shaft fillet surface, for example, can receive a 48% increase in fatigue strength through hammer peening as opposed to a 24% increase by surface rolling, as compared to a surface without cold-working [6].

### 2.2.4 Shot Peening

This will be discussed in more detail in par 2.4 below. Shot peening involves bombarding the treated surface with small ideally spherically shaped metal, glass or ceramic particles projected by a high speed impeller, through an air or water medium, or compressed air. The impact causes local plastic deformation which results in some impairment of the surface smoothness, an increase in surface hardness, and the generation of considerable surface compressive residual stresses. The beneficial effect of the compressive residual stresses far outweighs the sometimes detrimental effect of the surface roughness and thereby makes for improved fatigue properties.

Shot peening produces from 10% to 50% cold-working of the original surface layer. For the application of this research, it is the percentage decrease of the original cross-sectional area of the surface layer that remains after shot peening, which causes the crystals (or particles) to become smaller. The typical thickness of the remaining shot peened layer is from 0.2 to 1mm [13].

Shot peening has proved to be effective in overcoming potential fatigue weaknesses created in, or by, grinding, electro-discharge machining (EDM), anodising, plasma spraying, welding

and weld repair, decarburization in steels, austempered ductile iron (ADE), fretting, galling, cavitation damage, pitting, crack arrest, etc. An added advantage of shot peening over other cold-working procedures is that it may be applied to a greater variety of shaped parts, for external and internal applications <sup>[14]</sup>.

Another important application of shot peening is peen forming, which is especially useful for forming parts too large for conventional machinery, e.g. aircraft wing skins.

### 2.2.5 Laser Peening

Laser peening is entertained by the shot peening community as “shot peening without the shot” because of similar characteristic effects.

Laser (shock) peening was developed in the 1970's and has now moved from a laboratory curiosity to a more affordable, although not yet cheap, process for industry. The process could be considered to be in its infancy by industry because of its recently approaching viability and refinement. It cannot be viewed as a cold-working process (only 1% to 2%) because only single or a few deformation cycles are required.

High energy density lasers (100 to 300 J/cm<sup>2</sup>) with pulse lengths of tens of nanoseconds (about 30 ns) are used to strike (e.g. black painted) metal surfaces producing high pressure plasma bursts resulting in impulsive shock waves inertially confined by (e.g. water layer) above-surface tamping, resulting in the shock waves propagating downwards into the metal interior to form plastic deformation beneath surface residual compressive stresses suitable for fatigue life enhancement. A thin surface layer of black paint provides an excellent absorber of the light for the plasma bursts to take place while water tamping effectively contains the shock so that the wave propagates back into the material.

There are various advantages of this method. One is that it has deep compressive stress depth capabilities, greater than 1 mm, which are useful, for example, in preventing foreign damage (FOD) caused by sucked-in debris, and crack initiation to turbine blades.

Laser peening has been shown to be superior for strengthening new and previously damaged fan blades against fatigue failure. Another advantage is that the minimal cold working on the surface exhibits a striking resistance to thermal relaxation at low and reasonably high temperatures (425 °C in Ti6Al4V and Inconel 718). Yet another is the improvement over shot peening of stress corrosion cracking (SCC) of type 304 stainless steel.

The disadvantages have been inhibiting factors to industry. The major disadvantage has been the slowness of the operation and the general unavailability of sufficiently powerful laser systems. A recent US government contract for a laser to illuminate passing satellites led to the latest development of solid state laser technology, employing Nd (Neodymium) doped glass gain media and phase conjugation with an output of 100 J at 10 Hz, which has overcome most debilitating problems. The new increased repetition rate capabilities created thermal loading difficulties causing cracking of the glass which was overcome by a somewhat ingenious technique of zigzagging the laser beam through the glass and phase conjunction control, which led to better beam resolution and heat distribution gradients, allowing for more effective heat removal.

The overall acceptance of this technique in industry has not yet been established. No evidence could be found by the author on the extent of its effectiveness with Aluminium Alloys, although there is no denial of its possible usefulness. This process could become a serious contender to conventional fatigue life enhancement techniques if the remaining inhibiting factors could be effectively overcome, opening the door to some serious research possibilities <sup>[13]</sup>.

### **2.2.6 Other Varieties of Peening**

Other techniques are high pressure water peening, rotary flap process and a rather interesting gas detonation process utilising controlled explosions of propane-butane with oxygen to propel powdered materials between 600-1200 m/s so that they imbed about 0.2 mm into the metal creating a residual compressive stress <sup>[13]</sup>.

### **2.2.7 Summary**

The mechanical and laser methods of fatigue strengthening mentioned above all have their particular applications and limitations which must be taken into consideration when deciding optimum utilisation. Cold-working may be applied to most metals, even enhancing other required treatments (e.g. anodising), while laser peening is still establishing a name for itself.

It is in the treatment of non-ferrous metals, especially aluminium alloys as in the case of this research, that shot peening has shown few equals and can be regarded as one of the most valuable surface treatments to combat metal fatigue.

### 2.3 PHYSICAL CHARACTERISTICS OF 7075–T6 ALUMINIUM ALLOY

Table 1 Physical characteristics of 7075-T6 aluminium alloy. Excerpt from Appendix B

Properties	Value
Chemical Composition	Percentage Mass: Al 89.65, Zn 5.6, Mg 2.4, Cu 1.72, Cr 0.25, Fe 0.21, Si 0.13, Mn 0.03, Ti 0.01
Heat Treatment	470 °C, water cooled to 120 °C, 24 hours air cooled
Density	2.8 gm/cm <sup>3</sup>
Hardness, HV	175
Ultimate Tensile Strength	572 MPa, 644 MPa (Databook) <sup>[15]</sup> , 612 MPa (specimens)
Tensile Yield Strength (0.2 % Proof Stress)	503 MPa, 604 MPa (Databook), 560 MPa (specimens)
Elongation at Break	11 % (indicating ductility, see par 3.2.1.4)

### 2.4 SHOT PEENING

#### 2.4.1 Introduction

The purpose of shot peening in improving fatigue strength and fatigue life is fairly simple, as outlined above, and is well documented in many applications. The key to the role which the shot peening process plays in fatigue life, surface finish, stress corrosion and corrosion fatigue, is the manner in which shots interact with the target surface to engender post impact residual stresses as well as metallurgical changes. The explanations of how and what happens to the surface layer are mainly given in terms of plastic deformation caused by the impact of the shot, a physical analysis of the fractured parts, stress distribution, crack initiation and propagation, and cyclic loading, but much caution is displayed when explaining microstructural effects.

There are good reasons for this explanatory shortfall. One is that metals are not transparent and that there is no complete visual inspection available at the moment to observe microstructural behaviour during dynamic testing, leaving the researcher with the sense of almost shooting in the dark, or analysing the aftermath. Another is that target materials respond to multiple impact of shots in a complex manner. Researchers are therefore forced to impose certain physical conditions on tested specimens to elicit symptomatic responses for analysis to find out what is going on microstructurally. This difficult task has stimulated qualitative as well as quantitative explanations of metal fatigue with associated mechanistic models that have almost exclusively followed partly or fully empirical routes employing “best fit” formulae via some elegant techniques.

Paris and Forman, amongst others, have offered foundations for operational applications, but even they have imprecisions that need to be known, creating one of the practical pathways for researchers to investigate. One major difficulty for the researcher is to have an appreciation for the number of variables and complexities, and then judiciously deciding which ones are expedient to retain or affordable to exclude. The price paid is that symptoms may arise that mask the physical properties important to analysis.

#### **2.4.2 Types and Sizes of Shot**

Shot used for peening is generally of iron or steel, although some non-ferrous and non-metallic materials (e.g. ceramics) also are used. Shot is designated by numbers according to size, the number in approximate proportion to the size. For some 2xxx and 7xxx aluminium alloys S70 ( $\pm 0.2\text{mm}$ ), S230 ( $\pm 0.6\text{mm}$ ) and S550 ( $\pm 1.4\text{mm}$ ) cast steel shot applications have indicated up to a 34% increase in fatigue strength. The most popular size seems to be the S230 which is about the size of the larger grains found in the 7075-T6 microstructure. The shot, or media, should be spherical or well rounded, free from sharp edges and facets, and have a length (large diameter):width (small diameter) aspect ratio of less than 2:1.

Cast steel, or “regular”, shot, the most widely used, is made by blasting a stream of molten steel with water (atomising) that form globules which rapidly solidify into nearly spherical pellets. The pellets are screened for sizing, reheated for hardening, quenched, and tempered

to the desired hardness, somewhere between RC40 to 50. Its hardness reduces shot breakage and increases peening quality.

Cast (chilled) iron, or “hard”, shot with a hardness range of RC58 to 65 is brittle and breaks down rapidly but gives comparatively higher intensities. Cast (malleable) iron shot with a hardness range of RC20 to 35 is softer but leaves a carbon residue on the work pieces <sup>[13]</sup>. Cut wire shot is produced from chopped steel wire with its length equal to its diameter and the edges rounded off by blasting them repeatedly onto hardened plate. The initial expense is high but is justified by their durability since they rarely break, almost eliminating the problem of sharp edges, as well as having acceptable shot geometry <sup>[13]</sup>.

Glass beads are used for peening stainless steel, titanium, aluminium, and other metals that might be contaminated by iron or steel shot. They can be used in improving surface finish over and above their fatigue improving properties. They are available in small sizes, 0.05mm, which is useful for peening very small radii. Comparisons of intensities by using glass or steel shot have revealed minimal differences <sup>[13]</sup>.

Ceramic beads are made from zirconium oxide and are very hard and totally inert. They are reasonably durable but expensive and are particularly useful in applications where no foreign metal can be tolerated <sup>[13]</sup>.

### 2.4.3 Equipment

The principal components of shot peening equipment are a shot-propelling device, shot cycling arrangements and a work-handling conveyer. All portions of the equipment that are exposed to the stream of shot are enclosed, to confine the shot and permit it to be recycled. The shot is propelled by one of two methods, one with a motor driven bladed wheel rotating at high speed, and the other by a continuous stream of compressed air.

In the wheel method, the shot is propelled by a bladed wheel that employs a combination of radial and tangential forces to impart the necessary peening velocity to the shot <sup>[6]</sup>. See Figure 5. The position on the wheel from which the shot is projected is controlled to concentrate the blast in the desired direction. Wheel machines range from a single fixed wheel to multiple

wheels which may even have means of oscillation. Wheel speeds range from 600 to 4500 rpm resulting in shot velocities of 15 to 120 m/s. A typical wheel of 330mm outside diameter and 40mm wide will deliver up to 180kg of shot in an elongated pattern approximately 40mm wide  $\times$  600mm long, when the centreline of the wheel is 600mm from the work surface. Advantages of the wheel method are easy control of shot velocity, a high production capacity including wide peening areas and large quantities of small parts, and freedom from moisture problems encountered with compressed air.

The air-blast method introduces shot, either by gravity or by direct pressure (270 to 540 MPa), into a stream of compressed air directed through a nozzle onto the work piece to be peened. It is more economical for limited production quantities and can develop higher intensities with small shot sizes, permits the peening of deep holes and cavities (with a long nozzle), consumes less shot in peening small intricate parts, and has a lower initial cost <sup>[13]</sup>.

Shot recycling is made through devices that separate and remove spent (broken or undersize) shot, and add new shot. The shot separator shown in Figure 6 employs a closed air system, which maintains a constant velocity and volume of air throughout the separator and uniformly removes spent shot. Shot-adding devices automatically replenish and maintain an adequate quantity of shot in the machine at all times through a level controller in the storage hopper.

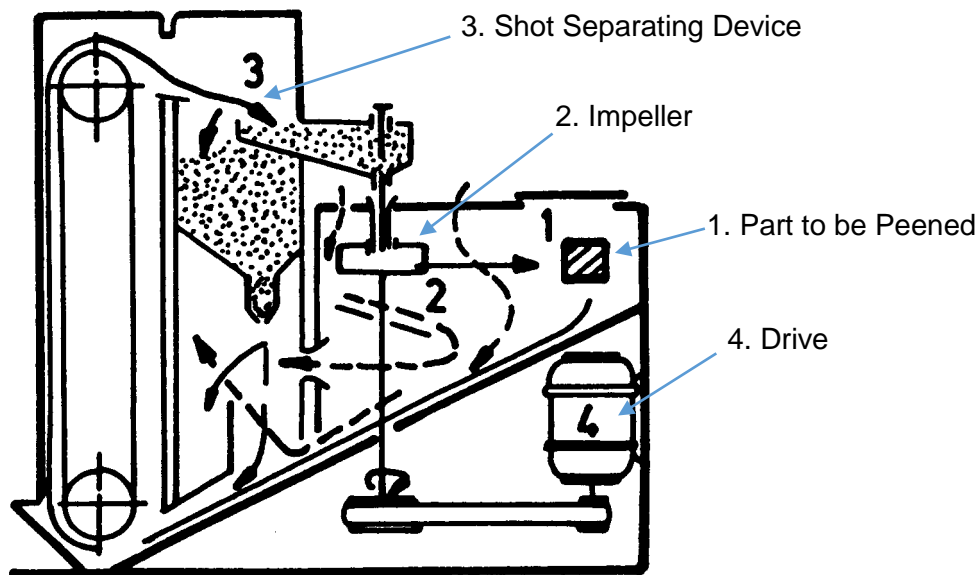
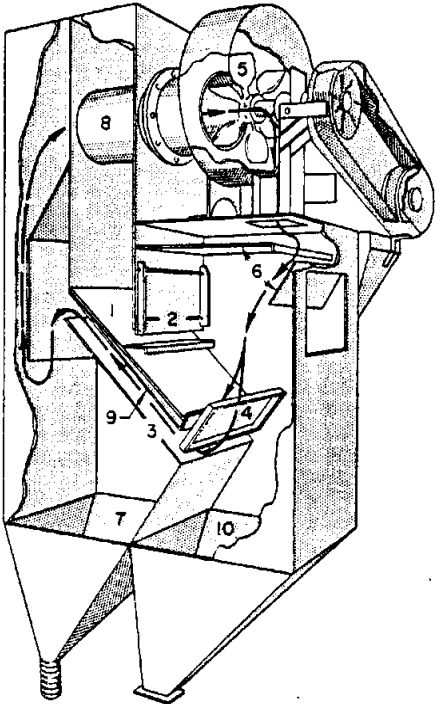


Figure 5 Schematic of shot peening machine <sup>[6]</sup>



Part No	Description
1	Inclined shed
2	Hinged winged gate
3	Outlet for spent shot
4	End baffle
5	Fan
6	Air baffles
7	Settling hopper for spent shot
8	Fan inlet
9	Adjustable baffle
10	Storage hopper for usable shot

Figure 6 Shot separator for use with a shot peening machine [16]



*Figure 7 Photo of shot peening in progress* <sup>[14]</sup>

The effectiveness of shot peening depends largely on peening intensity, and it is essential that all critical areas of a part be adequately exposed to the stream of shot. Proper exposure is facilitated by the use of efficient work handling fixtures, conveyers and mechanisms, which incorporate several basic motions for effective exposure of parts of a variety of shapes. Areas on the parts that do not require shot peening are masked with tape or steel carbide, aluminium, or moulded rubber which also double as holding fixtures. Masking is very expensive and should only be carried out if absolutely necessary <sup>[13]</sup>.

Dry or wet peening may be performed with glass beads. Dry peening procedures are similar to those used for metal shot, but separating the broken glass shot requires special methods. Wet peening uses very fine glass particles, usually mixed in water and contained in a suitable hopper. A mixer pump maintains a mechanical suspension of glass in water, and the feed pump forces the flow of slurry through the nozzle. The movement of the slurry through the nozzle is accelerated by compressed air. The nozzles are attached to an oscillating bar that directs the flow of slurry at the work piece. After making contact with the work piece, the slurry is fed back to the hopper and then recycled. The peening pattern of the slurry is controlled by the oscillating nozzles. Air pressure is controlled at each nozzle by separate regulators. Exposure time for the peening cycle is controlled by automatic timing devices. Because of the high fracture rate of glass particles, the separation of broken glass is particularly important if peening effectiveness is to be properly maintained. Control of the shot peening process depends on systematic, periodic testing to determine intensity, coverage, and other important control factors.

#### **2.4.4 Almen Test System**

Special mention is made of the Almen test system for intensity control because it has served as the foundation measure of process effectiveness to industry and the military in spite of certain technical shortcomings. Even shot peened processes with highly technical labels, e.g. micro-processor or computer controlled systems, typically use the Almen test system as their ultimate test of process effectiveness.

Almen found that if he shot peened one side of a steel plate it curved convexly toward the peened side, due to the restoring of the bending moments from the induced compressive stresses and the resistant forces in the metal, the amount of bending proportional to the intensity of the shot peening. The Almen test system shown in Figure 8 was developed and comprises essentially of three elements: (1) standardised strips of spring steel in a range of thicknesses to measure almost all peening intensity ranges, (2) steel blocks that support the Almen strips, and (3) a modified depth gauge that is used to read the arc height (bow) in the peened Almen strip. The arc height is used as a measure of the peening intensity. The strips are said to be "saturated" when the arc height increases by 10% for double the exposure time as shown in Figure 9. The Almen arc height number can also give an indication of the depth of compression on many metals at given intensities, as shown in Figure 10.

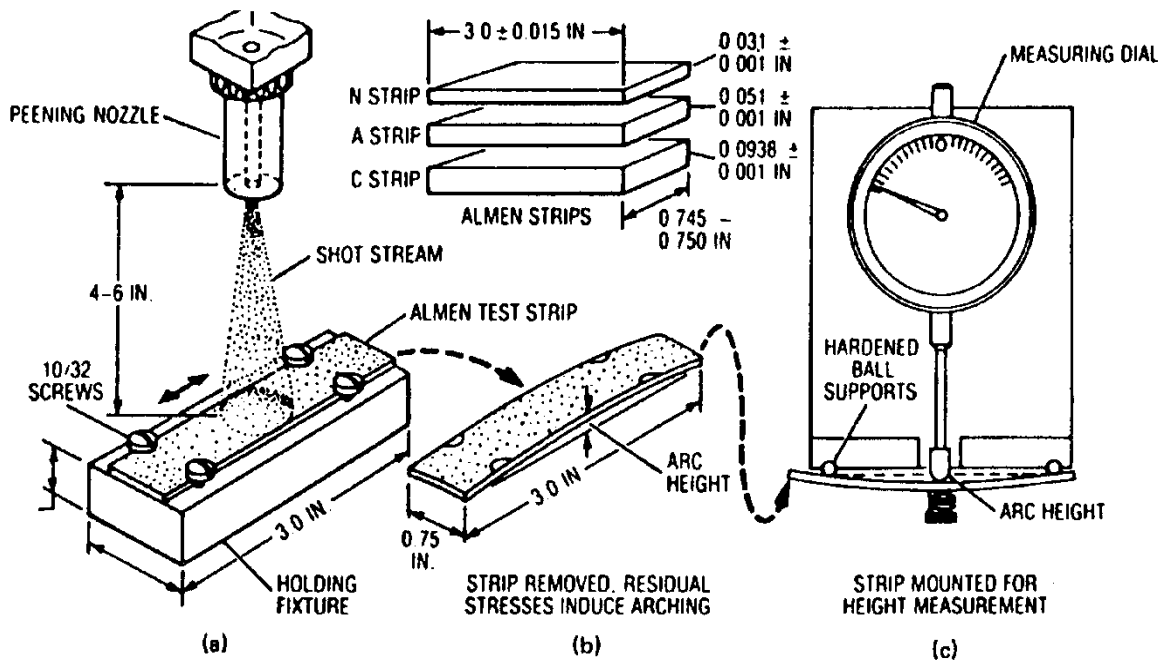


Figure 8 The Almen strip system employs standardized strips of spring steel that become curved when peened on one side only. The degree of curvature is proportional to the absorbed kinetic energy<sup>[3]</sup>

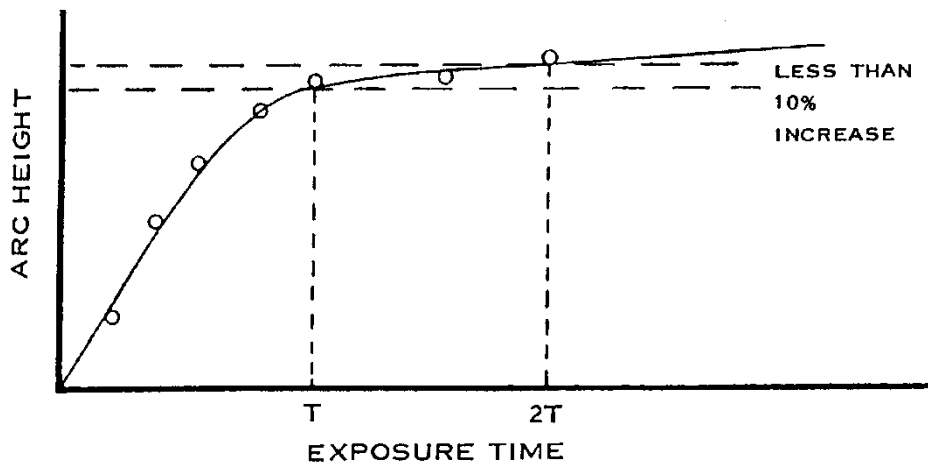


Figure 9 Saturation curve, developed by exposing individual Almen strips at increasing time increments until there is less than a 10% increase in curvature when the time is doubled. The Almen strips are said to be "saturated" at time T<sup>[3]</sup>

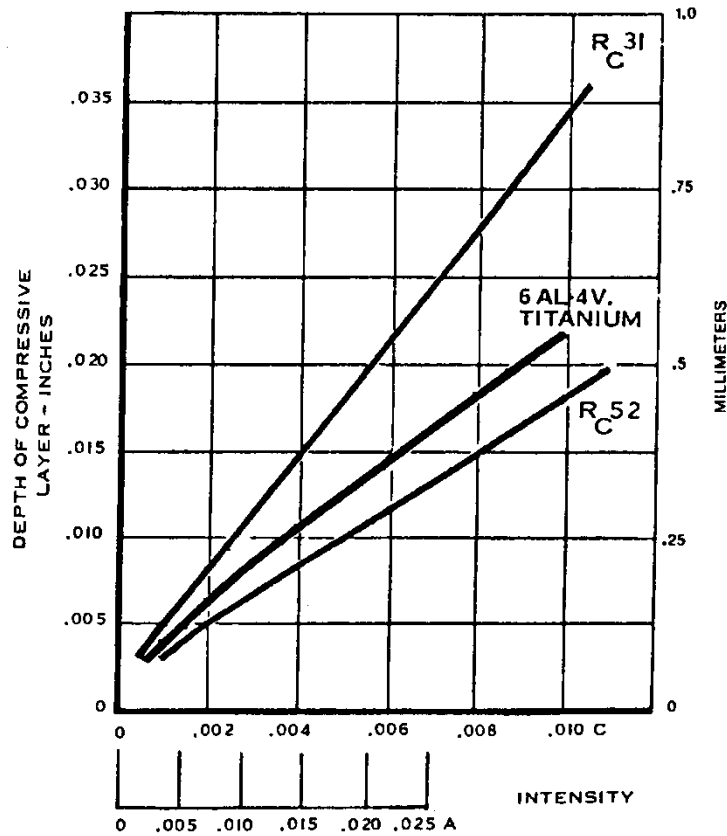


Figure 10 Depth of compression vs Almen arc height. Depth is proportional to the intensity and hardness of the material being peened [3]

The Almen scale shown above is rated in thousandths of an inch (0.0254mm). An Almen intensity, for example, of 12-16 A implies an arc height between 0.012 and 0.016 inches (0.3048 and 0.4064mm), although it is becoming more common to express the height in millimetres. Current research illustrated by Waterhouse [3] introduces the Almen number and the curvature, K, for small heights, where

$$K = \frac{8 \times \text{Almen Number}}{d^2} \tag{Equation 2.5}$$

and d is the distance over which the arc height is measured, usually 1.25 inches (31.75mm). Since the strip is able to deform, the sum of the bending moments must be zero. See Figure 11. Waterhouse refers to analysis where the bending moment is given by:

$$M = \int_{z_2}^{z_1} \sigma_{rr}(z^*) \cdot \left[ z - \left( \frac{t}{2} \right) \right] dz \tag{Equation 2.6}$$

where:  $\sigma_{rr}$  = surface stress  
 $t$  = thickness of the strip  
 $z$  = depth below the surface

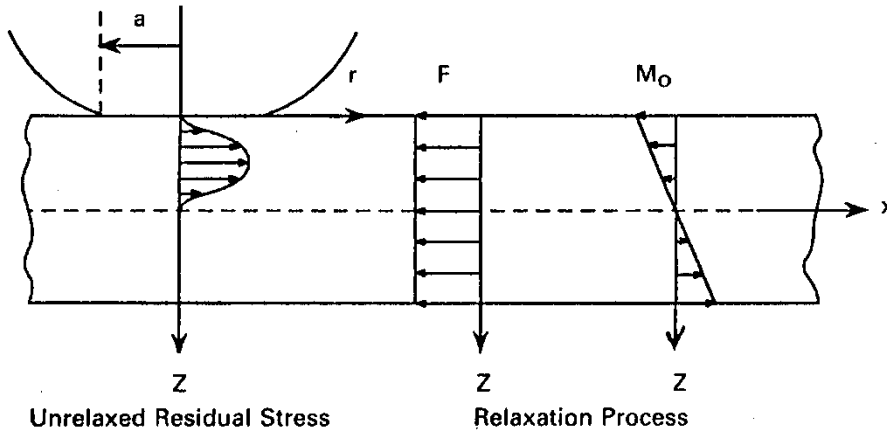


Figure 11 Geometry of residual stress fields due to direct and bending type relaxation [3]

The curvature is related to the bending moment by:

$$K = \frac{12M_o(1-\nu^2)}{Et^3} \quad \text{Equation 2.7}$$

where:  $\nu$  = Poisson's ratio

$E$  = Young's modulus

Integrating equation (2.6) and combining the results with equation (2.7) yields:

$$K = \frac{(5.966c - 5.53)k}{Ec^3a} \quad \text{Equation 2.8}$$

where  $c$  is the normalised Almen strip thickness  $t/a$ . Figure 12 is a plot of this equation for different values of  $c$  and indicates the curvature to be expected for various contact sizes. The graph may be used to determine the curvature which must be achieved to realise the maximum compressive residual stress under conditions of full coverage. This curvature can be converted to the appropriate Almen number using equation 2.5. The quantity that needs to be known is  $a$ , the radius of the impression created by a single impact. Since this is related to the diameter of the shot, some fraction of this value may be used. Alternatively the characteristic diameter of the dimples on the peened surface could provide the required information [3]

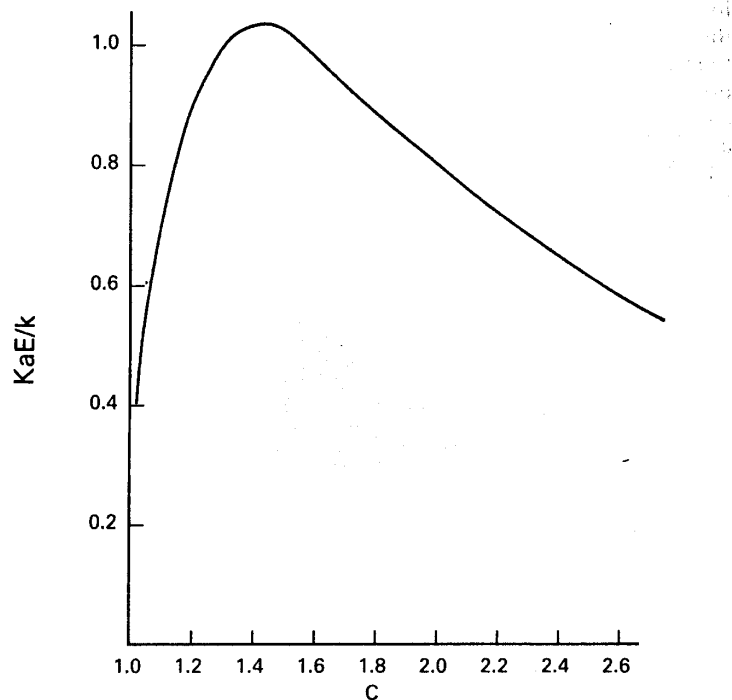


Figure 12 Expected curvature of Almen test strip for full coverage shot peening vs normalised Almen strip thickness <sup>[3]</sup>

#### 2.4.5 Control of Process Variables

Major variables in the shot peening process are shot size and hardness, shot velocity, peening intensity, surface coverage, angle of impingement, and shot breakdown. The quality and effectiveness of peening depend on the control of each of these independent variables. An increase in **shot size** will tend to increase the peening intensity and decrease coverage. Common practice is to select the minimum shot size capable of producing the required intensity in order to take advantage of the more rapid rate of coverage obtained with smaller shot. The selection of a particular shot size may be dictated by the configuration of the part to be peened.

In peening aluminium, a larger shot size than that required to achieve the desired intensity may be used to enhance surface appearance and to increase depth of penetration. When a surface appearance is required, the minimum shot size must be specified. Peening effect, at the same intensity, increases with shot size for aluminium Almen Intensity.

Variations in **hardness** of shot do not affect peening intensity, provided the shot is harder than the work piece.

**Peening intensity** increases with the velocity of shot, but an increase in the velocity will be offset by an increase in shot breakdown. Peening intensity is governed by the velocity, hardness, size and weight of the shot pellets and by the shot impingement angle to the work piece. Intensity is expressed as the arc height of an Almen test strip at full coverage, as shown in par. 2.4.4. The lowest peening intensity capable of producing the desired effect is deemed as the most efficient and economical, because of minimum shot size and exposure time. If the intensity is excessive the compressive stresses at the surface induce tensile stresses at the core that are too high, especially with thin parts.

The depth of the compressive stress layer from peening affects the choice of peening intensity where, for example, a compressive stress layer is required underneath a decarburised layer.

**Surface coverage** is a measure of how completely an area has been hit by the shot particles and may be defined as the ratio of the dimpled surface to the total surface. The SAE J443 quantitative relationship between surface coverage and exposure time is:

$$C_n = 1 - (1 - C_1)^n$$

where  $C_n$  = % coverage (expressed as a decimal) after  $n$  cycles. This formula has a limit approaching 100%, but since 98% is the practically measurable limit of accuracy it has become the arbitrary unit of full coverage. Higher coverages are given as multiples of the 98% coverage value.

Coverage is measured directly by visual and the Straub methods, and indirectly by the Valentine and residual stress measurement (e.g. X-ray diffraction) methods. Visual methods are usually used and include comparison of the surface with reference replicas with or without the aid of optical magnification, and comparing a transparent plastic replica photographic projection of the peened surface with reference replicas. The Metal Improvement Company has developed the Peenscan system which employs a tracer liquid that is painted, sprayed or dipped onto the part. After drying, the part is shot peened, and examined under UV light to reveal any unpeened areas. In softer materials, like aluminium, traces of Peenscan may still be seen uniformly distributed over the surface even when there is full coverage. In rotating bending tests on 7075 aluminium alloy 45% to 100% ranges of coverage gave fatigue life increases of 50% to over 150% respectively [3].

The **angle of impingement** between the shot blast stream and the surface of the work piece is normally 90° but if it is reduced the peening intensity also reduces. When small angles are unavoidable the shot size and velocity may have to be increased to improve the intensity.

The **shot breakdown** is controlled by a separator which must ensure that the quantity of full-size shot never falls below 85% (preferably higher) for consistent intensity to be maintained [3].

Computer monitored shot peening machines have the ability to monitor, control and document parameters critical to the verification of the shot peening process and are in frequent use today [3,14].

#### 2.4.6 Applications

The major application is to improve fatigue characteristics, but there are other important applications, mentioned in par 2.2.4, which will be treated in more detail here.

Residual tensile stresses and surface brittleness can be caused by the generation of high surface temperatures during severe **grinding** operations. These residual tensile stresses can approach the ultimate tensile stress and dramatically reduce the fatigue or corrosion stress resistance of the material. Shot peening after grinding can overcome the detrimental effect of these residual stresses as shown in Figure 13, where the fatigue life at a reversed bending stress amplitude of 100000 psi (689.5 MPa) after severe grinding plus shot peening is about 130 % higher than that with severe grinding only.

There are, however, new gentle grinding techniques using cubic boron nitride (CBN) grinding wheels that develop shallow layers of residual compressive stresses, which can be enhanced by the controlled shot peening process [14].

In electro discharge machining (EDM) not all the molten metal produced during discharge is expelled into the working gap. That which remains resolidifies to form a hard and brittle skin on the work surface. Accompanying thermal stresses, plastic deformation and shrinkage induce residual tensile stresses in the work piece which, under certain conditions, have been found to approach the ultimate tensile strength of the material near the surface. Shot peening over the hard surface can be very beneficial in restoring the fatigue strength [3,14].

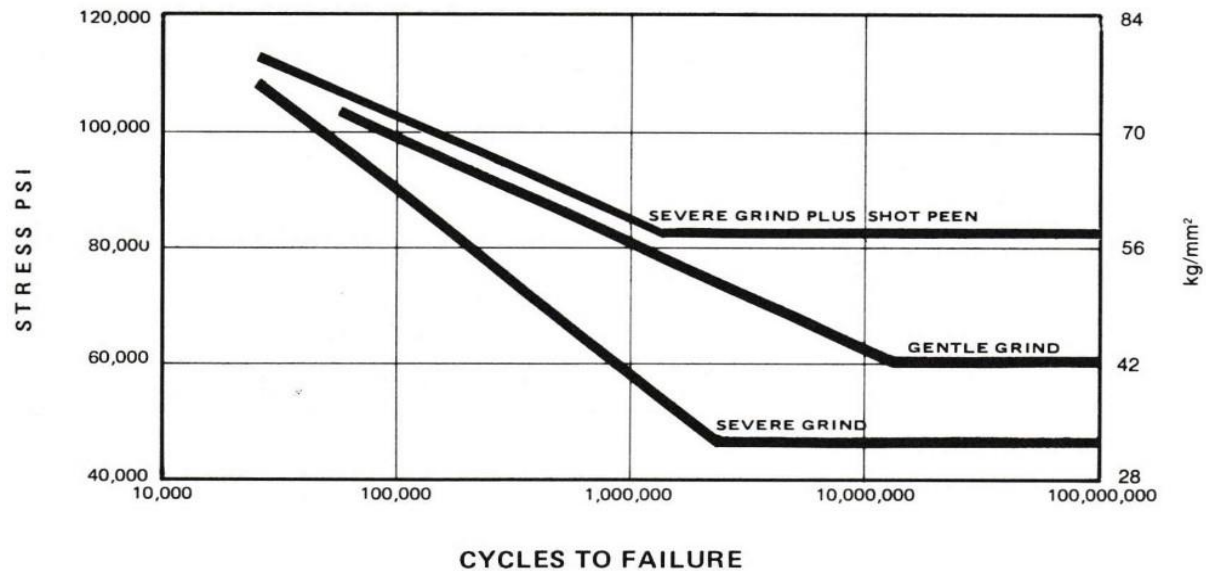


Figure 13 Reversed bending fatigue of flat bars of varying Rockwell hardness showing improved fatigue limit C45<sup>[14]</sup>

**Anodising and plasma spray** coatings tend to reduce fatigue resistance which will be improved if shot peened prior to these operations. Peening after plasma coating improves its surface finish. Waterhouse showed that anodising and shot peening reduced the coefficient of fretting on aluminium surfaces consequently reducing wear<sup>[3,14]</sup>.

Heat generated by **welding** often produces tensile stresses approaching the yield strength of the material in the heat-affected zone (HAZ). These stresses can be combated by improving the weld geometry and/or inducing residual compressive stresses by shot peening. Even after fatigue cracks have started and the weld repaired, shot peening may be used to induce beneficial compressive stresses<sup>[14]</sup>.

At **high hardness** levels, high strength steel loses fatigue strength due to increased notch sensitivity which can be substantially increased through shot peening<sup>[14]</sup>.

**Decarburization** can reduce the fatigue strength of high strength steels by up to 70% and lower strength steels by 45%. It is a detrimental surface phenomenon, not necessarily related to depth, and can induce residual tensile stresses in the surface. Shot peening has proven to be effective in restoring most, if not all, of the fatigue strength lost due to decarburization. Even though the decarburised layer is softer, it is not easily detectable on quantities of parts, and peening can ensure the integrity of these parts if decarburization is suspected<sup>[14]</sup>.

**Austempered ductile iron (ADE)** is being used for crankshafts, camshafts, gears and railroad wheels. Shot peening has shown to improve the fatigue strength substantially as well as increasing the surface hardness to improve wear resistance <sup>[14]</sup>

**Fretting** can develop when the relative motion of microscopic amplitude occurs between two metal surfaces. As the surfaces rub, fine abrasive oxides form, which contribute to the scoring of the surfaces. The fatigue strength reduces because of the damage caused by fretting. Shot peening increases the surface hardening and provides a residual compressive stress at the fretting surfaces. The minute indentations caused by shot peening act as small oil reservoirs and assist in lubrication retention. O'Hara refers to tests conducted on 2014 aluminium alloy, that after shot peening, the plain fatigue strength increased by 70% and the fretting fatigue strength increased by 300% <sup>[3]</sup>. For maintenance of fretting fatigue strength care must be taken not to remove surface indentations. Further tests revealed that, after removing the surface indentations to a fine finish, the plain fatigue strength increased but the fretting fatigue reduced <sup>[3,14]</sup>.

**Galling** is caused by strong adhesive forces whenever an imbalance of electrons exists between two mating metal surfaces. At low stresses, minute junctions form at contacting surfaces and small fragments of metal become detached when subsequent relative movement occurs. At higher stresses, however, much larger junctions are formed and actual seizure may occur, stalling the equipment or "freezing" the action of the part. The cold worked densified surface, generally obtained through shot peening makes the material more resistant to galling and the residual compressive stress retards crack growth and pit formation if a limited amount of galling occurs <sup>[14]</sup>.

**Cavitation damage** is the result of high relative motion between a metal and a liquid. If the pressure accompanying a high velocity motion drops to the vapour pressure, the liquid will vaporise and form a vapour cavity at the metal surface. At a slight increase in pressure, this bubble will collapse, causing a concentrated liquid impact resulting in erosion and pitting of the metal surface. Once initiated, the cavitation damage becomes progressive and cumulative. Shot peening, especially after work hardening, has been shown to reduce cavitation damage <sup>[14]</sup>.

**Pitting** is caused by oil (or some other liquid) being trapped in a surface microcrack by two metal surfaces in motion being pressed together (e.g. two rollers). The high pressure of the trapped oil in the crack generates high tensile stresses at the crack root, causing crack propagation and eventual pitting. The residual compressive stresses through shot peening

assists in preventing the initiation and propagation of the cracks required for pitting to take place <sup>[14]</sup>.

**Crack arrest** at the surface layer is performed when the residual compressive stress through shot peening is sufficient to overcome the tensile stress at the crack tip and prevent re-initiation and propagation of the crack. The crack would have to be shallow enough so that it is within the range of the shot peening effects <sup>[14]</sup>.

**Stress corrosion cracking** (SCC) is a progressive fracture mechanism in metals that is caused by the simultaneous interaction of a corrodent and a sustained tensile stress. Structural failure is often sudden and unpredictable and is frequently encountered in the absence of any other obvious kind of corrosive attack. Shot peening creates a surface residual compressive stress can be an effective measure for preventing SCC, regardless of the dominant SCC mechanism, the material, or corrosive environment <sup>[14]</sup>.

**Search peening** has been developed to meet the stringent mandatory requirements for corrosion control in inspection programmes for ageing civil aircraft, and is particularly useful in exposing latent corrosion. The surface to be tested is blasted to clean the surface and then control shot peened causing the surface layers to stretch and separate along weakened corrosion paths beneath the surface. Visible blistering and flaking at the surface shows up the hidden corrosion. The surface is dressed and the process repeated until no further blistering occurs. On completion the surface is shot peened to re-induce surface residual stresses for service. One major advantage of this method is that the part to be treated need not be removed from its structure unnecessarily <sup>[3]</sup>.

Another important (and possibly viewed as somewhat glamorous) application of shot peening is that of **peen forming** or shaping in, for example, aluminium alloy sheet used for the skin of aircraft wings. The residual compressive stress created by controlled shot peening on one side of the sheet causes the material to develop a compound, convex curvature to the desired shape. This process is ideal for forming large panel shapes where the bend radii are reasonably large without abrupt changes in contour, and within the metal's elastic range <sup>[3]</sup>. Marsh, quoting others, states that in fully machined panels with considerable variation of thickness for various built-in features, shot peen forming is the *only* method of manufacture possible, to create the severe double curvatures often required for efficient structures <sup>[3]</sup>.

### 2.4.7 Geometry

Sharp corners are sites of high stress concentrations and certainly points of crack initiation. They cannot be successfully peened due to the inability of round shot to reach them. Most specifications require that the shot diameter be no more than half the radius of the fillet. Although a large fillet radius is preferable, it should not be less than about 0.4mm for steel shot and 0.1mm for glass beads.

Outside corners can be severe stress concentration locations. Peening will roll over a sharp outside corner creating a burr, which may be unpeened and invite crack initiation. Burring from peening may also cause holes or slots to close up.

For peening to be successful, the depth of the layer of compression must extend beneath the deepest surface discontinuity.

Parts to be peened generally should not be thinner than 2.5 mm because of possible distortion <sup>[3]</sup>.

### 2.4.8 Limitations

Shot peening has few practical limitations in terms of the materials or of the size, shape, quantity, surface condition, and surface hardness of parts that can be peened. It is not so much the mechanical process that limits the effect of shot peening as an appreciation of the control of process variables, the size and shape of the work piece, surface conditions, and temperature limitations <sup>[16]</sup>.

### 2.4.9 Process After Peening

Since shot peening may be regarded as a finishing treatment, usually no further processing of peened work is required, except to prevent corrosion. Temperatures high enough to relieve the beneficial effects of peening should be avoided. If the peening depth is large enough, e.g. in aluminium, light grinding or machining may be applied without significant harm, but there should be knowledge of stress gradients beforehand <sup>[16]</sup>.

### 2.4.10 Summary

Shot peening has been applied with remarkable success and versatility over many years. Through careful management of the requirements mentioned above for effective shot peening, engineers have been provided with a very important technique to combat fatigue which is one of the most debilitating problems to overcome. A variety of shapes of parts and specifications required by engineers can be processed by computer controlled shot peening machines, which combine full control with maximum versatility, are being utilised by service providers.

## 2.5 RESIDUAL STRESSES INDUCED BY SHOT PEENING

### 2.5.1 Distribution of Residual Stresses

Surface residual tensile stress, through machining etc., is undesirable and can be superseded by a residual compressive stress imparted by shot peening, as shown in Figure 14. The effect of shot peening on the stress distribution with an applied load is shown in Figure 15 <sup>[3]</sup>.

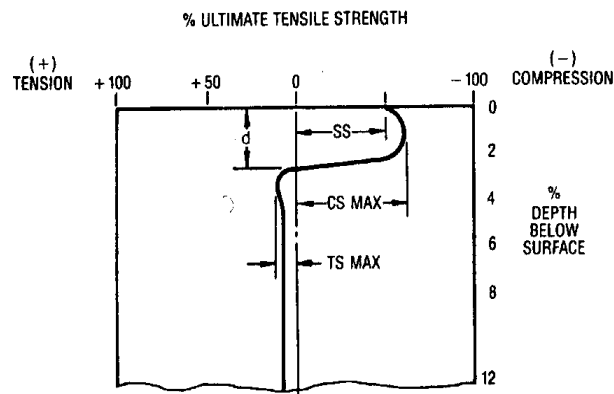


Figure 14 Example of residual compressive stress profile imparted by shot peening <sup>[3,14]</sup>

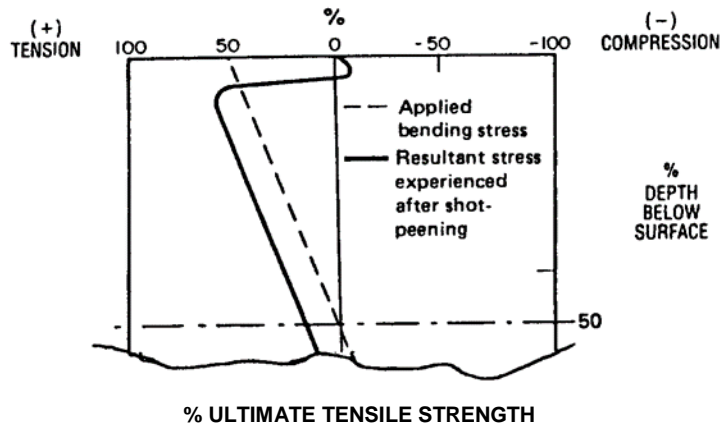
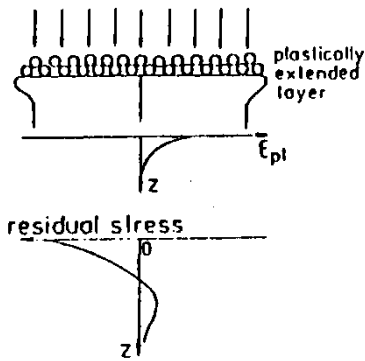


Figure 15 Combined residual and applied bending loading <sup>[3]</sup>

Shot peening produces residual compressive stresses with a maximum magnitude almost at the surface for soft metals and a little deeper for harder metals. According to Wohlfahrt both these types of stress distributions may be conceptualised by two different processes of localised plastic deformation and consequently residual stress generation <sup>[17]</sup>.

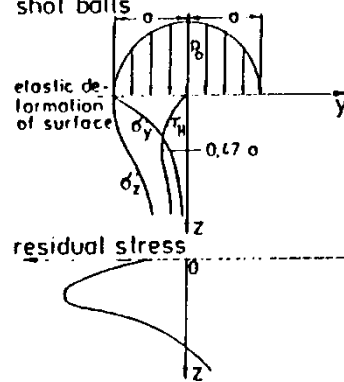
The first process is the direct plastic elongation of layers very close to the surface as a consequence of tangential forces due to numerous shot indentations, comparable to surface hammering, indicated by an increase of surface roughness and/or surface hardness. The elastic-plastic elongation of the surface layer results in residual compressive stresses at maximum magnitude at, or very near, the surface, shown in Figure 16 on the left, as a predominant effect <sup>[17]</sup>. Surface residual stresses are functions of the degree of plastic deformation of surface layers which may be approximately indicated by the surface roughness, if the surface roughness before peening is sufficiently small. Soft material will have a relatively high surface roughness after peening indicating that plastic deformation of surface layers should be the predominant process, especially with harder shot.

Stretching of a surface layer as a consequence of "surface hammering"



effect is marked with a hard shot and a soft workpiece

Hertzian pressure as a consequence of the vertical forces connected with the impact of shot balls



effect is possible with a soft shot and a hard workpiece

Figure 16 1st process on the left shows elastic-plastic elongation of surface layer with max residual stress at or near surface. The 2nd process on the right shows the maximum resultant shear stress at 0.47a below surface [17]

The second process can be Hertzian pressure due to the vertical force per ball (F). Hertz's theory analyses normal stresses induced below the surface on which a ball is pressed statically. As shown in Figure 16 on the right, the resulting shear stress has a maximum at a distinct distance,  $z_{\Gamma, \max}$ , below the surface, such that

$$z_{\Gamma, \max} = 0.47a \tag{Equation 2.9}$$

where "a" is the half-width of the contact zone.

Hertzian theory shows the following relations: -

$$p_o = \frac{3}{2} \times \text{mean contact pressure} = \frac{3}{2\pi} \cdot \frac{F}{a^2} \tag{Equation 2.10}$$

$$\tau_{\max} = 0.31 \cdot \frac{3}{2\pi} \cdot \frac{F}{a^2} \tag{Equation 2.11}$$

Where:  $p_o$  = Hertzian pressure

$\tau_{\max}$  = maximum shear stress

F = vertical pressure force

a = half width of the contact zone

If the Hertzian pressure becomes high enough, the maximum shear stress will exceed the flow stress at a depth of  $0.47a$  and the resulting plastic elongation will generate residual compressive stresses at that depth. The yielding occurs at this point when

$$\frac{P_o}{\text{yieldpoint in pure shear}} = 2.77.$$

As the load is increased a plastic region develops, initially surrounded by elastic material, but finally the material becomes fully plastic. If the ball is indented on the same spot several times, work hardening occurs and residual stresses are developed leading to a steady state

situation called the “shakedown limit” when  $\frac{P_o}{\text{yieldpoint in pure shear}} = 5.54.$

The degree of deformation at the maximum shear stress depth determines the magnitude of maximum residual stress.

It is assumed that the depth of the contact zone,  $h$ , is nearly equal to the measured surface roughness. The following equation could be used to find  $a$ :

$$a = \sqrt{2hr - h^2}$$

**Equation 2.12**

where:  $r$  = radius of the shot

$h$  = depth of the contact zone

Hertz equations are valid for hard materials, especially at low velocities, where plastic deformation of the surface and dynamic effects are not too predominant.

In materials of low hardness ( $HB \leq 285$ , 7075-T6 = 150HB), much of the kinetic energy of the shot is used for direct plastic deformation of the surface layers, and this will be the dominating process. The shot imprints have a relatively large depth and width resulting in low Hertz pressure.

If low shot energies, excluding very small shot, are used possibly all the kinetic energy is consumed for plastic deformation of the surface layers. The maximum surface residual stress may be analysed, depending on the variation of  $F$  and  $a$ , and the strain hardening characteristics. If the shot energy is limited to the steeper part of the stress-strain curve, where strain hardening exists, then the enlargement of the contact zone may remain relatively small. With increasing shot energy  $F$  may increase by more than  $a^2$ . According to

equations 2.10 and 2.11 the maximum shear stress may be raised sufficiently to produce a maximum residual stress below the surface. Shot peening of soft materials with markedly harder shot can result in a maximum residual stress at the surface if low shot energies are applied, and below the surface using medium shot energies. A smaller diameter shot favours the Hertzian pressure effect where the maximum residual stress is below the surface [3,17].

Al-Hassani shows how the residual stress field under each impact interacts with similarly produced neighbouring fields to finally produce a residual stress distribution varying in depth but uniform in planes, parallel to the surface. It is considered that the shot is rigid, impinging upon a rigid perfectly elastic target. This assists in predicting the depth of the dent produced in the target surface and then to estimate the plastic zone,  $h_p$ . Once  $h_p$  is predicted, it is then possible to predict the residual stress distribution in shot peened metal [18].

The equation of motion of the spherical shot normally impinging on the target surface is: -

$$\text{mass}_{\text{shot}} \times \text{acceleration}_{\text{shot}} = \text{area}_{\text{contact circle}} \times \text{pressure}_{\text{average}} \quad \text{Equation 2.13}$$

$$\frac{4\pi}{3} \rho R^3 \frac{dv}{dt} = -\pi a^2 \bar{p} \quad \text{Equation 2.14}$$

where:  $\rho$  = density

$R$  = radius of shot

$v$  = velocity of shot

$a$  = radius of the contact circle

$\bar{p}$  = average pressure resisting motion, given by: -

$$\frac{\bar{p}}{Y} = 0.6 + \frac{2}{3} \ln\left(\frac{Ea}{YR}\right) \quad \text{Equation 2.15}$$

where:  $Y$  = yield strength of the target

$E$  = Young's modulus of the target

The non-dimensional "deformation parameter",  $\frac{Ea}{YR}$ , effectively represents the ratio of the

imposed strain,  $\frac{a}{R}$ , to the capacity of the material to sustain elastic strain,  $\frac{Y}{E}$ . The elastic

limit is reached when  $\bar{p} = 1.07Y$  and yields at  $\frac{Ea}{YR} = 2$ . The fully plastic state is reached when

$\bar{p} = 3Y$ , yielding at  $\frac{Ea}{YR} = 36.6$ , comparing well with experimental values. For  $\frac{Ea}{YR} > 40$ , equation 2.15 will not apply and rigid plastic theory will be more appropriate. By substituting equation 2.15 into 2.14 and integrating, using  $\frac{dv}{dt} = v \frac{dv}{dz}$  gives:-

$$\frac{\bar{z}}{R} = \left(\frac{2}{3}\right)^{\frac{1}{2}} \left(\frac{\rho v_o^2}{\bar{p}}\right)^{\frac{1}{2}} Q \quad \text{Equation 2.16}$$

where:  $v_o$  = initial impact velocity

$\bar{z}$  = final indentation

$Q$  = a function of  $E$  and  $Y$

If  $\bar{p}$  is held constant during indentation the solution to (3.3.1.7) is:

$$\frac{\bar{z}}{R} = \left(\frac{2}{3}\right)^{\frac{1}{2}} \left(\frac{\rho v_o^2}{\bar{p}}\right)^{\frac{1}{2}} \quad \text{Equation 2.17}$$

The non-dimensional number  $\frac{\rho v_o^2}{\bar{p}}$  gives a measure of the severity of impact and is sometimes called the "Damage Number". Results from testing of aluminium, which is not as sensitive to strain rate, are close to equation 2.17. The impact generated plastic zone may be represented by:

$$\lambda = 3 \left(\frac{2}{3}\right)^{\frac{1}{4}} \frac{R}{h} \left(\frac{\rho v_o^2}{\bar{p}}\right)^{\frac{1}{4}} \quad \text{Equation 2.18}$$

where:  $\lambda = \frac{h_p}{h}$

$h$  = thickness of the target

An element at the contact surface undergoes cyclic tension-compression during each shot impact. As the point of maximum tension on the surface changes from yield in tension to plastic compression, a condition of reversed yield takes place, which may result in a sudden stress jump exceeding the yield stress. This is the Bauschinger effect. Fortunately, the reversed stress in most materials is normally less than the yield stress.

In shot peening, the far field stress due to one indenter adds to the stress below the other indenter if load application occurs simultaneously. Consequently, plasticity may be reached earlier and the plastically deformed depth may tend to be slightly shallower. However, in practice, the occurrence of impact is random and also includes multiple single as well as repeated impacts. The plastic zones below the shots join together to form an upper layer of residual compressive stress almost uniform over the active surface of the medium.

Residual stresses introduced by plastic flow due to initial impact act in a manner to inhibit plastic deformation during subsequent impacts. If the first impact were to introduce a biaxial residual stress of compression equal to the yield stress the mean pressure required in the second impact, if yield is to occur, should be doubled and the load made eightfold. If the same impact pressure were to be applied, yield will not take place in subsequent loading cycles and the surface is said to “shakedown”.

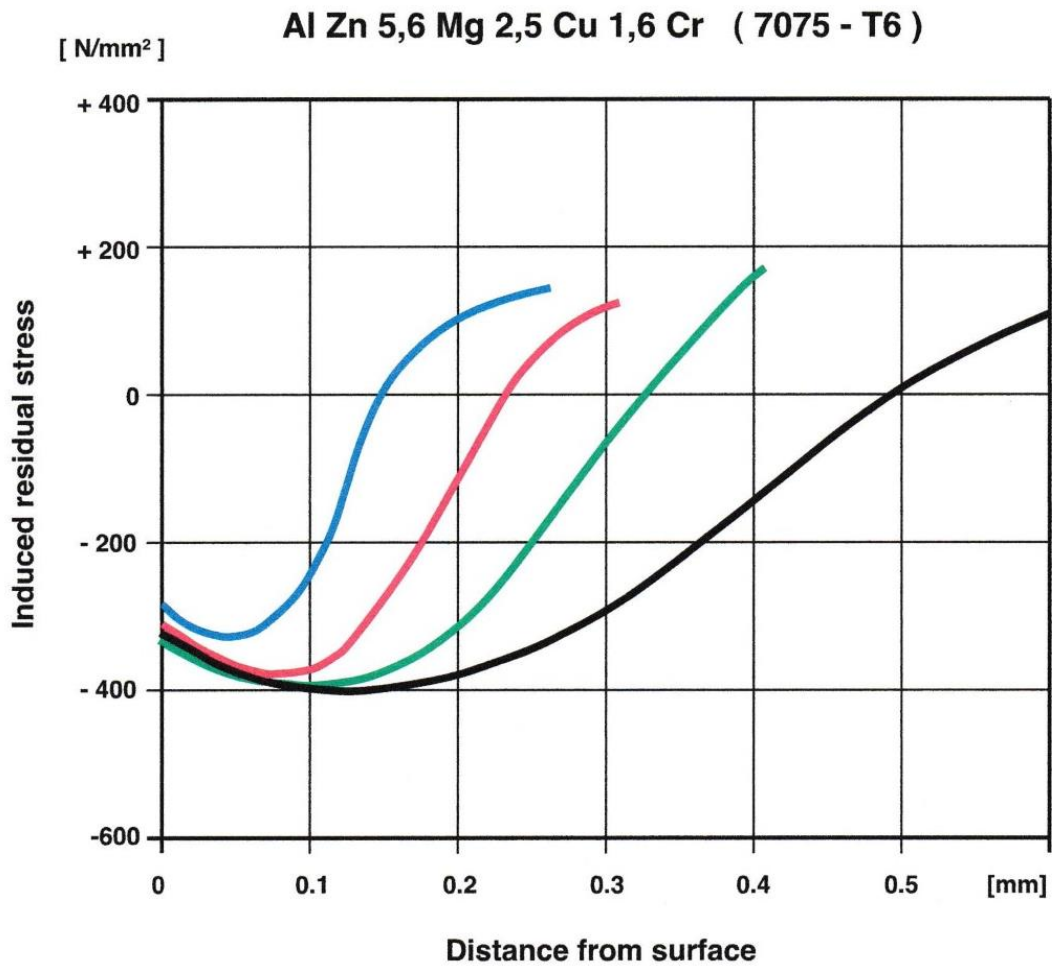
The overall residual stress in the shot peened target is the sum of all the fields caused by repeated impacts at each spot as well as progressive impacts to cover the whole surface of the target. It is beyond any theoretical analysis, according to Al-Hassini, to predict the instantaneous build-up of the residual stress distribution, but by making use of the measured patterns of residual stress in shot peened specimens, he attempts to show that the rest of the target reacts to the total sum of the residual stress distribution by exhibiting equivalent direct and bending stresses acting in a manner to balance the internal stresses. Consequently, these cause bending and axial strains which are manifested by curvature of the target towards the impinging shots. This action continues until such a time that when the arc height levels off and a state of saturation is reached. By envisaging that the bending moment and axial force are reacting to a causal stress or a “source stress”, a cosine function with some empirical combinations was derived, which predicted a residual stress distribution valid at regions below the surface agreeing with common measured residual stress distribution curves <sup>[18]</sup>.

### **2.5.2 Magnitude of Residual Stresses**

Variations in the shot peening process have little effect on the magnitude of the compressive stress induced as long as the shot used is at least as hard as or harder than the material being peened. The magnitude of the compressive stress is primarily a function of the material itself and has a value at least half of the yield strength of that material <sup>[14]</sup>.

The 0.2% proof stress of aluminium alloy 7075-T6 is given as 604 MPa [Databook on Fatigue Strength of Metallic Materials pg. 1660-1667] so the expected residual compressive stress induced by shot peening should be  $\geq 300$  MPa but less than the yield or proof stress <sup>[19]</sup>.

Typical residual compressive stresses for S230 steel shot using an Almen intensity of approximately 20A range between 300 and 400 MPa. Tests results published by OSK showed residual compressive stresses around 380 MPa under comparative shot peening specifications undertaken here as shown in Figure 17. These values will be taken into consideration when assessing residual compressive stress test results.



Line	Intensity [mm A]	Shot size [mm Ø]	Coverage
	0.18	0.5	98 %
	0.28	0.5	98 %
	0.35	0.7	98 %
	0.90	1.2	98 %

Figure 17 Magnitude and distribution of residual stress induced by different shot peening parameters on 7075-T6 Aluminium Alloy <sup>[19]</sup>

### 2.5.3 Depth of Residual Stresses

The depth of the compressive layer is influenced by variations in peening parameters as illustrated in Figure 17. In par 2.5.1 depth is included in the Hertzian pressure and Al-Hassini discussions and need not be repeated here. The depth of compression vs. Almen arc height is demonstrated in Figure 18.

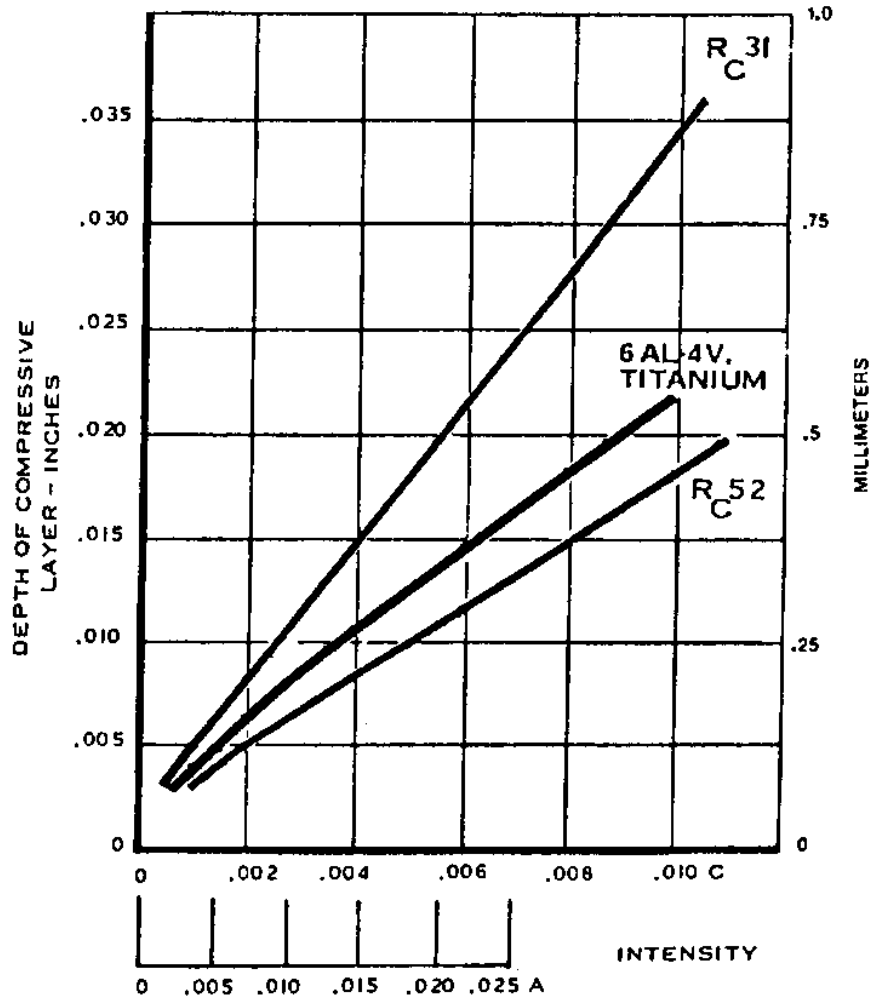
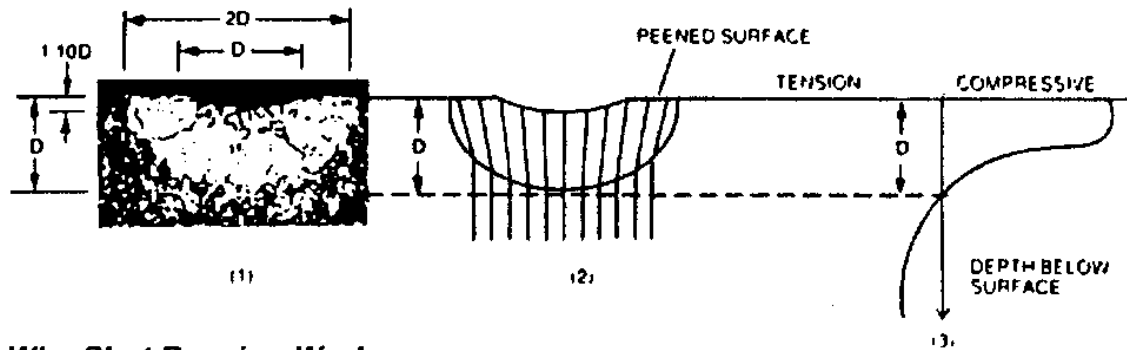


Figure 18 Depth of compression vs Almen arc height. Depth is proportional to the intensity and hardness of the material being peened <sup>[14]</sup>

Eckersley states that the impact of the pellet creates a dimple of diameter "D" and exerts a depression of about  $\frac{1}{10}D$  <sup>[3]</sup>. The surface is stretched by the impact to a depth of

approximately “D”, which is the approximate depth of the residual compressive stress shown in Figure 19. The core then exerts a compressive force in attempting to restore the surface to its original condition.



### **Why Shot Peening Works**

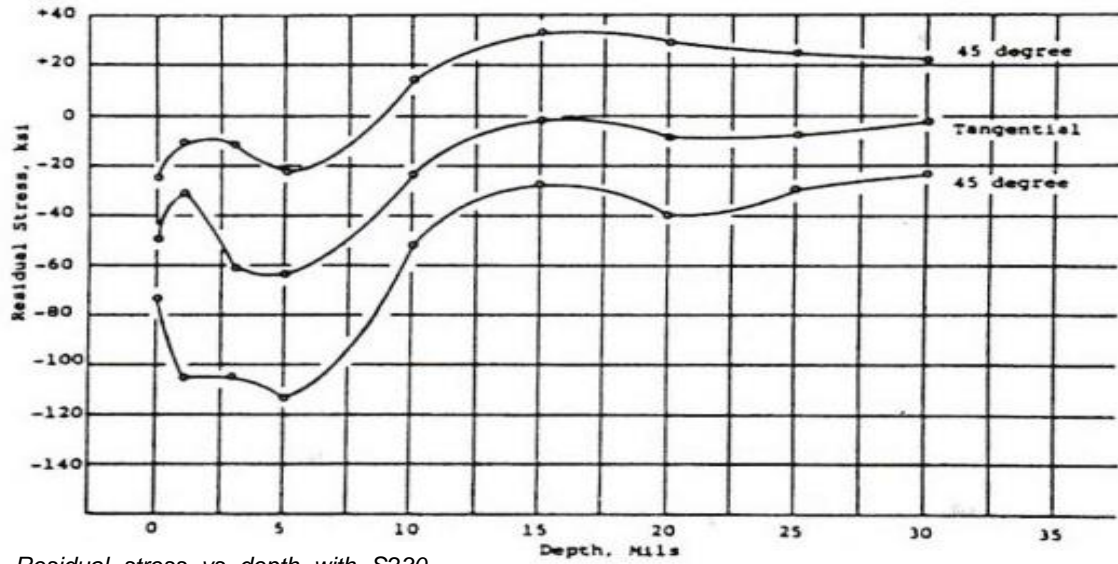
1. Impact of a high speed pellet creates a dimple of diameter “D”. The depression is about  $1/10 D$ .
2. The surface is stretched by the impact. The depth of the stretching is approximately “D”.
3. The “not stretched” core exerts a compressive force in attempting to restore the surface to its original condition.

Figure 19 Effects of shot peening dimple depression on the magnitude and distribution of residual stress <sup>[3]</sup>

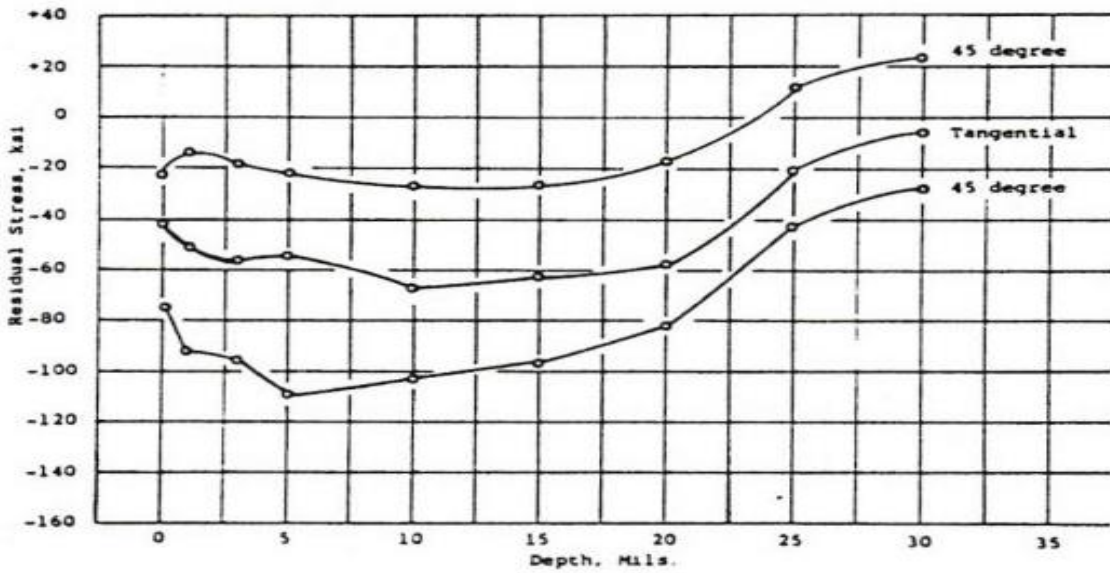
The size of shot has an effect on the depth of the residual compressive stress as shown in Figure 19 above.

It also has a different effect on the depth of the compressive layer in aluminium alloys than in other metals. An aluminium part peened to a given Almen intensity will have a deeper layer of compressive stress when peened with larger shot than smaller shot at the same intensity as shown in Figure 20.

S



Residual stress vs depth with S230



Residual stress vs depth with S660 shot

Figure 20 Residual stress vs depth using S230 and S660 shot [14]

According to Hughes applying the similar specimens, shot and intensity levels as here, the typical depth of the residual compressive stress is about 200  $\mu\text{m}$  below the surface of the metal [20].

#### 2.5.4 Relaxation of Residual Stresses

Waterhouse states that the two main causes of stress relaxation in practice are cyclic stressing (i.e. fatigue) and increased temperature [3]. Another cause is the application of a static tensile stress which reduces the surface residual compressive stress which will become permanent if the elastic limit is exceeded, a technique used to remove the effects of residual stress to determine the less noticeable effects of work hardening and surface roughness. This technique could prove useful in the attempt to reduce the somewhat high surface residual stress produced by shot peening to test its effect on fatigue life characteristics. Stress relaxation is a function of the level of cyclic stressing as shown in Figure 21.

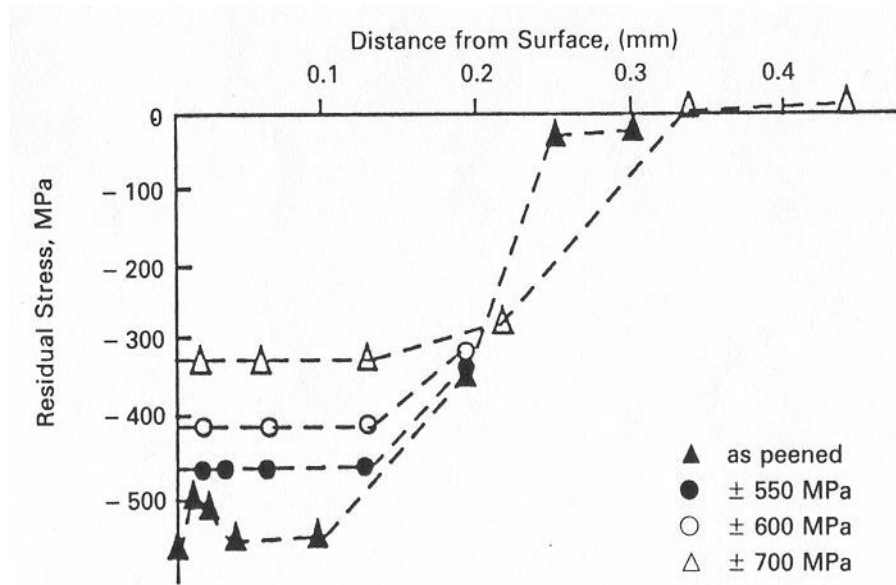


Figure 21 Relaxation of Residual Stress after One Cycle of Fatigue at 3 Levels of Alternating Stress (Rotating Bending) in Shot Peened Specimens [3]

### 2.5.5 Effect on Fatigue Life by Residual Stresses

Shot peening appreciably increases fatigue life in aluminium alloys as demonstrated by S-N graphs, e.g. Figure 22.

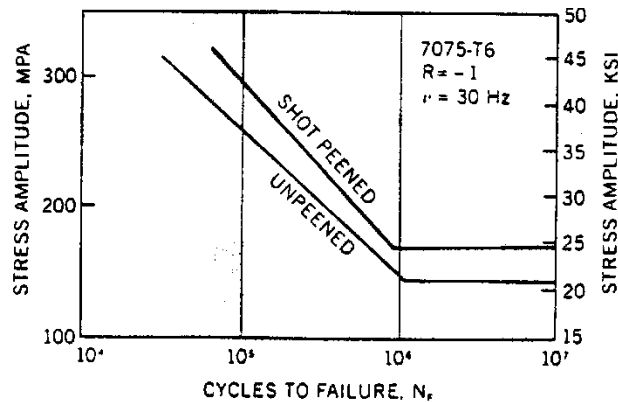


Figure 22 Results of reversed bending fatigue tests on unpeened and shot peened specimens of 7075-T6 Aluminium Alloy<sup>[3]</sup>

Wohlfhart refers to increases in the bending fatigue strength (at  $R = -1$ ) with increasing Almen intensity. Differences in fatigue life after peening with different intensities decrease with increasing stress amplitudes, presumably due to relaxation of residual compressive stresses during the first few cycles becoming more pronounced at higher stress amplitudes.

In cyclic bending tests of aluminium I-beams, a sufficiently high peening intensity and peening time with steel shot was necessary to obtain appreciable fatigue life improvement. Peening only with glass beads resulted in the lowest fatigue life whereas double peening with steel shot and thereafter with glass beads led to the longest life, possibly assisted by the surface smoothing effect of the glass beads<sup>[21]</sup>.

7075-T6 aluminium alloy specimens were shot peened with steel shot and fatigued giving a 300% increase in fatigue life. Some were given a second peening with glass beads before fatiguing and showed a further 50% improvement in fatigue life, partially attributed to a reduction in surface roughness by the glass beads. Others were initially cyclically loaded for a pre-determined number of cycles with improved fatigue life<sup>[22]</sup>.

Waterhouse made investigations into re-peening 7075-T6 aluminium alloy and a 0.43C steel (see Figure 23) concluding that it had no further effect on fatigue life, ascribing this phenomenon to the limited reduction in the residual compressive stress after 75 % of the fatigue life. He also found that 50 % of fatigue failures in the aluminium specimens initiated from below the surface where there would be less benefit from re-peening [3].

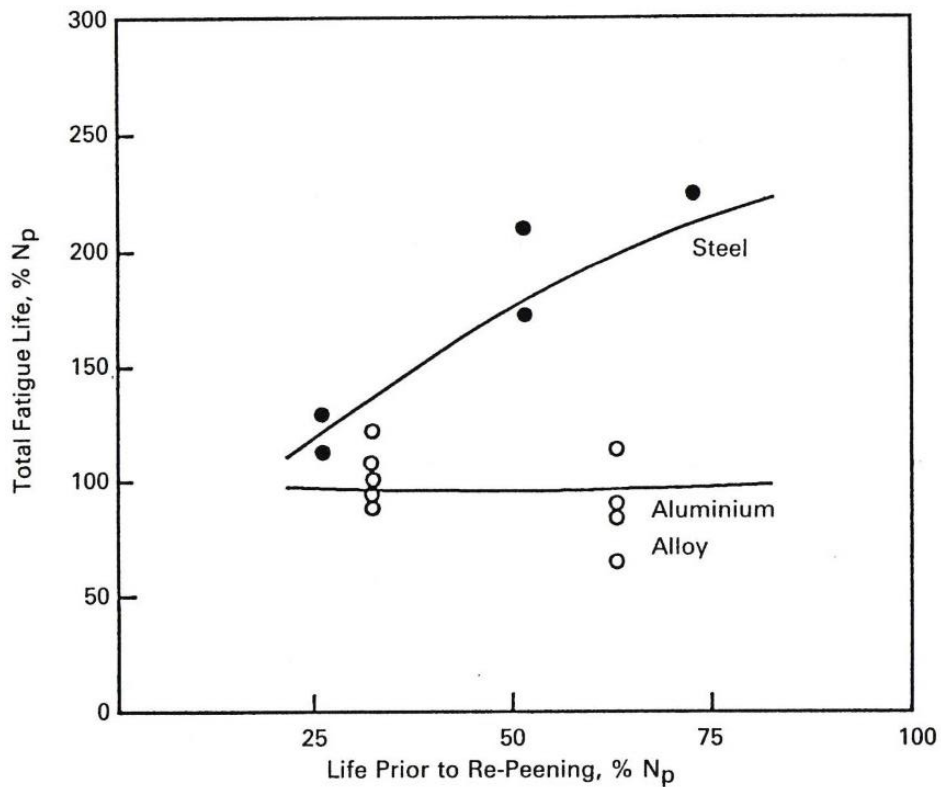


Figure 23 Effect of re-peening on the total fatigue life of 0.4C steel and 7075-T6 aluminium alloy [3]

Waterhouse conducted experiments on aluminium alloys which demonstrated that heavy peening had a greater effect in low cycle (high alternating stress) fatigue (LCF), and light peening a greater effect at high cycle (low alternating stress) fatigue (HCF) [3]. The reason given is that the LCF part of the curve is determined by propagation of a fatigue crack, since initiation of the crack will readily occur from defects or PSBs at these high stresses. Heavy peening increases the depth of the residual compressive stress layer, and therefore has a much greater retarding effect on the growth of the crack. The HCF region of the curve is concerned with the initiation of the crack. Light peening is less likely itself to introduce defects from which cracks will initiate at these low stresses and also it will close up or smooth out defects.

For the type of specimens and loading to be used in this research the Stress Intensity and Paris equations referred to in par 2.1.3 may play a significant role in generating fatigue characteristics. For brevity the formulae are repeated here.

The Stress Intensity Factor, with the compliance function, is given as

$$K = f\left(\frac{a}{W}\right) \cdot \sigma(\pi a Q)^{\frac{1}{2}} \quad \text{Equation 2.19}$$

and the Paris equation

$$\frac{da}{dn} = C(\Delta K)^m \quad \text{Equation 2.20}$$

where:  $\Delta K = \Delta\sigma(\pi a Q)^{\frac{1}{2}}$

### 2.5.6 Residual Stress Measurement: Centre Hole Drilling Method

Residual stresses can be measured by various methods divided into non-destructive, semi-destructive and destructive categories, with the technique selected on the type of material, geometry, required depth being analysed, the resolution required, as well as the expense.

Non-destructive methods include neutron diffraction, X-ray diffraction, ultrasonic and magnetic techniques. These techniques rely on the behaviour of wave mechanics to measure their effects on the crystallographic properties of materials.

Semi-destructive methods involve removing a small amount of material and leave the overall integrity of the structure intact and include centre hole, ring core, and deep hole drilling. This technique is based on the function of the amount of strain released, measured by a strain gauge rosette, corresponding to a small shallow drilled hole.

Destructive techniques result in irreparable structural change to the specimen. The strain release method is also used by cutting the material to relax the residual stress and then measuring the deformed shape. Techniques like the contour method, slitting, block removal and Sach's boring are used [23].

The approach applied in this research to the specimens was the hole-drilling technique which can be performed by the air abrasive or air turbine drilling methods. NMMU has a high speed air turbine hole drilling machine which is relatively simple and economical to use.

A hole is drilled at the centre of a specific three-element strain gauge rosette, with the removal of material under stress causing strain relaxation near the hole. The strain gauges detect the changes in material movement, or strain, and the results recorded at predetermined depths. These strain measurements are then used to calculate the stresses at the specific depths.

Residual stresses can be calculated in four optional techniques, the incremental strain, average stress, power series, integral, and Schwarz-Kockelmann methods.

The method applied to assess residual stress-depth values was the integral method because it is suitable and most generally used for abruptly varying residual stress fields. The calibration coefficients were evaluated using finite element calculations tabulated for a range of hole radii and depths <sup>[5]</sup>

### **2.5.7 Summary**

Residual compressive stresses induced by shot peening have a significant effect on fatigue life, depending on their distribution, magnitude, depth and relaxation characteristics.

Combined applied tensile and higher surface residual compressive stresses will inhibit crack initiation and extend fatigue life. In 7075-T6 the shot indentations are deeper than conventional steels resulting in surface plastic-elastic deformation which is predominantly a function of the residual stress distribution. The residual compressive stress can be viewed a function of the Hertzian pressure until a maximum is reached at the shakedown limit. Residual stress distribution can be shown to vary in depth in parallel planes of similar magnitude. Care must be taken that the Bauschinger effect does not result in damaging the surface and detrimentally affecting the surface stress distribution.

The dimple model shown by Eckersley could be of assistance in resolving the problem of creating an “unpeened” specimen with residual compressive stresses. If the shot peened surface is skimmed by an amount between  $\frac{1}{10}D$  and  $D$  where the level of deformation could

be regarded as insignificant in the presence of residual compressive stresses, the specimen could be regarded as “unpeened” for practical purposes.

The problem of inducing variation of residual compressive stresses in shot peened specimens, to analyse their effects on fatigue life, may be addressed by the stress relaxation technique of static tensile straining.

Since relatively low cycle fatigue testing will be utilised for the experimentation of this dissertation the effect of heavy peening will be an important consideration.

Compliance functions, depending on the geometries of the specimens to be tested, can be a useful tool in predicting fatigue life.

Residual stress testing is a vital component to the analysis of fatigue life and suitable techniques like the hole drilling method was utilised to measure these stresses. The results will be analysed in conjunction with microstructural criteria in the attempt to formulate a life prediction model.

## **2.6 MICROSTRUCTURE**

### **2.6.1 Surface and Sub-Surface Deformation**

Grain refinement and an increase in dislocation density will occur after shot peening, which may have a significant effect on fatigue performance with specific metals.

Waterhouse refers to microstructural changes by combining shot peening and heat treatment. Examination of transmission electron microscope (TEM) samples from shot peened material to study the dislocation arrangements in the microstructure has had little success. Work has been done using X-ray line broadening and microhardness traverses. An X-ray diffraction line for annealed material of suitable grain size has an intrinsic breadth depending on the optical system and Bragg angle. Very fine grain size and work hardening (i.e. increased dislocation density) result in line broadening. X-ray data is converted into a distortion factor involving the size of the coherent domains from which diffraction occurs and the micro-strain in the surrounding material. Figure 24 shows how this factor changes with cycles of fatigue in the shot peened surface of 2024-T351 aluminium alloy. It reflects the changes in the first 20 cycles with regard to stress relaxation, following a period of stability

up to 10000 cycles after which there is an increase related to general fatigue damage, such as the development of persistent slip bands (PSBs).

The dislocation density profile with the residual stress profile is shown in Figure 25<sup>[3]</sup>

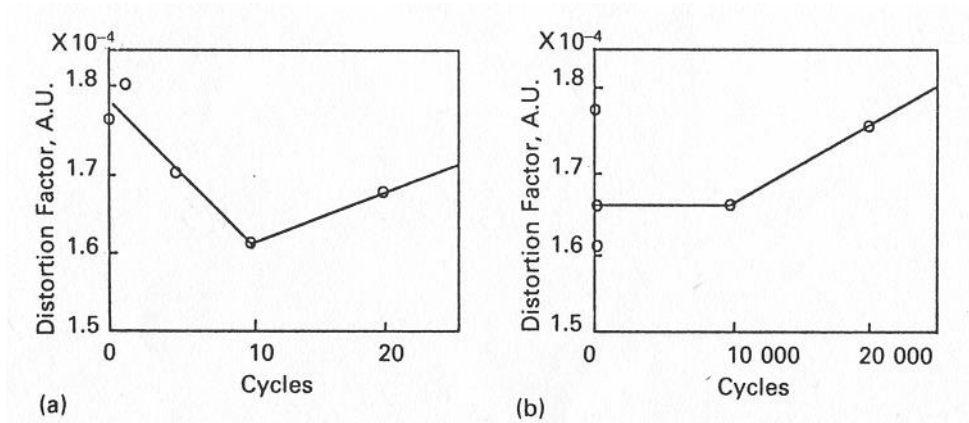


Figure 24 Distortion factor variation with cycles of fatigue for shot peened 2024-T351 aluminium alloy up to (a) 20 cycles and (b) 20000 cycles<sup>[3]</sup>

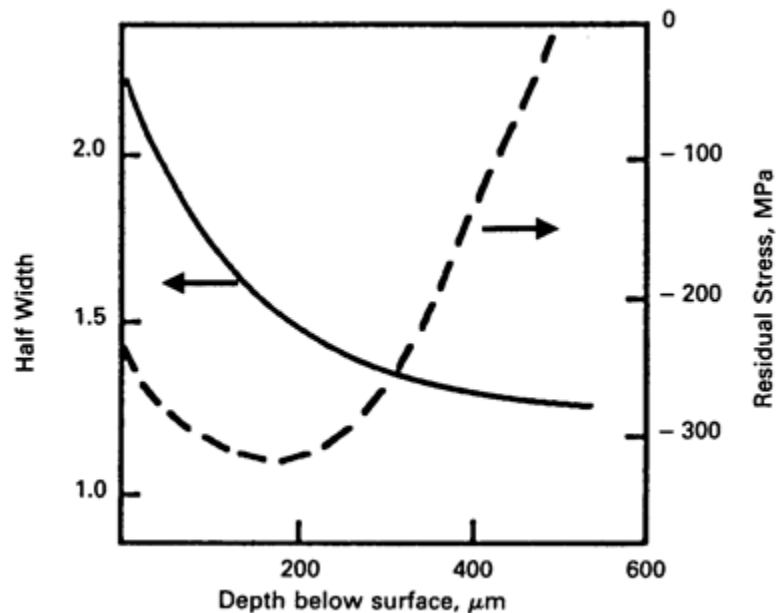


Figure 25 Dislocation density (solid line) and residual stress (dashed line) profile of shot peened 2024-T351 aluminium alloy<sup>[3]</sup>

The surface layer of 7075-T6 is consistent with the rest of the microstructure before shot peening, with a pancake shape along the largest dimension typically in the axial direction for round bars, but distorts significantly afterwards. If variations of surface residual compressive stresses can be imposed on the surfaces of specimens, i.e. unpeened (but “treated”) or shot

peened, then it may be possible to examine the relative importance of microstructural effects. The task of imposing varied surface residual compressive stresses with an acceptably normal microstructure is the tricky part.

One option to create residual stresses (motivated in par 2.5.7) in an “unpeened” specimen is to shot peen the surface, carefully remove the surface layer that includes the distorted structure, and test whether the compressive stress levels will hold and are sufficiently high enough. There may be partial intermingling of distorted and normal elements at those layers but these would hopefully not have significantly detrimental localised plastic strain effects. The depth of the shot peened layer, estimated to be marginally greater than 200  $\mu\text{m}$  according to par 2.5.3, will only be established by actual residual stress-depth tests in conjunction with SEM fractographs, making this approach not without risks.

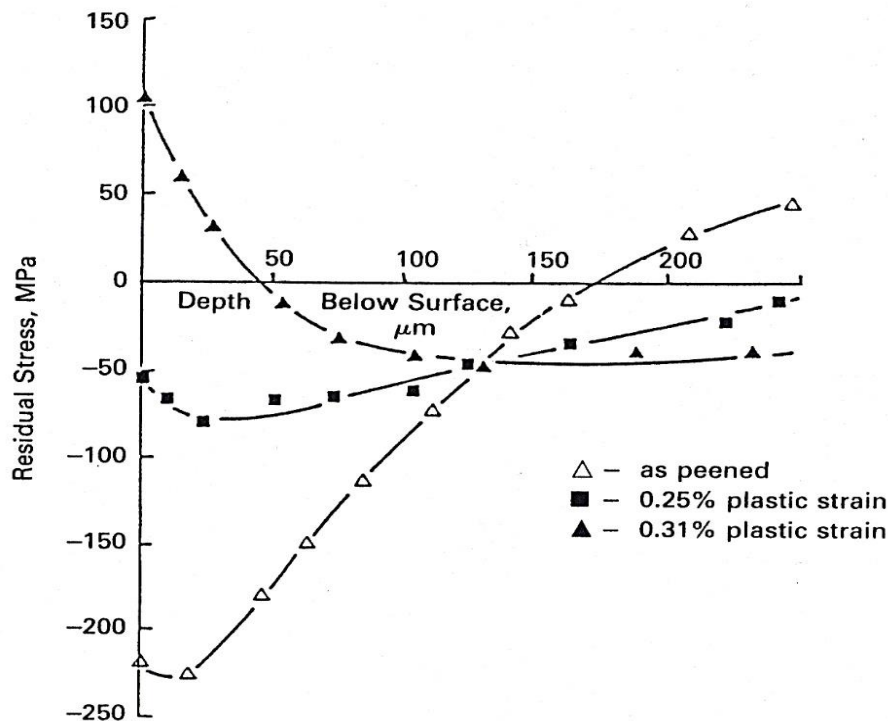
A possible approach to induce varied residual stresses in these “unpeened” and shot peened specimens (motivated in par 2.6.2) is to incrementally plastically strain them, as explained in par 2.5.4, which serves to incrementally reduce their original residual surface compressive stresses. A concern with 7075-T6 is with the tendency for the Zn, Ag and Mg, in particular, to produce microstructural instability and an unwanted increase in dislocation density. The specimens to be tensile tested for this dissertation will be checked for significant give-away serrated flow symptoms.

### **2.6.2 Effects of Small Plastic Strain**

Waterhouse, quoting Kirk, shows how the application of tensile stress to produce small plastic strain on shot peened specimens reduces the residual compressive stress until it becomes zero at a critical strain value <sup>[3]</sup>. The application of plastic strain has no effect on surface hardness according to Waterhouse. Interestingly, the application of a compressive stress with plastic strain also reduces the residual compressive stress but with less effect. Critical strain values range from 0.28% for copper to 1.25% for a selected steel utilising maximum applied tensile stresses ranging between 160 MPa and 375 MPa. See Table 2 and Figure 26 below, showing how a mere 0.25% plastic strain on shot peened copper reduces the residual compressive stress from about 225 MPa to about 75 MPa <sup>[3]</sup>. As stated in par 2.5.4 this behaviour may have useful applications in this research for residual stress variation effects without surface hardness concerns.

Table 2 Critical Strain and Maximum Tensile Residual Stress Values <sup>[3]</sup>

Material	Critical Strain %	Max Tensile Stress MPa
Copper (OFHC)	0.30	+ 160
Nickel (99.92%)	0.28	+ 185
0,05C Steel	1.10	+ 375
0,04C, 0,8Mn Steel	1.25	+ 300
0,3C, 0,5Mn, 4Ni, 1,25Cr, 0,3Mo Steel	0.30	+260

Figure 26 Residual stress profiles of shot peened copper after plastic straining <sup>[3]</sup>

Meininger shows that even under small applied dynamic cyclic axial loads, stress concentrations at notches and voids can lead to significant levels of local plastic strain and consequent regional fatigue failure, highlighting the importance of understanding microstructural and micromechanical processes that control cyclic plasticity <sup>[24]</sup>. Details of the cyclic stress-strain response and the microstructural features that control this response in

precipitation hardened aluminium alloys have not yet been fully described. They used commercially available 7075 in the T6 and T651 tempers to characterise the low cyclic deformation response to provide a mechanistic interpretation of the observed differences in behaviour.

Both tempers produced material in the peak-aged condition. Strengthening was provided by coherent and semicoherent GP (Guinier Preston) zones and precipitates which were expected to be shearable during cyclic deformation. These dislocations served as sites for heterogeneous nucleation of precipitates.

Applying 0.1% and 0.3% plastic strain amplitudes to plotting peak absolute compressive and tensile stresses to the number of cycles, it was found that the magnitude of the compressive stress always exceeded the applied tensile stress (by approximately 10%). Both peaks exhibited fairly stable behaviour for the first few cycles followed by gradual hardening to saturation. Significant softening was observed prior to failure only at amplitudes of 0.6% and greater. They referred to Li et al attributing the relative rapid hardening that precedes saturation to the formation of dense dislocation bands separating channels of lower dislocation density. The authors used an asymmetry factor, characterising the degree of asymmetry between tension and compression peaks, and found that it increased slightly with plastic strain amplitude, but remained at 3 to 4% for strain amplitudes above 0.3%.

They noted after SEM tests that the 7075-T6 exhibited a fairly flat fracture surface at low plastic strain amplitudes ( $\leq 0.2\%$ ) with a single primary crack initiating at the circumference of the specimen, growing transgranularly and perpendicularly to the loading axis. At higher plastic strain amplitudes (above 0.3%) the surface was characterised by coarse slip bands and intergranular cracking. Final fracture occurred by linking these small cracks, resulting in a macrocrack that grew at  $45^\circ$  to the loading axis. Specimens tested at high strain amplitudes exhibited coarse circumferential surface cracks oriented with the crack plane normal to the loading axis. The authors referred to Starke et al who (with plastic strain amplitudes above 0.4%) stated that cracks nucleated at coarse inclusions and that shear bands then linked the tips of the microcracks to cause final fracture. Starke et al noted the effects of concentrated slip and circumferential initiation of cracks followed by transgranular propagation. The observations of the fracture surfaces were generally consistent with the development of localised plastic deformation.

Meininger hypothesised that the asymmetry was attributable to the inhomogeneous nature of deformation of this alloy. 7075-T6 is known to exhibit strain localisation in which deformation is concentrated in bands as a consequence of two related effects.

In the **first mechanism**, the non-uniform thermal stresses that arise during quenching lead to regions of localised plastic deformation. In these quench bands, gliding dislocations lower the free vacancy concentration by rearranging them into dislocation loops. Upon ageing, there are insufficient vacancies to support homogeneous nucleation, resulting in the formation of coarse, lath-shaped precipitates in the quench bands. These quench bands are said to be relatively soft and serve as regions in which strain is initially localised.

In the **second mechanism**, strain localisation results when the coherent and semi coherent particles that form in this alloy at peak strengths are sheared by dislocations.

The localisation of deformation is most pronounced at low plastic strain amplitudes ( $\leq 0.3\%$ ). At higher amplitudes, deformation becomes more homogeneous due to activation of cross-slip and secondary slip at higher stresses. At the highest plastic strain amplitudes the larger asymmetry factor at saturation for the T6 temper may be associated with the onset of strain softening caused by particle shear.

They concluded that these asymmetries are related entirely to microstructural effects. Cyclic deformation of this precipitation strengthened alloy is controlled by dislocation substructure, inhomogeneities in particle distribution and dislocation/particle interactions <sup>[24]</sup>.

### 2.6.3 Effects on Fatigue Life

Microstructural compliance and integrity for the sustained retention of compressive residual stresses by withstanding stress relaxation, through cyclic loading, as long as possible is critically important to fatigue life. Effects, like grain orientation and size etc., can jeopardise and compromise the microstructure's capacity to provide resistance to fatigue.

Region 1 crack growth, which is highly dependent on the microstructure, can be resisted by closure mechanisms like plasticity-induced closure which is sensitive to the yield strength.

Surface strain hardening produced by shot peening increases the surface yield stress effectively relegating the applied stress due to cyclic loading to proportionately lower ratios, supposedly yielding extended fatigue life.

#### **2.6.4 Summary**

Post shot peening surface and subsurface deformation can be characterised by grain refinement and dislocation density. The distortion factor may be interpreted as a function of dislocation density assisting in the determination of stress relaxation effects to the possible development of persistent slip bands prior to final fracture.

The simulation of unpeened specimens with residual compressive stress may be possible by careful skimming of the surface layer of shot peened specimens. Stress variation may be obtained by limited incremental plastic straining of peened and simulated unpeened specimens so that any tendency towards microstructural instability and unwanted increases in dislocation density will be minimised.

Plastic straining must be less than the estimated critical strain value to ensure that significant residual compressive stresses remain. No literature could be found by the author to obtain critical strain values for 7075-T6 but it could be about 1% by comparison with known values of other metals.

The inclusion of axial fatigue testing by Meininger et al at small plastic strain levels was made to gain insight into possible effects of plastic straining on fatigue. Testing for this dissertation will be limited to applied bending stresses below the plastic limit but specimens which have been plastically strained before fatigue testing may reveal similar characteristics to Meininger's tests which may assist in explanations of microscopic behaviour, perhaps with the help of the two proposed mechanisms.

## 2.7 MICROHARDNESS

Hardness of materials, and their measurements, are well known to the materials science fraternity. It is a measurement of the resistance of a material to plastic deformation. This is done by indenting the surface by applying a test load to a diamond square-based pyramid shaped indenter, in the Vickers test, and applying predetermined dimensions of the indentation to elicit a hardness number. Hardness is not a definitive property but provides a relative comparison between different materials.

The term "microhardness" is commonly seen to describe the hardness testing of materials with low applied loads. In the Vickers test used in this research, a diamond indenter is impressed into the surface of the test specimen using a known applied force or test load of about 2 N for indentations of about 50  $\mu\text{m}$ .

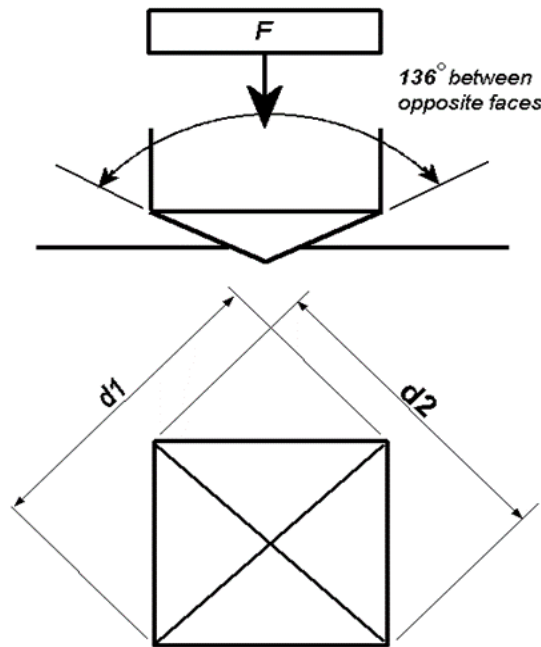


Figure 27 Indenter impression of Vickers microhardness tester [5,39]

The Vickers hardness test precision diamond indenter, shown in Figure 27, has a face angle of  $136^\circ$ , and the diagonal dimensions of indentation or impression surface area,  $d_1$  and  $d_2$ , are measured under a microscope, with their mean value applied to the formula to calculate the Vickers hardness number as follows:

$$HV = \frac{F}{A_s} = \frac{2F \sin\left[\frac{\alpha}{2}\right]}{d^2} = \frac{1.8544F}{d^2} \quad \text{Equation 2.21}$$

Where:        d = mean diagonal length in mm  
                   A<sub>s</sub> = area in mm<sup>2</sup>  
                   F = load in kgf (kilogram.force)

Microhardness testing can be used to observe changes in hardness on the microscopic scale and have been shown to be proportional to the maximum tensile strength of steels. It may prove useful if a similar relationship can be found with 7075-T6 aluminium alloy, although this is disputed by Davis who states that aluminium alloys are not as compliant as steels in this regard although Figure 28 demonstrates a broad relationship <sup>[25]</sup>.

Figure 28 shows Rockwell hardness ball (HRB) units which are converted to Vickers hardness (HV) units, used in this research, for the microhardness analysis in par 4.2.4.2.

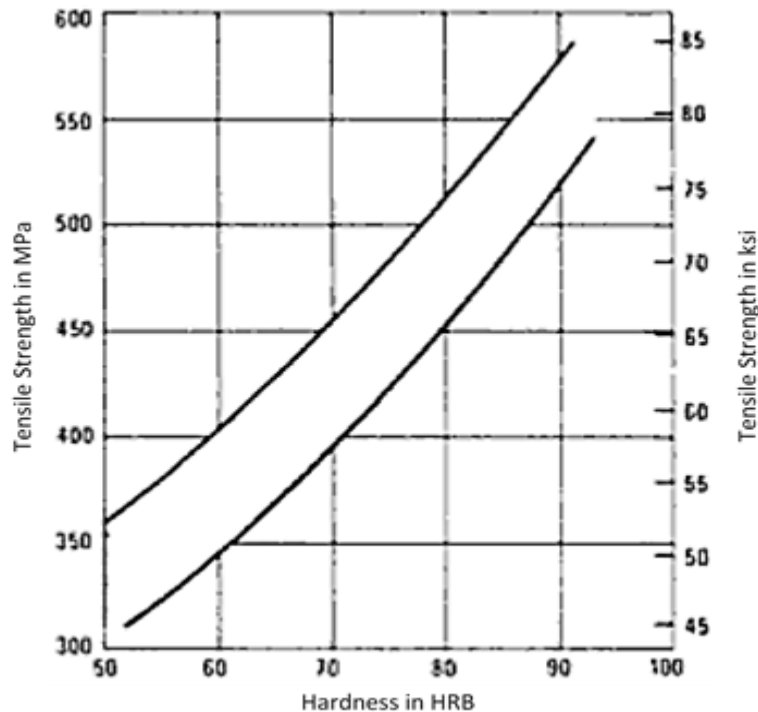


Figure 28 Tensile strength vs surface hardness for various aluminium alloys <sup>[25]</sup>

Solis Romero shows in Figure 29 that microhardness shows an initial increase which then decreases with depth in shot peened 2024 aluminium alloy. He ascribed the high microhardness at the shot peened surface to the intense plastic deformation induced by shot impacts that provoked work hardening and distortion of grain structure [26].

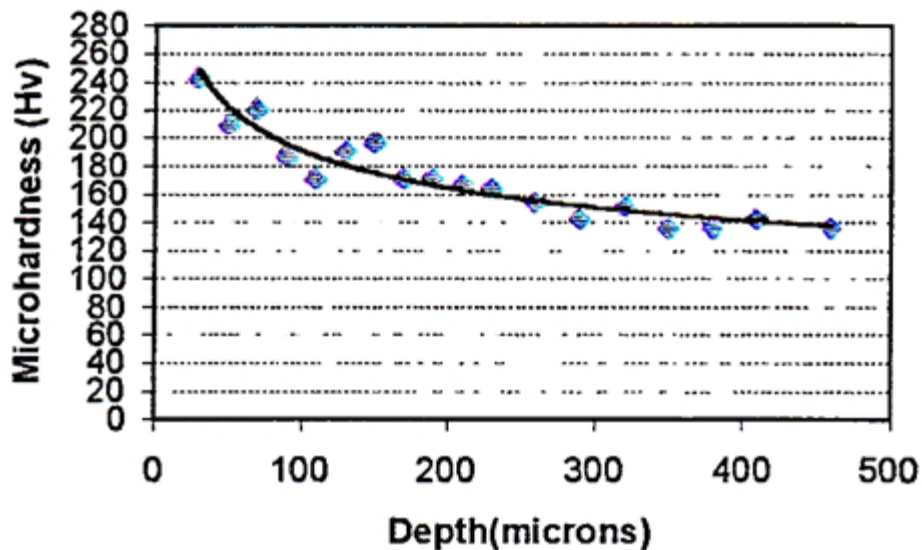


Figure 29 Microhardness profile of a 2024 aluminium alloy shot peened specimen [26]

Micro-hardness can be affected by strain hardening caused by shot peened surfaces and plastic straining throughout the material and it may be possible to establish relationships between the residual stress and hardness at corresponding depths, as well as fatigue life estimations [5,25].

## 2.8 FRACTOGRAPHY

The purpose of using fractographs taken by the scanning electron microscope (SEM) in this research is to inspect the fractured surfaces of fatigue tested specimens for fatigue characteristics such as striations, shear surfaces, voids, initiation and end cracking, and other microstructural effects that may reveal the nature of the types of fatiguing taking place.

The SEM produces images by scanning a sample with a focused beam of electrons which interact with the atoms of the sample producing various signals that can be detected and produce images that contain information about the sample's surface topography and composition.

The sample is cut to a suitable size and the surfaces are cleaned of any external impurities before being mounted on a specimen holder for scanning with magnifications that can range from 10 to 500000 times.

The diagrams in Figures 30 and 31 show how an electron gun emits a beam of electrons that is attracted by the anode, passes through magnetic fields and lenses which focus the electron beam on to the sample. When the beam hits the sample, electrons and X-rays are ejected from the sample. Detectors collect the X-rays, backscattered electrons, and secondary electrons and convert them into a signal that produces an image <sup>[27]</sup>.

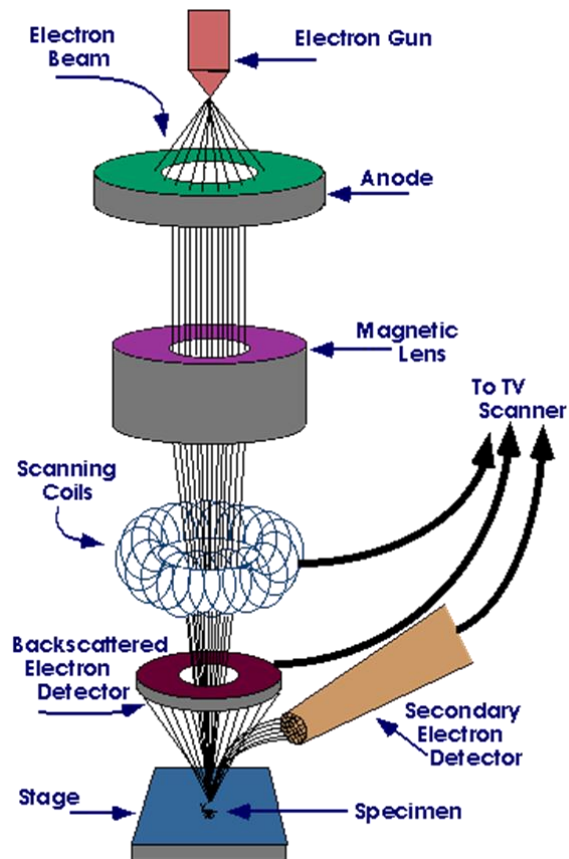


Figure 30 Principle of the SEM process <sup>[27]</sup>

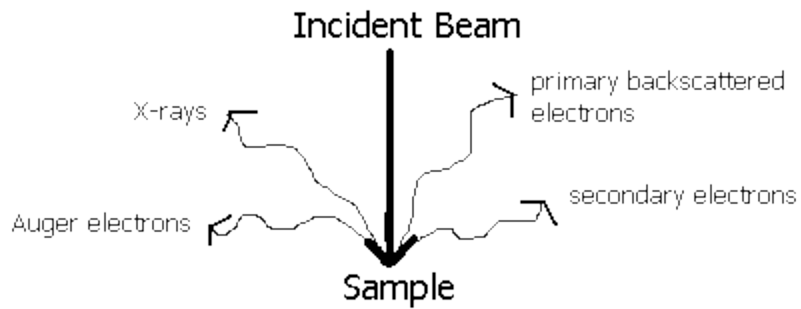


Figure 31 SEM incident electron beam showing ejected electrons and X-rays [27]

Interpretation of fractographs is important in identifying whether the fracture surface is ductile, brittle, intergranular or transgranular, voids, defects responsible for formations, cleavage planes, etc. These characteristics can assist in how and with what level of cyclic loading takes place, so that remedies may be found to prevent or offer longer fatigue life. Below are fractographs that help identify characteristics of fracture surfaces [27,28].

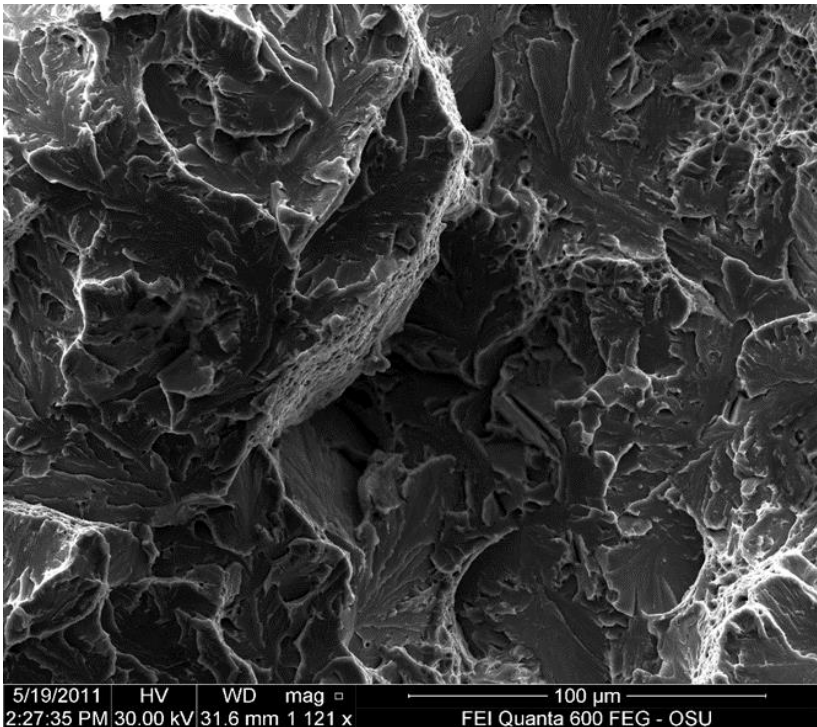


Figure 32 Brittle transgranular fracture of an unknown metal with flat cleavage planes and sharp edges along the atomic steps [37]

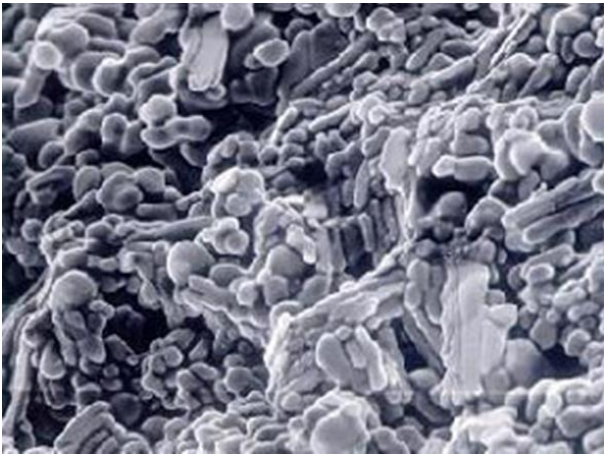
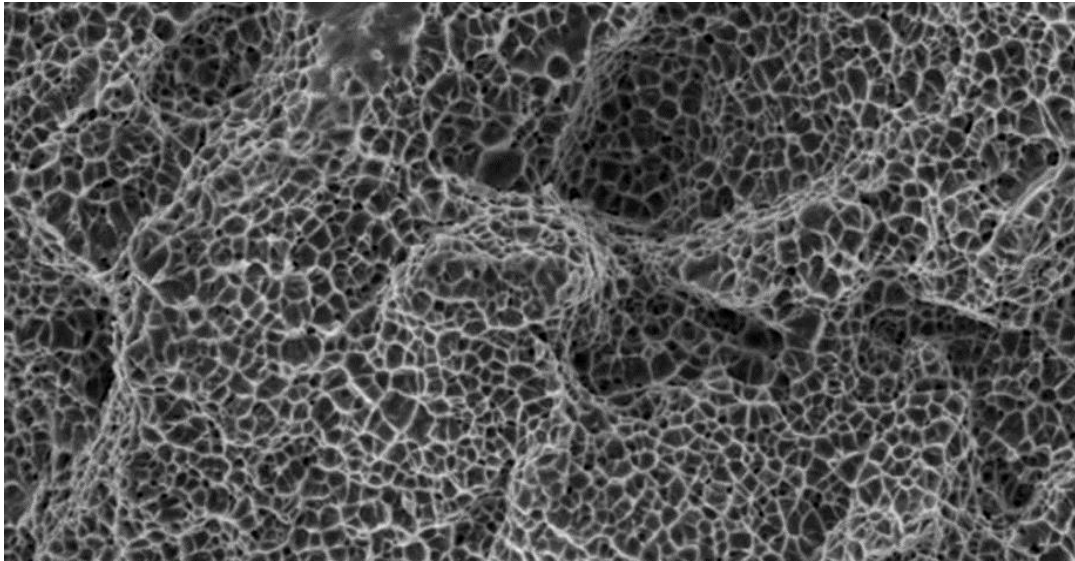


Figure 33 Surface of voids on the surface of an aluminium casting x 1000 [38]



*Figure 34 Equiaxed dimples from ductile overload of unknown metal [38]*

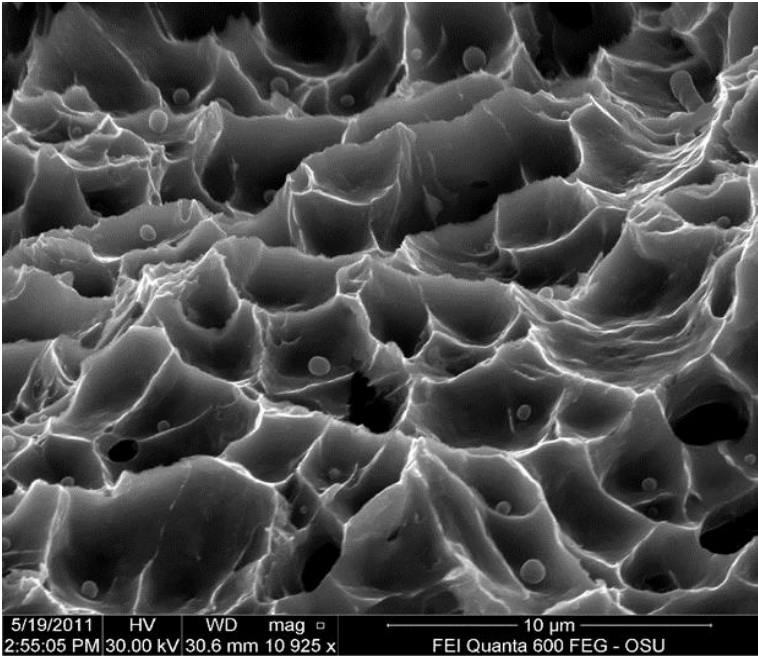


Figure 35 Ductile fracture of an unknown metal with clear ductile dimples (microvoids) with significant plastic deformation of the material between dimples. Many of the dimples show a defect in the centre of the dimple which may have been responsible for the dimple formation [37]

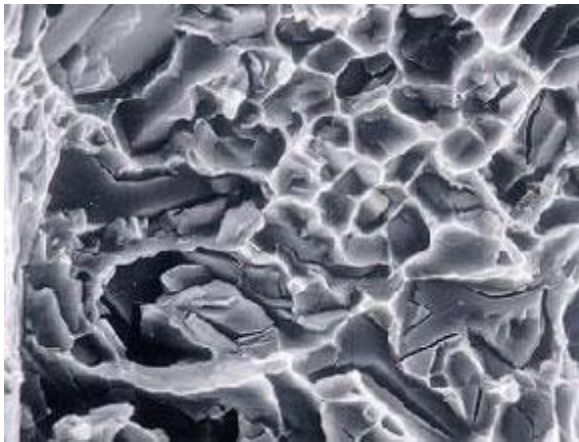


Figure 36 Brittle fracture surface of an aluminium casting x 1000. The angular silicon particles at the surface contribute to the brittleness [38]

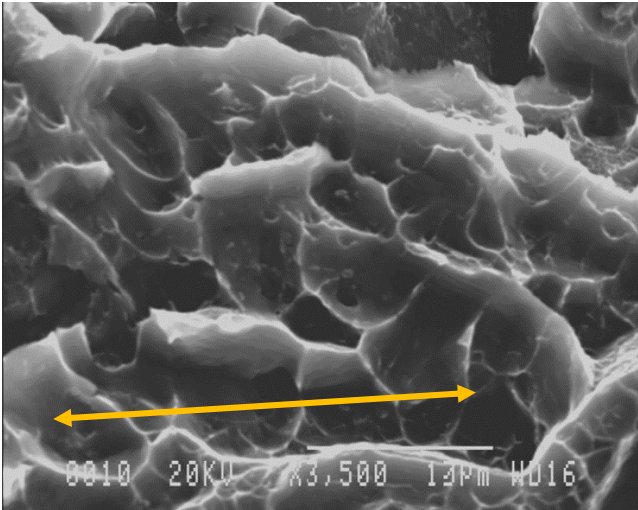


Figure 37 Microvoid coalescence in 8090-T8511 aluminium alloy formed by a combining of voids, some seen with precipitate particles at their centres [28]

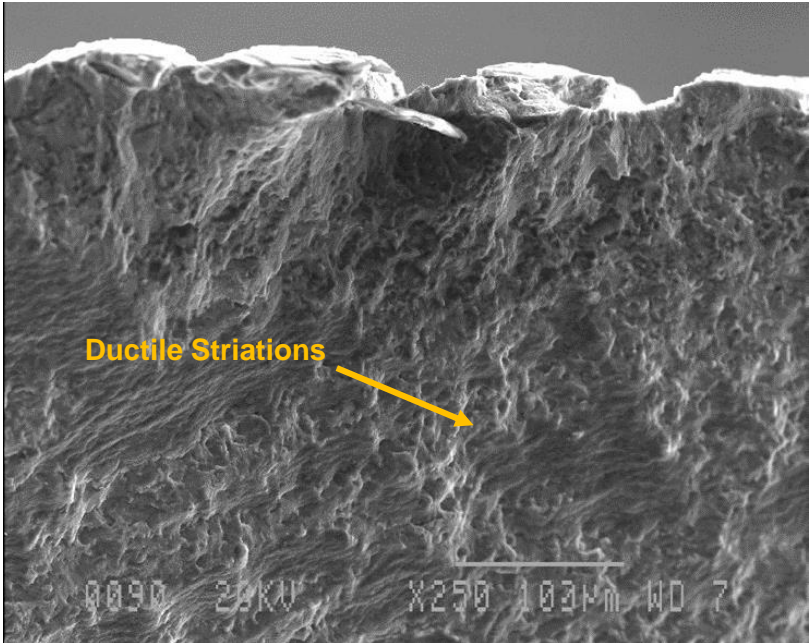


Figure 38 Low cycle fatigue of aluminium alloy 5383-H21 showing ductile striations causing transgranular fracture [28]

## 2.9 LIFE PREDICTION MODELS

### 2.9.1 Mean Stress Correction with Constant Amplitude Loading

Stress-life methods like those applied for S-N curves and mean stress applications are usually used for high cycle fatigue and are inaccurate for low cycle fatigue below 10000 cycles. Since the fatigue life of all specimens in this research is above 20000 cycles and averaging about 90000 cycles, stress-life methods should be valid.

Cyclic fatigue properties of materials are often obtained from completely reversed, constant amplitude tests, with zero mean stress, which usually serves as a general point of reference, or the norm, for the engineering community.

With non-zero mean stresses under constant amplitude loading, as is the case with this research, it would be expedient to convert the solutions to equivalent completely reversed values so that they can be compared to generally published results, and be more user-friendly.

To achieve this conversion, a mean stress correction has been devised, which converts the non-zero mean stress to an equivalent mean stress, and then applying it to find the equivalent alternating stress amplitude, using one of several empirical techniques including Gerber, Goodman and Soderberg theories, which use readily available static material properties like yield and tensile stresses along with S-N information.

The Goodman theory is more applicable to brittle materials and the Soderberg cautiously conservative (see Figure 41 in par 2.9.3 below) while the Gerber theory is more suitable for ductile materials like 7075-T6 aluminium alloy, and therefore more applicable [29,30].

### 2.9.2 Effects of the Stress and Fatigue Ratios

The stress ratio is given as  $R = \frac{\sigma_{\min}}{\sigma_{\max}}$  and is an important property in the analysis of fatigue.

The general standard, or point of reference, is  $R = -1$  for tension-compression applied stress where the mean stress is zero. The cyclic diagrams in Figure 39 below show the consequences of some typical variations of  $R$ , including the  $R = +0.1$  used in this research.

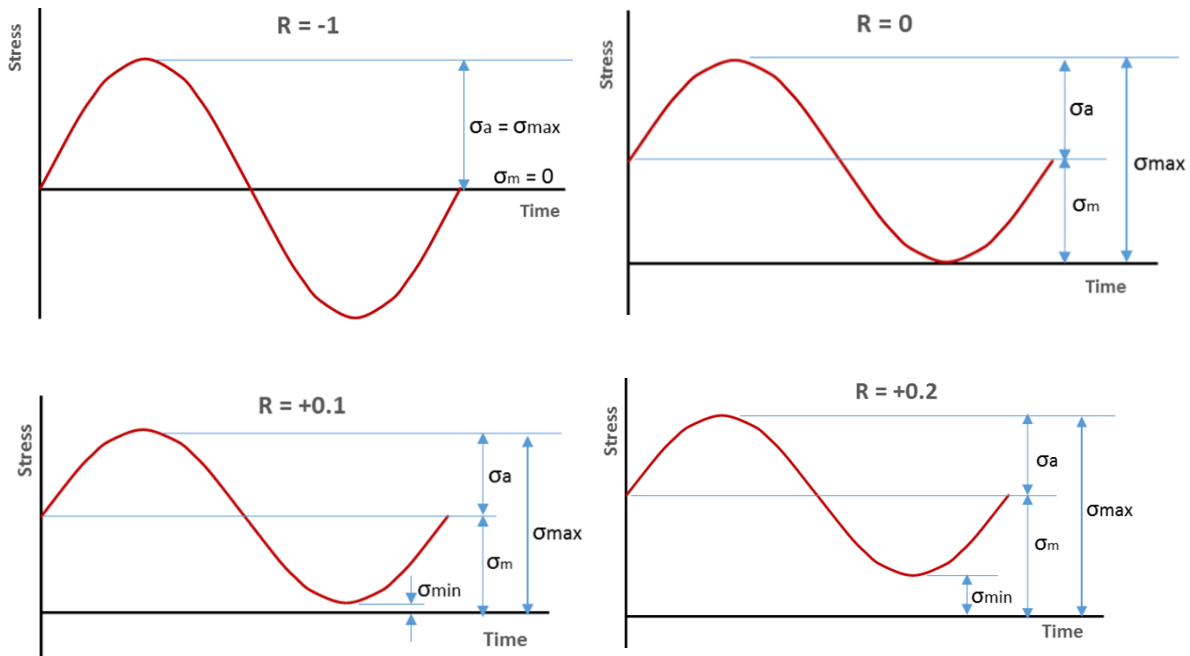


Figure 39 Fatigue cycle diagrams with typical variations of stress ratio  $R$  (adapted) <sup>[31]</sup>

The fatigue ratio which is given as the ratio of the effective endurance tensile stress to the ultimate tensile stress is an indicator of acceptability to use mean stress methods. Typical values range from 0.25 to 0.6 depending on the material. 7075-T6 aluminium alloy has a fatigue ratio of around 0.3 with a fairly wide tolerance due to the sometimes wide scatter of fatigue life cycles at the endurance limit.

Figure 40 shows the comparison between cyclic stresses at various mean stresses for the same fatigue life. Cycle (a) represents the fully reversible cycle at  $R = -1$  and cycle (d) most closely represents the tension-tension cycle used in this research where  $R = 0.1$ .

It can be easily seen that the stress amplitude for the fully reversible cycle (a) is significantly larger than that for cycle (d), giving an indication of what to expect in this research, aided by the Gerber equation <sup>[31]</sup>.

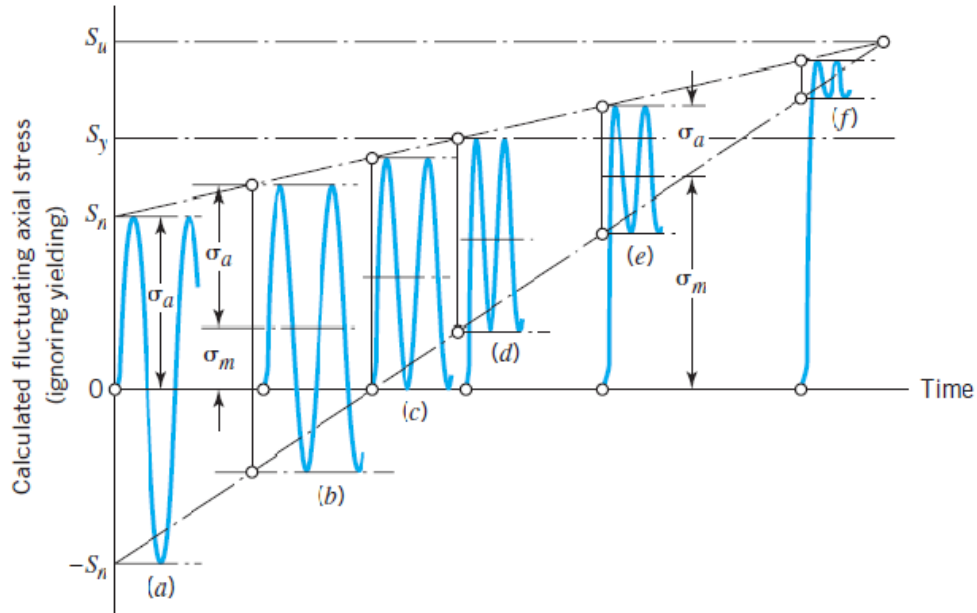


Figure 40 Various fluctuating uniaxial stresses corresponding to equal fatigue life <sup>[31]</sup>

### 2.9.3 Application of the Gerber Equation

In the pursuit of fatigue life prediction of materials within practical measurable parameters the Gerber equation offers a solution with ductile materials under a combination of a fatigue inhibiting residual compressive and fatigue producing applied tensile stresses.

The Gerber equation will be tested for its viability to predict fatigue life of specimens by comparing the effects of fairly constant shot peening and variable plastic straining inducing varying residual compressive stresses and microstructural effects, under constant bending stresses.

The majority of fatigue research has been carried out using a pulsating tension applied cyclic load with the minimum stress = 0 and therefore the stress ratio,  $R = 0$ .

Converting actual to effective mean stress can be a highly significant variable, influencing the number of cycles for crack initiation, the rate of crack propagation, and the critical crack size for final failure.

It has been generally accepted that the mean stress has a significant influence on fatigue

strength if the applied stress cycle is wholly tensile, although there is little experimental evidence to support this, as the majority of fatigue data have been published under alternating reverse cycles with  $R = -1$ .

It is hoped that the Gerber equation, based on empirical relationships, will be found applicable here to predict the effect of the mean stress by using the alternating stress at a given life, and the material ultimate tensile stress (UTS) <sup>[30]</sup>.

An attempt will be made to relate and compare the Gerber equation solutions to the standard S-N curves for 7075-T6 aluminium alloy and check their correlations.

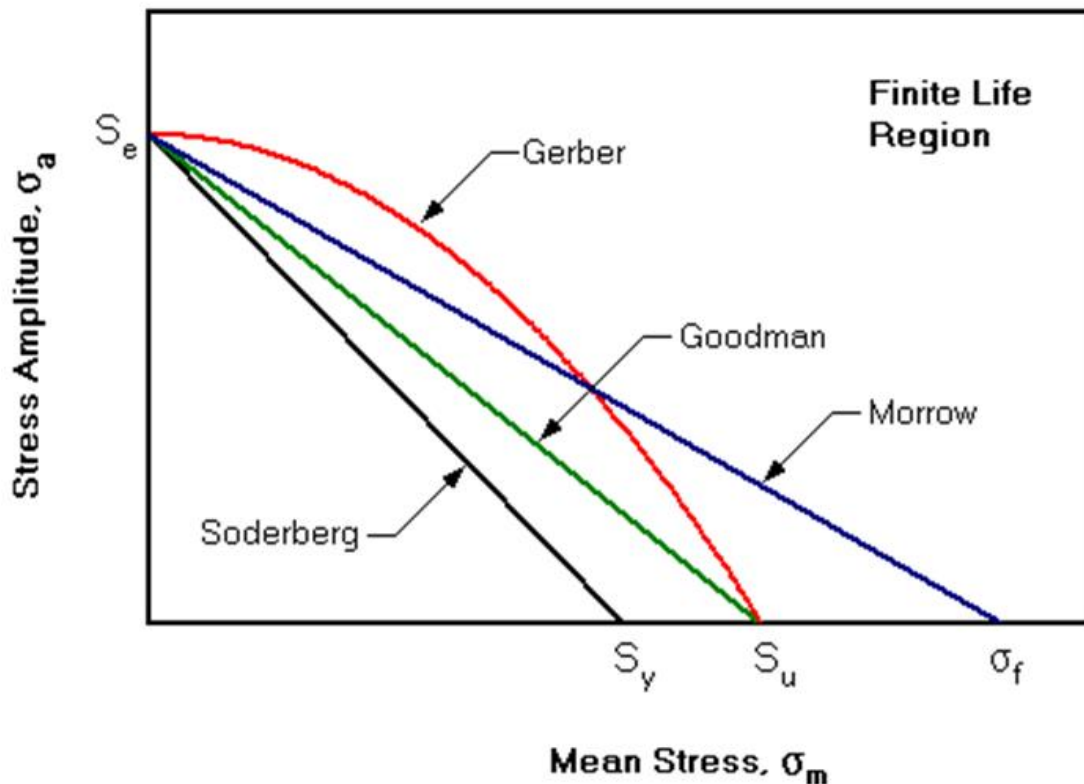


Figure 41 Graphical representation of the parabolic Gerber mean stress correction for fatigue life analysis. Also shown are the Morrow, Goodman and Soderberg lines <sup>[40]</sup>

In Figure 41 above:

$\sigma_e$  = endurance limit for fully reversible alternating stress

$S_y$  = yield stress

$S_u$  = ultimate tensile stress

$\sigma_f$  = true fracture stress

The Gerber equation is given generally as:

$$\frac{\sigma_{\text{Alternating (a)}}}{\sigma_{\text{Endurance Limit (n)}}} + \left[ \frac{\sigma_{\text{mean}}}{\sigma_{\text{uts}}} \right]^2 = 1$$

Which can be re-written as:

$$\sigma_n = \frac{\sigma_a}{1 - \left[ \frac{\sigma_m}{\sigma_u} \right]^2} \quad \text{Equation 2.22}$$

Where the effective mean stress is given by:

$$\sigma_m = \left[ \frac{\sigma_{\text{max}} + \sigma_{\text{min}}}{2} \right] + \sigma_{\text{residual}} \quad \text{Equation 2.23}$$

And, the equivalent stress amplitude given by:

$$\sigma_a = \left[ \frac{\sigma_{\text{max}} - \sigma_{\text{min}}}{2} \right] \quad \text{Equation 2.24}$$

Where:

- $\sigma_n$  = alternating stress amplitude for the completely reversible cycle ( $R = -1$ )
- $\sigma_a$  = applied alternating stress amplitude with respect to the mean stress
- $\sigma_u$  = ultimate tensile stress of the material
- $\sigma_{\text{max}}$  = maximum applied bending stress amplitude
- $\sigma_{\text{min}}$  = minimum applied bending stress amplitude [5]

#### 2.9.4 Application of the Juvinall and Marshek Life Prediction Method

In this approach the S-N curve is generalised into a linear graph between the reversible cyclic stress amplitude at 1000 cycles and the stress at the endurance limit. This yields a straight-line graph, as shown in Figure 42 below, with its accompanying simple equation of the type  $y = mx + c$ , which can be transposed to the semi-log form  $\text{Sn} = m \text{Log } N_f + C$  or the log-log form  $\text{Log Sn} = m \text{Log } N_f + C$ .

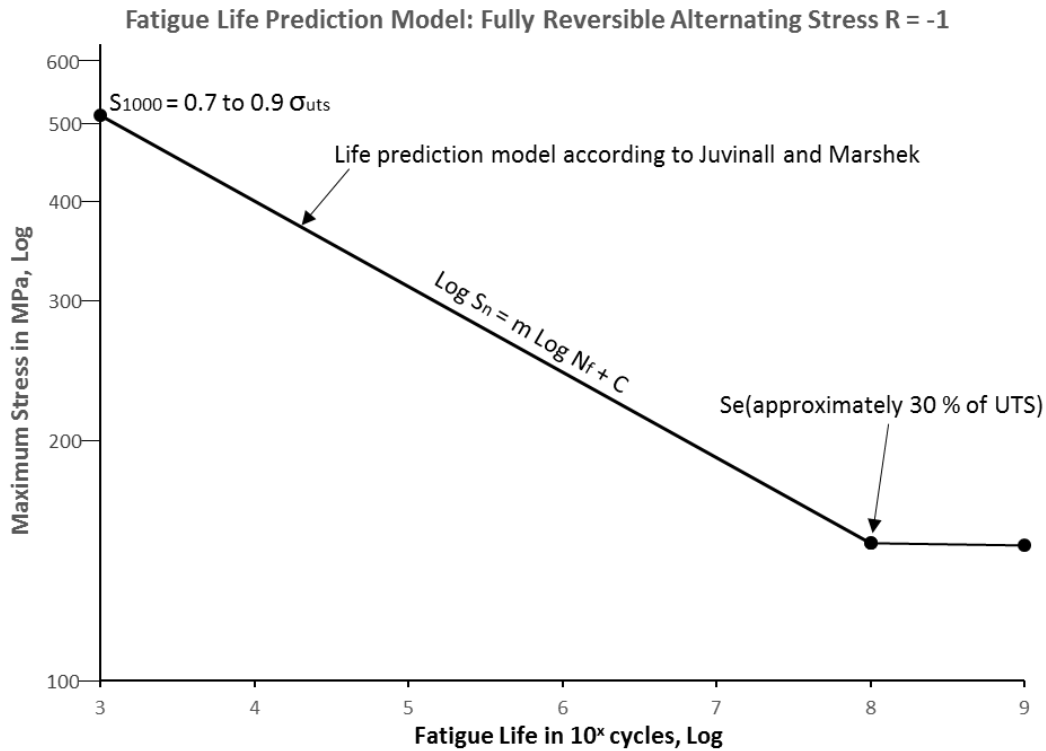


Figure 42 Graphical representation of the Juvinal and Marshek life prediction model [5,31]

The value for the ultimate tensile stress (UTS) for the specimens was tested to be 612 MPa. The stress amplitude at 1000 cycles is approximated to about 70 % to 90 % of the UTS for 7075-T6 aluminium alloy giving around 430 and 550 MPa, although there is a significant amount of variance beyond these stresses at 1000 cycles. All the cycles to failure were between 25000 and 320000 cycles which fits comfortably between the  $10^4$  and  $10^6$  cycle range.

The estimated fatigue, or endurance limit, as cited in 2.9.2, is approximately 30 % of the UTS. However, it was deemed more useful to read this value off reliable S-N diagrams [31].

The US Navy MIL-HDBK-5J handbook shows a wide and thoroughly worked range of fatigue testing. It also has the rare advantage of plotting S-N curves from various stress ratios which may be useful for comparison purposes. The curves shown in Figure 43 are all based on the stress intensity factor ( $k_t$ ) = 1 for smooth, un-notched specimens, applicable to this research.

It is unfortunate, though, that the S-N curves were for *axial* fatigue testing, but this is not a serious drawback, however, as these curves are very close to reverse bending fatigue testing with relatively easy standard conversion factors.

It can be seen from the curve for fully reversible stress, where  $R = -1$ , that the fatigue limit seems to be around  $10^6$  to  $10^8$  cycles if the scatter is to be considered [31,32]

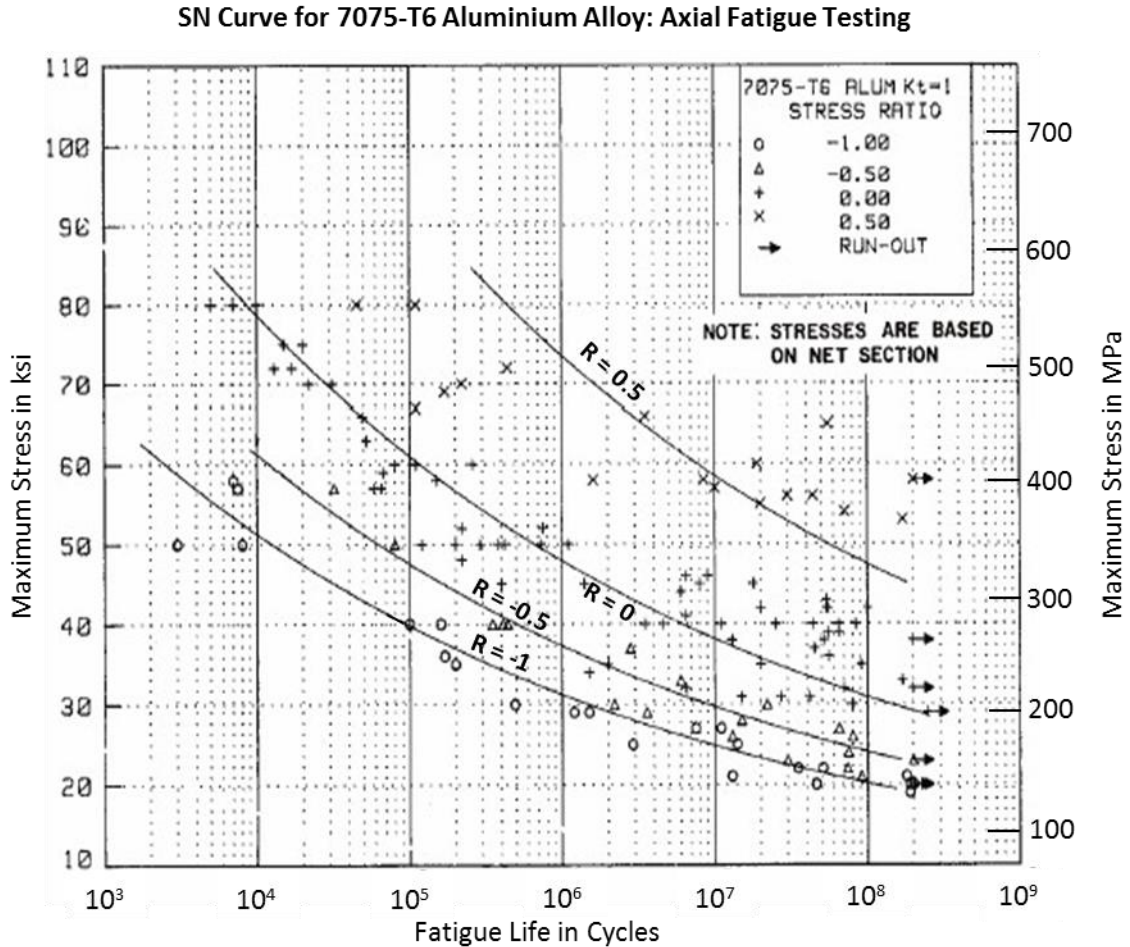


Figure 43 S-N Curves for axially loaded 7075-T6 aluminium alloy at various stress ratios. The lowest curve is for fully reversed cyclic stress amplitude where  $R = -1$  [32]

Another useful source is from the much used Atlas of Fatigue Curves by Howard E Boyer in Figure 44 below, showing a typical S-N curve for constant amplitude, fully reversed bending at  $R = -1$  for un-notched specimens of 7075-T6 aluminium alloy [33]. The cycle range is from the more common  $10^4$  up to  $10^7$  cycles rather than the  $10^8$  cycles shown in the MIL-HDBK-5J.

Once the Figure 43 has been converted from applied axial to bending stresses by an approximate 11 % increase, shown later in table 26 and Figure 113, it can be compared to Figure 44 as well as its generated table 27 and Figure 116. Even before these conversions have taken place, it can be seen that the Atlas of Fatigue Curves curve is positioned lower than that for the MIL-HDBK-5J. This apparent anomaly will be dealt with in the analysis section in par 4.3.1 where the application of generalised coefficients, introduced in par 2.9.5, will demonstrate the rationale behind it.

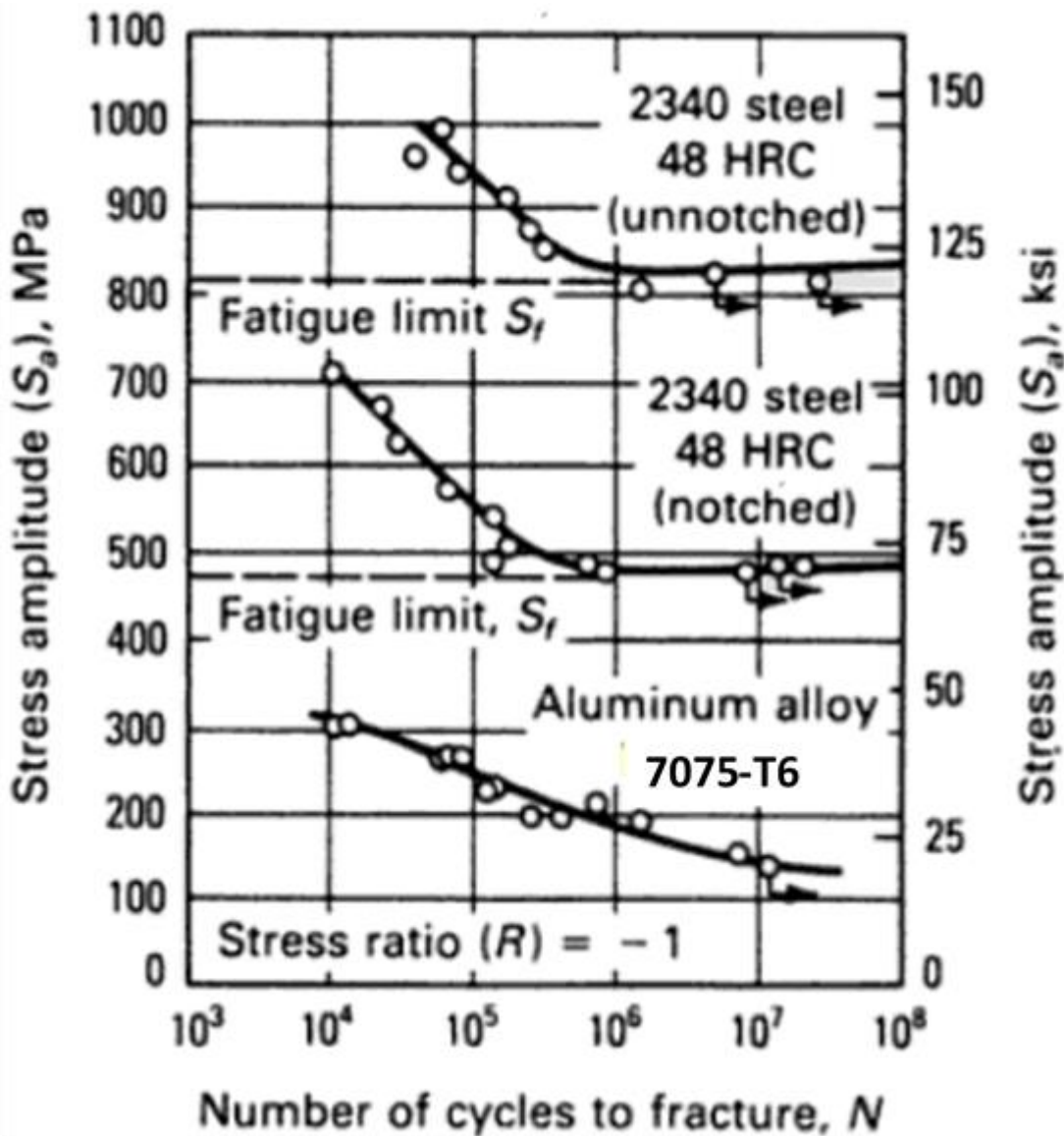


Figure 44 S-N graph showing 7075-T6 aluminium alloy under fully reversible cyclic bending fatigue [33]

Correlation with the life prediction model may be accommodated by the Haigh diagram showing the Gerber curves at various applicable lines of constant fatigue life, as shown in Figure 45 below.

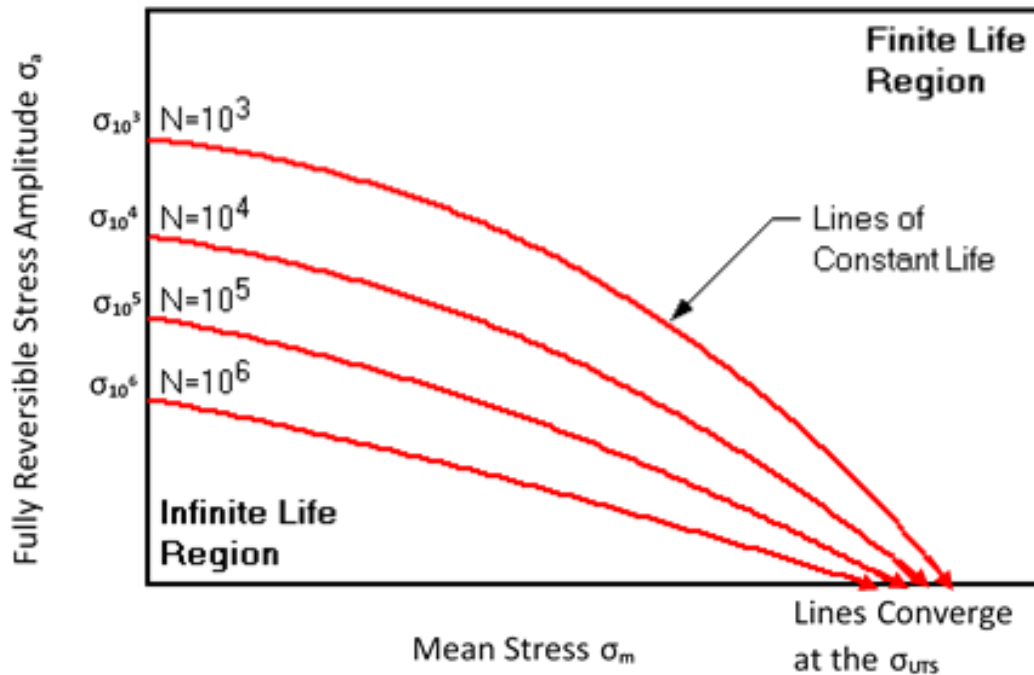


Figure 45 Haigh diagram showing Gerber lines of constant fatigue life (adapted) <sup>[40]</sup>

### 2.9.5 Approach to Combining the Gerber with Juvinall and Marshek Methods

Since the experimental stress values are assessed with a stress ratio of  $R = +0.1$  they must first be calibrated into fully reversible equivalent stresses where  $R = -1$  and zero mean stress, and to achieve this the Gerber equation is used.

The stress amplitudes can be compared to the S-N diagrams in Figures 43 and 44 to check whether they are within reasonable limits and operate as a type of plausibility parameter.

The stress amplitudes are then plotted on the Juvinall and Marshek life prediction diagram, by use of the line equation, to obtain the predicted cycles to failure.

It may occur that stress values, and therefore the cycle predictions to failure, found directly from the Gerber equation after substitution into the life prediction equation may not correlate

sufficiently well enough, primarily due to the number of specimens that were plastically strained and skimmed, causing microstructural effects from which strain hardening may alter the fatigue life significantly.

If this is the case a generalised fatigue strength factor will need to be calculated to adjust the fully reversible stress amplitudes so that they may be applied to the S-N and life prediction diagrams. Generalised fatigue factors are useful for ductile materials which correlate well with the maximum distortion energy theory partly due to their highly localised yielding <sup>[31]</sup>.

For bending stresses, endurance limit amplitudes may be calculated from the following equation:

$$S_n = S'_n \cdot C_L \cdot C_G \cdot C_S \cdot C_T \cdot C_R \quad \text{Equation 2.25}$$

Where:

- $S'_n$  = RR Moore endurance limit where  $S'_n$  is a percentage of the UTS
- $C_L$  = load factor = 1.0 for bending
- $C_G$  = gradient factor depending on the diameter of the specimen, normally between 0.9 and 1.0 for bending.
- $C_S$  = surface factor depending on surface and sub-surface conditions
- $C_T$  = temperature factor which is 1 here
- $C_R$  = reliability factor corresponding to a percentage of the standard deviation, e.g. 1 for 50 %, 0.897 for 90 %, 0.868 for 95 %, 0.753 for 99.9 % reliability.

The gradient factor,  $C_G$ , is related to the diameter range of the specimens. For 10 to 14 mm diameter specimens used in this research, a factor of 0.9 is recommended <sup>[31]</sup>.

The surface factor,  $C_S$ , considers surface finishes like scratches or roughness, differences in the metallurgical character of the surface layer or sub-surface, the presence of residual stresses, or any other form of “surface damage”. The reference surface is the mirror polish finish which has  $C_S = 1$  shown in Figure 46. The “machined or cold-drawn” curve may have closer practicality for this research for unpeened and possibly skimmed specimens. This may be useful in finding a more representative endurance limit for the unpeened life prediction model which can serve as a point of reference for other treatments.

Juvinall and Marshek clearly state that these factors serve as a “very rough guide” and that other facets could be considered if necessary, which may be the case here.

There was no specific generalised factor to cover treatments like plastic strain or strain hardening which can permeate the whole depth of the specimen and would be just as reasonable to include it. Strain hardening could be given as  $C_{SH}$ , for example, or  $C_{PS}$  for plastic strain, etc. [31].

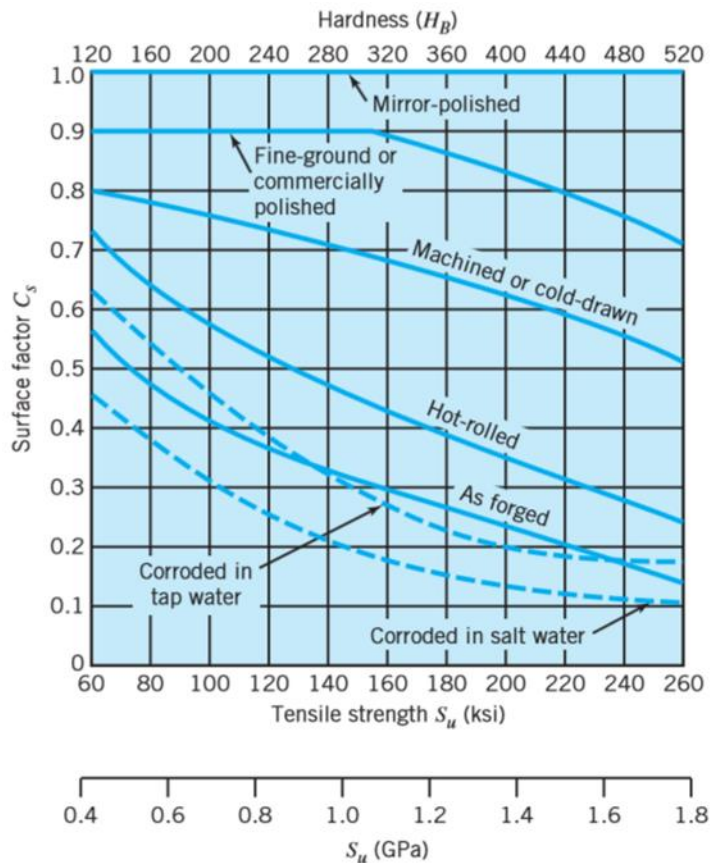


Figure 46 Surface factor vs tensile strength and hardness for steel [31]

For the  $10^3$  cycle limit, the stress amplitude  $S_{1000} = 0.9 \sigma_u$  for ferrous metals but is fairly variable for aluminium alloys and will need to be approximated from S-N diagrams which usually give stress values around  $10^4$  rather than  $10^3$  cycles with a fairly wide scatter. By inspection, values of  $S_{1000}$  even around  $0.7 \sigma_u$  can be considered reasonable [31].

Finally, a representative mathematical life prediction model will hopefully be determined.

### 2.9.6 Summary

Life prediction models have been utilised to create more user friendly mechanisms for engineers to predict the fatigue life more practically by applying generally available properties of materials being used.

The aim here is to find a life prediction model, applying the Juvinall and Marshek method, when specimens are tested at a non-zero mean stress, and recalibrating the applied stress amplitudes to equivalent values for zero mean stress and fully reversible cycles, by means of the Gerber equation, so that fatigue life may be assessed relatively easily. This is due to the generally common availability of data under fully reversible cyclic conditions.

The effects of “surface damage”, residual stresses, microstructural effects as found in plastic straining and strain or work hardening, will need to be considered in the equivalent stress amplitude calculations, which may be possible by finding generalised factors which make the stress amplitudes more representative.

## **CHAPTER 3. EXPERIMENTAL DETAILS**

### **3.1 INTRODUCTION**

In support of the problem statements expressed in par 1.4, the experimentation was planned to help understand the effectiveness of shot peening in promoting the fatigue life of 7075-T6 aluminium alloy round bar, taking into consideration surface residual stresses, micro-structural and micro-hardness parameters.

The details given below explain the development and implementation of the various types of tests performed, as well as the practical issues involved in trying to achieve solutions to the problem statement and accompanying sub-problems, and at the same time bearing in mind the delimitations.

### **3.2 FATIGUE TESTING**

#### **3.2.1 Specimen Details**

##### **3.2.1.1 Material and Machining**

7075-T6 aluminium alloy was purchased from a commercial supplier in the form of 25mm diameter bar. A total of 30 specimens were machined to the diagram shown in Figure 47. All specimens were dog-bone shaped round bars with 120 mm total length and 50 mm effective testing length.

Two specimens, reserved for tensile testing, were of 8 mm diameter to suit the tensile testing machine at UCT.

26 specimens were prepared for fatigue testing of which 22 were of 14 mm diameter, 1 of 12 mm diameter, and 3 of 10 mm diameter. This was done to check for any significant variances in fatigue characteristics. The diagram below shows the 14 mm diameter specimen details. The same profile was adopted for the 10 and 12 mm diameter specimens and they were machined accordingly.

Three of the 22 specimens of 14 mm diameter were reserved as the untreated unpeened benchmark (“as received”) samples, to serve as a point of reference for the others, referred to in par 1.7.8.

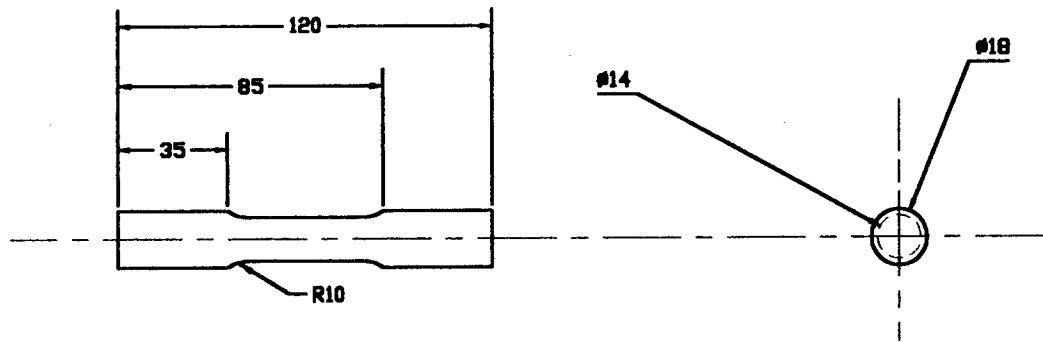


Figure 47 Specimen diagram showing 14 mm testing diameter. The 12 mm and 10 mm test diameter specimens were to the same profile.

### 3.2.1.2 Shot Peening

23 specimens were shot peened according to the Almen metric scale, using cast steel S230 shot, with a 150% covering.

10 specimens, all 14 mm diameter, were sent to the SAA Denel laboratories to the 8 to 14 Almen range.

13 specimens were shot peened by the CPUt laboratories, 9 of 14 mm diameter, 1 of 12 mm diameter, and 3 of 10 mm diameter, all to the 20 to 36 Almen range which was higher than requested.

Fortuitously, although a uniform Almen range was envisaged, to test the fatigue effects on fatigue life and microstructure on some specimens, the higher value was viewed as beneficial to the purposes of this dissertation as the actual values on the Almen test strip were only 22 to 24 A. Heavier shot peening on this material has an effect on the depth of the shot peened layer but not a significant effect on the magnitude of the residual stress.

### 3.2.1.3 Specimen Preparation

**Surface Preparation.** Before fatigue testing the surfaces of all the specimens were prepared by starting with 600 grit and ending with 1200 grit paper, after which they were polished on a rotary machine with lamb's wool, to maintain a consistent surface smoothness with selected samples checked on the surface tester. The surface roughness was tested on the Talysurf surface testing machine at UCT and kept to about  $\pm 0.1 \mu\text{m}$ . This was done to control surface

roughness and reduce stress raisers that encourage early crack initiation, as well as for easier observation of crack initiation identification and growth on the optical microscope.

**Plastic Straining.** 17 specimens, peened and unpeened, were given small incremental plastic strains from 0,1% to 1% microstrain, on the tensile testing machine at CPUT in an attempt to vary surface residual stresses and cause strain hardening to identify fatigue and microstructural effects.

**Radial Skimming.** 9 peened specimens were given a 200  $\mu\text{m}$  radial skim in an attempt to create simulated “unpeened” specimens with surface residual compressive stresses, to investigate the effect on fatigue life for a reasonably normalised microstructure and smooth surface.

**Surface Residual Stress Tests.** Nine specimens were tested on the NMMU Residual Stress Analyser (RESTAN) air turbine centre hole drilling machine, representing unpeened, shot peened, and plastic straining effects. One specimen, shot peened at SAA, was tested at the UCT laboratories on their Air Abrasive Hole Drilling machine.

#### **3.2.1.4 Tensile Test**

Two specimens, DP 31 and 32, were tensile tested to establish the 0.2 % proof stress and ultimate tensile strength of the supplied material. The specimens were machined to the same profile as the other specimens according to Figure 47 but with the smaller diameter at 8 mm to suit the tensile testing machine at UCT.

The tensile testing machine was a Zwick 1484, with 200 kN loading capacity, and 100 kN grips.

The datasheet and load extension graphs generated by the tensile testing machine software program are shown below.

PARAMETER			
7083.100			
a/d $\emptyset$	8.	mm	
L $\emptyset$	36.	mm	
FV	500.	N	
dF	15000.	N	
DIM	2.	MPa	
FORMAT	222.		
V 1	2.	mm/min	
V 2	2.	mm/min	
V MAX	100.0	mm/min	
L-1	0.		
1	509.12	22.08	50.27 - DP31
2	514.72	22.94	50.27 - DP31

Figure 48 Tensile Tester Datasheet for DP 31 & 32

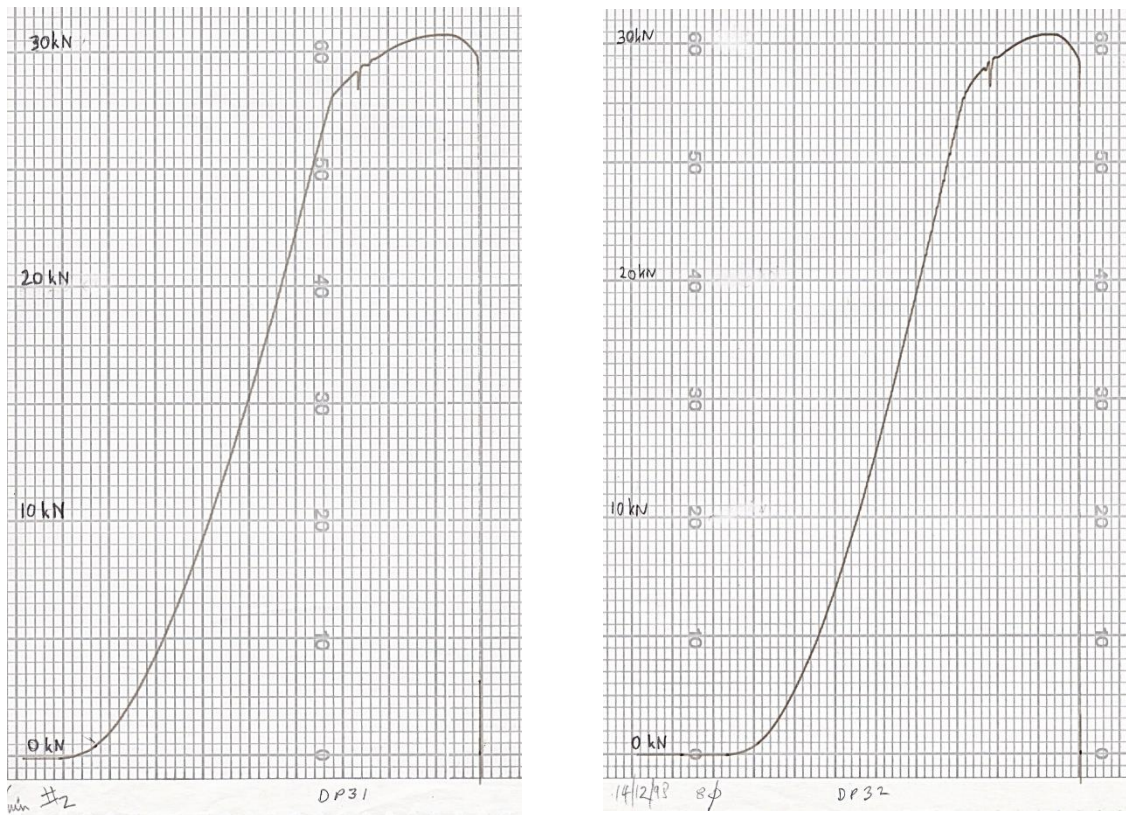


Figure 49 Tensile tester load-extension graphs for DP 31 & DP 32

From the datasheet in Figure 48 it shows the programmed calculations of the ultimate tensile strength as 614.72 MPa for DP 31 and 609.12 MPa for DP 32.

The extension rate was 2 mm per minute.

The average between the two ultimate tensile strengths gave a value of 612 MPa which was used for this research.

From table 1 in par 2.3 it shows the tensile 0.2 % proof stress:ultimate strength as 604:644 MPa taken from the Databook on Fatigue Strength of Metallic Materials Volume 2, and a significantly different 503:572 MPa from the table of physical properties, giving an average of 554:608 MPa with a very large 50/36 MPa margin of tolerance! As can be seen, this is not an uncommon experience. The load-extension graphs in Figure 49, averaged 557 MPa with a  $\pm 6$  MPa margin of tolerance. With such wide margins of tolerance and the proof stress playing a comparative role it was decided to round the 0.2 % proof stress to 560 MPa for convenience and practicality, although making allowances for variances if justified.

The proof stress will be used as a guideline point of reference in the analysis of results when assessing total stresses due to bending and residual effects exceeding yielding limits.

From Figure 49, the clear extension of the elastic-plastic and plastic regions at the top of the graph demonstrates the ductility of 7075-T6 aluminium alloy, as opposed to brittle materials where this region is much closer to the elastic region.

### **3.2.2 Specimen Fatigue Testing**

#### **3.2.2.1 Fatigue Machine**

Fatigue tests were performed by the researcher on the E.S.H. universal servo hydraulic testing machine, shown in Figure 50, at UCT under the supervision of Prof Tait.

Servo hydraulic machines have a continuous feedback system which are ideally suited for fatigue testing.

The servo-controller compares the desired command signal with the actual measured performance by displaying an error signal which is amplified and conveyed to the servo valve. This, in turn, corrects the actuator (piston) movement in the relevant direction ensuring accurate load outputs. The machine has a 50 kN actuator but with a 5 kN load cell so precautions had to be taken not to cause any overloading.

Monitoring, measuring and recording were done through a digital panel meter, oscilloscope, load cell, linear variable differential transformer (LVDT) to measure linear displacement, and cycle counter.

Control, command signal and feedback are done through gain control, limit detectors, ramp and signal generators, and the amplitude measurement unit.

All this offers a bumpless transfer from the stroke to load controls, giving a desirable smooth operation to the specimen being tested.

Specimens were mounted for three point bending on the machine which was set up according to the supervisor's guidelines.

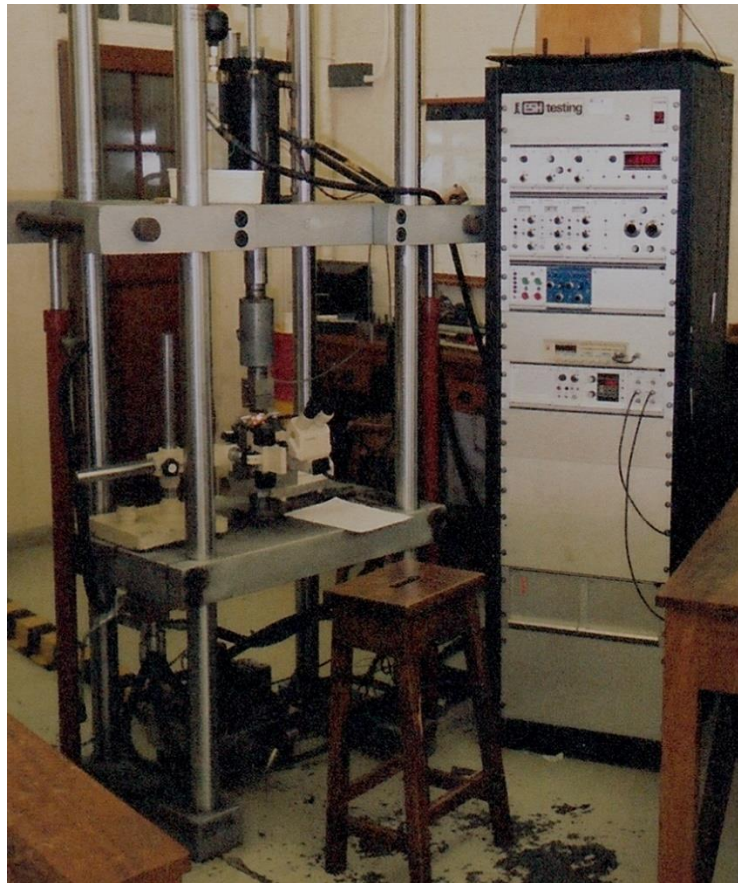


Figure 50 The ESH fatigue testing machine at UCT

The operational capacity of the ESH machine is as follows:

Maximum Load	100 kN
Cyclic Load	50 kN
Frequency	0-15 Hz
Cross-head Speed	> 0.025 mm/sec

### 3.2.2.2 Specimen 3 Point Bending Fatigue Test

Individual specimens were mounted horizontally on two vertical supports 100 mm apart for the oscillating load to be applied downwards at the centre of the specimen, shown below in Figure 51.

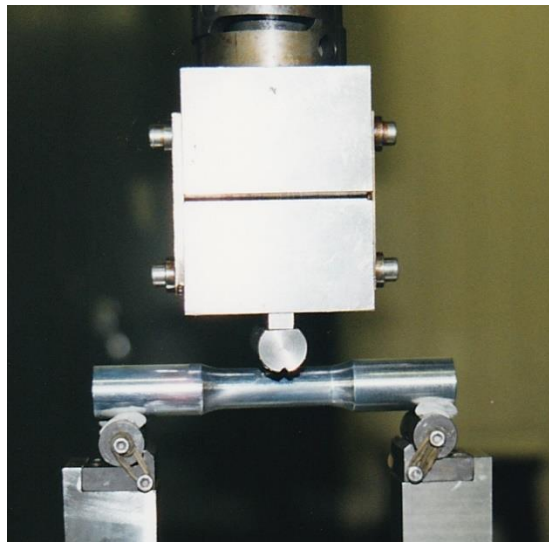


*Figure 51 Specimen mounted on two supports with the cross-head supplying the cyclic load*

All necessary pre-operational settings were made and the optical microscope mounted underneath the centre of the specimen (see Figure 52) to observe crack initiation and propagation during the test.

The minimum and maximum bending stresses were initially set at 48 and 480 MPa tensile for the first 6 specimens, and increased from 52.5 to 525 MPa at the request of the supervisor to make it closer to the yield/proof stress of 560 MPa for the supplied material as discussed in par 3.2.1.4. so the 9,3 % increase of bending stress was justified to test low cycle fatigue tendencies more effectively. This increase of bending stress was taken into account.

During fatigue testing the machine would be stopped to detect any signs of crack initiation after which the number of cycles would be noted. The machine would then be run for a short number of cycles and stopped to record crack lengths with the corresponding number of cycles, until final fracture.

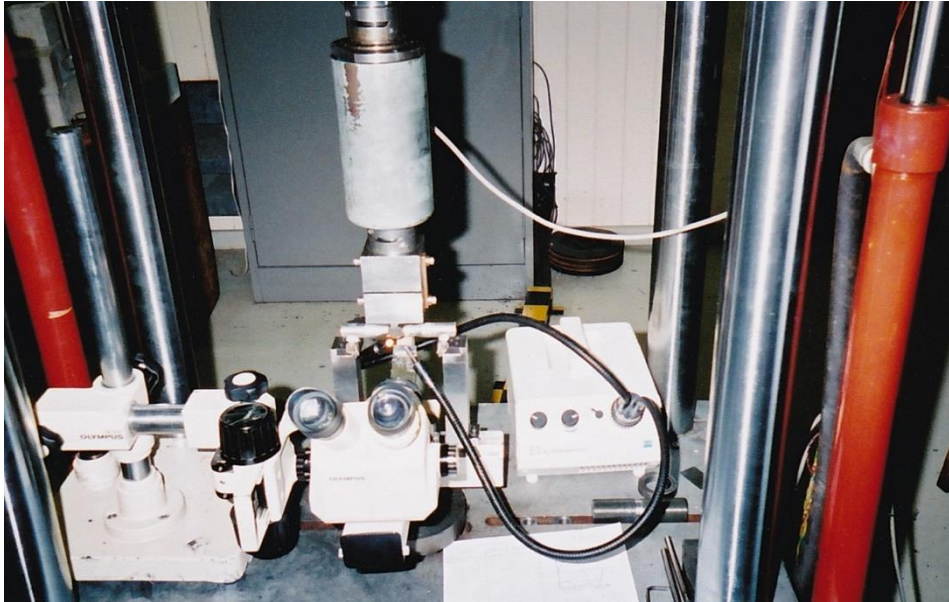


*Figure 52 The complete setup showing the cross-head, load cell, mounted specimen, and optical microscope*

Crack initiation and propagation length observations were made by use of an optical microscope with the corresponding number of cycles recorded at regular intervals from the cycle counter.

Three of the peened specimens were removed from fatigue testing after 20000 cycles, before their expected crack initiation, sent for re-peening to SAA, and then fatigue tested to failure to evaluate whether any significant extension of fatigue life may be found.

The ESH also had an optional “trip on fracture” function which could be used for specimens being fatigue tested overnight. This was the case for DP 38 which took about 7 hours to fracture after a total of 241420 cycles! This would have taken at least an additional 4 hours to stop the machine periodically to inspect for any crack formations.

The downside of this function was that only the number of cycles to final fracture were recorded and not the crack initiation and growth to final fracture. This, however, was fortuitously of relatively little concern for this research, after some changes in direction were

made to the original research at CPUT, as only the number of cycles to final fracture were required.

A total of 26 specimens were fatigue tested. To assist in checking fatigue characteristics, three specimens with 10 mm and one with 12 mm diameters, but with the same profile, were tested on the E.S.H. machine.

### 3.3 RESIDUAL STRESS TESTING

It needs to be noted that, as stated in par 1.1, the residual stress testing was outsourced to NMMU while the author was registered at CPUT. The Figures below are from the actual testing on specimens for this research. The brief description, in par 3.3.1 and par 3.3.2, of the residual stress testing given below is to explain the procedure as it would have taken place, and is covered for the sake of completeness.

#### 3.3.1 Residual Stress Drilling Assembly

NMMU tested the selected specimens on their air turbine hole drilling machine referred to in par 2.5.6, as shown in Figures 53 and 54 below.



Figure 53 Air turbine hole drilling machine at NMMU

The hole drilling assembly consists of a work centre with three axes, a vertical head holding an overhead microscope and drill head containing a high speed air turbine. The microscope

is used to align the drilling axis to the centre of the strain gauge rosette as well as measuring the hole diameter and eccentricity after drilling.

To ensure alignment, the drill head is rotated  $45^\circ$  out of alignment with the optical centring device (OCD) which is adjusted by means of the three axes. When centring has been achieved the drill head is rotated back into alignment with the OCD and hole location.

Drilling is then perpendicular to the work piece.

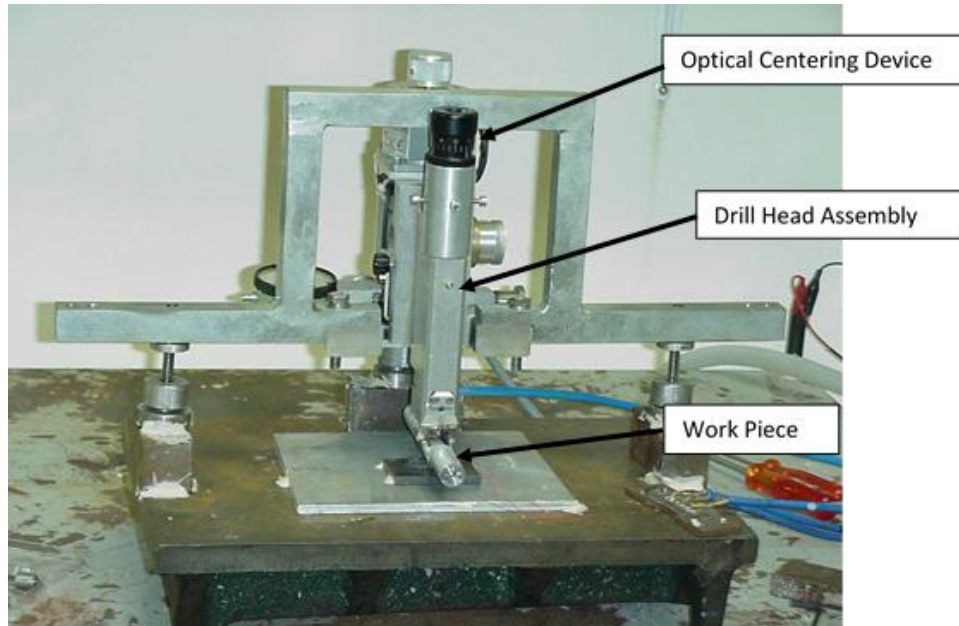


Figure 54 Air turbine hole drilling assembly showing the main components

### 3.3.2 Residual Stress Measurement

The REsidual STress ANalysis (RESTAN) system is fully automatic and its functions are software controlled.

A strain gauge rosette, with three grids connected to a strain amplifier, is attached to each specimen when tested. The drilling assembly, strain amplifier, electronic control unit and computer make up the complete unit. The electronic control unit controls the air supply to the air turbine located at the drilling head of the drilling device. The amplifier, controlled by the software programme measures the strain magnitudes detected by the strain gauges. The software programme controls all the sequential steps during the drilling operation.

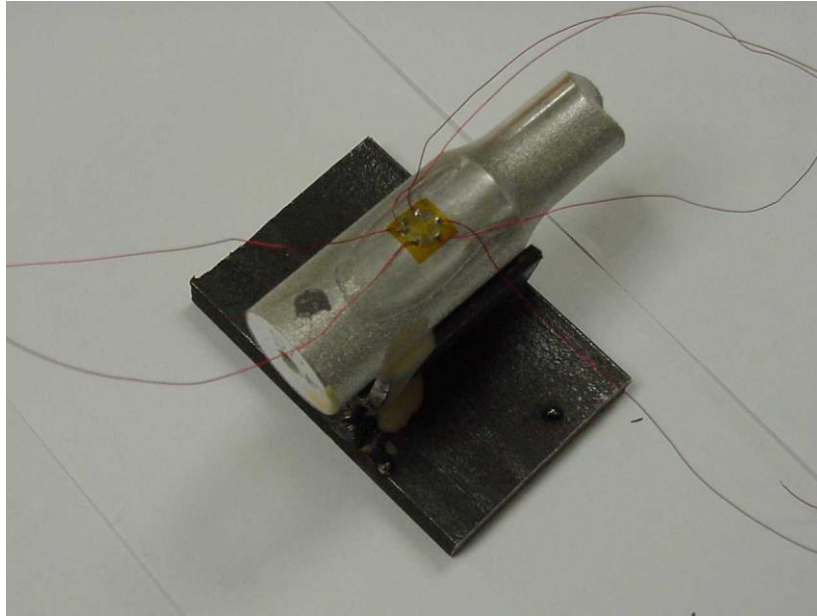


Figure 55 Specimen with strain gauge rosette attached showing the wire connections

The strain gauges were attached after specimen surface preparations according to the manufacturer's directions. The EA-06-031RE-120 type of strain gauge rosette was selected for all tests according to the recommendations on the manufacturer's gauge data sheet enclosed with the set gauges, as shown in Figure 56 below.

The standardised procedure for residual stress analysis by the hole drilling method was then applied as described in ASTM E837.

The drilling was done with 10 to 20 incremental steps ranging from 0.01 to 0.05 mm to a depth of about 0.5 mm, 20 % of the strain gauge radius, depending on the programming. The measurements were entered into the software and the strain results processed. From the three strain values the residual stresses were calculated and transposed into a principal stress format on to a results sheet according to the Integral method as shown in Figure 57.

This information was received by the researcher and used to calculate the residual stress components acting in the same line of action as the applied bending stress values at the corresponding depths. The bulk residual tensile stresses were used to find the equivalent stress for the Gerber equation, and residual stresses were algebraically added together to find the combined resultant stresses at corresponding depths, for analysis <sup>[5]</sup>.

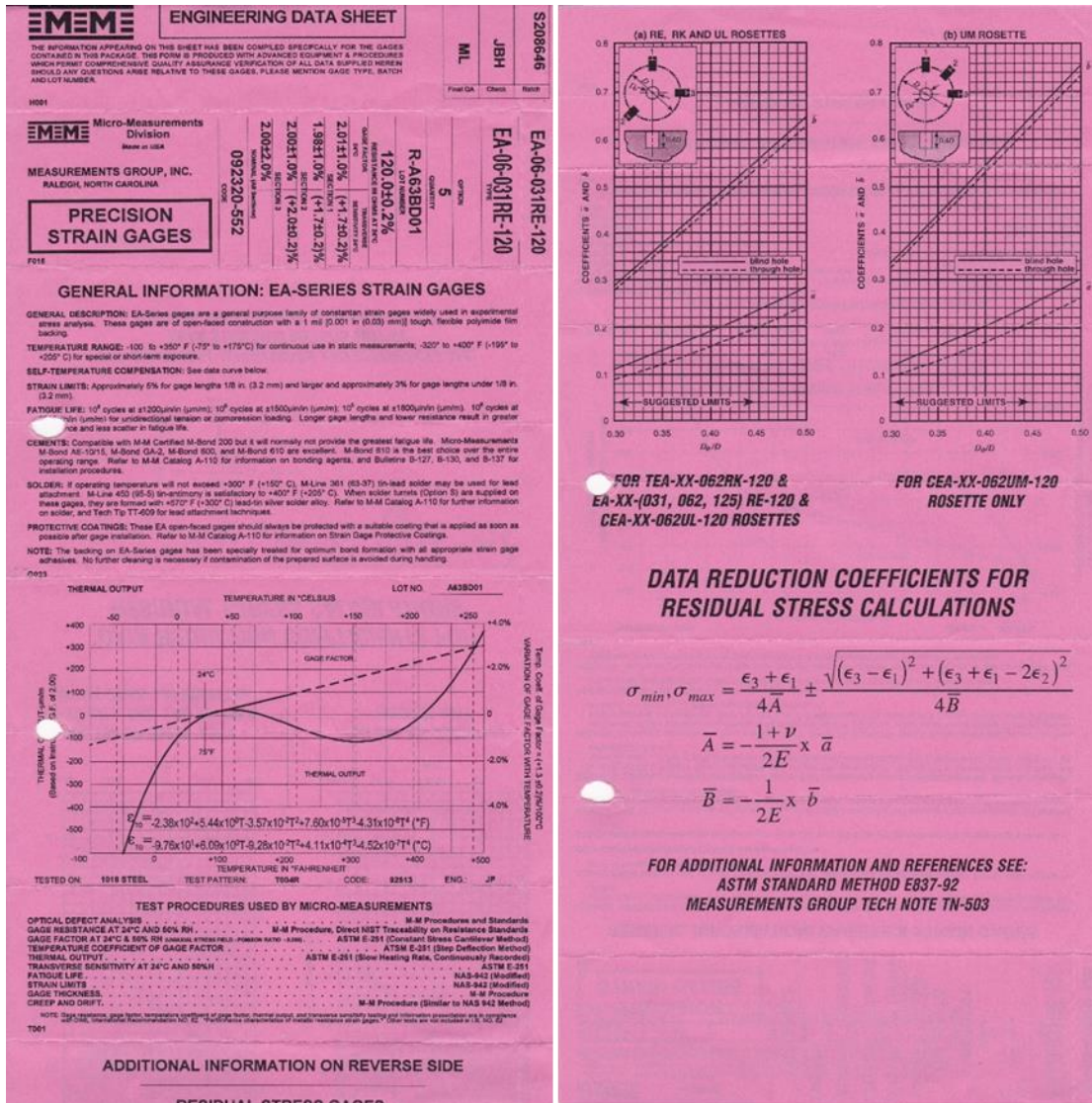


Figure 56 Data sheet for strain gauge rosette EA-06-031RE-120

<b>Residual Stress Analysis</b>						
Dat	2001-11-2					
Descripti	Dp 15 for Don Peters					
Materi	Aluminium 7075					
Treatme	T73					
Strain Gau	EA-031RE-120					
<b>Interpolated values of measured strains and stress calculation results</b>						
(Calculation Metho INTEGRAL )						
Depth [m]	a [1e-	b [1e-	c [1e-	Alfa Angle [°]	$\sigma_{mi}$ [N/mm	$\sigma_{ma}$ [N/mm
0.03	26.77	65.54	26.50	-45.10	-1663.34	-40.19
0.07	72.76	208.88	114.69	-39.84	-3058.07	-365.41
0.12	171.75	394.07	284.07	-35.66	-3666.36	-2151.72
0.17	322.08	569.07	481.31	-32.28	-3428.86	-2569.06
0.23	494.51	705.04	655.76	-29.09	-3034.37	-1328.48
0.28	655.38	798.85	783.53	-25.55	-2664.62	-678.02
0.33	782.43	861.15	864.45	-21.30	-1763.05	-171.26
0.37	869.91	904.36	910.49	-17.45	-675.92	445.52
0.42	925.08	936.38	935.35	-25.09	-5.55	556.87
0.47	960.51	959.97	948.94	-68.91	339.74	784.42

Figure 57 Raw residual stress analysis data sheet showing parameters and principal stresses

### 3.3.3 Magnitude and Calibration of Residual Stresses

The residual stress test results from the NMMU laboratory had values which were found to be unrealistically high, as can be seen from the example in Figure 57 under the principal stress ( $\sigma_{mi}$  and  $\sigma_{ma}$ ) columns, by a factor of approximately 10, compared to typical results found elsewhere, although the proportions of stress distribution were acceptably comparable, necessitating some scaling of the stress values to typically tested values. The reason for this inconsistency could not be ascertained.

To overcome this difficulty, it was decided to match the average highest residual compressive stress value to comparable tests of those found in the tests for this research and proportionately recalculate them by applying a realistic and workable conversion factor.

The typical stress from comparative shot peening on this material of similar dimensions was found from two sources.

In the first source residual stress tests performed at UCT by a final year BSc student, who did some similar fatigue testing as the author, on his set of 3 identical specimens, referred as DP 50 for convenience, to those used in this research with the same shot peening specifications from SAA, the average maximum residual stress was found to be 370 MPa [20]. In the second source, published maximum residual stresses on 7076-T6 aluminium alloy by OSK ranged from 350 to 400 MPa with an approximate average 380 MPa, as described in par 2.5.2.

It seems reasonable to this researcher that a conservatively comparative average maximum residual compressive stress value of 380 MPa will be suitable for the purposes of this research to obtain acceptably accurate results, as the primary value intended to be applied will be the much lower residual tensile bulk stress within the tested region, ranging from 20 to 40 MPa (10 to 15 %) of the maximum residual compressive peak values, which effectively negates stress spikes producing acceptably low error margins.

The highest maximum residual compressive stress components, in line with the applied bending stress, in tests done at NMMU on two specimens were found to be 4233 MPa which was shot peened at SAA (DP4), and 4832 MPa which was shot peened at CPUT (DP38), giving an average maximum of 4533 MPa.

This means that all residual stress values found in the specimens would need to be reduced to a scale by a factor of  $380/4533 = 0,0838$ , which is a ratio of 1: 11,93.

It is expected that this will yield more realistic stress values to validate the analysis. In residual stress test results on commonly used materials widely researched by this author, results should be within acceptable experimental fatigue testing parameters.

This will apply to the scaled residual tensile average (or bulk) stress values needed to calculate the effective mean stress required by Gerber's equation to be applied to the life prediction model, and comparisons with hardness values and fatigue life.

An example of the spreadsheet calculations and stress-depth diagrams, using the values of Figure 57 above, is given in table 3 (especially columns 8 and 9 showing the tested and calibrated values) and Figure 58 for the same specimen DP 15, to illustrate the benefits of the reduction factor.

The residual stress profile of the (benchmark) unpeened specimens is expected to be low in compression and tension, especially when compared to the maximum bending stress. In

Chapter 4, Figure 74 shows the residual stress-depth profile of the untreated DP 1 demonstrating this trend. The low residual stresses were unable to combat the tensile bending stress leading to a low fatigue life average of 32167 cycles.

Detailed calculations and diagrams for all specimens tested for residual stresses will be given as part of the analysis of results.

Table 3 Spreadsheet sample of stress calculations for DP 15 specimen

Depth	$\theta$	$\sigma_2$	$\sigma_1$	$\sigma_{centre}$	R	$2\theta$	$\sigma_{x \text{ res}}$	$\sigma_{x \text{ res}}$	$\sigma_{Bend \text{ Max}}$	$\sigma_{Bend \text{ Min}}$	$\sigma_{x \text{ Tot Max}}$	$\sigma_{x \text{ Tot Min}}$
(mm)	( $^\circ$ )	(MPa)	(MPa)	(MPa)	(MPa)	(Rad)	(MPa)	Calibrated	(MPa)	(MPa)	Calibrated	Calibrated
0								-50	525.0	52.5	475.0	2.5
0.03	-45.1	-1663.3	-40.2	-851.8	811.6	-1.57	-854.6	-71.6	524.5	52.0	452.9	-19.6
0.07	-39.8	-3058.1	-365.4	-1711.7	1346.3	-1.39	-1470.6	-123.3	523.8	51.3	400.5	-72.0
0.12	-35.7	-3666.4	-2151.7	-2909.0	757.3	-1.24	-2666.5	-223.5	523.0	50.5	299.4	-173.1
0.17	-32.3	-3428.9	-2569.1	-2999.0	429.9	-1.13	-2814.3	-235.9	522.1	49.6	286.2	-186.3
0.23	-29.1	-3034.4	-1328.5	-2181.4	852.9	-1.02	-1731.7	-145.2	521.1	48.6	376.0	-96.5
0.28	-25.6	-2664.6	-678.0	-1671.3	993.3	-0.89	-1047.6	-87.8	520.3	47.8	432.5	-40.0
0.33	-21.3	-1763.1	-171.3	-967.2	795.9	-0.74	-381.3	-32.0	519.4	46.9	487.5	15.0
0.35								0.0	519.1	46.6	519.1	46.6
0.37	-17.5	-675.9	445.5	-115.2	560.7	-0.61	344.7	28.9	518.8	46.3	547.7	75.2
0.42	-25.1	-5.6	556.9	275.7	281.2	-0.88	455.7	38.2	517.9	45.4	556.1	83.6
0.47	-68.9	339.7	784.4	562.1	222.3	-2.41	397.3	33.3	517.1	44.6	550.4	77.9

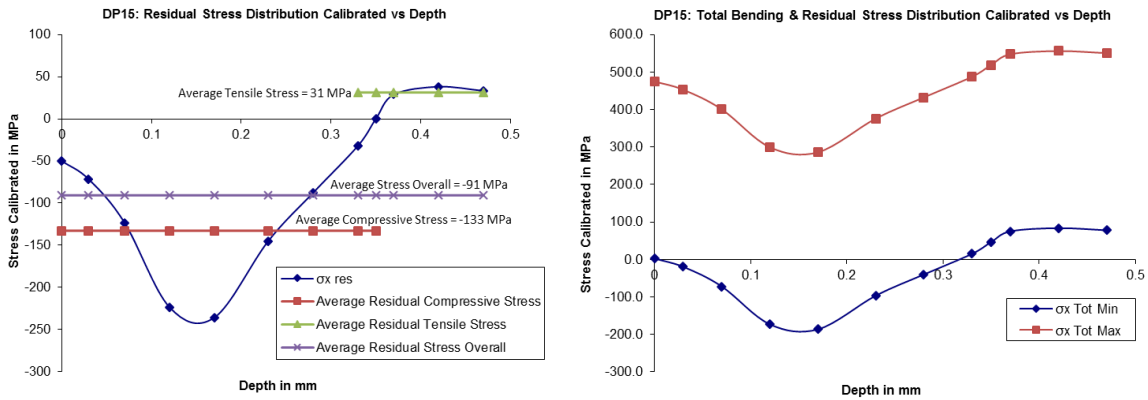


Figure 58 Example of stress-depth diagrams for DP15 specimen

### **3.4 SHOT PEENING AT CPUT**

As mentioned in par 3.2.1.2, 14 specimens were shot peened on the shot peening machine at the CPUT laboratories. The laboratory technician, assisted in part by the researcher, performed the tests.

The Almen tests were done by testing 4 strips in turn by fastening them to the base, as described in par 2.4.4, and the assembly bolted to the shot peening machine table.

The shot peening machine was set according to the specifications in Tables 4, 5 and 6 below.

Table 4 Shot peening machine test settings record at CPUT

	<b>Cape Kaapse Technikon</b>	<b>School of Mechanical Engineering</b> <b>Skool vir Meganiese Ingenieurswese</b> P. O. Box 652, Cape Town, 8000 Posbus 652, Kaapstad, 8000  Tel. –2721 460 3010, Fax / Faks –2721 460 3708

### Shot peening Test Record Haelklopwerk Toetsregister

Lot number and other production control numbers Lot nommer en ander produksiebeheer nommers	
Part number / Onderdeel nommer	
Number of parts in lot / Aantal dele in lot	
Date Peened / Datum geklop	12/12/2000
Shot peening machine used Haelklopwerkmasjien gebruik	No.1
Manual or Automatic, if Automatic record program on table 1 Met die hand of Outomaties, as Outomaties teken program aan op tabel 1	Auto
Specified peening intensity Gespesifiseerde haelklop intensiteit	A 0.20 – 0.36
Actual peening intensity by teststrip #1 Werklike haelklop intensiteit per toetsstuk #2 #3 #4	A 0.24
<b>Shot / Hael</b>	
Type / Tipe	S-230
Hardness / Hardheid	
Number of deformed shapes per sample size Hoeveelheid verformende dele per monster See table 2 / Sien tabel 2	20
Standoff / Wegstaan	100 mm
Exposure time / Blootstellingstyd	7,5 min
Shot flow rate / Hael vloei tempo	544 g/min
Percentage coverage / Persentasie bedekking	150%
Air pressure / Lugdruk	1.7 bar on gauge

Table 5 Program used in automatic peening mode at CPUT

	<b>Cape Kaapse Technikon</b>	<b>School of Mechanical Engineering</b> <b>Skool vir Meganiese Ingenieurswese</b> P. O. Box 652, Cape Town, 8000 Posbus 652, Kaapstad, 8000  Tel. –2721 460 3010, Fax / Faks –2721 460 3708
---	--------------------------------------	--

Table 1. Program used in Automatic peening mode  
 Tabel 1. Program wat vir die Outomatiese wyse gebruik is.

Step Stap	Position Posisie			Speed Spoed			Pressure Lugdruk
	X	Y	Z	X	Y	Z	
1	275	566		40 mm/s	50 mm/s	60 RPM	1950 hPa
2	275	705		40	8	60	1950
3	275	566		40	8	60	1950
4	275	705		40	8	60	1950
5	275	566		40	8	60	1950
6	275	705		40	8	60	1950
7	275	566		40	8	60	1950
8	275	705		40	8	60	1950
9	275	566		40	8	60	1950
10	275	705		40	50	60	1950

Number of repeats?  
 Hoeveelheid herhalings ? ...3.....

Operator  
 Operateur.....A. C. Esterhuyse

Table 6 Specifications for various types of shot at CPUT. S230 steel shot was used

	<p><b>Cape Kaapse Technikon</b></p>	<p><b>School of Mechanical Engineering Skool vir Meganiese Ingenieurswese</b> P. O. Box 652, Cape Town, 8000 Posbus 652, Kaapstad, 8000</p> <p>Tel. –2721 460 3010, Fax / Faks –2721 460 3708</p>
---	---	---

Table 2. Maximum allowable number of unacceptable deformed shapes.  
Tabel 2. Maksimum toelaatbare hoeveelheid onaanvaarbaar vervormde fatsoene.

Cast iron Shot Sizes	Cut Wire Sizes	Glass Bead Sizes	Ceramic Bead Sizes	Sample Size	Maximum Allowable Number of Unacceptable Deformed Shapes
Gietyster Hael Groottes	Gesnyde Draad Groottes	Glaskraal Groottes (mm)	Keramiek-kraal Grootte (mm)	Monster Grootte (mm)	Maksimum toelaatbare hoeveelheid onaanvaarbaar vervormde fatsoene
930		3.3528 - 2.3876		25 x 25	8
780		2.8194 - 2.0066		25 x 25	11
660	CW-62	2.3876 - 1.6764		25 x 25	16
550	CW-54	2.0066 - 1.4224		25 x 25	22
460	CW-47	1.6764 - 1.1938		25 x 25	32
390	CW-41	1.4224 - 0.9906		25 x 25	45
330	CW-35	1.1938 - 0.84074	1.1684	12.5 x 12.5	16
	CW-32			12.5 x 12.5	18
280	CW-28	0.9906 - 0.70612		12.5 x 12.5	23
230	CW-23	0.84074 - 0.59436	0.8382	12.5 x 12.5	32
190	CW-20	0.70612 - 0.50038		12.5 x 12.5	45
170		0.59436 - 0.4191	0.6096	6.3 x 6.3	16
130		0.50038 - 0.35306		6.3 x 6.3	23
110		0.4191 - 0.29718	0.4318	6.3 x 6.3	32
70		0.35306 - 0.24892		6.3 x 6.3	45
		0.29718 - 0.21082	0.3048	3.2 x 3.2	16
		0.24892 - 0.1778		3.2 x 3.2	22
		0.21082 - 0.14986	0.1524	3.2 x 3.2	31

Some clarity of tables 4, 5 and 6 is required.

Table 4 shows the peening intensity setting to be A 0.20 to 0.36 with the actual value obtained as A 0.24. These values should be read as A 20, A 36 and A 24 respectively to conform to standard formatting.

Table 5 shows 3 repeats, meaning the first test and 3 subsequent tests on the Almen strips shown in Table 4.

The number of deformed shots was 20 in Table 4 for the actual test which was well within the maximum allowable amount of 32 shown on Table 6.

The pressure given as 1.7 bar in Table 4 corresponds to 1700 hPa gauge which is 1801 hPa absolute pressure, 149 hPa (7.6 %) below the designated pressure of 1950 hPa in Table 5, possibly explaining the peening intensity of A 24 instead of a higher amount, which turned out to be a more favourable option.

From Table 4, it can be seen that the test had an exposure time of 7.5 minutes with the S230 cut wire shot at a flow rate of 544 g/min at the required 150 % coverage.

The shot peening machine was set to operate at the same settings as in Table 4 so that the specimens would receive the same treatment as the Almen strips.

All 13 specimens were then shot peened in turn.

### **3.5 MICROSTRUCTURAL TESTING**

Microstructural testing consisted of four components, plastic straining, diametral skimming, Vickers microhardness tests, and scanning electron microscope (SEM) tests.

#### **3.5.1 Plastic Straining**

The purpose of plastic straining was to reduce the residual stresses induced by shot peening and see whether it had any significant effect on the microstructure to influence the fatigue life.

Plastic straining was performed at the CPUT (then Cape Technikon) tensile testing laboratory.

18 specimens, 3 unpeened, 6 shot peened at SAA, and 9 shot peened at CPUT, were successfully plastically strained on their tensile testing machine. The specimens had strain

gauges, with their data sheet shown in Figure 59, attached to them by using the same procedure as with the residual stress testing at NMMU.

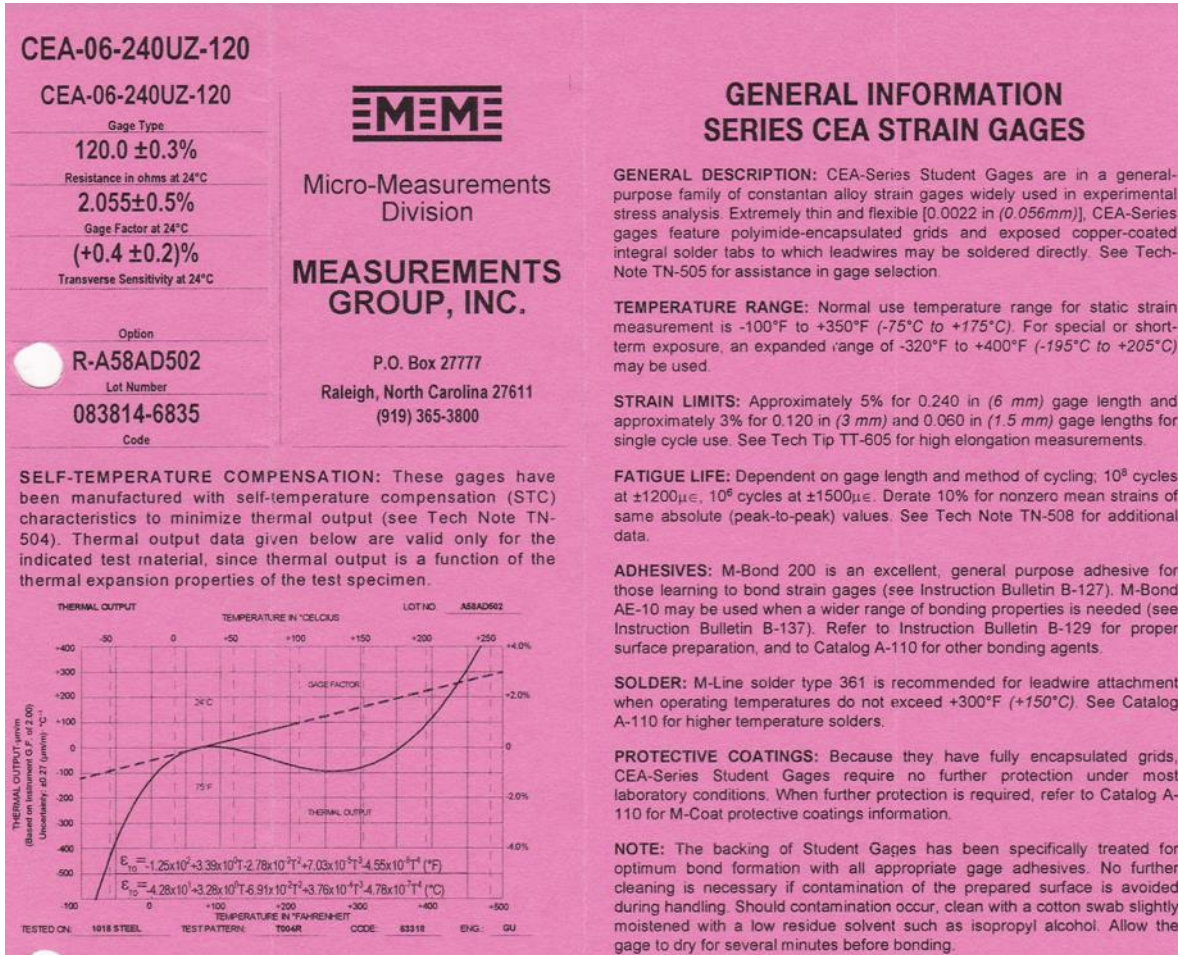


Figure 59 Data for strain gauge used for plastic straining at CPUT

For the 14 mm diameter specimens the loading was taken up to 80 kN when the early stages of plastic straining started taking effect. The load was increased incrementally with the strains noted until the strain level was an estimated value above the intended plastic strain, aware that the material was in the elastic-plastic range, so that when the load was relaxed the material would have plastically strained at a slightly lower required value. When the desired estimated applied strain was reached the load was decreased to check whether there was the required permanent plastic strain, and if not, the load was taken to its previous level and incrementally increased again.

It was sometimes necessary to repeat this procedure on a trial and error basis, especially at the beginning of the testing before more familiarity with the straining behaviour of the specimens became evident, until the required permanent plastic strain was reached. The necessity of repeating the procedure may have been the reason why the final load was not always comparatively proportional to the final permanent strain because 7075-T6 aluminium alloy has a tendency to dynamically recover as the load is increased. This trend was striking when the two other specimens (DP 31 and 32) earmarked for tensile strength testing were tensile tested to fracture.

The 10 mm diameter specimens were loaded up to 40 kN before plastic strain started taking effect. A similar loading procedure was followed to attain the desired strains. Table 7 refers.

Table 7 Specimens that were plastically strained

No of Specimens	Specimen No DP	Specimen Diameter in mm	Load in kN	Plastic Strain in % Microstrain
1	5	14	85	0.5000
2	13	14	85.6	0.4103
3	18	14	84	0.2094
4	19	14	85	0.1703
5	20	14	86	0.4885
6	21	14	85.2	0.3865
7	24	14	80	0.2000
8	25	14	85.8	1.0072
9	26	14	87	0.5960
11	28	14	86	0.2026
12	29	14	85	0.5767
13	34	14	88	0.6000
14	35	14	80	0.2815
15	36	14	86.6	0.5106
16	41	10	43	0.1500
17	42	10	43	0.3506
18	43	10	43	0.4617

### 3.5.2 Diametral Skimming

The aim of diametral skimming, as described in par 2.5.7 and 2.6.1, is to remove the shot peened layer to reveal an “unpeened” surface where the level of plastic deformation could be regarded as insignificant, but where there may be compressive residual stresses present. The depth of the shot peened layer is around 200  $\mu\text{m}$ , as described in par 2.5.3, so it was decided to skim the surface of the specimens on a lathe by that amount and then fatigue test them to gauge the effect on fatigue life.

9 specimens, all shot peened at CPUT, were selected for skimming, 2 with no plastic straining and the balance with varied degrees of plastic straining. One specimen was not fatigued and used for micro-hardness testing.

The results are shown in table 8 below.

Table 8 Fatigue life of shot peened specimens with various plastic straining and a 200  $\mu\text{m}$  surface skim

No of Specimens	Specimen No DP	Plastic Strain in % Microstrain	Fatigue Life, $N_f$ cycles to failure
1	25	1.0072	57840
2	26	0.5960	38740
3	27	0.8265	51890
4	34	0.6000	34180
5	36	0.5106	N/A
6	37	0	309240
7	42	0.3506	40890
8	43	0.4617	41130
9	45	0	282210

Although the results and analysis will be discussed later in chapter 4, it is easily seen that specimens with no plastic straining revealed the highest fatigue life by a high margin, and it may also be interesting to note the perhaps unexpected *increase* in fatigue life with an increase in plastic straining! This may reveal some interesting characteristics of microstructural effects compared to the residual stresses in these specimens.

### 3.5.3 Microhardness Tests

As stated in par 2.7, microhardness can be used to observe changes in hardness on a microscopic scale, and the tests done were to offer some indication whether this change was evident, and what significance could be ascertained from the results.

Microhardness tests were performed on 3 specimens by applying the Vickers test. The specimens were prepared by cutting the specimens directly through the diameter, as shown in Figure 27 in par 2.7, and the diametral surface prepared for the test.

A diamond indenter was impressed in the diametral surface by a 200 gram load at 0.15 mm increments along the diameter to a depth of 2.05 mm and then 0.5 mm increments to a depth of 9.05 mm on the specimens.

In each case the  $d_1$  and  $d_2$  measurements were recorded across the indentations by use of the microscope and substituted into the formula for the hardness value with the results shown in table 9.

Table 9 Vickers hardness - diametral depth experimental values

Description	Value/No			Unit
	DP 20	DP 36	DP 45	
Specimen	DP 20	DP 36	DP 45	
Peening	8 to 14	20 to 36	20 to 36	A
$\epsilon_{pl}$	0.4885	0.5106	0	% $\mu$ Strain
$K_{1c}$	28.6	28.6	28.6	MPa.m <sup>1/2</sup>
Skim	0	200	200	$\mu$ m
$N_{failure}$	116250	N/A	282210	cycles
$\sigma_{uts\ ave}$	612	612	612	MPa
$\sigma_{yield\ ave}$	560	560	560	MPa
$R_{stress\ ratio}$	0.1	0.1	0.1	
$\sigma_{bend\ min}$	52.5	582.5	52.5	MPa
$\sigma_{bend\ max}$	525	525	525	MPa
Diameter	14	14	12	mm
Hardness	Vickers	Vickers	Vickers	200gm

Test Position	Depth (mm)	HV Number		
		DP 20	DP 36	DP 45
1	0.10	171	156	162
2	0.25	176	161	176
3	0.40	177	175	166
4	0.55	178	170	164
5	0.70	181	171	163
6	0.85	177	156	166
7	1.00	186	163	166
8	1.15	178	164	163
9	1.30	174	163	169
10	1.45	176	165	166
11	1.60	170	161	167
12	1.75	174	162	164
13	1.90	172	164	162
14	2.05	181	163	168
15	2.55	171	159	162
16	3.05	167	158	166
17	3.55	169	155	163
18	4.05	176	160	166
19	5.05	157	156	170
20	6.05	166	157	158
21	7.05	164	156	159
22	9.05	164	161	154
Average		173.0	161.6	164.5

The trendlines in the graphs of the 3 specimens in Figure 60 show a steady reduction on HV numbers with depth, although with a fairly wide scatter.

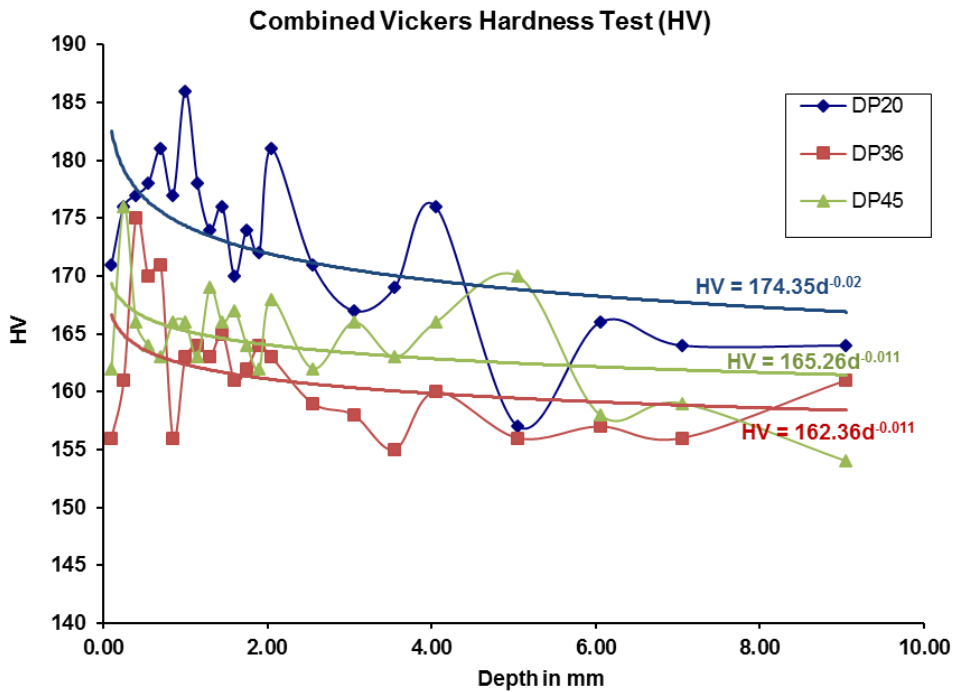


Figure 60 Vickers hardness vs diametral cross-section for 3 specimens

### 3.5.4 Scanning Electron Microscope (SEM) Tests

Six specimens, DP 19, 20, 27, 36, 37, and 45, were given SEM tests to show the fractured surfaces to highlight microstructural features, crack initiation and end crack fast fracture characteristics.

Selected fractographs of characteristics common to all of the tested specimens with various magnifications are shown in the Figures below. Comments on specific characteristics relating to fatigue are given with the fractographs.

Fractographs will be shown including details of their features in the analysis in Chapter 4.

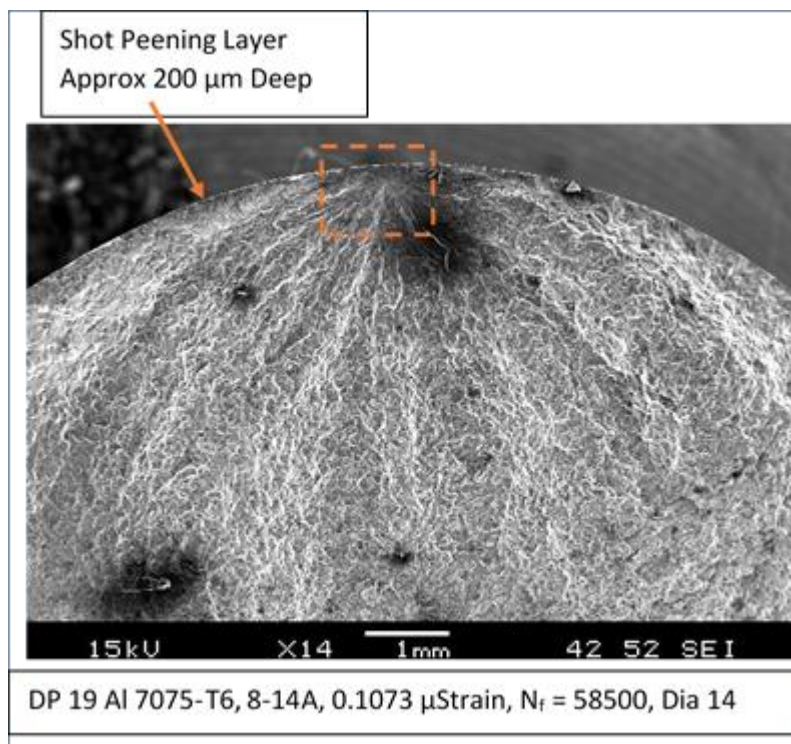


Figure 61 DP 19 showing the crack initiation site and next frame

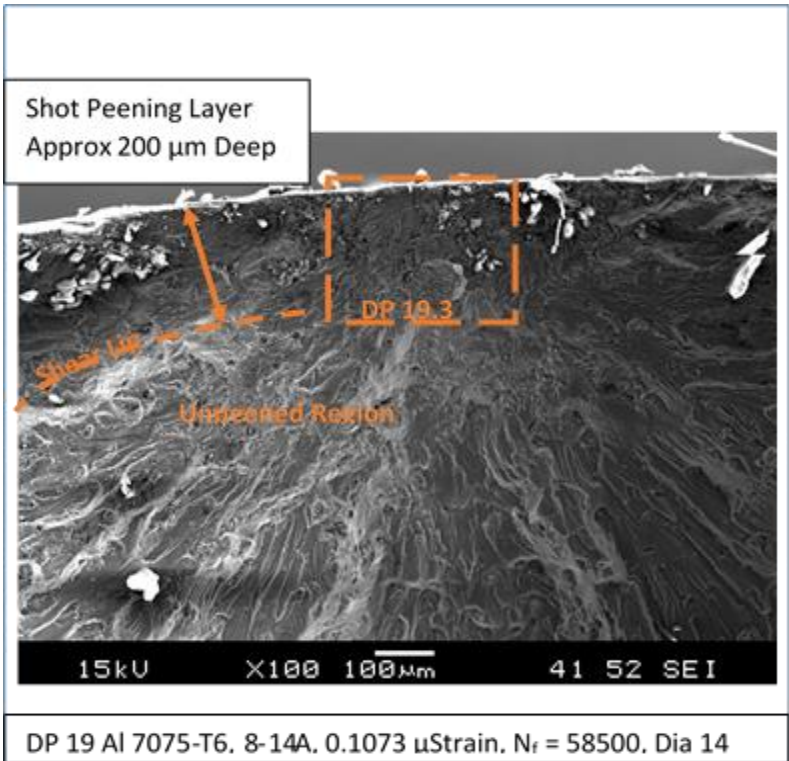


Figure 63 DP 19 clearly showing the sub-surface crack initiation site on the right, the shot peened layer and unpeened region

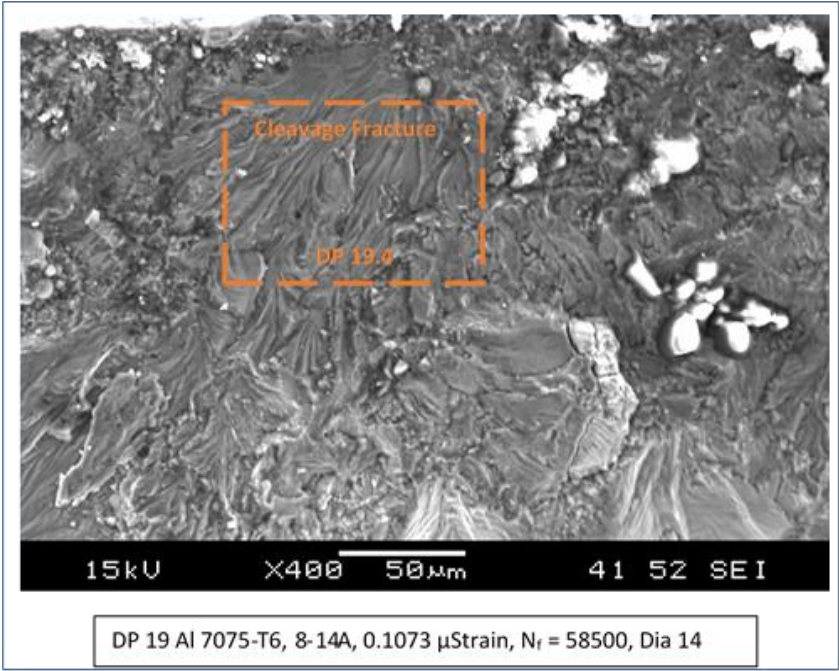


Figure 62 DP 19 showing the whole shot peened depth

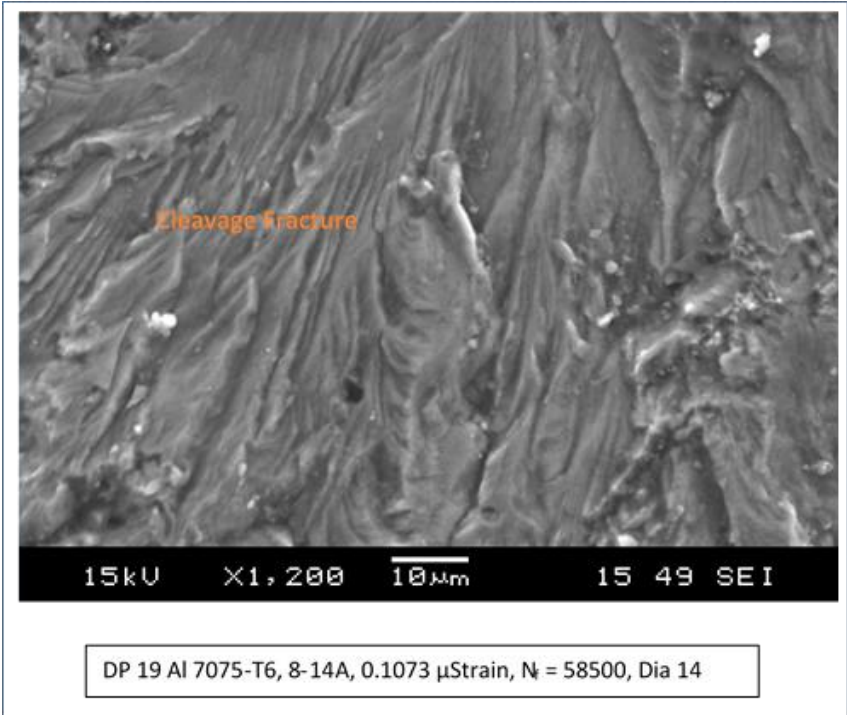


Figure 65 DP 19 showing magnification of the shot peened region and the typical shear cleavage with high atomic steps of ductile materials

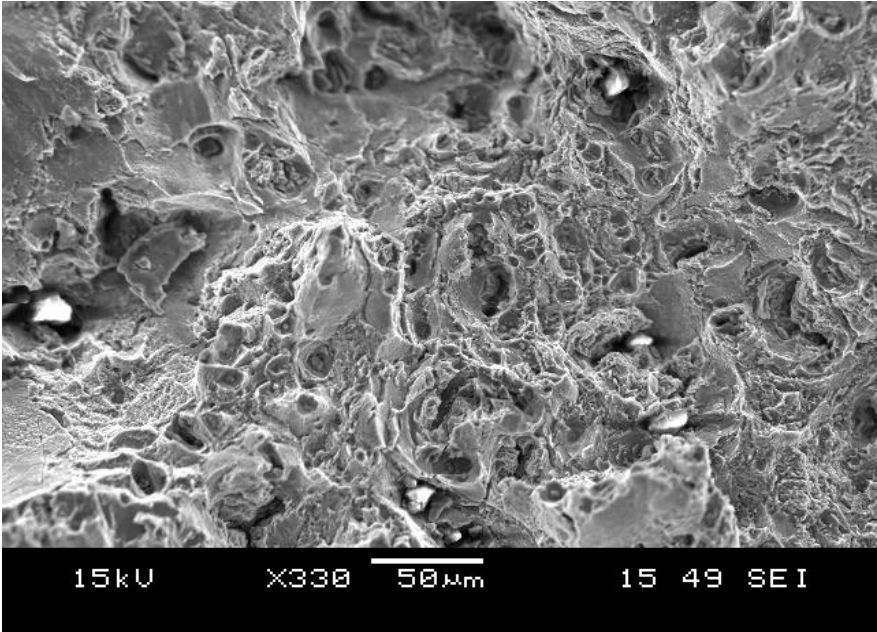


Figure 64 DP 20. Commonly seen ductile dimples with significant plastic deformation between dimples. White coloured defects can be seen at the centres of some dimples which may have contributed to the dimple formation

The following three fractographs show transgranular and intergranular cracks amidst ductile dimples with embedded defects.

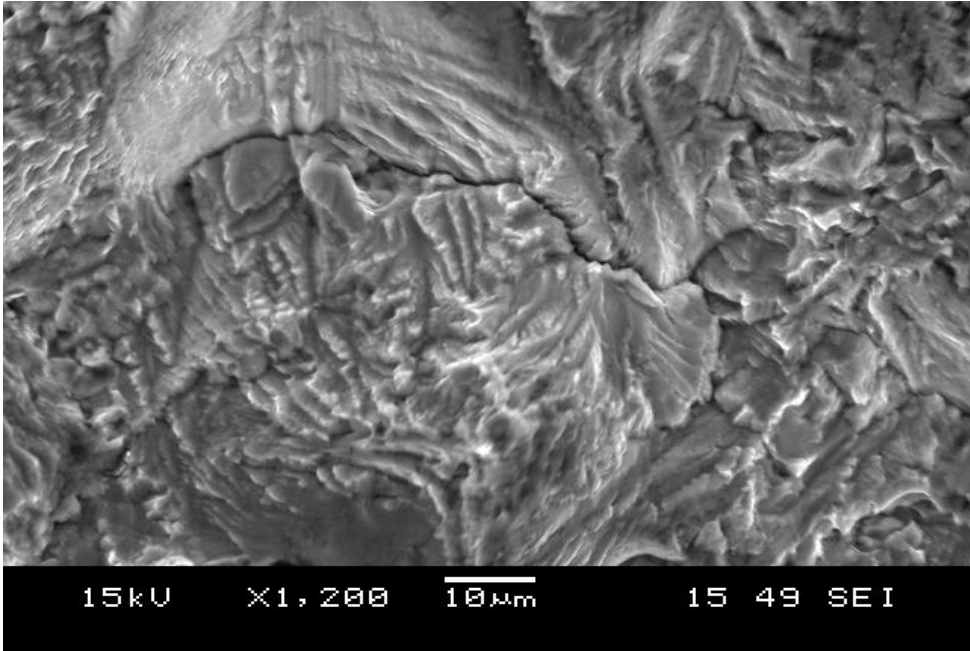


Figure 67 Crack initiation site of DP 27. Transgranular cracking shown at the centre with small intergranular cracking branching off on the right end of the crack

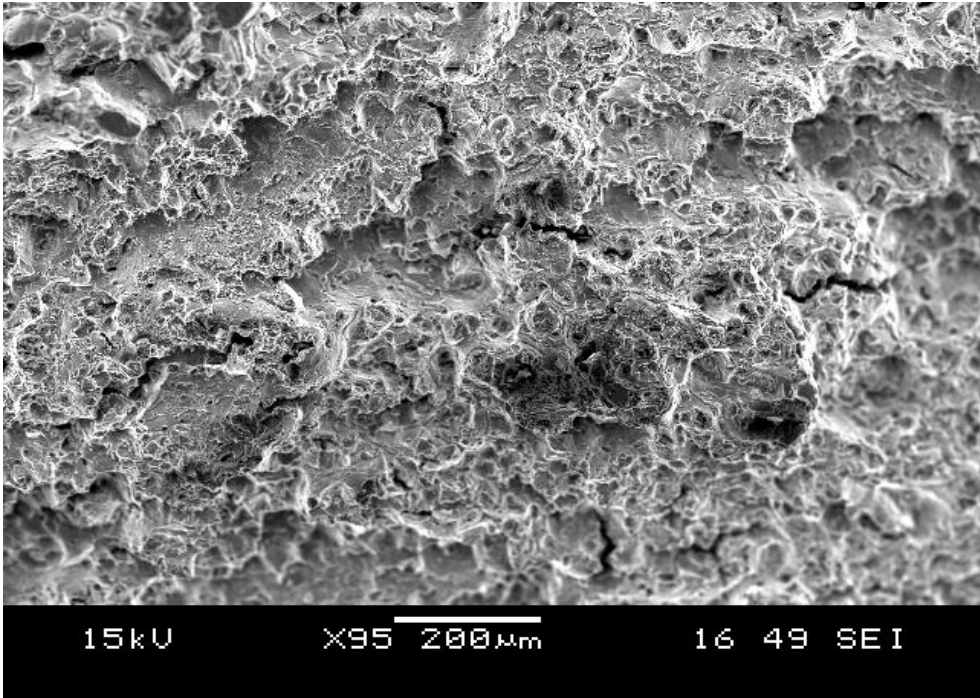


Figure 66 DP 27. Fast fracture site at the specimen centre. Multiple cracks can be seen in the ductile dimpled region

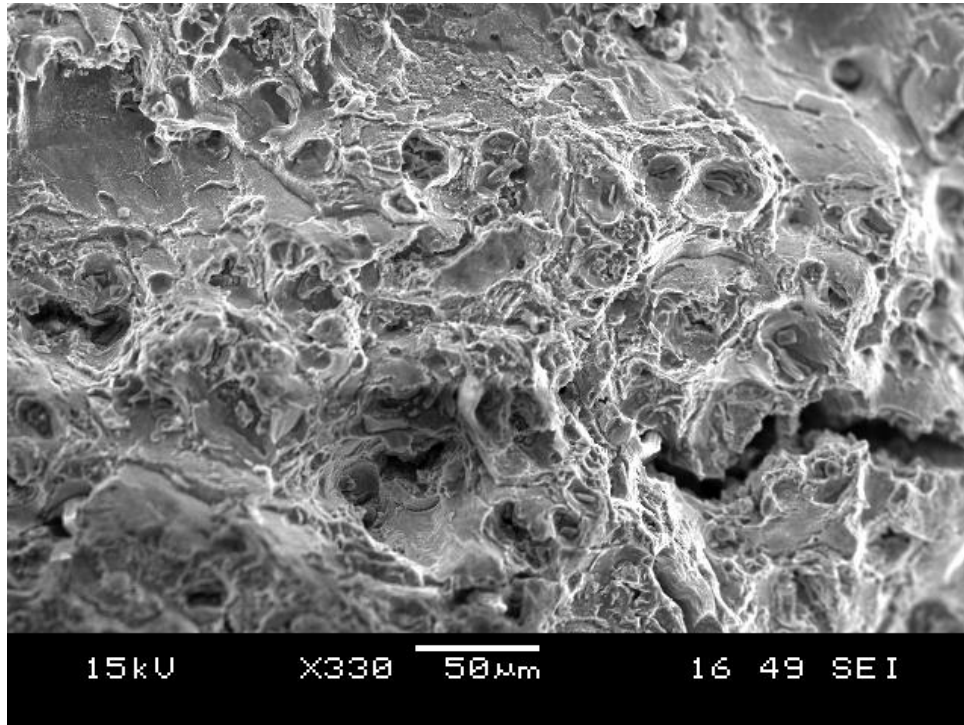


Figure 68 DP 27. Magnification of centre- right hand crack in figure 61 showing the crack extension through the centres of the dimples where probable defect elements are embedded, as seen on the dimple to the left of the crack

### 3.6 SUMMARY

Experimentation was divided into four main sections which were fatigue testing, residual stress testing, shot peening, and microstructural testing.

The **fatigue testing** section involved the preparation of total of 30 specimens by initially machining them to the required size from commercially supplied raw bar, selection of the number of specimens for specific treatments, and finally fatigue testing 26 specimens.

Three specimens were left untreated to serve as a fatigue life benchmark and 2 unpeened specimens were reserved for tensile testing at UCT.

23 specimens, 10 at the 8 to 14 Almen range at SAA and 13 at the 20 to 36 Almen range at CPUT, were shot peened using S230 shot with 150 % covering. The shot peening at CPUT was done at a higher range than required but turned out to be between 22 and 24 Almen which proved to be beneficial to this research.

17 specimens, unpeened and shot peened, were given small incremental plastic strains from 0.1 % to 1 % microstrain and 9 peened specimens were given a 200  $\mu\text{m}$  radial skim. 9 specimens were sent for residual stress testing at NMMU and 1 set of 3 specimens was tested at UCT.

Fatigue tests were done on the ESH universal servo hydraulic testing machine at UCT, which has an ideally suited continuous feedback system for fatigue testing. The specimens were fatigue tested by using horizontally mounted 3 point bending.

A cyclic bending stress ratio of 0.1 was applied, initially set at 48 MPa and 480 MPa for 6 specimens, and the changed to 52.5 MPa and 525 MPa at the request of the supervisor to make it closer to the 560 MPa proof stress.

During the fatigue testing the machine was stopped to check for any fatigue cracks, by using an optical microscope, where the crack length and number of cycles was recorded, until final fracture. Three unpeened specimens were prefatigued to 20000 cycles and sent for shot peening before being fatigued to failure.

**Residual stress testing** was done at NMMU for the researcher on their air turbine hole drilling machine applying the RESTAN fully automatic system with software control. A three grid strain gauge rosette was attached to each specimen and connected to the strain amplifier. The strains were recorded at depths from 0.3 mm up to 0.5 mm and the principal stresses recorded at each depth increment.

The recorded stresses were found to be too high compared to typical values found in literature, although were in good proportion. A conservative average maximum residual compressive stress of 380 MPa was found from literature and the residual stress-depth tests at UCT to be suitable for this research.

A conversion factor of 0.0838 was calculated between the 380 MPa average maximum residual stress decided upon, and the average of the two maximum residual stresses found in the test. This factor was used to calibrate all the residual stress results to conform to more realistic values.

The calibrated average residual tensile stresses required for application in the Gerber equation were found to be within acceptable margins.

**Shot peening at CPUT** was done on 13 specimens. Almen tests were done on 4 testing strips and used to set the shot peening machine. The actual peening intensity was found to be 22 to 24 Almen at a gauge pressure of 1.7 bar, exposure time of 7.5 minutes at a flow rate of 544 g/min, at 150 % coverage. The higher peening intensity turned out to be beneficial.

**Microstructural testing** was in the form of plastic straining, diametral skimming, Vickers microhardness tests, and scanning electron microscope (SEM) tests.

Plastic straining was done on the tensile testing machine at CPUT on 18 specimens, 3 unpeened, 6 shot peened at SAA, and 9 shot peened at CPUT. Strain gauges were attached to the specimens and the wires attached to an amplifier. A tensile load was slowly placed on the specimens, relaxed periodically to check whether permanent plastic strain had been achieved, and loaded again until the required plastic strain had been reached. The plastic strains ranged incrementally from 0.1703 % to 1.072 % microstrain with the results shown in table 7.

**Diametral skimming** to a depth of 200  $\mu\text{m}$  was performed on 9 specimens that were shot peened at CPUT of which 2 specimens had no plastic straining. The results in table 8 show plastic straining reduced fatigue life overall but also experienced an unexpected increase in fatigue life approximately directly proportional to the plastic strain.

**Microhardness tests** were performed on 3 specimens by applying the Vickers hardness test using a diamond indenter with a 200 gram load at incremental gaps along the diametral surface. Indentation measurements were made and the hardness values found with the results shown in table 9 and Figure 60. The results are to be used to find any possible relationship between the microhardness and residual stress.

**Scanning electron microscope (SEM) tests** were performed on 6 specimens representing the various designated treatments to show microstructural features on the fractured surfaces. Fractographs shown in Figures 61 to 68 demonstrated crack initiation and end crack fast fracture, shot peened depth, shear cleavage, plastic deformation between dimples, as well as transgranular and intergranular cracking.

The results of the different experiments performed will be analysed in the next chapter.

## **CHAPTER 4. ANALYSIS OF RESULTS**

### **4.1 INTRODUCTION**

The purpose here is to analyse the results bearing in mind the parameters articulated in the problem statement and sub-problems, together with the hypothesis and delimitations.

The approach will be to cover the parameters topically and then combine the relevant ones to analyse the overall effect so that a balanced and useful life prediction may be found.

The topics will start with the overall fatigue analysis profiling which will be analysed groupwise according to the various specimen treatments and tests with regard to fatigue life, residual stress-depth, microstructural effects including plastic straining, microhardness, and fractography.

The analysis of the fatigue life of specimens with various treatments will be compared to that of the untreated unpeened specimens, which will serve as the point of reference benchmark for this research, as stated in par 1.7.8.

The final part will include the roles of the topics covered to applying the Gerber equation together with the Juvinall and Marshek life prediction model to produce life prediction models for the 7075-T6 aluminium alloy bar used in this research.

### **4.2 FATIGUE ANALYSIS PROFILES**

Fatigue testing results have been categorised into groups of common treatment to generate general trends for analysis. Spreadsheets together with fatigue life performance graphs will be used for each group to highlight their characteristics and fatigue life relation to each other.

#### **4.2.1 General Test Specimen List and Groupings**

The spreadsheet below in Table 10 is a groupwise list of all the specimens used in this research, a summary of their treatments, types of testing, and final fatigue life.



It will be evident from the specimen number sequence that some specimens are missing from this list. The reason for this is that 3 were damaged and the rest were part of the previous research and not applicable here.

It will also be seen that there is a set of 3 specimens numbered as a single specimen DP 50, referred to in par 3.3.3, in Group 9 included in the list to serve for fatigue life and residual stress reference purposes, with permission, to represent specimens that were shot peened at SAA with Almen intensity 8 to 14, for comparison with DP 38 which was shot peened at CPUT with Almen 20 to 36.

DP 4 in Group 9 and DP 36 in Group 11 were fatigue tested but problems were experienced during the tests compromising the fatigue results, rendering them unusable and effectively with the status of being “not fatigued” for this research. However, DP 4 was given a residual stress test, and DP 36 a Vickers microhardness (HV) and scanning electron microscope (SEM) tests which will be useful for the analysis.

The specimens have been split up into the 11 groups, according to common or comparative treatments, described under the “Notes” column on the extreme right, which correspond to the treatment columns UP (unpeened), UP PS (unpeened, then plastically strained), UP PF SP<sub>saa</sub> (unpeened, plastically strained, and then shot peened at SAA), etc. The abbreviations are explained in the table legend.

#### **4.2.2 Fatigue Tests: Groupwise**

The groups are arranged into five comparative tests to analyse the fatigue life patterns for various treatments and their relation, if any, to different groups. Fatigue life comparisons relative to specimens in each grouping and other groups will be made to assess fatigue life improvements per treatment process, with possible reasons for them.

Although the graphs show fatigue life related to plastic strain it will serve for reference purposes in this section as plastic strain will be analysed in its own section.

##### **Test 1: Groups 1, 2 and 9**

The purpose is to compare the fatigue lives of unpeened (UP) specimens in group 1 to unpeened and plastically strained (UP, PS), as well as unpeened, plastically strained and

shot peened at CPUT (UP, PS, SP<sub>ct</sub>) in group 2. Group 9 with shot peened specimens is for comparison purposes to unpeened specimens.

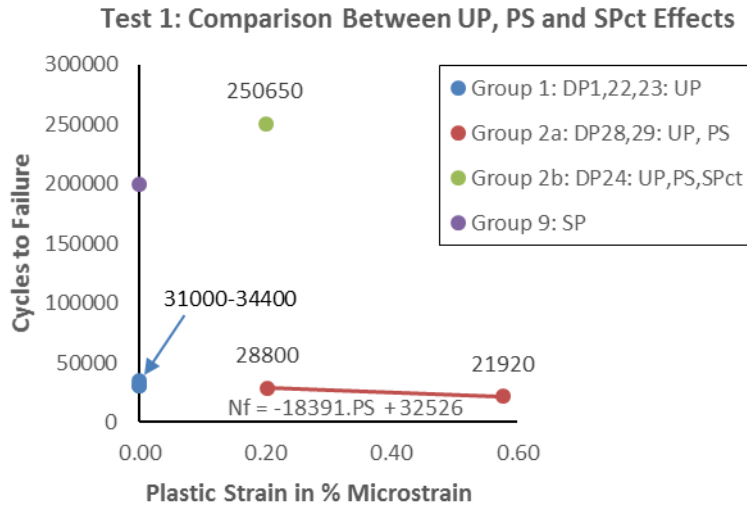


Figure 69 Fatigue test 1: comparison for groups 1, 2 and 9

Figure 69 demonstrates that the UP and PS specimens in group 2a (DP 28 and 29) performed the worst, which was expected, with an average fatigue life of 25360 cycles. The UP specimens of group 1 were the second worst at an average of 32167 cycles, with the UP, PS and SP<sub>ct</sub> specimen of group 2b (DP 24) having the highest fatigue life of 250650 cycles, demonstrating the marked improvement provided by shot peening after plastic straining. Group 9, serving as the point of reference for shot peened specimens at an average fatigue life of 200000 cycles was surprisingly less than that which included plastic straining in group 2b.

### Test 2: Group 3

In this test all 3 specimens were pre-fatigued to 20000 cycles at a maximum bending stress of 480 MPa and then shot peened at SAA. The first 2 specimens, DP 14 and 17 were then fatigued to failure at a maximum bending stress of 480 MPa, and the third specimen, DP15, at 525 MPa.

The purpose of this test is to investigate the effect of pre-fatiguing unpeened specimens to about 60 % of its unpeened fatigue life, then shot peen them and fatigue to failure, to find out any fatigue life implications.

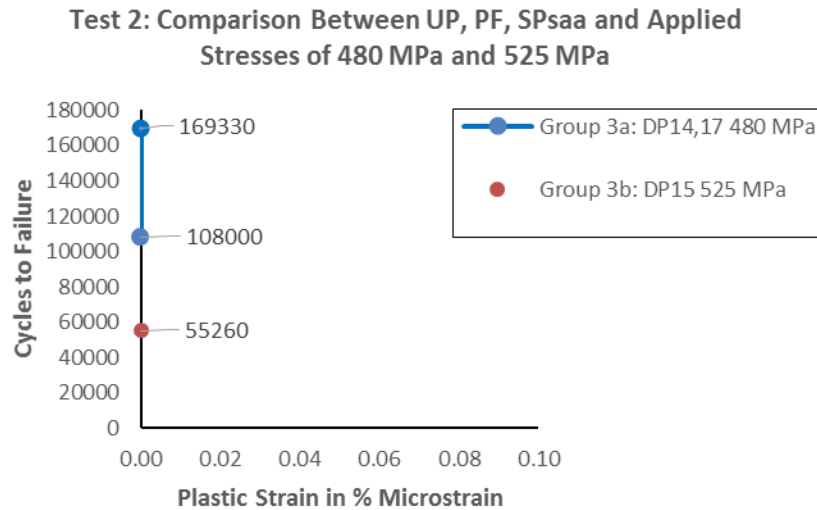


Figure 70 Fatigue test 2: comparison for group 3

From Figure 70 it can be seen that specimens pre- and post-fatigued at 480 MPa maximum bending stress had a higher average fatigue life of 138665 cycles as opposed to the specimen with only 55260 cycles with 525 MPa post-fatigued maximum bending stress by a surprising 151 % improvement. The high discrepancy in fatigue life between the specimens finally fatigued at 480 and 525 MPa seems too high compared to 69 % in reverse stress order with DP 13 and DP 5 in Group 4 (even though there was almost equal plastic straining involved), where they were fatigued at the different stresses throughout their tests. There is a suspicion that some flaw may have occurred with DP 15 which may explain why it failed so soon, and hinder attempts at life prediction modelling.

### Test 3: Group 4

This test is to compare two specimens of similar plastic straining, the same shot peening at SAA, but fatigued at different maximum bending stresses, 480 MPa and 525 MPa.

Contrary to test 2, the specimen fatigued at 480 MPa and 0.5 % plastic strain fatigued sooner at 32750 cycles, while the one with a bending stress of 525 MPa and 0.4103 % plastic strain fatigued at 55490 cycles which is a 69 % increase.

The role of a lower plastic straining may have played a role, although the specimen without plastic strain in test 2 also with a maximum bending stress of 525 MPa had almost the same fatigue life at 55260 cycles.

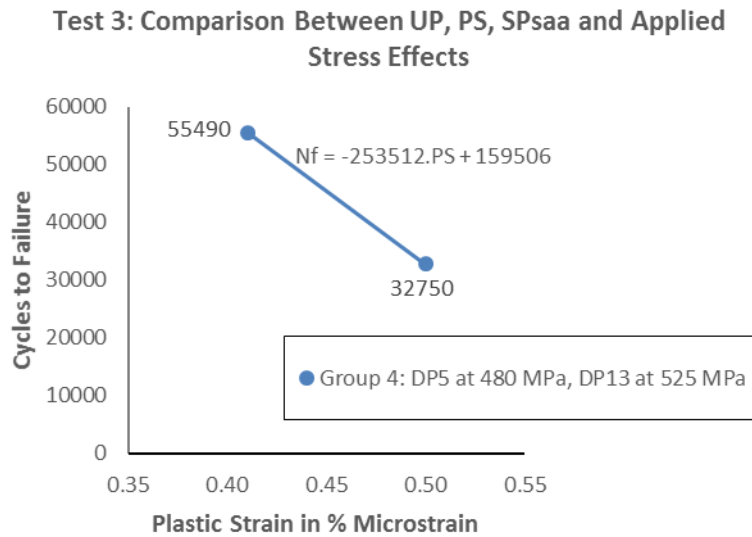


Figure 71 Fatigue test 3: comparison for group 4

#### Test 4: Groups 4a and 5

In this test the purpose was to determine a relationship between the effects of steadily increasing plastic strain on fatigue life with all specimens shot peened at SAA.

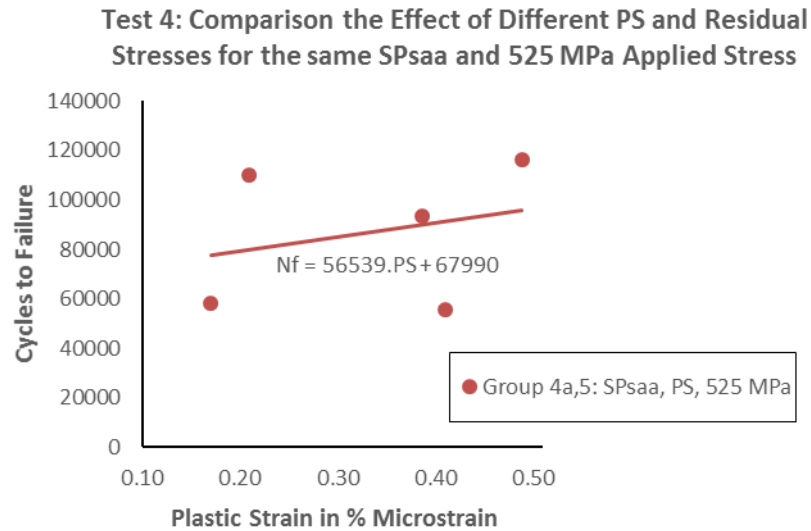


Figure 72 Fatigue test 4: comparison for groups 4a and 5

Specimens from group 5 and DP 13 from group 4 were plastically strained from 0.1703 up to 0.4885 % with initially surprising results. Although the fatigue life scatter was significantly wide the trendline showed a steady *increase* as shown by the linear equation gradient of 56539! This finding, however may not result in a definitive solution due to the scatter profile. DP 13 was the odd one out with the others showing a higher increase in fatigue life with strain. This phenomena will be of interest to the microstructural analysis in par 4.2.4 below.

### Test 5: Groups 6, 7 and 8

The aim here is to find a relationship with the effects of increasing plastic strain and a radial skimming of 200  $\mu\text{m}$  for specimens shot peened at CPUT, involving groups 6, 7 and 8. Group 6 specimens had plastic strain and no radial skim, group 7 had no plastic strain and radial skim, while group 8 had both plastic strain and radial skim.

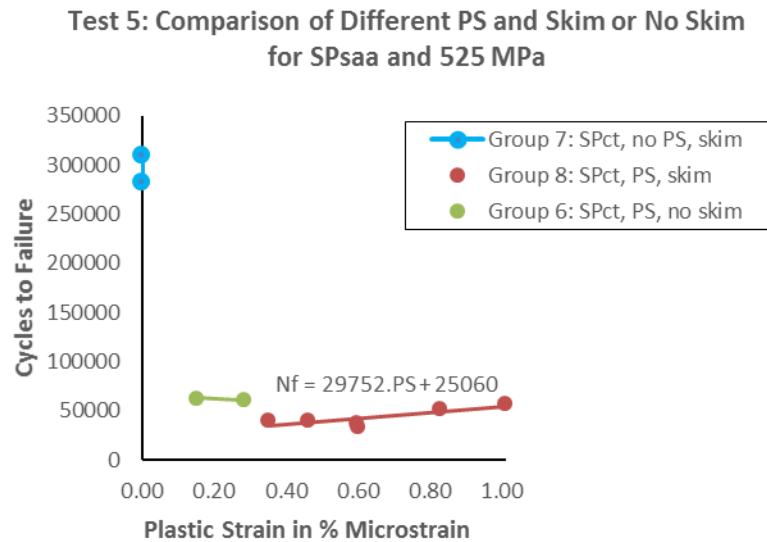


Figure 73 Fatigue test 5: comparison for groups 6, 7 and 8

The purpose of the skimming is to essentially remove the shot peened layer leaving a relatively “unpeened” simulated surface, but with a remaining residual compressive stress to hopefully extend fatigue life. If it succeeds then it may indicate a parameter for the role of the microstructure in fatigue life.

As can be seen from Figure 73, the group 7 specimens without plastic strain but with skim had fatigue lives averaging 295725 cycles, far exceeding the others with plastic strain which averaged 48697 cycles. Group 6 without skim performed slightly better than group 8 with both plastic strain and skim.

It is of microstructural interest, however, that in group 8 with all specimens skimmed, the fatigue life *increased* with an increase in plastic strain, also evident in test 4, as shown by the trendline gradient, a partly unexpected characteristic implying microstructural influences, which would be of interest to any researcher, and will be analysed in par 4.2.4.

### 4.2.3 Residual Stress-Depth Tests

Ten specimens were given residual stress-depth tests as detailed in par 3.3, of which one, DP 50 (a set of 3), was done at UCT on their air abrasive centre hole drilling (AACHD) machine, and the 9 others at NMMU.

The 9 specimens, indicated in table 10 for residual stress testing (RST) at NMMU, were selected to check correlations in their differences, if any, in residual stress profiles and magnitudes, as a function of their treatments.

The average stress values shown on the residual stress-depth graphs were calculated using Simpson's area rule, where the areas were divided into strips for each incremental depth shown in the left column of tables 11 to 22 and matched with the corresponding average residual stress ( $\sigma_{x \text{ res calibrated}}$ ) of each strip.

The common purpose of these tests is to analyse the role, nature, depth, and effects of the residual stresses in conjunction with the bending stresses, with fatigue life for various listed surface treatments.

This section is divided into 7 tests as follows.

### Test 1: Group 1:

DP 1: unpeened and fatigued to failure with a maximum bending stress of 480 MPa.

Table 11 DP 1: unpeened specimen

Depth (mm)	$\theta$ (°)	$\sigma_2$ (MPa)	$\sigma_1$ (MPa)	$\sigma_{\text{centre}}$ (MPa)	R (MPa)	$2\theta$ (Rad)	$\sigma_{x \text{ res}}$ (MPa)	$\sigma_{x \text{ res}}$ Calibrated (MPa)	$\sigma_{\text{Bend Max}}$ (MPa)	$\sigma_{\text{Bend Mn}}$ (MPa)	$\sigma_{x \text{ Tot Max}}$ Calibrated (MPa)	$\sigma_{x \text{ Tot Mn}}$ Calibrated (MPa)
0								-60	480.0	48.0	420.0	-12.0
0.02	41.1	-1078.2	-463.6	-770.9	307.3	1.43	-728.9	-61.1	479.7	47.7	418.6	-13.4
0.05	-73.6	-771.4	323.0	-224.2	547.2	-2.57	-684.2	-57.4	479.2	47.2	421.9	-10.1
0.08	-65.8	-312.9	420.8	54.0	366.8	-2.30	-189.2	-15.9	478.8	46.8	462.9	30.9
0.10							0.0	0.0	478.5	46.5	478.5	46.5
0.12	-65.3	139.5	164.7	152.1	12.6	-2.28	143.9	12.1	478.1	46.1	490.2	58.2
0.15	-65.5	-22.2	409.7	193.7	216.0	-2.29	52.0	4.4	477.7	45.7	482.0	50.0
0.18	-62.7	-64.4	490.7	213.1	277.6	-2.19	52.7	4.4	477.2	45.2	481.6	49.6
0.22	-19.0	-28.0	459.3	215.7	243.6	-0.66	407.7	34.2	476.6	44.6	510.8	78.8
0.25	-2.4	-15.7	380.5	182.4	198.1	-0.08	379.8	31.8	476.1	44.1	508.0	76.0
0.28	-3.9	-15.0	368.4	176.7	191.7	-0.14	366.6	30.7	475.7	43.7	506.4	74.4
0.32	-6.7	-23.4	354.1	165.4	188.7	-0.23	348.9	29.3	475.1	43.1	504.3	72.3
0.35	-8.8	-32.9	322.3	144.7	177.6	-0.31	314.0	26.3	474.6	42.6	500.9	68.9
0.38	-9.8	-97.0	223.1	63.0	160.1	-0.34	213.7	17.9	474.1	42.1	492.1	60.1
0.42	-10.0	-51.9	240.6	94.4	146.2	-0.35	231.7	19.4	473.5	41.5	492.9	60.9
0.45	-9.7	-24.5	202.8	89.2	113.6	-0.34	196.4	16.5	473.1	41.1	489.5	57.5
0.48	-9.1	6.5	172.7	89.6	83.1	-0.32	168.5	14.1	472.6	40.6	486.7	54.7

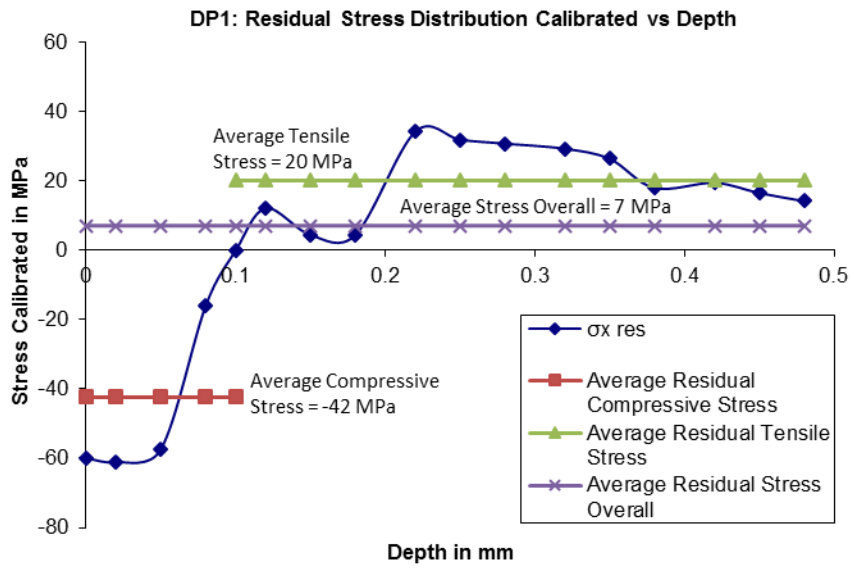


Figure 74 DP 1: unpeened: residual stress vs depth

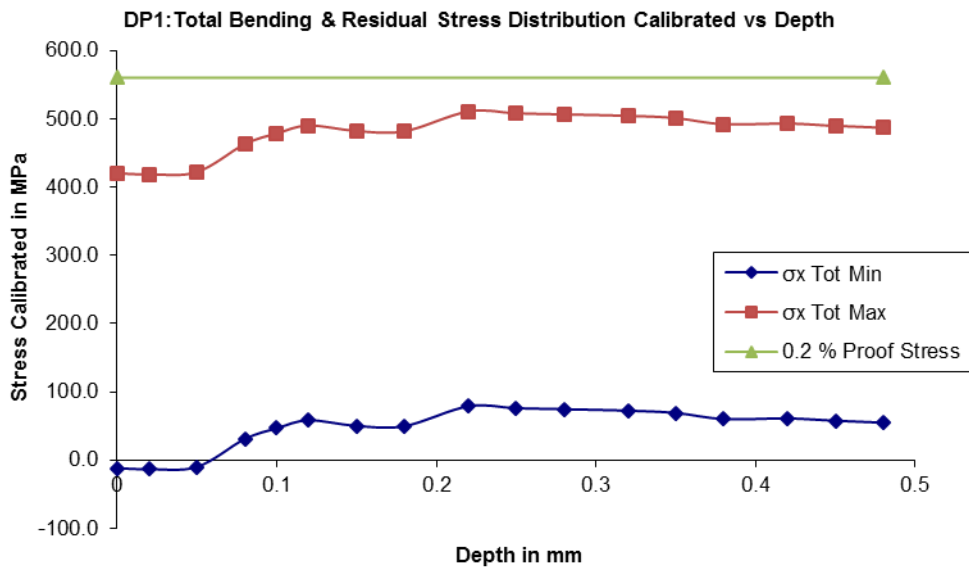


Figure 75 DP 1: unpeened: total bending and residual stress vs depth

As would be expected of an unpeened specimen, there was a relatively low residual compressive stress averaging 42 MPa over a depth of 0.1 mm with the rest averaging 20 MPa tensile, and overall average stress of 7 MPa tensile across the tested region. This resulted in the combined bending and residual stress all being effectively tensile with average fatigue failure occurring at 32167 cycles for group 1. The highest combined maximum bending and residual tensile stress of 510.8 MPa, as shown in Figure 75, was reasonably within the yield proof value of 560 MPa.

### Test 2: Group 3:

DP15: shot peened at SAA, prefatigued to 20000 cycles at a maximum bending stress of 480 MPa, then shot peened at SAA, and fatigued to final fracture at the maximum bending stress of 525 MPa. The other two specimens of group 3, DP 14 and 17, were fatigued to failure at 480 MPa.

Table 12 DP 15: unpeened, prefatigued to 20000 cycles and shot peened at SAA

Depth (mm)	$\theta$ (°)	$\sigma_2$ (MPa)	$\sigma_1$ (MPa)	$\sigma_{\text{centre}}$ (MPa)	R (MPa)	$2\theta$ (Rad)	$\sigma_{x \text{ res}}$ (MPa)	$\sigma_{x \text{ res}}$ Calibrated (MPa)	$\sigma_{\text{Bend Max}}$ (MPa)	$\sigma_{\text{Bend Min}}$ (MPa)	$\sigma_{x \text{ Tot Max}}$ Calibrated (MPa)	$\sigma_{x \text{ Tot Min}}$ Calibrated (MPa)
0								-50	525.0	52.5	475.0	2.5
0.03	-45.1	-1663.3	-40.2	-851.8	811.6	-1.57	-854.6	-71.6	524.5	52.0	452.9	-19.6
0.07	-39.8	-3058.1	-365.4	-1711.7	1346.3	-1.39	-1470.6	-123.3	523.8	51.3	400.5	-72.0
0.12	-35.7	-3666.4	-2151.7	-2909.0	757.3	-1.24	-2666.5	-223.5	523.0	50.5	299.4	-173.1
0.17	-32.3	-3428.9	-2569.1	-2999.0	429.9	-1.13	-2814.3	-235.9	522.1	49.6	286.2	-186.3
0.23	-29.1	-3034.4	-1328.5	-2181.4	852.9	-1.02	-1731.7	-145.2	521.1	48.6	376.0	-96.5
0.28	-25.6	-2664.6	-678.0	-1671.3	993.3	-0.89	-1047.6	-87.8	520.3	47.8	432.5	-40.0
0.33	-21.3	-1763.1	-171.3	-967.2	795.9	-0.74	-381.3	-32.0	519.4	46.9	487.5	15.0
0.35								0.0	519.1	46.6	519.1	46.6
0.37	-17.5	-675.9	445.5	-115.2	560.7	-0.61	344.7	28.9	518.8	46.3	547.7	75.2
0.42	-25.1	-5.6	556.9	275.7	281.2	-0.88	455.7	38.2	517.9	45.4	556.1	83.6
0.47	-68.9	339.7	784.4	562.1	222.3	-2.41	397.3	33.3	517.1	44.6	550.4	77.9

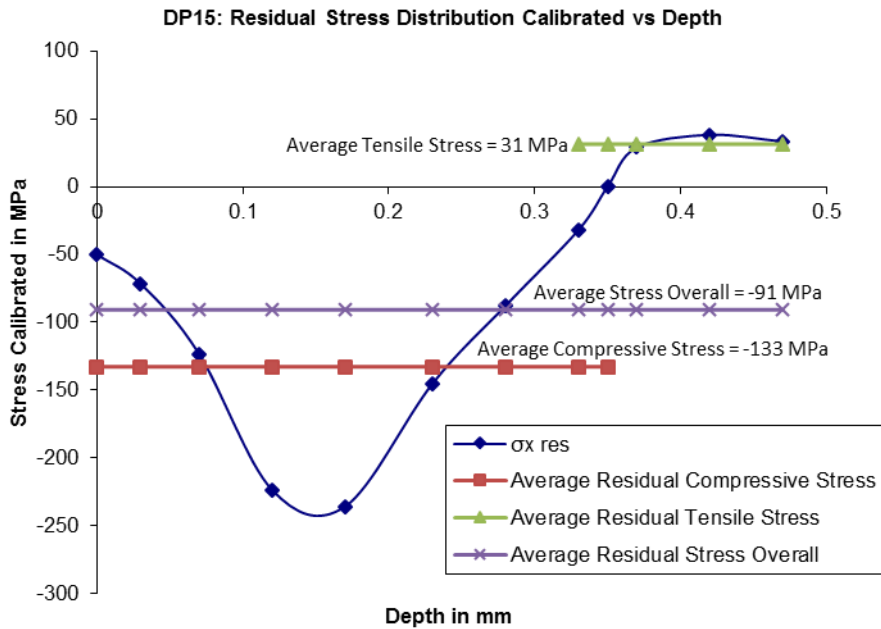


Figure 76 DP 15: unpeened, prefatigued to 20000 cycles, shot peened at SAA: residual stress vs depth

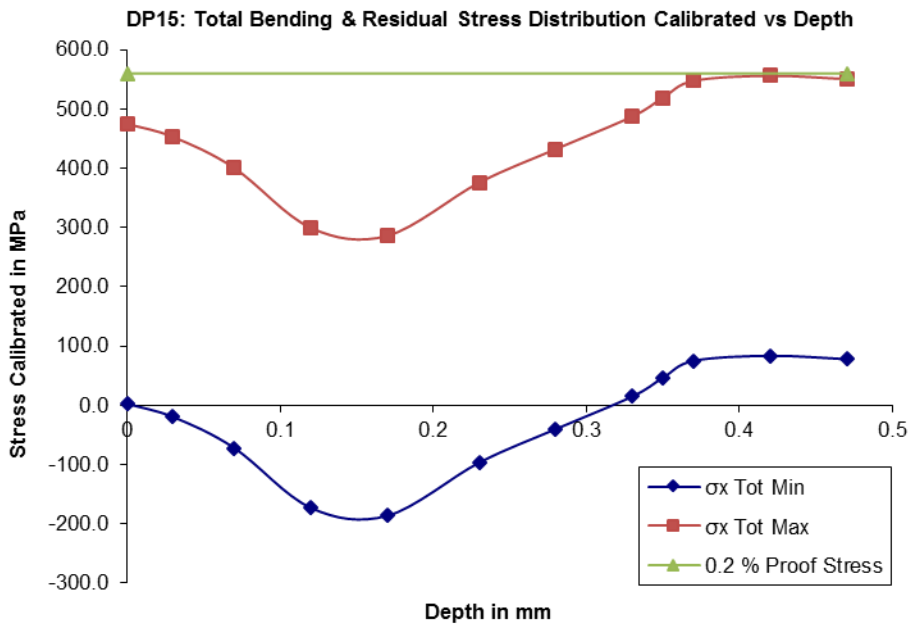


Figure 77 DP 15: unpeened, prefatigued to 20000 cycles and shot peened at SAA: total bending (525 MPa) and residual stress vs depth

The results here show well-proportioned graphs with lower residual compressive stresses, due to prefatiguing followed by shot peening before fatiguing to final failure, than those shot peened without prefatiguing as with group 9 in test 7.

The average residual stresses of 133 MPa compressive, 91 MPa overall compressive and 31 MPa tensile over the tested region, can be taken as conservatively representative of group 3, seeing that the fatigue life of DP 15 tested here was the lowest and half of the group average of 110863 cycles.

This specimen was finally fatigued at a maximum bending stress of 525 MPa while the other two specimens were fatigued earlier on at the initially lower 480 MPa, possibly explaining their higher fatigue life within the group. Also, the lower bending stress possibly led to less residual compressive stress relaxation during the fatigue tests thereby extending their fatigue life.

Table 13 DP 14, 17: estimated unpeened, prefatigued to 20000 cycles, and shot peened at SAA

Depth (mm)	$\sigma_x$ res Calibrated (MPa)	$\sigma_{Bend}$ Max (MPa)	$\sigma_{Bend}$ Min (MPa)	$\sigma_x$ Tot Max Calibrated (MPa)	$\sigma_x$ Tot Min Calibrated (MPa)
0	-50	480	48	430	-2
0.03	-72	480	48	408	-24
0.07	-123	479	47	356	-76
0.12	-224	478	46	255	-177
0.17	-236	477	45	241	-191
0.23	-145	476	44	331	-101
0.28	-88	476	44	388	-44
0.33	-32	475	43	443	11
0.35	0	475	43	475	43
0.37	29	474	42	503	71
0.42	38	474	42	512	80
0.47	33	473	41	506	74

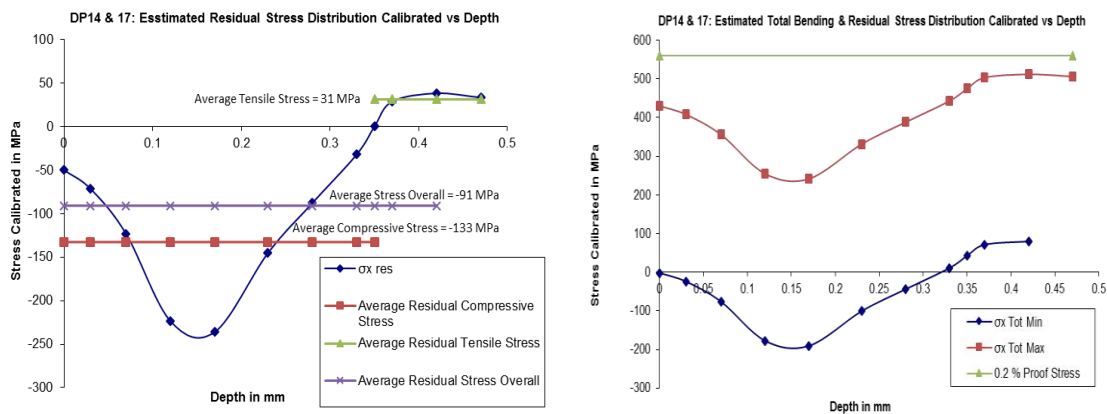


Figure 78 DP 14, 17: estimated residual stress and total bending & residual stress distribution vs depth

The 31 MPa average tensile residual stress for DP 15 contributed to a maximum combined bending and residual tensile stress of 556 MPa at a depth of 0.42 mm which is virtually at the yield value of 560 MPa, as shown in Figure 77, contributing to its shorter fatigue life.

The other two specimens, DP 14 and 17, may have had comparable residual stress values, and would have had a maximum combined bending and residual tensile stress around 512 MPa at the same depth, within a safer stress region as shown in Figure 78.

Unfortunately, the disproportionate gap in fatigue lives between DP 15 and the others raises sufficient doubt whether there was some flaw in DP 15 to draw a useful conclusion to this gap.

### Test 3: Group 4:

DP 5: shot peened at SAA, 0.5 % plastic strain, 480 MPa

DP 13: Shot peened at SAA and 0.4103 % plastic strain, 525 MPa

Table 14 DP 5: shot peened at SAA with 0.5 % plastic strain and a maximum bending stress of 480 MPa

Depth (mm)	$\theta$ (°)	$\sigma_2$ (MPa)	$\sigma_1$ (MPa)	$\sigma_{\text{centre}}$ (MPa)	R (MPa)	$2\theta$ (Rad)	$\sigma_{x \text{ res}}$ (MPa)	$\sigma_{x \text{ res}}$ Calibrated (MPa)	$\sigma_{\text{Bend Max}}$ (MPa)	$\sigma_{\text{Bend Min}}$ (MPa)	$\sigma_{x \text{ Tot Max}}$ Calibrated (MPa)	$\sigma_{x \text{ Tot Min}}$ Calibrated (MPa)
0								-20	480.0	48.0	460.0	28.0
0.03	6.6	-903.5	-350.2	-626.9	276.6	0.23	-357.6	-30.0	479.5	47.5	449.6	17.6
0.07	7.3	-1589.4	-773.1	-1181.2	408.2	0.25	-786.1	-65.9	478.9	46.9	413.0	-19.0
0.12	7.8	-1862.0	-1079.0	-1470.5	391.5	0.27	-1093.4	-91.7	478.1	46.1	386.5	-45.5
0.17	7.1	-1291.4	-782.2	-1036.8	254.6	0.25	-790.1	-66.2	477.4	45.4	411.1	-20.9
0.23	5.8	-513.1	-268.3	-390.7	122.4	0.20	-270.8	-22.7	476.5	44.5	453.8	21.8
0.28	4.4	-201.9	-13.7	-107.8	94.1	0.15	-14.8	-1.2	475.7	43.7	474.4	42.4
0.33	3.2	-81.1	81.2	0.1	81.2	0.11	80.7	6.8	474.9	42.9	481.7	49.7
0.37	2.5	18.5	201.5	110.0	91.5	0.09	201.2	16.9	474.3	42.3	491.2	59.2
0.42	2.1	34.7	165.6	100.1	65.4	0.07	165.4	13.9	473.5	41.5	487.4	55.4
0.47	1.8	66.1	176.5	121.3	55.2	0.06	176.4	14.8	472.7	40.7	487.5	55.5

Table 15 DP 13: shot peened at SAA with 0.4103 % plastic strain and a maximum bending stress of 525 MPa

Depth (mm)	$\theta$ (°)	$\sigma_2$ (MPa)	$\sigma_1$ (MPa)	$\sigma_{\text{centre}}$ (MPa)	R (MPa)	$2\theta$ (Rad)	$\sigma_{x \text{ res}}$ (MPa)	$\sigma_{x \text{ res}}$ Calibrated (MPa)	$\sigma_{\text{Bend Max}}$ (MPa)	$\sigma_{\text{Bend Min}}$ (MPa)	$\sigma_{x \text{ Tot Max}}$ Calibrated (MPa)	$\sigma_{x \text{ Tot Min}}$ Calibrated (MPa)
0								-90	525.0	52.5	435.0	-37.5
0.03	-5.2	-2131.3	-1240.2	-1685.7	445.5	-0.18	-1247.6	-104.6	524.5	52.0	419.9	-52.6
0.07	-4.5	-2550.3	-1687.6	-2118.9	431.3	-0.16	-1692.8	-141.9	523.8	51.3	381.9	-90.6
0.12	-5.1	-2449.2	-1661.8	-2055.5	393.7	-0.18	-1667.9	-139.8	523.0	50.5	383.2	-89.3
0.17	-5.3	-1607.4	-994.0	-1300.7	306.7	-0.19	-999.3	-83.8	522.1	49.6	438.4	-34.1
0.23	-5.2	-595.2	-207.6	-401.4	193.8	-0.18	-210.9	-17.7	521.1	48.6	503.4	30.9
0.28	-5.1	-248.6	30.9	-108.9	139.8	-0.18	28.7	2.4	520.3	47.8	522.7	50.2
0.33	-5.0	16.6	168.0	92.3	75.7	-0.17	166.9	14.0	519.4	46.9	533.4	60.9
0.37	-5.1	274.6	313.7	294.2	19.6	-0.18	313.4	26.3	518.8	46.3	545.0	72.5
0.42	-5.3	261.9	325.6	293.8	31.8	-0.19	325.1	27.3	517.9	45.4	545.2	72.7
0.47	-5.6	252.6	321.8	287.2	34.6	-0.19	321.2	26.9	517.1	44.6	544.0	71.5

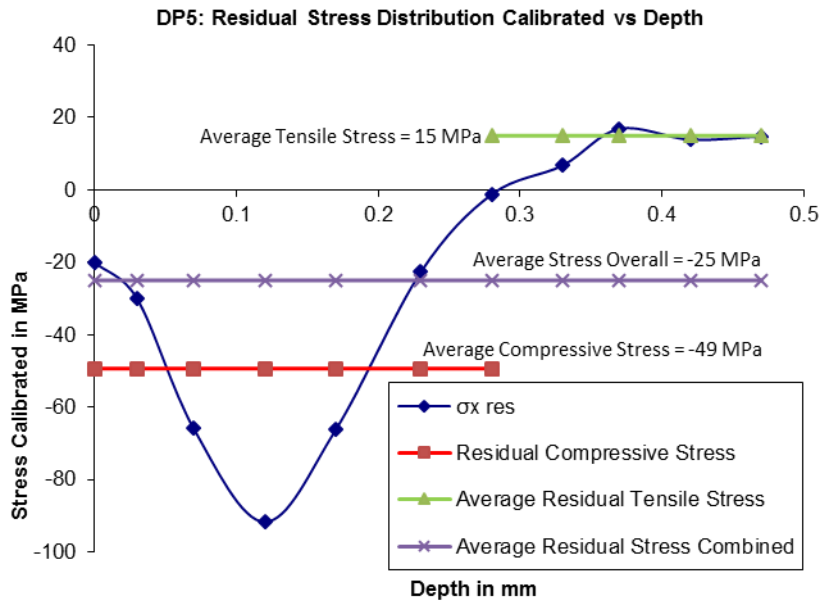


Figure 80 DP 5: shot peened at SAA with 0.5 % plastic strain: residual stress vs depth

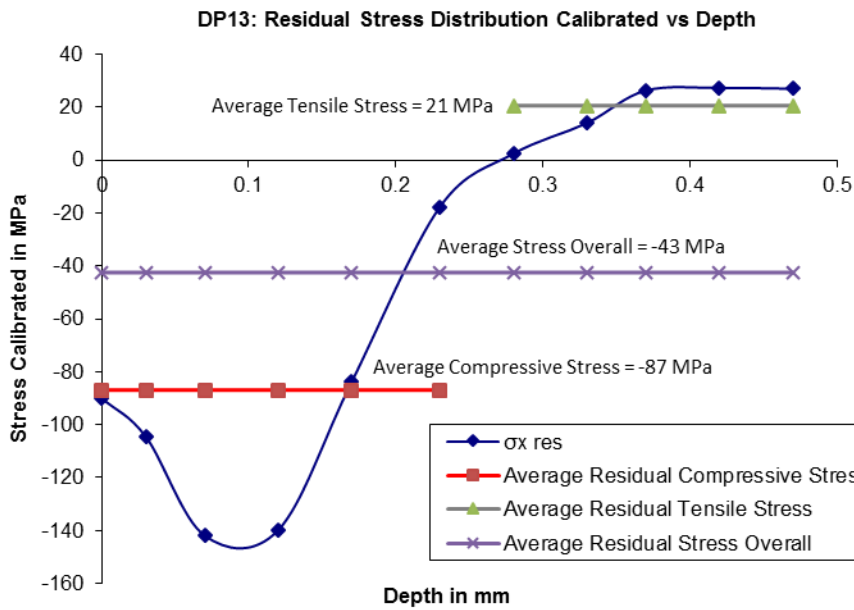


Figure 79 DP 13: shot peened at SAA with 0.4103 % plastic strain: residual stress vs depth

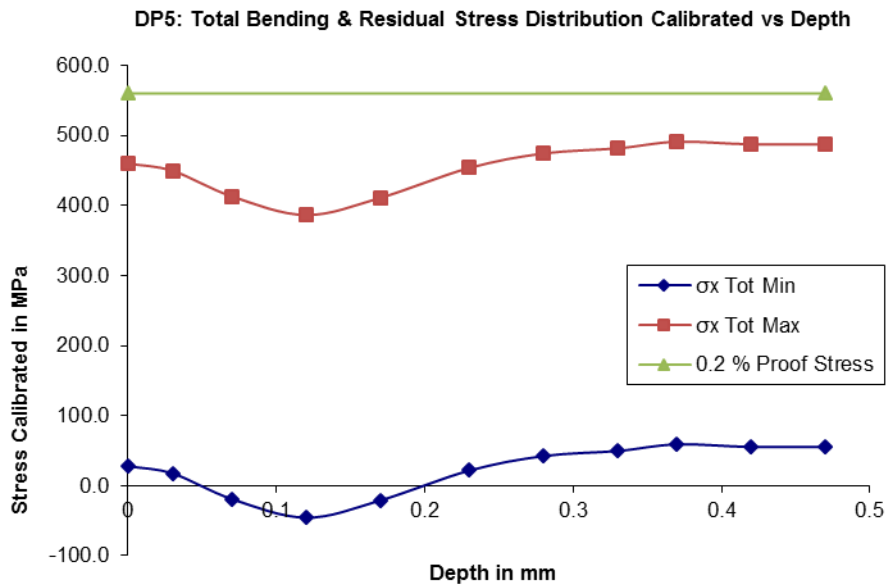


Figure 81 DP 5: shot peened at SAA with 0.5 % plastic strain: total bending (maximum 480 MPa) and residual stress vs depth

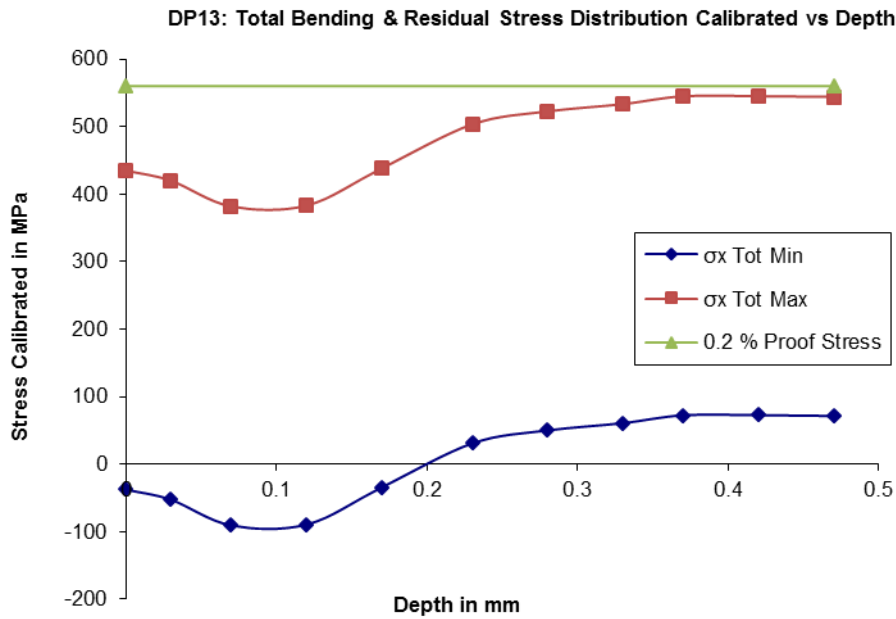


Figure 82 DP 13: shot peened at SAA with 0.4103 % plastic strain: total bending (maximum 525 MPa) and residual stress vs depth

Both specimens belonging to this group underwent residual stress tests. They were shot peened at SAA but had different plastic straining as well as maximum bending stresses.

All the graphs show good proportion and profiling, illustrating the effects of plastic straining and different bending stresses.

DP 5 with 0.5 % plastic strain showed a lower residual stress profile than DP 13 with 0.4103 % plastic strain as might be expected due to the higher plastic strain producing greater stress relieving of DP 5.

The maximum combined bending and residual tensile stress for DP 5 reached a relatively safe 491 MPa but with DP 13 it was a high 545 MPa, as shown in Figures 81 and 82, which was very close to the 560 MPa proof stress, implying that it might fail earlier, which was not the case.

The trendlines in Figure 83 show the higher rate of increase of residual stress as well as total bending and residual stress with depth at gradients at more than double the rate for DP 13 with 0.4103 % plastic strain and maximum bending stress of 525 MPa (fatigue life of 55490 cycles) over DP 5 with 0.5 % plastic strain and maximum bending stress of 480 MPa (fatigue life of 32750 cycles).

The aspect ratio of fatigue crack depth/crack length is seldom less than 0.5 for 7075-T6 aluminium alloy <sup>[34]</sup>. This means that at a crack depth of 0.325 mm, at the trendline interception points in both diagrams of Figure 83, the approximate crack length would be at around 0.65 mm, conservatively. The fatigue crack length at 0.65 mm depth was achieved at 28030 cycles for DP 5 (see Appendix C) and 53040 cycles for DP 13, indicating that DP13 took about twice the time to achieve microcrack initiation before uniform crack extension. Also, DP 5 needed only another 4720 cycles to failure while DP 13 took another 27460 cycles after the intercept point where the residual tensile stress increased at a higher rate than for DP 5.

With a higher bending and residual stress rate than DP 5, DP 13 still outperformed it. Since the shot peening was the same the only remaining applied variable was the plastic strain which was lower in DP 13, and seems to indicate that the stress relieving caused by the 0.4103 % plastic strain in DP 13 was not enough to decrease the residual compressive stress, as shown in Figure 80, as much as with DP 5 with 0.5 % plastic strain, shown in Figure 79.

This shows the effect of plastic strain in relieving residual compressive stress and therefore the fatigue life, even when the plastic strain difference was only 0.0897 % plastic strain or about 22 %. The relation between plastic strain and fatigue life will be discussed in more detail in the next section.

Table 16 DP 5 & 13: residual stress vs depth and total bending & residual stress vs depth values, showing their variances

Depth (mm)	Residual Stress (MPa)		Bend & Res Str (MPa)		Variance
	DP 5 0.5% PS	DP 13 0.41% PS	DP 5 0.5% PS	DP 13 0.41% PS	
0	-20	-90	460.0	390.0	70.0
0.03	-30.0	-104.6	449.6	375.0	74.6
0.07	-65.9	-141.9	413.0	337.0	76.0
0.12	-91.7	-139.8	386.5	338.3	48.2
0.17	-66.2	-83.8	411.1	393.6	17.5
0.23	-22.7	-17.7	453.8	458.8	-5.0
0.28	-1.2	2.4	474.4	478.1	-3.6
0.33	6.8	14.0	481.7	488.9	-7.2
0.37	16.9	26.3	491.2	500.6	-9.4
0.42	13.9	27.3	487.4	500.8	-13.4
0.47	14.8	26.9	487.5	499.7	-12.1

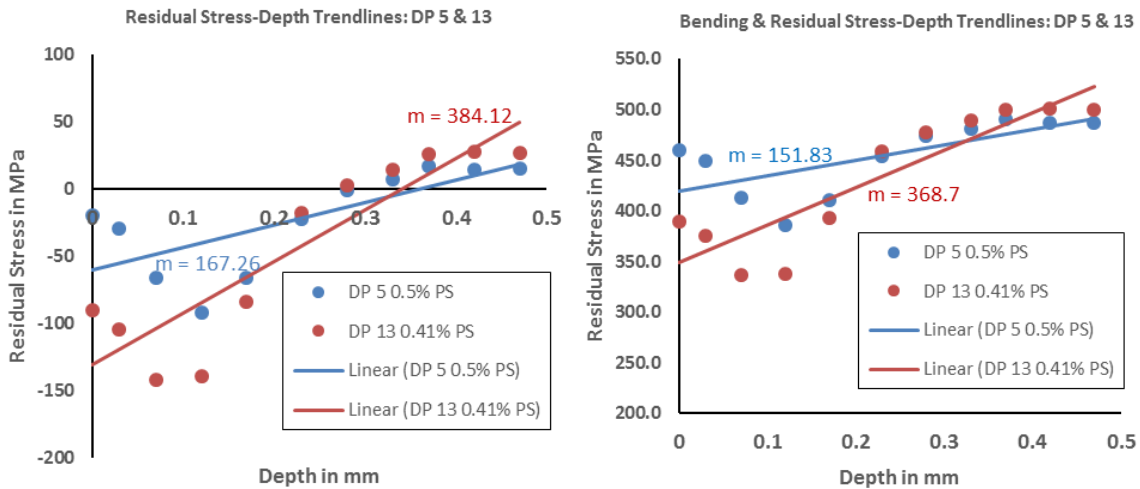


Figure 83 DP 5 & 13: Trendlines of residual stress vs depth and bending and residual stress vs depth

**Test 4: Groups 4a and 5:**

DP 19: shot peened at SAA and 0.1703 % plastically strain, 525 MPa.

DP13 in Test 3, Group 4, can be included in this test due to the same maximum bending stress and treatment, and with 0.4103 % plastic strain. Table 15, Figures 80 and 82 will be considered for this test.

*Table 17 DP 19: shot peened at SAA with 0.1703 % plastic strain*

Depth (mm)	$\theta$ (°)	$\sigma_2$ (MPa)	$\sigma_1$ (MPa)	$\sigma_{\text{centre}}$ (MPa)	R (MPa)	$2\theta$ (Rad)	$\sigma_{x \text{ res}}$ (MPa)	$\sigma_{x \text{ res}}$ Calibrated (MPa)	$\sigma_{\text{Bend Max}}$ (MPa)	$\sigma_{\text{Bend Min}}$ (MPa)	$\sigma_{x \text{ Tot Max}}$ Calibrated (MPa)	$\sigma_{x \text{ Tot Min}}$ Calibrated (MPa)
0								-40	525.0	52.5	485.0	12.5
0.03	80.5	-874.8	-643.8	-759.3	115.5	2.81	-868.5	-72.8	524.5	52.0	451.7	-20.8
0.07	56.4	-2427.7	-1566.5	-1997.1	430.6	1.97	-2163.8	-181.4	523.8	51.3	342.4	-130.1
0.12	58.5	-2963.7	-2180.6	-2572.2	391.6	2.04	-2749.7	-230.5	523.0	50.5	292.5	-180.0
0.17	-35.5	-2941.4	-1131.0	-2036.2	905.2	-1.24	-1741.8	-146.0	522.1	49.6	376.1	-96.4
0.23	-34.3	-1920.4	-130.9	-1025.7	894.8	-1.20	-699.7	-58.7	521.1	48.6	462.5	-10.0
0.28	-33.3	-1248.0	193.6	-527.2	720.8	-1.16	-241.0	-20.2	520.3	47.8	500.1	27.6
0.33	-32.3	-529.8	262.4	-133.7	396.1	-1.13	36.4	3.1	519.4	46.9	522.5	50.0
0.37	-31.3	223.3	493.4	358.4	135.1	-1.09	420.6	35.3	518.8	46.3	554.0	81.5
0.42	-30.4	237.1	648.1	442.6	205.5	-1.06	543.0	45.5	517.9	45.4	563.4	90.9
0.47	-29.6	182.3	700.0	441.1	258.8	-1.03	573.8	48.1	517.1	44.6	565.2	92.7

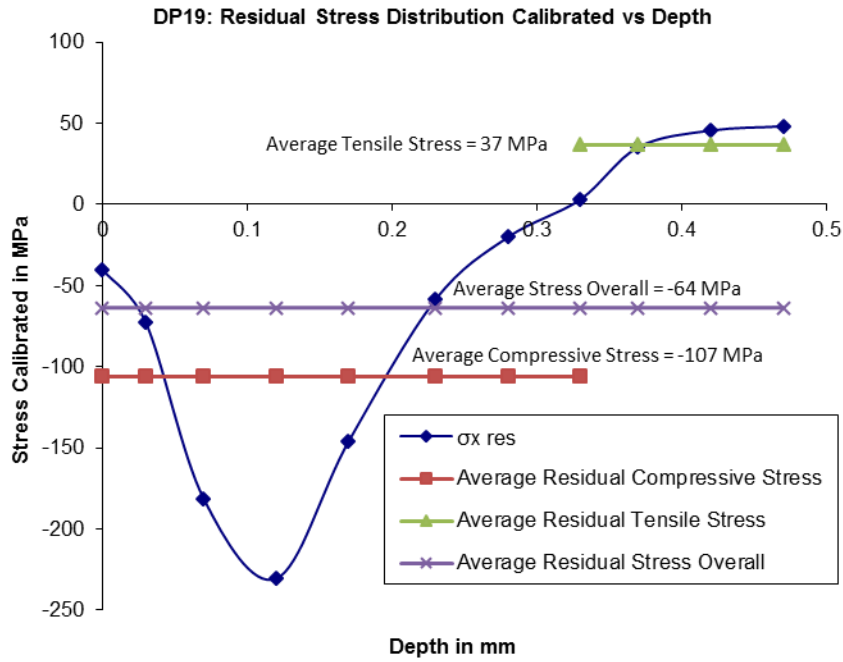


Figure 84 DP 19: shot peened at SAA with 0.1703 % plastic strain: residual stress vs depth

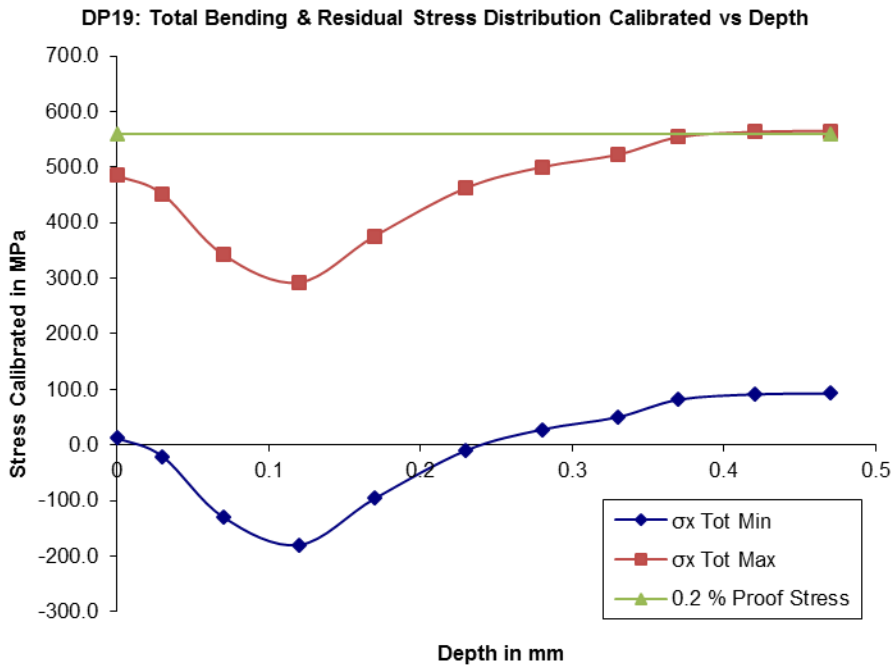


Figure 85 DP 19: shot peened at SAA with 0.1703 % plastic strain: total bending and residual stress vs depth

As with Test 3, there will be two specimens to analyse regarding residual and bending stresses and their application to fatigue life for treatment common to Group 5.

DP 19 received 0.1703 % plastic straining with average residual stresses of 107 MPa compressive, 64 MPa compressive overall, and 37 MPa tensile, and a fatigue life of 58500 cycles.

DP 13 received 0.4103 % plastic straining with average residual stresses of 87 MPa compressive, 43 MPa compressive overall, and 21 MPa tensile, and a fatigue life of 55490 cycles.

It can be seen that with the lower plastic strain of DP 19, the average residual compressive stresses were higher due to less tensile stress relieving effects from plastic straining, and a longer fatigue life by 5 %.

This plastic strain of DP 19 relative to DP 13 has a difference of 0.24 %, or a 141 % decrease which is somewhat out of balance with the residual compressive stress difference of 20 MPa or 19 % increase.

Also, the 3010 cycles or 5 % increase in fatigue life corresponds to a 20 MPa or 19 % increase in residual compressive stress of DP 19.

The maximum combined bending and residual tensile stress for DP 19 was a very high 565 MPa marginally exceeding the 560 MPa proof stress, as shown in Figure 85, implying that the specimen was encroaching into the plastic region at that point where the depth was 0.47 mm and becoming strain hardened there.

All 5 specimens received different levels of plastic strain which was the only applied independent variable and fatigue life as the dependent variable, implying that there may be a useful relationship between the two variables which may assist in finding a fatigue life prediction coefficient.

The relation between the plastic strain and the residual compressive stress with fatigue life will be analysed in the next section.

#### **Test 5: Group 6:**

DP 35: shot peened at CPUT and 0.2815 % plastically strain, 525 MPa

Table 18 DP 35: shot peened at SAA with 0.2815 % plastic strain

Depth (mm)	$\theta$ (°)	$\sigma_2$ (MPa)	$\sigma_1$ (MPa)	$\sigma_{\text{centre}}$ (MPa)	R (MPa)	$2\theta$ (Rad)	$\sigma_{x \text{ res}}$ (MPa)	$\sigma_{x \text{ res}}$ Calibrated (MPa)	$\sigma_{\text{Bend Max}}$ (MPa)	$\sigma_{\text{Bend Min}}$ (MPa)	$\sigma_{x \text{ Tot Max}}$ Calibrated (MPa)	$\sigma_{x \text{ Tot Min}}$ Calibrated (MPa)
0								-60	525.0	52.5	465.0	-7.5
0.03	-52.17	-1078.32	-693.81	-886.07	192.26	-1.82	-933.68	-78.3	524.5	52.0	446.2	-26.3
0.07	-44.40	-2331.20	-814.06	-1572.63	758.57	-1.55	-1556.74	-130.5	523.8	51.3	393.3	-79.2
0.12	-50.60	-3529.29	-2384.50	-2956.90	572.40	-1.77	-3068.07	-257.2	523.0	50.5	265.8	-206.7
0.17	-56.35	-3547.50	-2908.04	-3227.77	319.73	-1.97	-3351.16	-280.9	522.1	49.6	241.2	-231.3
0.23	-61.96	-2965.03	-1959.82	-2462.43	502.61	-2.16	-2742.90	-229.9	521.1	48.6	291.2	-181.3
0.28	-70.41	-2665.75	-1246.47	-1956.11	709.64	-2.46	-2506.20	-210.1	520.2	47.7	310.1	-162.4
0.33	78.00	-1901.07	-462.22	-1181.65	719.43	2.72	-1838.87	-154.2	519.4	46.9	365.2	-107.3
0.37	43.70	-939.58	404.83	-267.38	672.21	1.53	-236.88	-19.9	518.7	46.2	498.9	26.4
0.39							0.00	0.0	518.5	46.0	518.5	46.0
0.42	36.47	-345.63	610.21	132.29	477.92	1.27	272.50	22.8	517.9	45.4	540.7	68.2
0.47	33.89	148.76	678.08	413.42	264.66	1.18	513.50	43.0	517.0	44.5	560.1	87.6

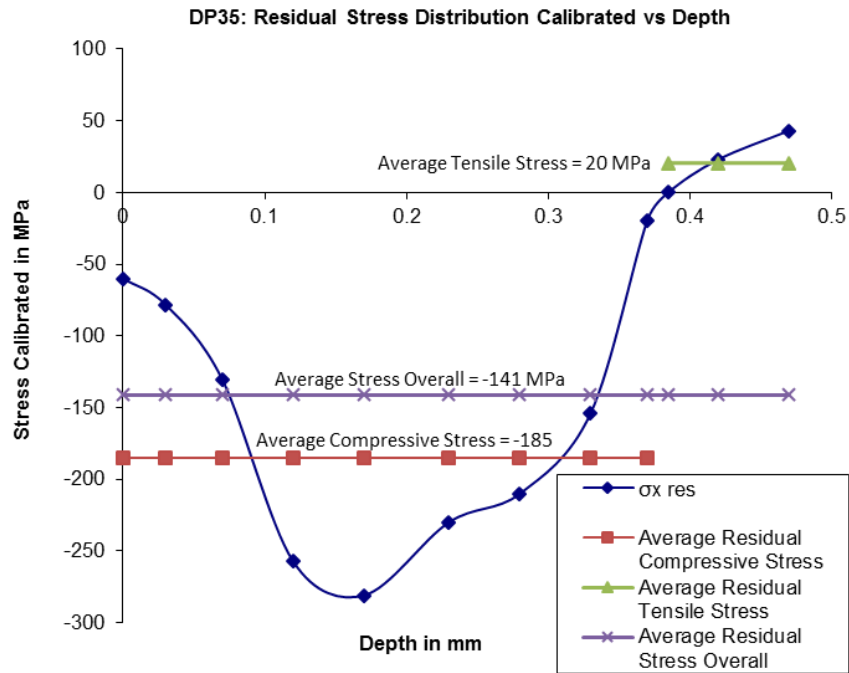


Figure 86 DP 35: shot peened at SAA with 0.2815 % plastic strain: residual stress vs depth

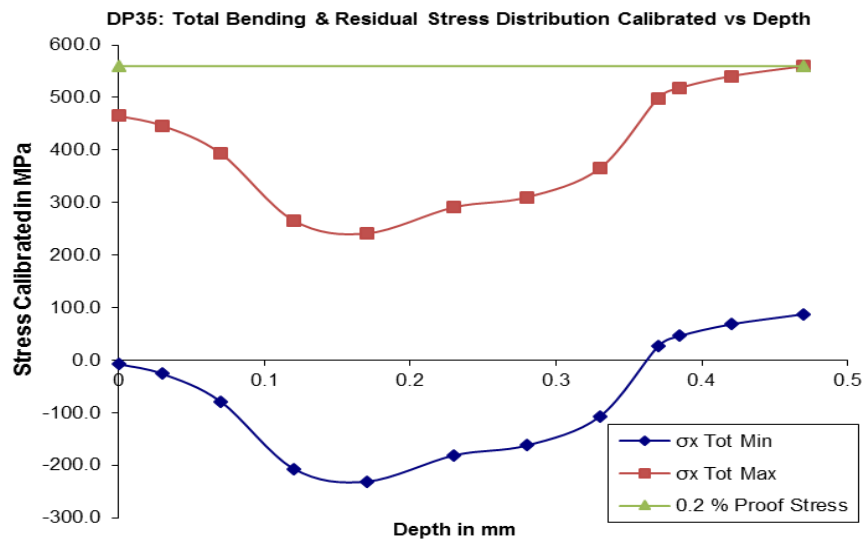


Figure 87 DP 35: shot peened at SAA with 0.2815 % plastic strain: total bending and residual stress vs depth

This is the first test in this section to analyse specimens shot peened at CPUT.

The residual stress-depth and total stress-depth graphs in Figures 86 and 87 show good profiles.

DP 35 received 0.2815 % plastic straining with average residual stresses of 185 MPa compressive, 141 MPa compressive overall, and 20 MPa tensile, and a fatigue life of 61480 cycles.

The other specimen in group 6, DP 41 with 0.15 % plastic straining and the same bending stress conditions had an expected higher fatigue life of 63420, which was 1940 cycles or 3 % higher than DP 35, although a 0.1315 % or a 47 % drop in plastic straining gives the impression that differences in small magnitudes of plastic straining will not make significant changes in fatigue life of shot peened specimens. It is expected then that the amount of residual compressive stress relaxation was probably fairly small in this group.

The combined bending and residual tensile stress of DP 35 reached a very high 560 MPa at a depth of 0.47 mm which was effectively at the yield proof stress, as shown in Figure 87, with the specimen probably experiencing local yield and some strain hardening there.

During the fatigue test of DP 35, at about 54000 cycles the crack length had reached only 0.47 mm, which increased slowly to about 2 mm, beyond the shot peened region, over the

next 5000 cycles indicating that there may have been some strain hardening resisting crack growth and extending fatigue life.

### Test 6: Group 8:

DP 25: shot peened at CPUT, 1.0072 % plastically strain, and a 200  $\mu\text{m}$  skim.

Table 19 DP 25: shot peened at CPUT with 1.0072 % plastic strain and 200  $\mu\text{m}$  skim

Depth (mm)	$\theta$ ( $^{\circ}$ )	$\sigma_2$ (MPa)	$\sigma_1$ (MPa)	$\sigma_{\text{centre}}$ (MPa)	R (MPa)	$2\theta$ (Rad)	$\sigma_{x \text{ res}}$ (MPa)	$\sigma_{x \text{ res}}$ Calibrated (MPa)	$\sigma_{\text{Bend Max}}$ (MPa)	$\sigma_{\text{Bend Min}}$ (MPa)	$\sigma_{x \text{ Tot Max}}$ Calibrated (MPa)	$\sigma_{x \text{ Tot Min}}$ Calibrated (MPa)
0								-15	525.0	52.5	510.0	37.5
0.03	5.0	-357.0	-84.1	-220.5	136.5	0.17	-86.1	-7.2	524.5	52.0	517.3	44.8
0.07	-0.1	65.2	326.1	195.6	130.4	0.00	326.1	27.3	523.8	51.3	551.1	78.6
0.12	0.5	102.8	325.4	214.1	111.3	0.02	325.4	27.3	522.9	50.4	550.2	77.7
0.17	3.2	21.5	224.5	123.0	101.5	0.11	223.8	18.8	522.0	49.5	540.8	68.3
0.23	6.3	-57.0	122.8	32.9	89.9	0.22	120.6	10.1	521.0	48.5	531.1	58.6
0.28	9.2	-111.7	63.0	-24.3	87.3	0.32	58.5	4.9	520.1	47.6	525.0	52.5
0.33	11.8	-103.0	45.0	-29.0	74.0	0.41	38.8	3.3	519.2	46.7	522.5	50.0
0.37	14.0	-127.1	10.7	-58.2	68.9	0.49	2.6	0.2	518.5	46.0	518.7	46.2
0.42	15.8	-102.8	15.8	-43.5	59.3	0.55	7.0	83.5	517.7	45.2	601.1	128.6
0.47	17.1	-65.4	26.9	-19.2	46.1	0.60	18.9	1.6	516.8	44.3	518.4	45.9

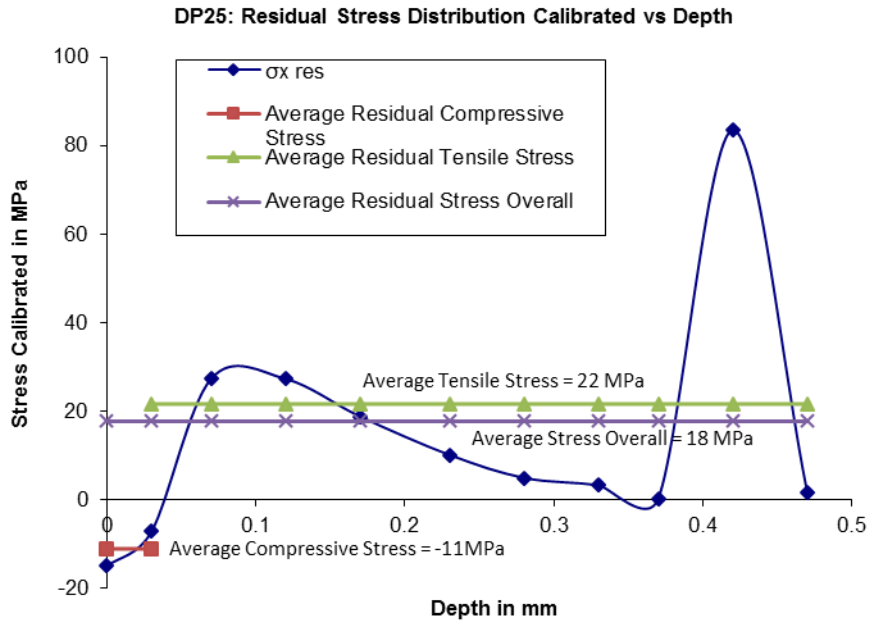


Figure 88 DP 25: shot peened at CPUT with 1.0072 % plastic strain and 200  $\mu$ m skim: residual stress vs depth

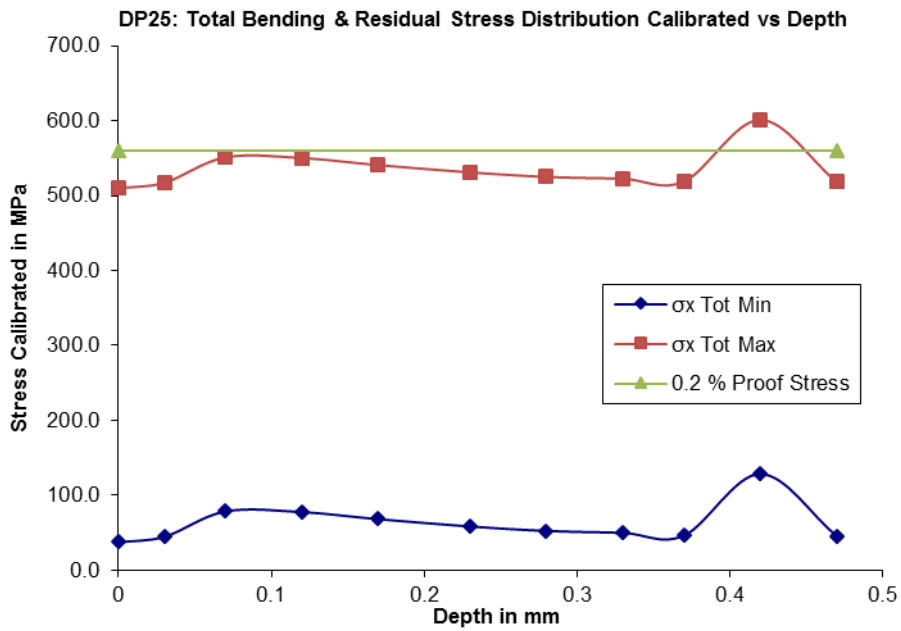


Figure 89 DP 25: shot peened at CPUT with 1.0072 % plastic strain and 200  $\mu$ m skim: total bending and residual stress vs depth

This is the first residual stress test in this section where a specimen has received a 200  $\mu\text{m}$  radial skim, as well as the highest plastic strain of 1.0072 % and was expected to yield high residual compressive stress relaxation, which was the case.

This group was earmarked to represent the “unpeened” specimen by skimming off most of the shot peened layer with the hope that some residual stress had remained to offer extended fatigue life, and then to test the effects of plastic straining as well.

It received low average residual stresses of 11 MPa compressive, 18 MPa tensile overall and 22 MPa tensile, but with an unexpected relatively high fatigue life of 57840 cycles, the highest in the group where all the specimens were also skimmed and had lower % plastic straining with an average fatigue life of 44112 cycles!

The reason for this inversely proportional high fatigue life performance with regard to low residual compressive stress and high plastic strain was remarked upon in par 3.5.2 referring to the results in table 8, and is intriguing.

Since the residual stress does not seem to have played a significant role in the relatively high fatigue life, probably due to the skimming of the shot peened surface, the other credible parameter is in the plastic straining affecting the microstructure and playing some work hardening role to extend fatigue life.

The maximum combined bending and residual tensile stress attained a very high 601 MPa spike at a depth of 0.42 mm, which exceeds the proof stress by 41 MPa, as shown in Figure 89, and only 11 MPa below the ultimate tensile strength, normally implying early fracture which was not the case.

The number of cycles at a depth of 0.42 mm and approximate crack length of 0.84 mm was 53750 cycles, increasing to 2.5 mm at 56000 cycles after which it failed fairly quickly. After a depth of 0.47 mm the residual stress profile dropped steeply towards the compressive stress region.

Unfortunately, the residual stress was not scheduled to be tested beyond this depth but it is feasible after viewing the residual stress profile and crack growth behaviour, that it became compressive from 0.5 up to a possible 2 mm, or resisted crack growth due to dynamic recovery especially after such high plastic straining as shown during the tensile testing, as well as rapid hardening preceding saturation to the formation of dense dislocation bands separating channels of lower dislocation density as described in par 2.6.2.

In contrast, the two specimens in group 7, DP 37 and 45 were also shot peened at CPUT and skimmed without plastic straining, and had a very high average fatigue life of 295725 cycles, as shown in par 4.2.2 test 5 in Figure 73.

Specimens shot peened at CPUT and skimmed were shown to have comparable fatigue lives to normal specimens shot peened only at CPUT.

However, with all the specimens of group 8 shot peened at CPUT and undergoing this test, where they had the combination of plastic straining and skimming, there is a persuasive impression that this combination was generally detrimental to fatigue life primarily due to the involvement of plastic straining.

The apparent contradiction, demonstrated in Figure 73 which was generated by table 8, is that an increase in plastic straining also increased the fatigue life of these specimens, seemingly posing as simulated “unpeened” specimens with microstructural empowerment! The microstructural analysis will need to attempt to supply some rational suggestions how this phenomena works.

**Test 7: Group 9:**

DP 38: shot peened at CPUT and fatigued at 525 MPa maximum bending stress.

DP 50: (set of 3) shot peened at SAA and fatigued at 525 MPa maximum bending stress

DP 4: shot peened at SAA but not fatigue tested.

The purpose of this test is to establish a point of reference for a specimen shot peened at CPUT and SAA to compare with other specimens receiving other treatments such as plastic straining, skimming, and microhardness tests.

Table 20 DP 38: shot peened at CPUT

Depth (mm)	$\theta$ (°)	$\sigma_2$ (MPa)	$\sigma_1$ (MPa)	$\sigma_{centre}$ (MPa)	R (MPa)	$2\theta$ (Rad)	$\sigma_{x \text{ res}}$ (MPa)	$\sigma_{x \text{ res Calibrated}}$ (MPa)	$\sigma_{Bend \text{ Max}}$ (MPa)	$\sigma_{Bend \text{ Min}}$ (MPa)	$\sigma_{x \text{ Tot Max Calibrated}}$ (MPa)	$\sigma_{x \text{ Tot Min Calibrated}}$ (MPa)
0								-200	525.0	52.5	325.0	-147.5
0.03	39.2	-3846.1	-2324.5	-3085.3	760.8	1.37	-2933.4	-245.9	524.5	52.0	278.6	-193.9
0.07	51.6	-5254.9	-3911.8	-4583.3	671.5	1.80	-4735.8	-397.0	523.8	51.3	126.8	-345.7
0.12	63.1	-5099.1	-3791.3	-4445.2	653.9	2.20	-4831.6	-405.0	523.0	50.5	117.9	-354.6
0.17	73.2	-3313.1	-2063.7	-2688.4	624.7	2.55	-3208.5	-269.0	522.1	49.6	253.1	-219.4
0.23	81.3	-1260.0	-193.7	-726.9	533.1	2.84	-1235.6	-103.6	521.1	48.6	417.5	-55.0
0.28	87.2	-594.2	343.0	-125.6	468.6	3.04	-592.0	-49.6	520.2	47.7	470.6	-1.9
0.33	-89.0	-87.9	549.6	230.9	318.7	-3.11	-87.7	-7.3	519.4	46.9	512.0	39.5
0.335							0.0	0.0	519.3	46.8	519.3	46.8
0.37	-87.0	521.1	896.0	708.6	187.4	-3.04	522.2	43.8	518.7	46.2	562.5	90.0
0.42	-86.2	563.2	800.3	681.7	118.5	-3.01	564.2	47.3	517.9	45.4	565.2	92.7
0.47	-86.1	527.8	832.9	680.3	152.6	-3.00	529.2	44.4	517.0	44.5	561.4	88.9

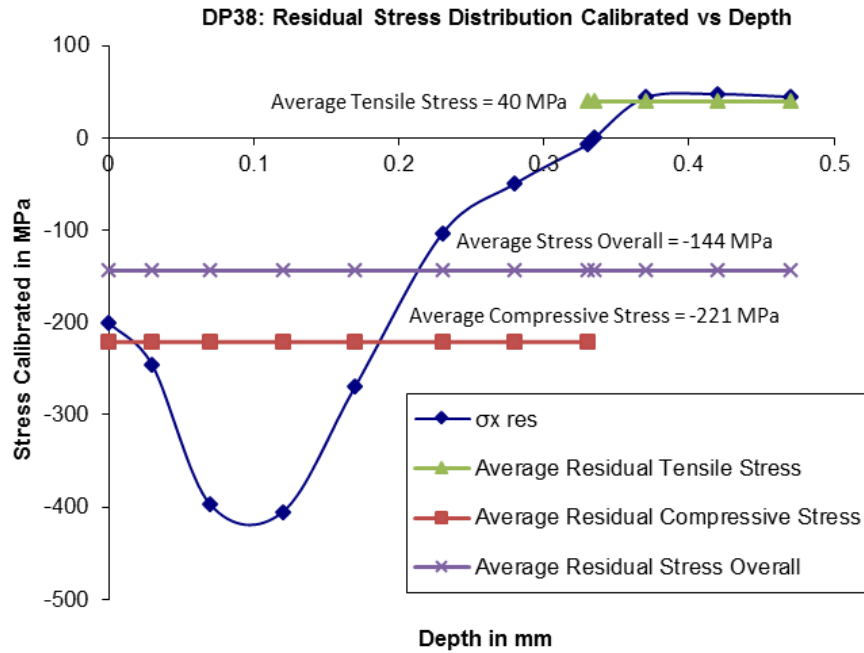


Figure 90 DP 38: shot peened at CPUT: residual stress vs depth

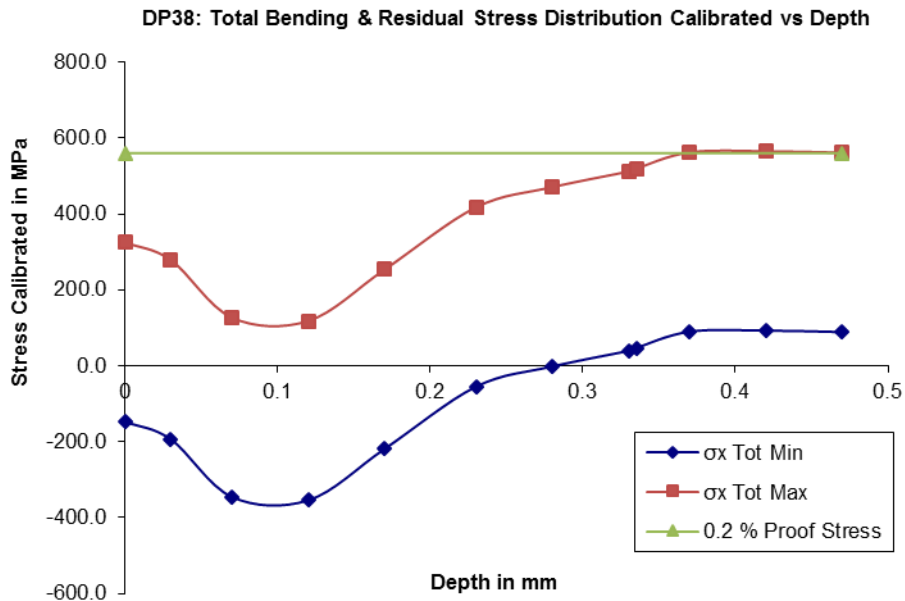


Figure 91 DP 38: shot peened at CPUT: total bending and residual stress vs depth

The graphs show very good stress-depth profiles with the bending tensile stresses being relatively neutralised over the first 0.2 mm of depth resulting in many cycles before crack initiation and then fatigue failure

As can be seen from the graphs, the average residual stresses were found to be 221 MPa compressive, 144 MPa overall compressive and 49 MPa tensile, and a fatigue life of 241420 cycles.

In contrast, DP 50, the set of 3 specimens tested at UCT referred to in par 3.3.3 and 4.2.3, had a maximum residual compressive stress of 370 MPa and a fatigue life of 158580 cycles, giving an average of 200000 cycles for the group.

If the residual stress profile is proportionally similar to that of DP 38 due to the residual stresses at the same incremental depths it would be approximately a factor of the maximum residual compressive stresses or  $370/405 = 0.914$ , giving 202 MPa compressive, 132 MPa overall compressive and 36 MPa tensile as shown in Figure 92, representing the shot peening at SAA.

The estimated values are given in table 21 and graphs in Figures 92 and 93 are shown below:

Table 21 DP 50: shot peened at UCT estimated residual stress vs depth

Depth (mm)	$\sigma_{x \text{ res}}$ Calibrated (MPa)	$\sigma_{\text{Bend Max}}$ (MPa)	$\sigma_{\text{Bend Min}}$ (MPa)	$\sigma_{x \text{ Tot Max}}$ Calibrated (MPa)	$\sigma_{x \text{ Tot Min}}$ Calibrated (MPa)
0	-182.8	525.0	52.5	342.2	-130.3
0.03	-224.8	524.5	52.0	299.7	-172.8
0.07	-362.9	523.8	51.3	161.0	-311.5
0.12	-370.2	523.0	50.5	152.8	-319.7
0.17	-245.8	522.1	49.6	276.3	-196.2
0.23	-94.7	521.1	48.6	426.4	-46.1
0.28	-45.4	520.2	47.7	474.9	2.4
0.33	-6.7	519.4	46.9	512.7	40.2
0.335	0.0	519.3	46.8	519.3	46.8
0.37	40.0	518.7	46.2	558.7	86.2
0.42	43.2	517.9	45.4	561.1	88.6
0.47	40.5	517.0	44.5	557.6	85.1

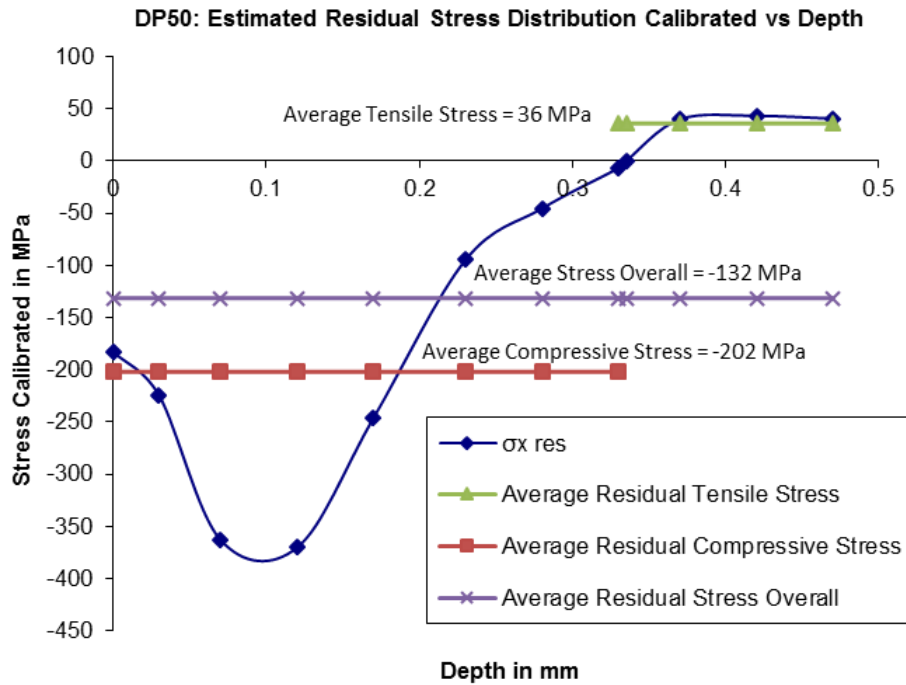


Figure 92 DP 50: estimated residual stress vs depth

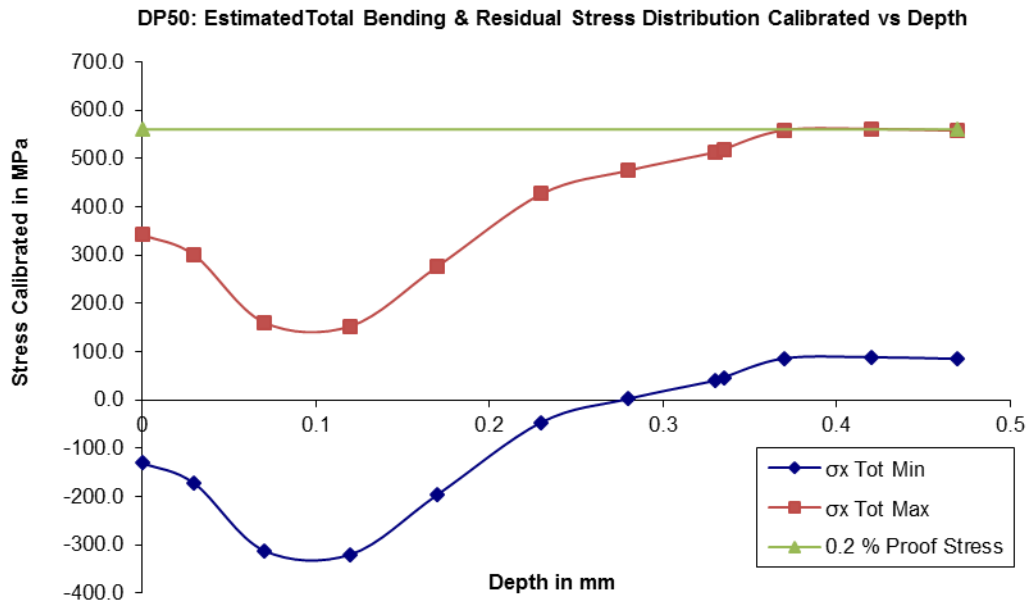


Figure 93 DP 50: shot peened at SAA, estimated total bending and residual stress vs depth

DP 4 was the only specimen in group 9 not to be fatigue tested but can serve as a point of reference for residual stress distribution with specimens shot peened at SAA.

Table 22 DP 4: Shot peened at SAA, not fatigued: residual stress vs depth

Depth (mm)	$\theta$ (°)	$\sigma_2$ (MPa)	$\sigma_1$ (MPa)	$\sigma_{centre}$ (MPa)	R (MPa)	$2\theta$ (Rad)	$\sigma_{x,res}$ (MPa)	$\sigma_{x,res}$ Calibrated (MPa)	$\sigma_{Bend Max}$ (MPa)	$\sigma_{Bend Min}$ (MPa)	$\sigma_{x,Tot Max}$ Calibrated (MPa)	$\sigma_{x,Tot Min}$ Calibrated (MPa)
0								-100			-100.0	-100.0
0.02	-79.2	-1475.4	-1254.8	-1365.1	110.3	-2.76	-1467.6	-123.0	0.0	0.0	-123.0	-123.0
0.05	-74.0	-2980.6	-2386.2	-2683.4	297.2	-2.58	-2935.4	-246.1	0.0	0.0	-246.1	-246.1
0.08	-88.4	-3926.1	-3487.1	-3706.6	219.5	-3.08	-3925.7	-329.1	0.0	0.0	-329.1	-329.1
0.12	63.3	-4456.5	-3347.1	-3901.8	554.7	2.21	-4232.7	-354.8	0.0	0.0	-354.8	-354.8
0.15	50.2	-4050.6	-2624.3	-3337.4	713.2	1.75	-3465.4	-290.5	0.0	0.0	-290.5	-290.5
0.18	45.3	-3047.9	-1675.5	-2361.7	686.2	1.58	-2369.4	-198.6	0.0	0.0	-198.6	-198.6
0.22	42.9	-1859.2	-754.1	-1306.6	552.6	1.50	-1266.0	-106.1	0.0	0.0	-106.1	-106.1
0.25	41.3	-892.3	-48.9	-470.6	421.7	1.44	-416.4	-34.9	0.0	0.0	-34.9	-34.9
0.28	40.1	-814.1	-131.1	-472.6	341.5	1.40	-413.9	-34.7	0.0	0.0	-34.7	-34.7
0.32	38.9	-369.1	137.5	-115.8	253.3	1.36	-62.5	-5.2	0.0	0.0	-5.2	-5.2
0.35	37.9	-126.5	271.8	72.6	199.2	1.32	121.7	10.2	0.0	0.0	10.2	10.2
0.38	36.9	445.8	767.5	606.6	160.9	1.29	651.7	54.6	0.0	0.0	54.6	54.6
0.42	36.0	328.8	635.9	482.3	153.5	1.26	529.9	44.4	0.0	0.0	44.4	44.4
0.45	35.2	404.2	691.7	548.0	143.7	1.23	596.2	50.0	0.0	0.0	50.0	50.0
0.48	34.6	463.1	739.7	601.4	138.3	1.21	650.7	54.5	0.0	0.0	54.5	54.5

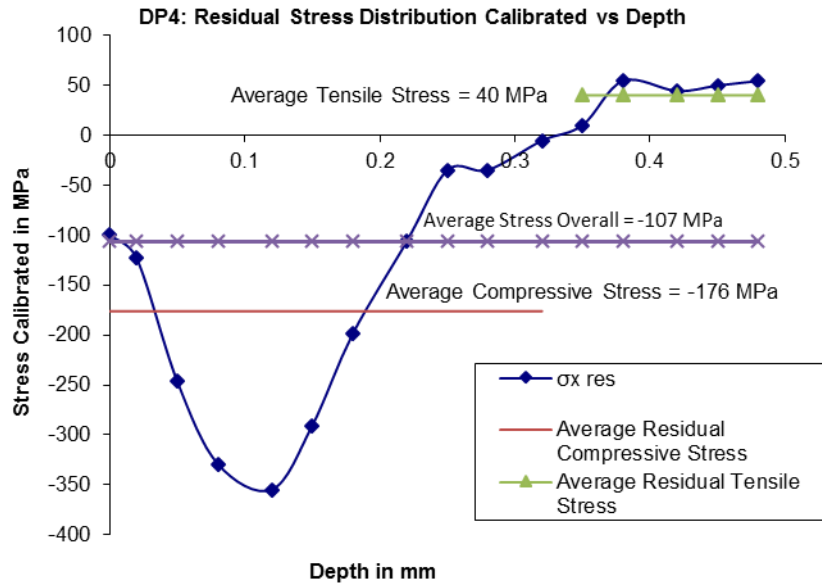


Figure 94 DP 4: Shot peened at SAA, not fatigued: residual stress vs depth

The graph in Figure 94 shows a fairly continuous stress-depth profile with the average residual stresses calibrated at 176 MPa compressive, 107 MPa overall compressive and 40 MPa tensile.

The maximum combined bending and tensile residual stress for DP 38 was 565 MPa at a depth of 0.42 mm, and an estimated 561 MPa for DP 50. Both specimens reached the region of the proof yield stress of 560 MPa, as shown in Figures 91 and 93, so it can be reasonably expected to receive sufficient strain hardening around that depth. Unfortunately, no crack length details are available for depth and crack length comparisons in this case as the fatigue machine was set to “trip on fracture” conditions for overnight testing which would have taken almost 7 hours.

These results can be compared to those of group 7, DP 37 and 45, where the specimens were shot peened at CPU4 and skimmed, having an average fatigue life of 295725 cycles, which is unexpectedly higher than DP 38 that had no skimming.

On the lighter side, it may be worth noting that the patience of the researcher was sorely tested while fatigue testing DP 37 which took 9 hours and 20 minutes of running plus frequent

machine stops in-between to check whether any cracks had formed, waiting before the first crack of a mere 1.35 mm was seen! It then, thankfully, took only another 15 minutes for final fracture! The total fatigue test lasted an afternoon with the machine stopped overnight, the morning of the next day and stopping the machine again, and the third day when it finally failed. Such was the determination of the then much fatigued researcher to resist the temptation to passively switch over to “trip on fracture” this time to obtain crack growth data for such an admirably enduring specimen. It earned the prestige of having the highest fatigue life of 309240 cycles.

Its, also enduring, partner in group 7, DP 45, took almost 8 hours of machine running to fatigue for 282210 cycles with approximately a further 3 hours for stopping to inspect for crack initiation. This was the 12 mm diameter specimen of the fatigue testing, demonstrating that the 2 mm smaller diameter was not a serious liability.

The unusual fatigue life results of Test 6 compared to those in this test will present some challenging parameters for the microstructural analysis.

#### **4.2.4 Microstructural Effects**

This section will include analysis on the effects on the microstructure through plastic straining, microhardness, and fractography testing. The role of these factors will be assessed regarding their effects on strain or work hardening contributing to fatigue life.

##### **4.2.4.1 Plastic Straining**

As stated previously the purpose of the plastic straining was to relieve residual compressive stresses to analyse the effect of varied values, as well as to possibly provide strain or work hardening to assess their influence on fatigue life.

An attempt will be made here to contribute towards determining a life prediction model by analysing the role of fatigue life vs % plastic strain.

All the graphs, including comments relating to plastic strain effects, in sections 4.2.2 and 4.2.3 will apply here.

A portion of table 10 is shown below as table 23 for convenient reference as well as Figure 95, a graph in showing plastic strain vs fatigue life ( $N_f$ ) for all groups and relevant trendlines with their gradients. The gradients of the trendlines are directly relative to the graph where:

$$m = \frac{\Delta N_f}{\Delta(\% \text{ Microstrain})} \quad \text{Equation 4.1}$$

The groups of interest are the ones with specimens that were plastically strained which were groups 2, 4, 5, 6, 8, and DP 36 of 11.

Table 23 Portion of Table 10 to highlight surface treatment, plastic strain, skim and fatigue life

Group No	Spec No DP	UP	UP PS	UP PF SPsaa	UP PS SPct	SPsaa 8-14 A	SPct 20-36 A	SPsaa 8-14A PS	SPct 20-36A PS	Skim 200 μm	PS %Micro Strain	HV Test	Fatigue Life Nf	Fatigue Life Ave	RST MPa	Max Stress MPa
1	1	1									0		34400		20	480
	22	1									0		31100			480
	23	1									0		31000	32167		480
2	28		1								0.2026		28800			525
	29		1								0.5767		21920	25360		525
	24				1						0.2000		250650	100457		525
3	14			1							0		108000		(31)	480
	17			1							0		169330	138665	(31)	480
	15			1							0		55260	110863	31	525
4	13							1			0.4103		55490		21	525
	5							1			0.5000		32750	44120	15	480
5	19							1			0.1703		58500		37	525
	18							1			0.2094		110260			525
	21							1			0.3865		93590			525
	20							1			0.4885	1	116250	94650		525
6	41								1		0.1500		63420			525
	35								1		0.2815		61480	62450	20	525
7	37					1				1	0		309240			525
	45					1				1	0	1	282210	295725		525
8	42								1	1	0.3506		40890			525
	43								1	1	0.4617		41130			525
	26								1	1	0.5960		38740			525
	34								1	1	0.6000		34180			525
	27								1	1	0.8265		51890			525
	25								1	1	1.0072		57840	44112	22	525
9	4					1					0				40	
	50					1					0		158580		(36)	525
	38						1				0		241420	200000	40	525
10	31	1														
	32	1														
11	36							1	1	0.5106	1					
TOTAL	31	5	2	3	1	2	3	6	9	9	0.4363	3	95493		27	
											Ave		Ave		Ave	

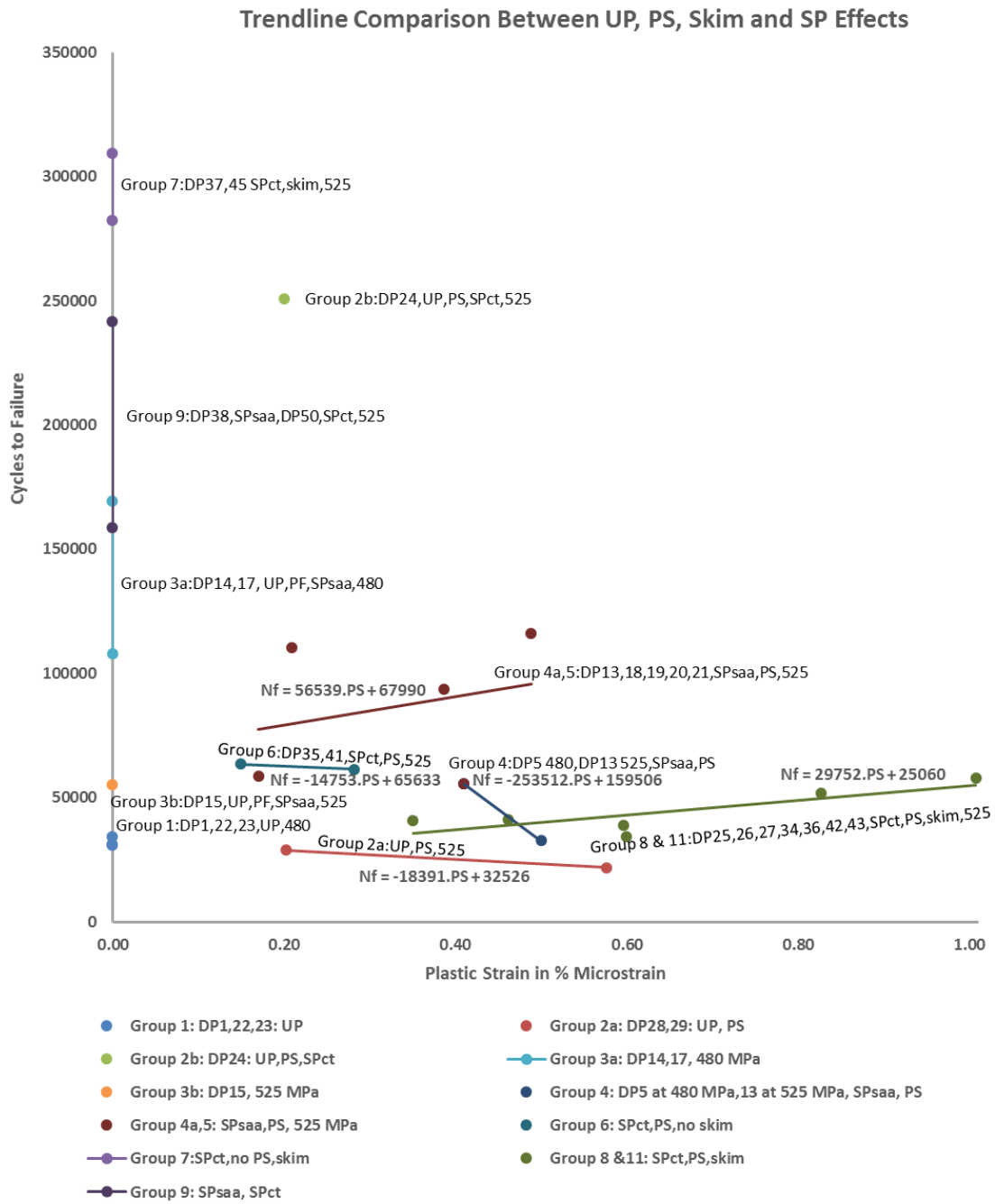


Figure 95 Graph showing all groups and relevant trendlines with gradients

**Group 2:** with specimens DP 28 and 29 which were unpeened and plastically strained had the worst fatigue lives in all fatigue testing, averaging 25360 cycles to failure, which is 27 % short of the standard unpeened specimens in group 1. In this case the plastic straining made the already generally tensile residual stresses before straining even more so, making them more susceptible to early fatigue failure, with little effective evidence of strain or work hardening.

This may be due to the unpeened specimens reaching near the critical plastic strain value for the unpeened specimens as described in par 2.6.2, where even the small amount of average residual compressive stress of 42 MPa over a depth of 0.1 mm, illustrated in Figure 74 in test 1 of par 4.2.3, would be overcome by the plastic straining.

The line gradient shown in Figure 95 shows a negative gradient  $m_{2a} = -18391$ , although small in context with the units, illustrating the detrimental effects of plastic straining on unpeened specimens.

In contrast, as described in par 4.2.2 test 1, shot peening after plastic straining had a dramatically beneficial effect on the fatigue life. In group 2b, DP 24 which was plastically strained to 0.2 % and then shot peened at CPUT had an increase in fatigue life of 770 % over the unpeened and same plastic straining as DP 28, marginally exceeding DP 38 in group 9, shot peened at CPUT without other treatment, by 4 % (9230 cycles).

The higher intensity shot peening at CPUT may have played a role in providing a deeper and slightly higher residual compressive stress as seen in par 4.2.3 test 7 on group 9 when comparing DP 38 shot peened at CPUT with 20 to 36 Almen, to DP 50 shot peened at SAA with 8 to 14 Almen intensity.

**Groups 4a and 5:** with specimens all shot peened at SAA. DP 13, 18, 19, 20, and 21, of groups 4a and 5, were fatigued at a maximum bending stress of 525 MPa, all with varying degrees of plastic straining.

Some aspects of plastic straining were discussed in par 4.2.2 test 3 and 4, and especially par 4.2.3 test 3 and 4.

In groups 4a and 5 it was pointed out that there was an overall increase in fatigue life with an increase in plastic strain, with a significantly wide scatter, although with an average of only

43 % of the fatigue life of specimens shot peened at SAA without other treatments. There was still an impressive 125 % increase in fatigue life over the unpeened specimens.

Figure 95 shows a partially unexpected positive trendline gradient of  $m_{4a,5} = 56539$  showing the increase.

It was partially *unexpected* because the increase in plastic straining reduced the residual compressive stress levels, as shown in Figures 80 for DP 13 and 84 for DP 19 compared to Figure 92 for the unstrained DP 50, required to combat the tensile bending stress leading to earlier failure.

It was also partially *expected* due to microstructural effects imposed on the specimens, leading to the main alternative explanation, which is that the effect of shot peening and plastic strain on the microstructure caused sufficient strain or work hardening which in turn increased the tensile proof stress as well as the dislocation density.

There was little evidence of localised strain softening suggested by Meininger's mechanisms in par 2.6.2. Waterhouse's findings of the fine grain size and work hardening in par 2.6.1 and 2.6.2, resulting in an increase in dislocation density, causing a significant delay in crack initiation and growth before reaching the softened regions in the microstructure which weaken the material so that it fatigues relatively quickly thereafter, seem a more viable proposition to explain the longer fatigue life.

It was also found, and hoped for, that the depth of the compressive residual stress was deeper than the originally estimated 0.2 mm (or 200  $\mu\text{m}$ ), the chosen skim depth. The average depth of the residual compressive stress on specimens shot peened from SAA was 0.32 mm below the surface although slightly reduced depending on the degree of plastic straining.

Table 24 and Figure 96 below show the depth of the residual compressive stress after plastic strain with respect to the source of shot peening.

The depth reduction with an increase in plastic strain is small and does not appear to be too significant, except for DP 25 from group 8 with the maximum 1 % plastic strain.

Table 24 Plastic strain vs depth of residual compressive stress

Specimen Number DP	Type of Shot Peening	% Plastic Strain	Depth of Comp Res Stress (mm)	Ave Res Stress at 200-300 $\mu$ m
50 (estimated)	SAA	0	0.335	-85
19	SAA	0.1703	0.33	-50
13	SAA	0.41	0.3	-25
5	SAA	0.5	0.3	-20
38	CPUT	0	0.335	-95
35	CPUT	0.28	0.39	-130
25	CPUT	1.0072	0.03	5

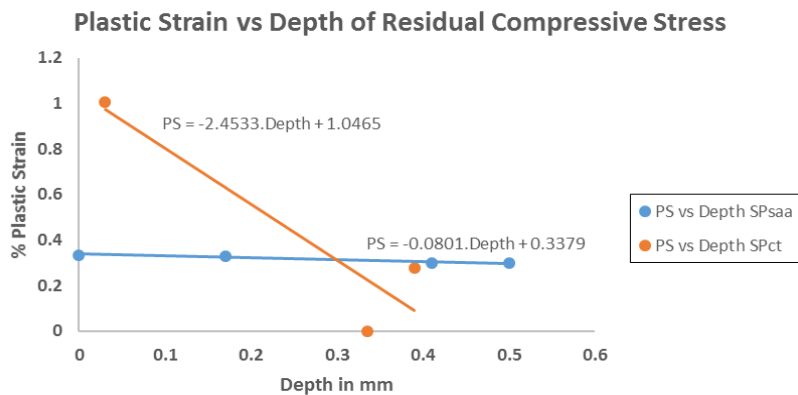


Figure 96 Plastic strain vs depth of residual compressive stress

**Groups 6, 7, 8 and 11:** with all specimens shot peened at CPUT and, except for DP 35 and 41 in group 6, a 200  $\mu$ m radial skim.

DP 37 and 45 were not plastically strained while the rest, DP 25, 26, 27, 34, 35, 36, 42, 43 and 45 were plastically strained by incremental amounts between 0.15 to 1 %.

As shown in par 4.2.2 test 5, the skimmed but not plastically strained specimens in group 7 had a very high average fatigue life of 295725 cycles, 6.7 times more than the skimmed plastically strained specimens in group 8, and 4.7 times more than the unskimmed specimens in group 6, implying that plastic straining severely reduced the fatigue life of shot peened specimens.

However, within the skimmed plastically strained specimens in group 8, there was an increase in fatigue life from 40890 to 57840 cycles reasonably directly proportional to the plastic strain, as was experienced above in groups 4a and 5. The trendline in Figure 95 shows a line gradient of  $m_{8,11} = 29752$  with a fairly narrow scatter.

It may be worth noting that the line gradient with shot peening from CPUT, an average of 0.64 % plastic strain, a 200  $\mu\text{m}$  skim and an average fatigue life of 44112 cycles had about half the gradient of groups 4a and 5 shot peened at SAA, an average 0.32 % plastic strain, no skim and an average fatigue life of 86818 cycles. This shows for both cases there is a trend that, for shot peened specimens, an increase in plastic strain will lead to a localised increase in fatigue life, contrary to unpeened specimens as shown for group 2.

Group 6, however, showed a marginal decrease in fatigue life with a small 0.14 % increase in plastic strain, but with only two specimens, the trendline may not be sufficiently representative.

Once it is acknowledged that the 200  $\mu\text{m}$  radial skim left a remaining layer of about 130  $\mu\text{m}$  of residual compressive stress, as shown in table 24, it fortuitously provided a limited restraint against the tensile bending stress. The average fatigue life performance was still significantly higher than that of the unpeened specimens in group 1 by a reasonable factor of 1.37 in the case of the plastically strained and skimmed specimens in group 8 and a staggering factor of 9.19 in the case of skimmed specimens in group 7 without plastic straining.

This implies that the remaining residual stress after skimming is able to assist in providing a significant increase in fatigue life.

The effects of shot peening on the surface can be seen from the fractographs in par 3.5.4 showing the surface distortion to be about 200  $\mu\text{m}$  deep, similar to the fractograph of DP 27, shot peened at CPUT as well as skimmed and plastically strained by 0.8265 %, which shows the affected depth around 100  $\mu\text{m}$  (see Appendix D).

From the residual stress-depth diagrams of shot peened specimens throughout par 4.2.3 (specifically Figures 76,79,80,84,86,90 and 94), it shows that the compressive stress measured at the 200  $\mu\text{m}$  depth to zero residual stress at the 300  $\mu\text{m}$  depth gives a useful guide to their contribution to fatigue life. This would indicate an average compressive stress between these points to be about half of the compressive stress at a depth of 0.2 mm as the shape of the curve to zero residual stress is approximately triangular.

Taking the general trend for all specimens tested in this research for residual stress-depth profiles in that region, the approximate stresses would range from 20 to 130 MPa compressive with a weighted average of 70 MPa compressive.

DP 25 which was skimmed and had 1 % plastic straining gave a small residual tensile stress of approximately 5 MPa. This seems to indicate that the 1 % plastic strain with skim could serve as the residual stress near-zero limit in the region beyond 200  $\mu\text{m}$ .

Table 24 and Figure 97 give the average residual stress trends between 200 and 300  $\mu\text{m}$  depths for groups 4a and 5 to represent shot peening at SAA, and the 100  $\mu\text{m}$  depth for groups 7, 8 and 11.

It can be seen that the residual compressive stress imposed by the higher intensity CPUT shot peening was greater than that from SAA in that region, with the trendline gradients almost the same, although the scatter for the CPUT shot peened specimens was higher than that of SAA.

The outcome for group 8, then, is that after shot peening from CPUT, a 200  $\mu\text{m}$  skim and various plastic straining, there remains a shallow compressive stress layer, within the region, of around 100  $\mu\text{m}$  material depth with an approximate residual compressive stress distribution shown by the trendline in Figure 96, contributing to an average 37 % improvement in fatigue life.

The plastic straining alters the microstructure not only to reduce residual stress but also to work harden it to greater strength to increase the fatigue life, demonstrating a notable contribution of the microstructure to the fatigue life of these specimens.

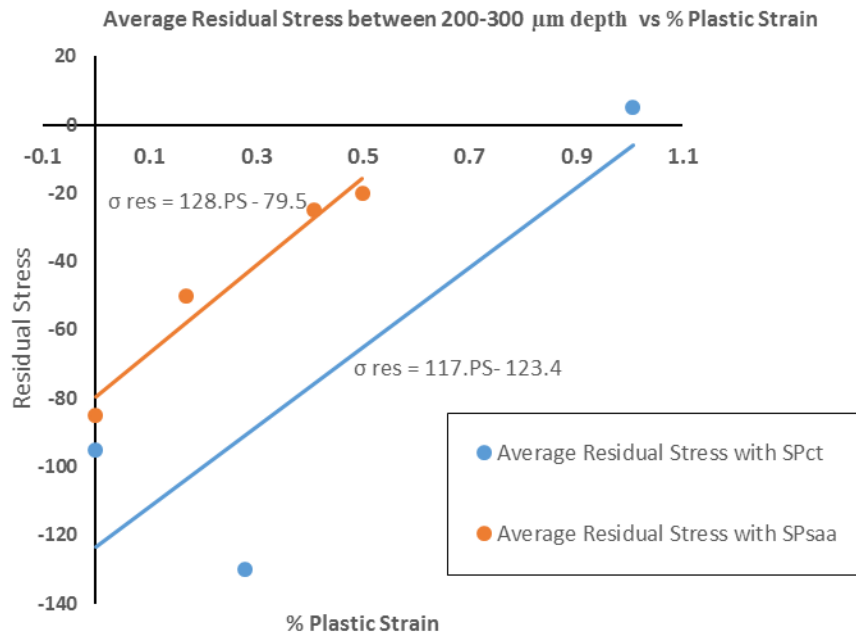


Figure 97 Average residual stress between 200-300  $\mu\text{m}$  depth vs plastic strain

#### 4.2.4.2 Microhardness

Three specimens, DP 20, 36 and 45, were given microhardness testing shown in par 3.5.3. The Figures 28 and 29 in par 2.7 indicate relationships between microhardness with tensile strength and depth with aluminium alloys.

Unfortunately, the spectrum of values is too broad and the highest stress too low in Figure 28 to apply precise values here. Only ranges of stress values can be investigated.

If the hardness of 175 HV (87 HRB) from table 1 is plotted on Figure 28 the upper and lower stresses in the spectrum are 557 MPa and 495 MP respectively, which is well below the maximum tensile strength of 612 MPa and more in line with the 0.2 % proof stress of 560 MPa.

If the proof stress is in line with the upper stress line of Figure 28, it would be more useful to this research as plastic straining and strain or work hardness are more inclined to increase the yield point, one of the primary motivations for understanding increased fatigue life with increased plastic strain with shot peened specimens.

The proof stress of 560 MPa corresponding to the normal material hardness of 175 HV could then be used as a point of reference for other hardness values found in the tests on the specimens with their corresponding yield stress points.

Matching known Vickers hardness values within the required range of this research and their corresponding Rockwell hardness B values were extracted from commercial tables <sup>[35]</sup> and inserted into appropriate fields in table 25. These values were then used to plot Figure 98 to find a general conversion equation between them.

This equation was then used to fill in the remaining unknown Rockwell hardness B values of table 25. These Rockwell hardness B values were used to obtain the corresponding stresses from Figure 28, which were then used to draw Figure 99 to obtain an equation to calculate all the stresses needed to generate table 25. Finally, the correlation between diametral depth and estimated proof stress could be demonstrated in Figure 100.

Part of Table 9 is given here for convenient identification.

Extract of Table 9 showing treatments given to each specimen

Description	Value/No			Unit
Specimen	DP 20	DP 36	DP 45	
Peening	8 to 14	20 to 36	20 to 36	A
$\epsilon_{pl}$	0.4885	0.5106	0	% $\mu$ Strain
$K_{1c}$	28.6	28.6	28.6	MPa.m <sup>1/2</sup>
Skim	0	200	200	$\mu$ m
$N_{failure}$	116250	N/A	282210	cycles
$\sigma_{uts\ ave}$	612	612	612	MPa
$\sigma_{yield\ ave}$	560	560	560	MPa
$R_{stress\ ratio}$	0.1	0.1	0.1	
$\sigma_{bend\ min}$	52.5	582.5	52.5	MPa
$\sigma_{Bend\ max}$	525	525	525	MPa
Diameter	14	14	12	mm
Hardness	Vickers	Vickers	Vickers	200gm

Table 25 Conversion from Rockwell hardness B to Vickers hardness and stress against incremental depth

Test Position	Depth (mm)	DP 20			DP 36			DP 45		
		HV	HRB	MPa	HV	HRB	MPa	HV	HRB	MPa
1	0.10	171	87	559	156	82	531	162	84	543
2	0.25	176	88	567	161	84	541	176	88	567
3	0.40	177	88	569	175	88	566	166	85	551
4	0.55	178	88	570	170	86	558	164	85	547
5	0.70	181	89	575	171	87	559	163	84	545
6	0.85	177	88	569	156	82	531	166	85	551
7	1.00	186	90	581	163	84	545	166	85	551
8	1.15	178	88	570	164	85	547	163	84	545
9	1.30	174	87	564	163	84	545	169	86	556
10	1.45	176	88	567	165	85	549	166	85	551
11	1.60	170	86	558	161	84	541	167	86	552
12	1.75	174	87	564	162	84	543	164	85	547
13	1.90	172	87	561	164	85	547	162	84	543
14	2.05	181	89	575	163	84	545	168	86	554
15	2.55	171	87	559	159	83	537	162	84	543
16	3.05	167	86	552	158	83	535	166	85	551
17	3.55	169	86	556	155	82	529	163	84	545
18	4.05	176	88	567	160	84	539	166	85	551
19	5.05	157	83	533	156	82	531	170	86	558
20	6.05	166	85	551	157	83	533	158	83	535
21	7.05	164	85	547	156	82	531	159	83	537
22	9.05	164	85	547	161	84	541	154	82	526
Average		173.0	87.1	562.0	161.6	84.0	541.9	164.5	84.8	547.6

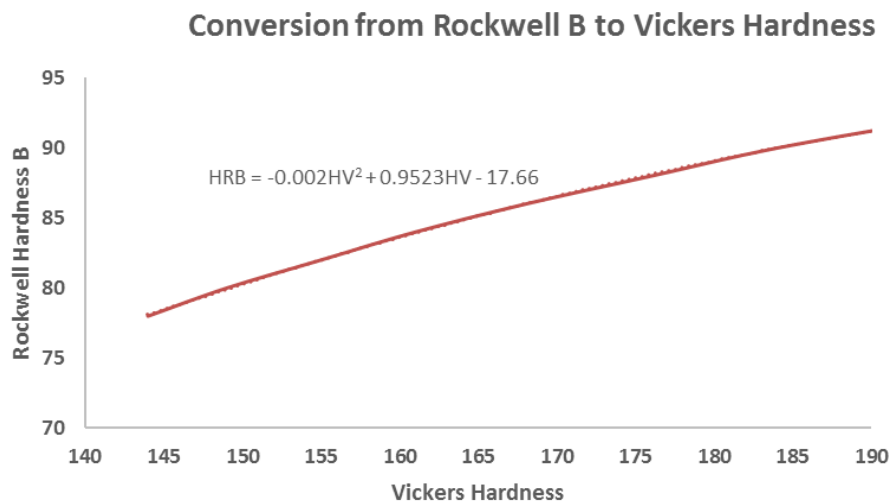


Figure 98 Graph showing conversion between Vickers and Rockwell B hardness

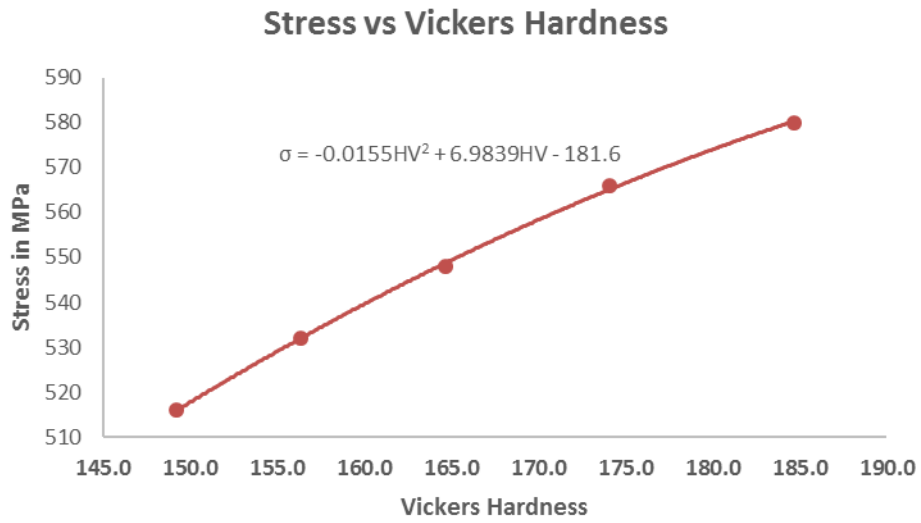


Figure 99 Vickers hardness vs Stress derived from figure 28

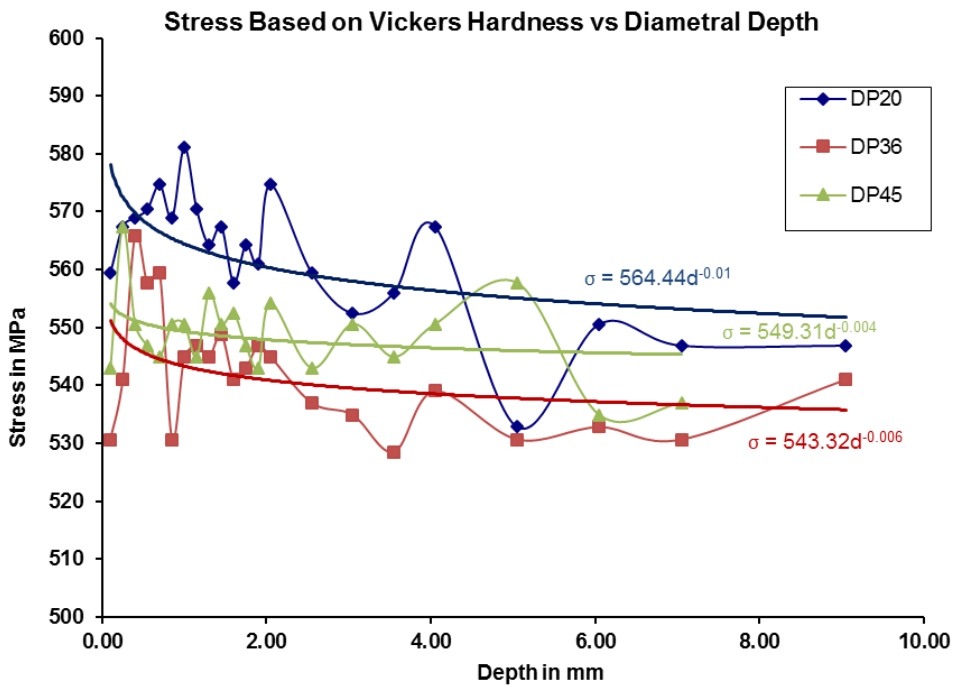


Figure 100 Diametral depth vs estimated proof stress derived from Vickers hardness values

The trendlines of the Vickers hardness vs diametral depth in Figure 60 show a close correlation to the stress vs diametral depth in Figure 100, although with the stress vs diametral depth trendline gradients somewhat steeper.

This implies that there is some correlation between Vickers hardness and proof stress, which should correspond with the ultimate tensile strength as well. The precision of the stress values here relies heavily on the relation of the highest stress line of the bandwidth between material strength of aluminium alloys and Rockwell hardness B values in Figure 28. Using the highest stress line may be justified as 7075-T6 is amongst the strongest of aluminium alloys.

The next issue is whether the microhardness contributes to indicators of significant microstructural inferences to fatigue life due to the various treatments and physical properties of the specimens.

In all cases the specific microhardness and stress values increase in the subsurface region before gradually decreasing through the diametral depth towards closer convergence.

This indicates the increase in proof stress in the shot peened region most probably due to the resulting high plastic deformation and work hardening, which would inhibit crack initiation and extend fatigue life.

The 200  $\mu\text{m}$  radial skim of DP 45 may have played a role in reducing the subsurface microhardness and stress due to the removal of most of the plastically deformed surface due to shot peening, compared to DP 20 with no skim and a deeper layer, but with no significant correlation to fatigue life.

The 0.4885 % plastic straining in conjunction with shot peening of DP 20 were perhaps the most significant contributors to the microhardness and proof stress increase for this specimen.

The role of microhardness and indicated proof stress through the diametral depth gave limited evidence of its effect on the microstructure on fatigue life here. This may be due to the unreliability factor of aluminium for microhardness to predict its strength accurately enough, as stated by Davis referred to in par 2.7.

#### 4.2.4.3 Fractography

The SEM fractographs clearly demonstrate microstructural properties as to the shot peened layer, types of fracture, ductility and crack features.

The fractographs in par 3.5.4 showing typical microstructural characteristics found in all specimens tested will be highlighted in this section with additional fractographs.

**Groups 4a and 5:** with specimens all shot peened at SAA. DP 13, 18, 19, 20, and 21, were fatigued at a maximum bending stress of 525 MPa, all with varying degrees of plastic straining.

DP 19 with 0.1703 % microstrain and fatigue life 58500 cycles, and DP 20 with 0.4885 % microstrain and fatigue life 116250 cycles, were given SEM tests.

The following fractographs will show DP 19 on the left and DP 20 on the right for comparison.

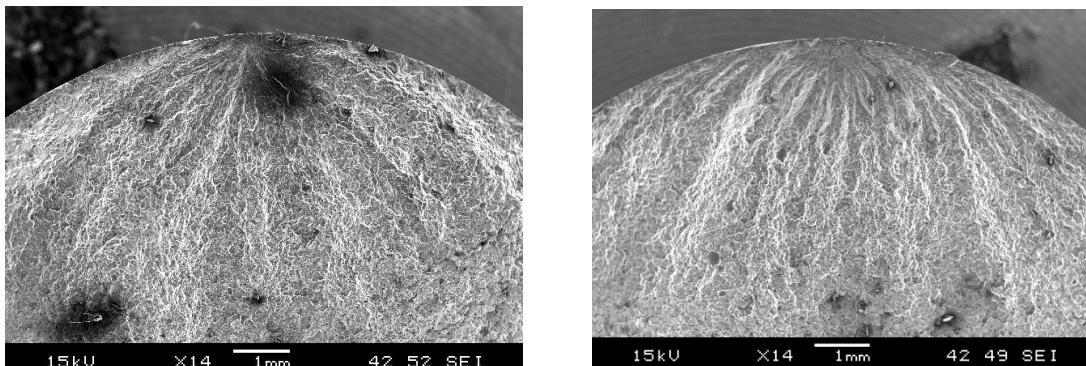


Figure 101 DP 19 and 20 fractographs of the crack initiation sites showing similar fracture surface features

From Figure 101 it can be seen that, besides the general fracture surface similarities, there are more marked dimples with DP 20 which may be due to the additional plastic strain stretching the material around harder impurities as shown in Figure 105.

Figure 102 shows the shot peened layers about 200  $\mu\text{m}$  deep and shear cleavage markings which are at about  $45^\circ$  to the surface.

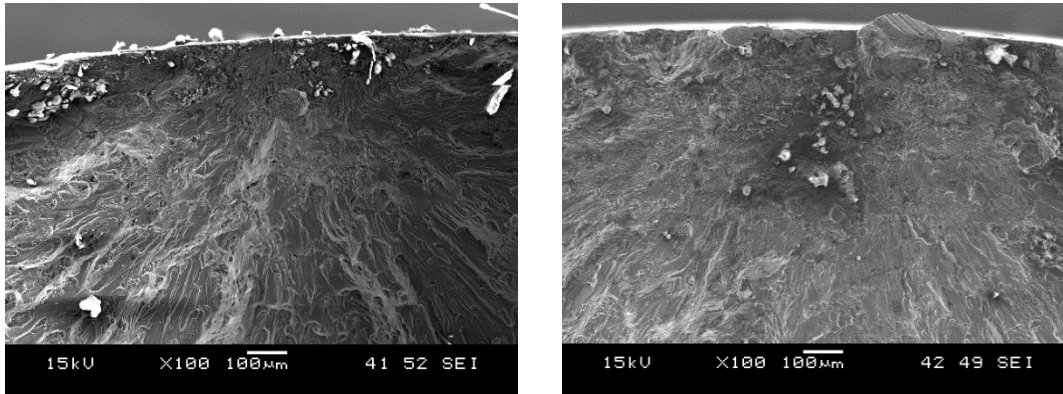


Figure 102 Close up views of the crack initiation sites of DP 19 and 20 showing the shot peened layers close to the surface and cleavage fracture on the planes of maximum shear

Figure 103 shows magnified views of the top left of both fractographs in Figure 102 with shear the cleavage planes clearly visible.

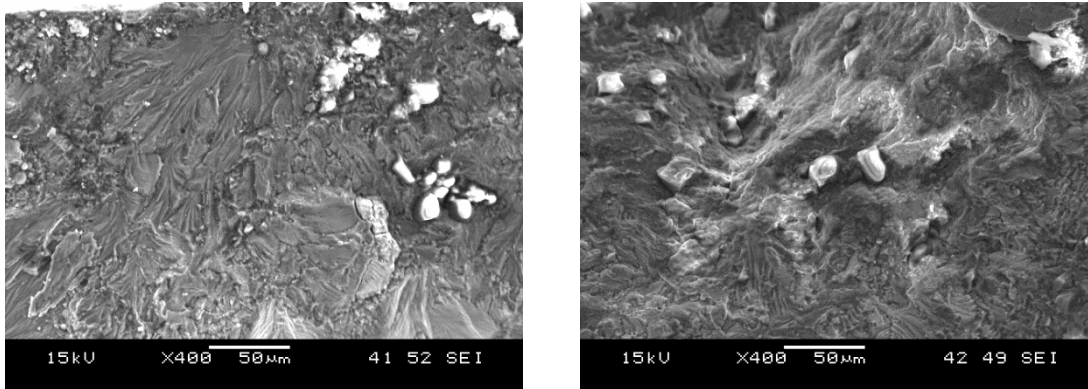


Figure 103 Magnification of Figure 101 showing shot peened region with flat cleavage planes (left) and fracture trough at crack initiation (right)

Figure 104 shows cleavage with typical ductile striations. On the right DP 20 possibly shows what could be termed as “tyre tracks”, perpendicular to the direction of crack propagation or growth, which are striation-like markings produced by relative movement between the two fracture surfaces during cyclic loading and crack extension as well as probable fatigue crack growth. This requires the presence of hard inclusions with combined Mode 1 (tension) and

Mode 2 (shear in the direction of the crack growth), or Mode 1 and 3, referred to in par 2.1.2 and appendix A.

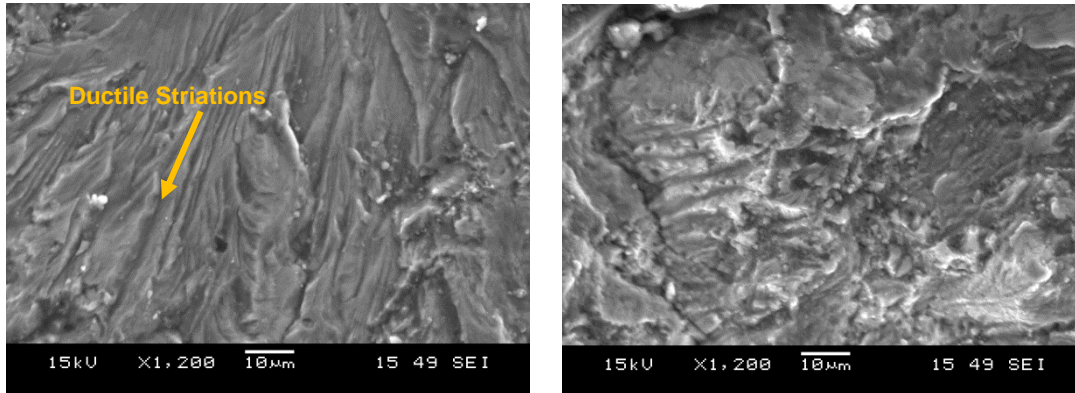


Figure 104 Further magnification of Figure 102 showing shear cleavage and high atomic steps of the ductile region

Figure 105 shows typical dimples, or microvoids, and clear coalescence of up to 6 microvoids indicated by the arrow, in the fast fracture region, indicating transgranular cracking. These particle precipitates in the dimple centres effectively resist fatiguing forces causing persistent slip bands, shown somewhat stacked in the right hand picture of figure 104.

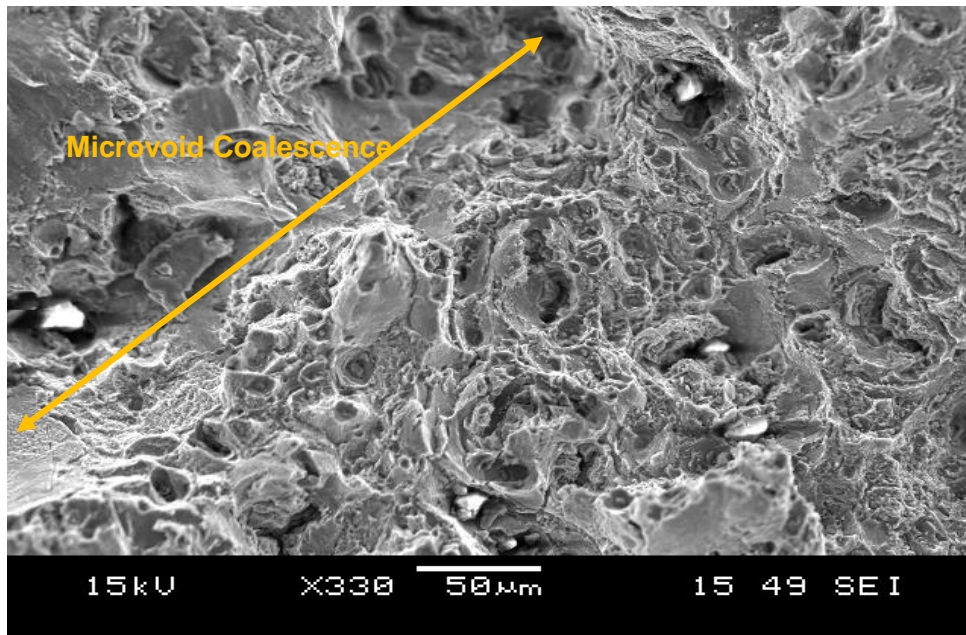


Figure 105 DP 20 showing ductile dimpled microvoids due to tensile overload with high plastic deformation between the dimples and white coloured precipitate particle defects at their centres. Intergranular microvoid coalescence is also shown.

**Groups 6, 7, 8 and 11:** with all specimens shot peened at CPUT and, except for DP 35 and 41 in group 6, a 200  $\mu\text{m}$  radial skim.

DP 37 and 45 were not plastically strained while the rest, DP 25, 26, 27, 34, 35, 36, 41, 42 and 43 were plastically strained by incremental amounts between 0.15 to 1 %.

SEM tests were given to four specimens.

DP 37 and 45 had skimming but no plastic straining with fatigue lives of 309240 and 282210 cycles respectively.

DP 27 received 0.8265 % microstrain and skimming with a fatigue life of 51890 cycles

DP 36 received 0.5106 % microstrain and was skimmed but fatigue results not available.

Figure 101 of groups 4a and 5 were similar for this group and so will not be repeated here. The effects of the heavier CPUT shot peening, plastic strain and skim on the microstructure will be of particular interest here.

Figures 106 and 107 show the less deep shot peened layers of around 100  $\mu\text{m}$  on DP 37 and 45

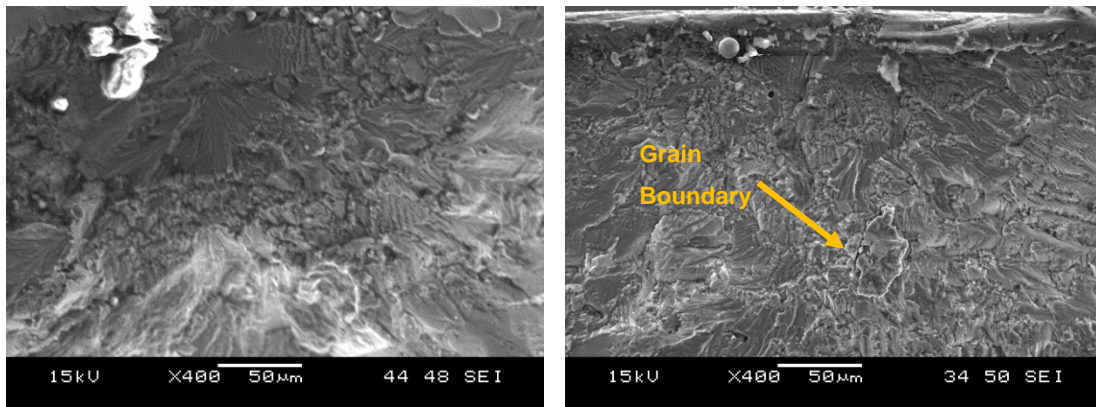


Figure 106 DP 37 and 45 at crack initiation sites showing the much smaller shot peened depth due to skimming. Notice the much darker compacted surface from the heavier shot peening

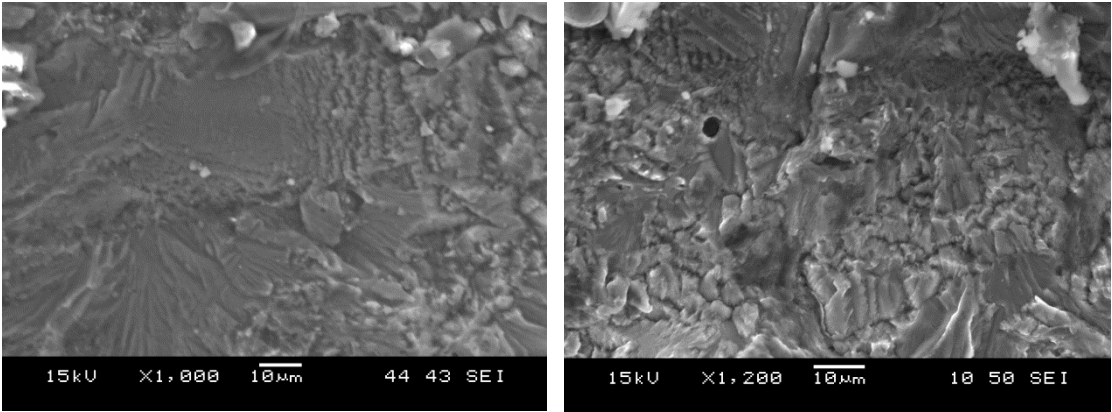


Figure 107 DP 37 and 45. Magnifications near the surface of Figure 105 of the top centre

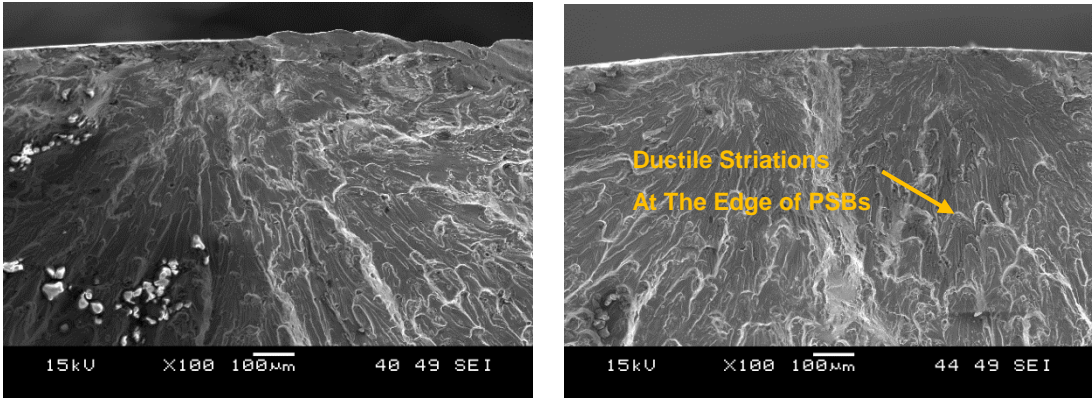


Figure 108 DP 27 and 36 showing shot peened surfaces and shear cleavage with atomic steps and ductile striations

Persistent slip bands (PSBs) can be seen in Figure 108, typical of the near crack initiation region, and amplified in Figure 109.

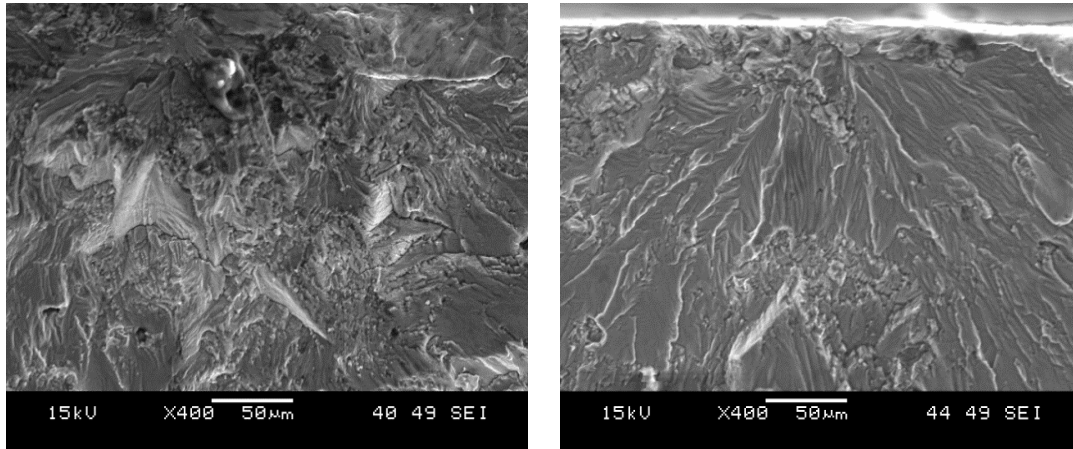


Figure 109 DP 27 and 36 showing magnifications of figure 107 at the top surface near the centre

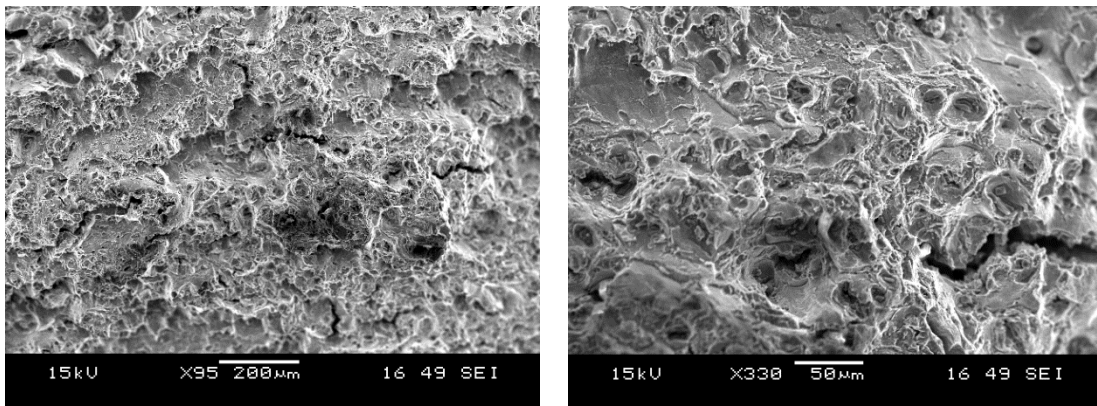


Figure 110 DP 27 with two images of the fast fracture region showing intergranular microvoid coalescence cracking, typical of ductile materials

Microstructural properties are demonstrated by the fractographs above and illustrate the intensity of shot peened layers, shear cleavage at the slow crack initiation region, dimpled ductile fast fracture surfaces with transgranular microvoid coalescence and cracks.

What was not so clear from these fractographs were the effects of plastic strain.

However, the identified properties can be used to assist in the analysis of life prediction modelling.

### 4.3 LIFE PREDICTION MODELLING

Par 2.9 describes combining the properties of the Gerber equation, to transform stress amplitudes of non-zero to zero mean stresses, with the Juvinall and Marshek life prediction model, to produce an effective stress amplitude vs fatigue life equation that may be used within the low cycle fatigue region.

This equation will need to have the flexibility to include microstructural effects in unpeened and shot peened conditions with a limited range of plastic straining. To this end a generalised fatigue strength factor, or factors, may be required to “shape” the life prediction equation model to achieve sufficient accuracy.

The strategy to be used will be to obtain raw values to establish operating equation parameters and then fine tune these to representative values through applicable generalised fatigue factors until sufficiently representative solutions, or ranges of solutions, are found.

It needs to be emphasised that the life prediction analysis will only be applied to specimens that underwent residual stress tests, and to the groups they belonged to, as the residual stress profiles are required to obtain the fully reversible stress amplitudes found by the Gerber equation.

#### 4.3.1 S-N Curve Selection

The purpose in this section is to find a working correspondence reference between the number of cycles to failure in the test groups to the alternating stress for fully reversible bending where  $R = -1$ , purely from the S-N diagram perspective.

Finding a reliable S-N curve to use as a point of reference is not trivial. Too many S-N curves have insufficient ranges of accuracy to be considered.

The most consistent S-N curves found by the author are in Figures 43 and 44 described in par 2.9.4 based on the MIL-HDBK-5J, for axial fatigue testing, and the Atlas of Fatigue Curves, for bending fatigue testing, respectively.

According to Juvinall and Marshek in their book, “Fundamentals of Machine Component Design”, practical stress conversion factors from axial to bending tests are given for the endurance limit and  $10^3$  cycles, essential for their life prediction model.

For the endurance limit the stress for axial reverse testing is about 0.9 times that for reverse bending and about 0.8 to 0.9 times at  $10^3$  or  $10^4$  cycles <sup>[31]</sup>.

It needs to be noted that aluminium alloys do not exhibit genuine endurance limits but, to align with the Juvinal and Marshek life prediction model, a working endurance value had to be found. The preference by the researcher was to find a value practically, but useably, remote enough so as not to detrimentally affect the results.

By careful inspection of the behaviour of the curves in Figure 43, and therefore Figures 111 to 113 below on which it is based,  $10^8$  cycles appeared to be the most suitable option, and was adopted throughout.

**Firstly**, for the recalibration of **MIL-HDBK-5J** curves shown in Figure 43, the conversion factors from axial to bending over the whole stress range, based on Figure 111 and adaptations for aluminium alloys from Juvinal and Marshek, were done by plotting the factors at endurance and  $10^3$  cycles and then finding the linear equation between them, as shown in Figure 112 <sup>[31]</sup>. In general, the axial stress is approximately 90 % of the bending stress.

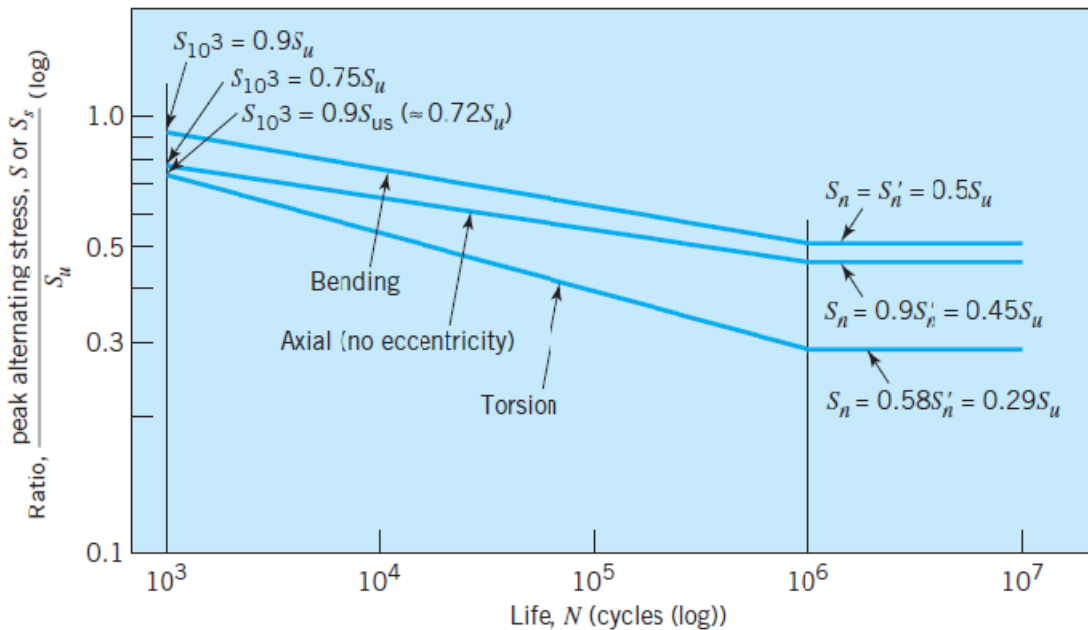


Figure 111 Generalised S-N curves for polished 7.6 mm diameter steel specimens <sup>[31]</sup>

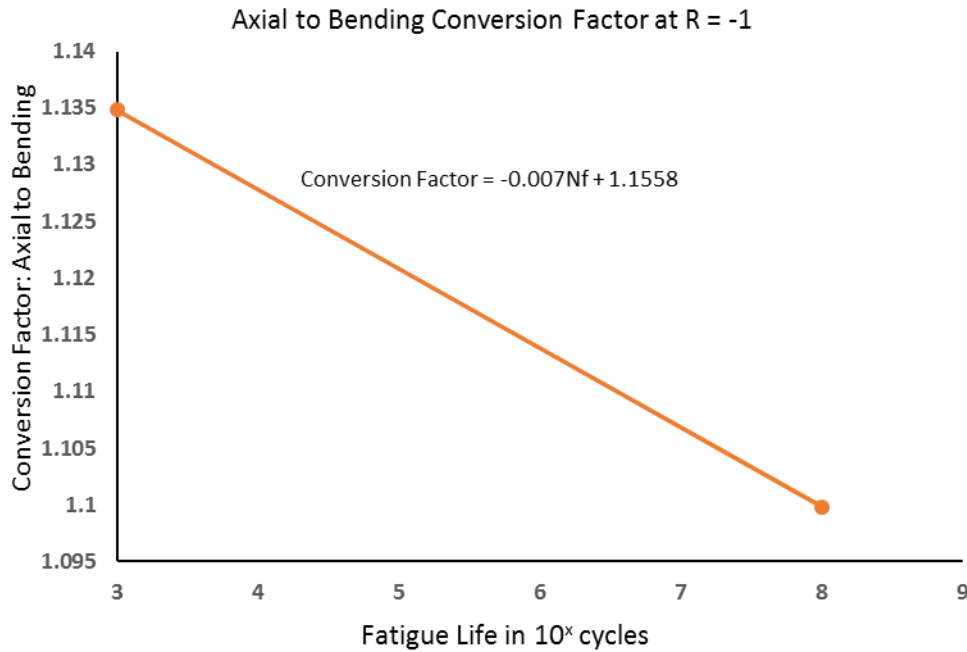


Figure 112 Axial to bending conversion line for S-N diagram

These conversion factors were used in table 26 to plot the points for reversible bending on the S-N diagram in Figure 113.

From figure 113 and table 26 it can be seen that the endurance bending stress rated at  $10^8$  cycles is 154 MPa.

In addition, for the sake of versatility, a best fit trendline needed to be aligned to the fully reversible bending line in figure 113 by applying Microsoft Excel trendline equations.

The best fit equation for reversible bending for Sn proved to be a polynomial of the 3<sup>rd</sup> order, and the equation generated as follows:

$$S_n = -0.9477 (\text{Log } N_f)^3 + 26.717 (\text{Log } N_f)^2 - 276.05 \text{Log } N_f + 1137.4 \quad \text{Equation 4.2}$$

This equation was used to calculate the  $S_{1000}$  value and was found to be 524 MPa which came to an acceptable 85.6 % of the UTS.

One drawback is that the MIL-HDBK-5J handbook does not offer stresses at  $10^3$  cycles, from which Figure 43 is taken, and warns that no values beyond those shown in the diagram should be assumed. This implies that the 524 MPa can only serve as an estimated guideline

and token stress for the sake of the life prediction model analysis, unless it proves sufficiently unreliable.

Also, since values from  $10^4$  cycles at a stress of 400 MPa in table 26 are more certain, it may become necessary to use this as the primary point of reference instead.

The Log Nf values from column 1 in Table 26 were then substituted into the generated equation above to formulate column 5, showing a close correlation with the plotted values in column 4 with minimal percentage variances in the required range of values used in this research, as shown in column 6.

Table 26 Axial to bending conversions for unpeened specimens for  $R = -1$

Log Nf	Stress MPa R = -1 Axial	Conversion Factor Axial to Bending	Stress Sn in MPa R = -1 Bending		Log Nf Equation	% Variance in Log Nf	Log Sn R = -1 Axial	Log Sn R = -1 Bending	Log Sn R = -1 Bending Equation
			Factor	Equation					
3	462	1.1348	524	524	2.91	2.91	2.66	2.72	2.71
3.5	405	1.1313	458	458	3.46	1.20	2.61	2.66	2.66
4	355	1.1278	400	400	4.00	-0.08	2.55	2.60	2.60
4.5	310	1.1243	349	350	4.54	-0.98	2.49	2.54	2.55
5	275	1.1208	308	307	5.08	-1.53	2.44	2.49	2.50
6	215	1.11	239	238	6.10	-1.59	2.33	2.38	2.39
7	170	1.1068	188	189	7.03	-0.38	2.23	2.28	2.28
8	140	1.0998	154	154	7.86	1.69	2.15	2.19	2.17

The Log Sn values for bending are shown in column 9 and the generated equation values in the final column 10, again demonstrating a very close and useful correlation.

The log Nf vs Log Sn graph is shown in Figure 114 producing a linear graph with a trendline equation of:

$$\text{Log Sn} = -0.1074 \text{ Log Nf} + 3.032 \quad \text{Equation 4.3}$$

This equation and graph can be used as a pre-calibrated point of reference towards finding a life prediction model for all the specified types of (unpeened, shot peened, plastically strained, and skimmed) specimen treatments for this research.

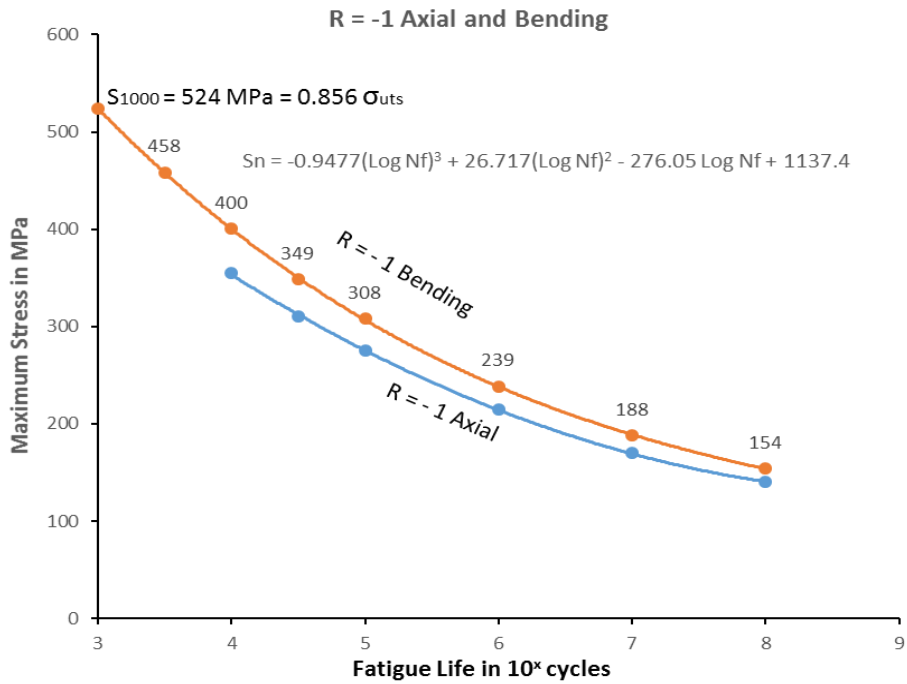


Figure 113 S-N diagram showing axial and bending lines for R = -1

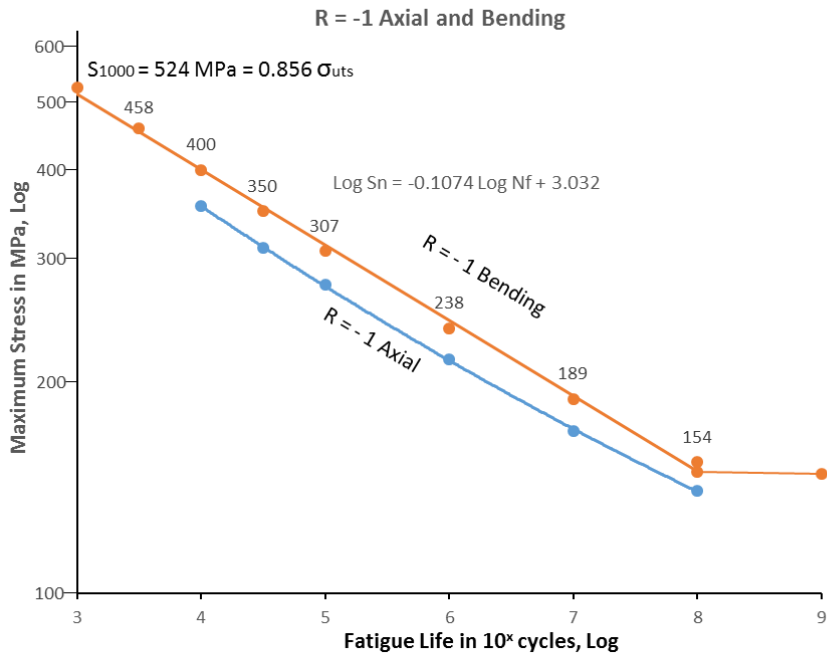


Figure 114 Log S-Log N diagram for axial and bending lines for R = -1

It now becomes appropriate to apply the generalised factors, described in par 2.9.5 to recalibrate Figure 114 for smooth untreated specimens to the testing conditions for this research by using equation 2.25, to find a working endurance limit.

From equation 2.25:

$$S'_n = 154 \text{ MPa}$$

$$C_L = 1$$

$C_G = 0.9$  for the 10 to 14 mm diameters within the limits of  $10 \text{ mm} < \text{diameter} < 50 \text{ mm}$ . The specimens tested for the MIL-HDBK-5J S-N curves were 5 mm in diameter where  $C_G = 1$

$C_S = 0.77$  to  $0.9$  from Figure 46 for machined for cold-drawn and fine ground steels for a UTS of 612 MPa (88.8 ksi). The only information for aluminium alloys found by the author was on the Yellowflight Engineering website which gave a diagram with similar parameters to Figure 46 with an almost identically correlating range of  $0.75$  to  $0.9$ . By inspecting the diagrams, a value of  $0.9$  was deemed the most suitable.

$C_T = 1$  as stated in par 2.9.5

$C_R = 0.897$  for 95 % reliability which is the estimate for the testing for this research

$$\begin{aligned} S_n &= S'_n \cdot C_L \cdot C_G \cdot C_S \cdot C_T \cdot C_R = 154 \times (1) \times (0.9) \times (0.9) \times (1) \times (0.897) = 112 \text{ MPa} \\ &= 0.727 S'_n = 18 \% \text{ of the UTS for these conditions} \end{aligned}$$

This value will be used as the endurance limit at  $10^8$  cycles for the untreated (unpeened) specimens in Group 1 and the S-N diagram to be used as a point of reference.

The Gerber equation is to be used to find the fully reversible alternating stress for Group 1.

DP1 was the only specimen in group 1 that was given residual stress – depth testing and will be evaluated here for compliance with the S-N diagram as follows:

Maximum bending stress = 480 MPa

Applied stress amplitude =  $0.5(\sigma_{\max} - \sigma_{\min}) = 0.5(480 - 48) = 216$  MPa

Applied mean stress =  $0.5(\sigma_{\max} + \sigma_{\min}) = 0.5(480 + 48) = 264$  MPa

Residual tensile stress = 20 MPa

Effective mean stress = applied mean stress + residual tensile stress =  $264 + 20 = 284$  MPa

Substituting into the Gerber equation (2.21) yields a corresponding fully reversible alternating stress at  $R = -1$  of:

$$\sigma_n = \frac{\sigma_a}{1 - \left[\frac{\sigma_m}{\sigma_u}\right]^2} = \frac{216}{1 - \left[\frac{284}{612}\right]^2} = 275.3 \text{ MPa}$$

Since DP 1 failed at 34400 cycles, it will need to be on, or a very close point on, the Log-Log S-N line to ensure 95 % reliability. The generated diagram is shown below in Figure 115.

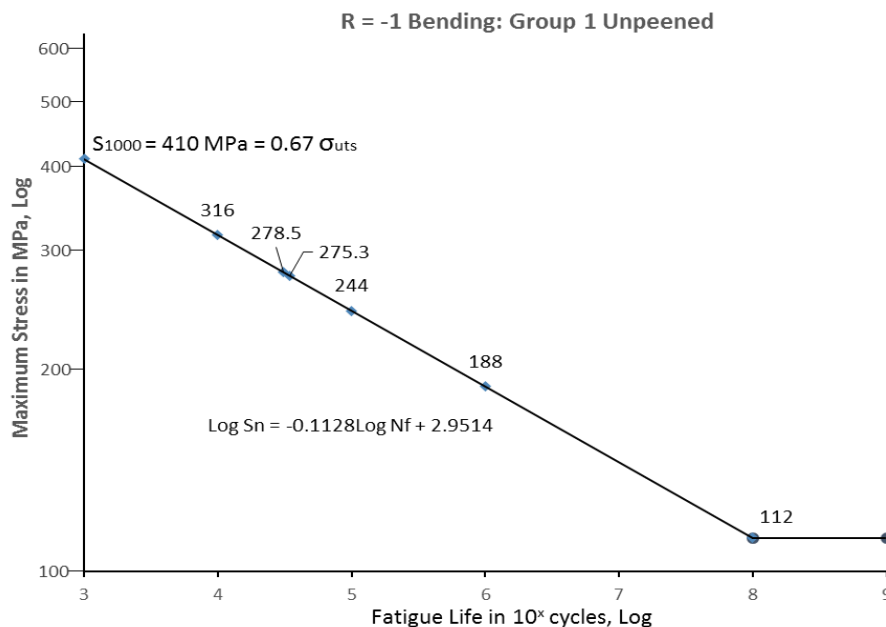


Figure 115 Log S-Log N showing the MIL-HDBK-5J diagram of Group 1 for unpeened specimens for  $R = -1$

The line equation of the calibrated graph in Figure 115 is:

$$\text{Log } S_n = -0.1128 \text{ Log } N_f + 2.9514 \quad \text{Equation 4.4}$$

The stress at  $10^3$  cycles was extrapolated from the line equation at 410 MPa which, at 67 % of the 612 MPa UTS, is a bit low. If the UTS were to be 572 MPa, according to Table 1, or 565 MPa according to the MIL-HDBK-5J handbook, then it would be around 72 %.

This discrepancy of UTS values may call into question the level of compliance between the 565 MPa used by the MIL-HDBK-5J test to that of the 612 MPa obtained in the tensile tests on the two specimens, DP 18 and 19, implying an inevitable variance in solutions. It is hoped that the generalised factors will reduce any significance to them.

By applying this approach all the specimens of Group 1 all the specimen values are reliably close to the line and should be useful to other fatigue tests on similar specimens.

**Secondly**, for the recalibration of the **Atlas of Fatigue Curves** shown in Figure 44, only the application of the generalised factors need be used as the curves are for bending fatiguing already.

Values from Figure 44 are shown in Table 27 and used to generate Figure 116 to replicate it as well as the equation of the line.

Table 27 S-N and log-log values calculated from the Atlas of Fatigue Curves<sup>[33]</sup>

Nf cycles	Log Nf	Stress in MPa R = -1 Bending		Log Sn	Sn Log-Log Equation	% Variance in Log Nf
		Diagram	Equation			
1000	3.00	440	440	2.59	391	12.78
10000	4.00	330	327	2.50	313	4.34
31100	4.49		282	2.45	281	0.36
34400	4.54	275	279	2.44	279	0.00
100000	5.00		243	2.40	251	-3.34
1000000	6.00	186	185	2.30	202	-8.42
10000000	7.00	148	148	2.21	162	-8.35
100000000	8.00	130	130	2.11	130	0.00
1000000000	9.00	130	130	2.11	130	0.00

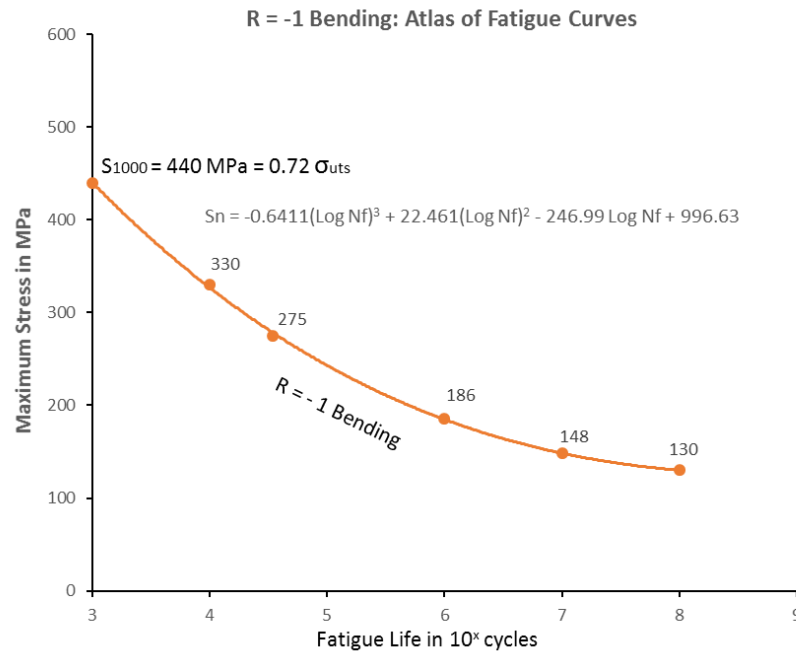


Figure 116 S-N diagram showing the Atlas of Fatigue Curves line for R = -1

The best fit generated equation for Sn proved to be a polynomial of the 3<sup>rd</sup> order, for the line in Figure 116 representing Figure 44 is:

$$S_n = -0.6411 (\text{Log } N_f)^3 + 22.461 (\text{Log } N_f)^2 - 246.99 \text{ Log } N_f + 996.63 \quad \text{Equation 4.5}$$

This equation was used to calculate the  $S_{1000}$  value which was found to be 440 MPa which came to 72 % of the UTS.

The log Sn-log Nf values were plotted to form a straight line graph in the same way as with Figure 114 giving Figure 117 and the generated linear equation 4.6 shown below.

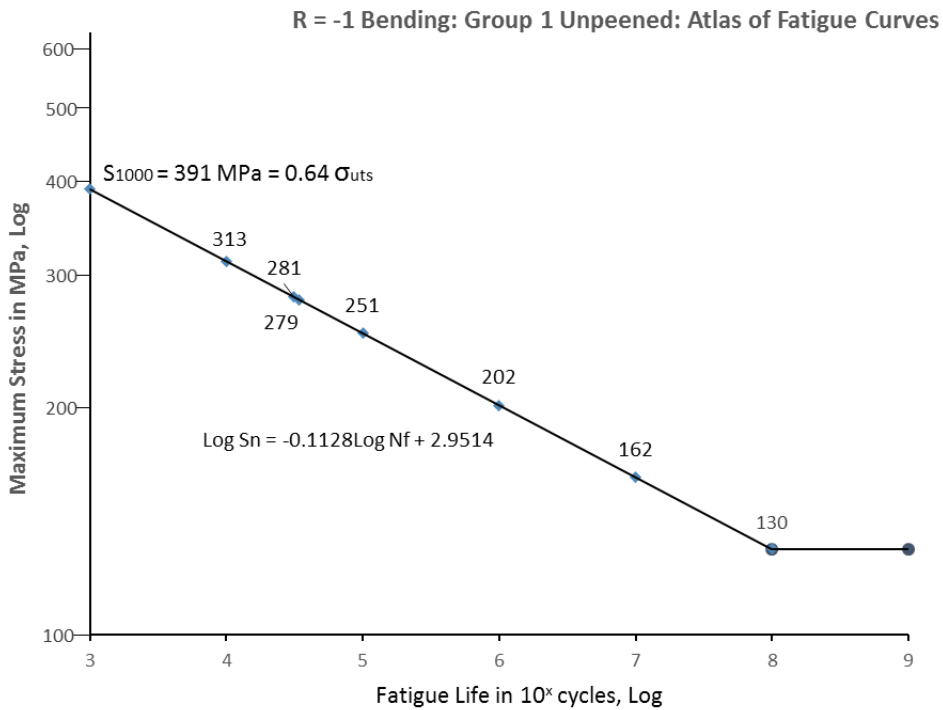


Figure 117 Log S-Log N diagram of Group 1 showing the Atlas of Fatigue Curves line for R = -1

The stress at 10<sup>3</sup> cycles was extrapolated from the line equation at 391 MPa which, at a low 64 % of the 612 MPa UTS, or about 69 % of the 572 MPa, according to Table 1, or 565 MPa according to the MIL-HDBK-5J handbook.

Again, by applying this approach all the specimens of Group 1 all the specimen values are reliably close to the line and could be used with fatigue tests on similar specimens.

The linear equation becomes:

$$\text{Log } S_n = -0.1128 \text{ Log } N_f + 2.9514 \quad \text{Equation 4.6}$$

By applying the same generalised factors to the endurance stress:

$$S_n = 0.727 \times 130 = 94.5 \text{ MPa} = 15 \% \text{ of the UTS for these conditions.}$$

The correlation and percentage variances shown in Table 27 are higher than with the MIL-HDBK-5J based graph in Figure 114 and the application of generalised factors resulting in only 95.5 MPa would drive the line unrealistically too low.

It was, therefore, decided that the MIL-HDBK-5J Log Sn-Log Nf based graph shown in Figure 115 was more reliable for this research.

The life prediction model for Group 1, then, will be equation 4.4

### 4.3.2 Groupwise Life Prediction Modelling

Now that the prediction model for unpeened specimens in Group 1 has been found in par 4.3.1 with Figure 115 and equation 4.4, as the primary lower parameter, it may serve as the model of reference for the other groups, so that prediction models may be found for each group process.

This will be attempted by applying the data and line equation 4.4 linked to Figure 115, adapting them to each group process, to generate a revised line equation and S-N diagram. Inspection of log-log S-N graphs show that they are generally reasonably parallel to each other, especially for the range of values covered in this research, meaning that the same line gradient may be applied which should yield more conservative results.

The remaining primary requirement will be to find the constant of the log-log linear equation. One concern is that the fatigue lives of shot peened specimens did not have the reliability confidence levels of unpeened specimens in some cases, making it difficult to estimate with too much precision.

The order of group testing is arranged according to the priority of the process and not the group number.

The order of analysis per group will be as follows:

- Use the Gerber equation to find the fully reversible alternating stress for those specimens that have had the residual stress-depth test.

- Substitute the reversible alternating stress and number of cycles to failure in the generalised form of equation 4.4, while maintaining the same gradient, to find the equation constant and adapted equation of the line. Since the primary generalised factors were previously applied to determine equation 4.4, they will not need to be repeated again.
- Find the stress values at  $10^3$  and  $10^8$  cycles by substituting them into the new equation. This will offer sufficient co-ordinate points to generate the linear Log Sn-Log Nf table and diagram after the pattern of Table 26 and Figure 115.
- Find the estimated stresses for the other specimens of the group.

The next step will be establish a parameter for specimens which are only shot peened in Group 9.

#### 4.3.2.1 Group 9: Specimens Shot Peened Only.

The shot peening of specimens at CPUT and SAA will need to be calculated separately.

DP 38, **shot peened at CPUT**, was the only specimen in the group that underwent a residual stress test at the NMMU laboratories as well as being fatigue tested, making it relevant for calibrating a suitable S-N diagram.

The Gerber equation is to be used to find the fully reversible alternating stress for Group 9.

DP 38 will be evaluated here for compliance with the S-N diagram as follows:

Maximum bending stress = 525 MPa

Applied stress amplitude =  $0.5(\sigma_{\max} - \sigma_{\min}) = 0.5(525 - 52.5) = 236.25$  MPa

Applied mean stress =  $0.5(\sigma_{\max} + \sigma_{\min}) = 0.5(525 + 52.5) = 288.75$  MPa

Residual tensile stress = 40 MPa

Effective mean stress = applied mean stress + residual tensile stress  
=  $288.75 + 40 = 328.75$  MPa

Substituting into the Gerber equation 2.21 yields a corresponding fully reversible alternating stress at  $R = -1$  of:

$$\sigma_n = \frac{\sigma_a}{1 - \left[\frac{\sigma_m}{\sigma_u}\right]^2} = \frac{236.25}{1 - \left[\frac{328.754}{612}\right]^2} = 332 \text{ MPa}$$

The number of cycles to failure of DP 38 must be closely matched to the reversible stress amplitude by using equation 4.4:

$$\text{Log } S_n = -0.1128 \text{ Log } N_f + C$$

Substituting  $N_f = 241420$  cycles and  $S_n = 332$  MPa yields:

$$\text{Log } 332 = -0.1128 \text{ Log } 241420 + C$$

$$C = 3.128$$

The equation for the graph representing shot peening at CPUT becomes:

$$\text{Log } S_n = -0.1128 \text{ Log } N_f + 3.128$$

**Equation 4.7**

At  $10^8$  cycles the endurance limit stress can be found:

$$\text{Log } S_n = -0.1128 \text{ Log } 10^8 + 3.128 = 2.2256$$

$$S_n = 168 \text{ MPa}$$

Also, the stress at  $10^3$  cycles becomes:

$$\text{Log } S_n = -0.1128 \text{ Log } 10^3 + 3.128 = 2.7896$$

$$S_{1000} = 616 \text{ MPa}$$

DP 50, the UCT specimen set, **shot peened at SAA**, underwent residual stress tests at UCT with estimated residual tensile results in par 4.2.3 Test 7: Group 9 and Figure 92.

DP 50 will be evaluated here for compliance with the S-N diagram as follows:

Maximum bending stress = 525 MPa

Applied stress amplitude =  $0.5(\sigma_{\max} - \sigma_{\min}) = 0.5(525 - 52.5) = 236.25$  MPa

Applied mean stress =  $0.5(\sigma_{\max} + \sigma_{\min}) = 0.5(525 + 52.5) = 288.75$  MPa

Residual tensile stress (estimated) = 36 MPa

Effective mean stress = applied mean stress + residual tensile stress  
 $= 288.75 + 36 = 324.75$  MPa

Substituting into the Gerber equation 2.21 yields a corresponding fully reversible alternating stress at  $R = -1$  of:

$$\sigma_n = \frac{\sigma_a}{1 - \left[\frac{\sigma_m}{\sigma_u}\right]^2} = \frac{236.25}{1 - \left[\frac{324.75}{612}\right]^2} = 329 \text{ MPa}$$

The number of cycles to failure of DP 50 must be closely matched to the reversible stress amplitude by using equation 4.4:

$$\text{Log } S_n = -0.1128 \text{ Log } N_f + C$$

Substituting  $N_f = 158580$  cycles and  $S_n = 329$  MPa yields:

$$\text{Log } 329 = -0.1128 \text{ Log } 158580 + C$$

$$C = 3.1035$$

The equation for the graph representing shot peening at SAA becomes:

$$\text{Log } S_n = -0.1128 \text{ Log } N_f + 3.1035$$

**Equation 4.8**

At  $10^8$  cycles the endurance limit stress can be found:

$$\text{Log } S_n = -0.1128 \text{ Log } 10^8 + 3.1035 = 2.2$$

$S_n = 159 \text{ MPa}$

The stress at  $10^3$  cycles becomes:

$$\text{Log } S_n = -0.1128 \text{ Log } 10^3 + 3.1035 = 2.77$$

$$S_{1000} = 582 \text{ MPa}$$

DP 4, shot peened at SAA was not fatigue tested but was given a residual stress-depth test making it worthwhile to find out the estimated number of cycles to failure at a maximum bending stress of 525 MPa.

$$\text{The effective mean stress} = 288.75 + 47 = 335.75 \text{ MPa}$$

Substitution into the Gerber equation gives a fully reversible alternating stress of 338 MPa, and after substituting this stress into equation 4.8, the number of cycles to failure is estimated to be 124115 cycles.

S-N diagrams representing shot peening curves are typically reliable higher than  $10^4$  to  $10^5$  cycles so the value of  $S_{1000}$  is of token value only to create the log-log line.

Table 28 and Figure 118 show the Log Sn–Log Nf values and lines, as shown below:

*Table 28 S-N and log-log values for group 9: shot peening*

Nf (cycles)	Log Nf	Log Sn SPct R = -1 Equation	Sn (MPa) SPct R = -1 Equation	Log Sn SPsaa R = -1 Equation	Sn (MPa) SPsaa Equation
1000	3.00	2.79	616	2.77	582
10000	4.00	2.68	475	2.65	449
100000	5.00	2.56	366	2.54	346
158580	5.20	2.54	348	2.52	329
200000	5.30	2.53	339	2.51	320
241420	5.38	2.52	332	2.50	314
1000000	6.00	2.45	283	2.43	267
10000000	8.00	2.23	168	2.20	159

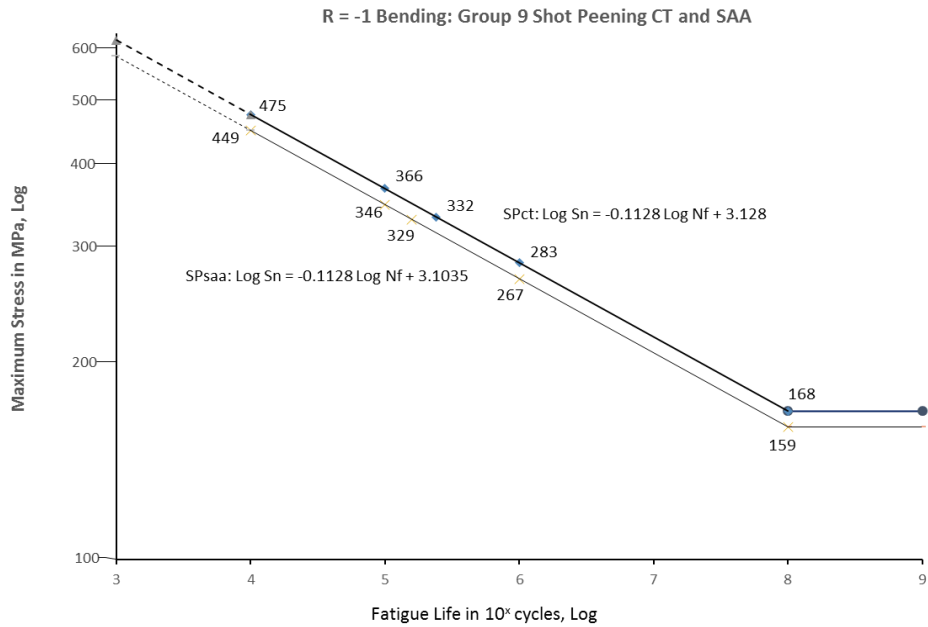


Figure 118 Log S-Log N of Group 9 for shot peened specimens at CPUT and SAA for R = -1

#### 4.3.2.2 Groups 4a and 5: Specimens Shotpeened at SAA and Plastically Strained.

This is a comparatively large group of 5 specimens fatigued at a maximum bending stress of 525 MPa, and one specimen (DP 5) fatigued at 480 MPa.

DP 5, 13 and 19 all underwent residual stress-depth tests at NMMU.

Unfortunately, DP 5 was the only specimen fatigued at 480 MPa, rendering it unrealistic to formulate a life prediction model for it.

In light of this the focus will need to be on those specimens fatigued at 525 MPa. This also has the advantage of a common mean stress and stress amplitude used previously in par 4.3.2.1 at R = 0.1. The only variable for the Gerber equation will be the residual tensile stresses required to find the effective mean stresses.

For DP 13 and 19 the residual tensile stresses were is 21 and 37 MPa respectively.

DP 13: effective mean stress = 288.75 + 21 = 309.75 MPa

DP 19: effective mean stress = 288.75 + 37 = 325.75 MPa

Substituting these values into the Gerber equation 2.21 yields:

DP 13:  $S_n = 318$  MPa at 55490 cycles to failure

DP 19:  $S_n = 330$  MPa at 58500 cycles to failure

These values are substituted into equation 4.4 to establish a new constant for this process.

$$\begin{aligned} \text{DP 13:} \quad & \log S_n = -0.1128 \log N_f + C_{13} \\ & \log 318 = -0.1128 \log 55490 + C_{13} \\ & C_{13} = 3.03757 \end{aligned}$$

$$\begin{aligned} \text{DP 19:} \quad & \log S_n = -0.1128 \log N_f + C_{19} \\ & \log 330 = -0.1128 \log 58500 + C_{19} \\ & C_{19} = 3.05625 \end{aligned}$$

The other relevant parameter is the plastic straining which will need to be an independent function of C

From par 4.2.2 Test 4 for Groups 4 and 5 the general trendline equation, for Groups 4a and 5 combined, relating the number of cycles to plastic strain is given in Figure 72 to be:

$$N_f = 56539 \text{ PS} + 67990$$

The equivalent number of cycles according to the plastic strains (in % microstrain) of DP 13 and 19 yield:

$$\text{DP 13:} \quad N_{f_{13}} = 56539 (0.4103) + 67990 = 91188 \text{ cycles}$$

$$\text{DP 19:} \quad N_{f_{19}} = 56539 (0.1703) + 67990 = 77619 \text{ cycles}$$

Both these values are far too high above the actual number of cycles to failure to be acceptable. The constant for the equation of 67990 cycles was an immediate giveaway. It was stated in the comments on Test 4 referred to that the fatigue scatter was fairly wide off the trendline, which has shown to be unusable here.

The fatigue lives of the other 3 specimens in this group show a closer correspondence between plastic strain and cycles to failure and it is a pity that residual stress-depth tests

could not have been performed on them so they could have been tested with the Gerber equation to help establish a more reasonable life prediction model.

Although a life prediction model can be created between DP 13 and 19 due to their close results, it will be contradicted by the results of the other 3 specimens.

The contradiction of a partially expected and unexpected fatigue life behaviour was commented on under the discussion on the microstructure in par 4.2.4.1 Groups 4a and 5, indication that the tests for this grouping were inconclusive for life prediction modelling within the scope of this research, so no attempt will be made to analyse it further, however tantalising a problem such as this may be to solve.

#### **4.3.2.3 Groups 6: Specimens Shotpeened at CPUT and Plastically Strained**

Only two specimens, DP 35 and 41 were tested under these conditions, with DP 35 undergoing a residual stress-depth test at NMMU.

The purpose of this group was to find a life prediction model indicator for specimens which were shot peened at CPUT and plastically strained without skimming (in contrast with group 8), although the sample size is somewhat small.

As with par 4.3.2.1 only the effective mean stress is to be calculated for the Gerber equation.

The residual tensile stress = 20 MPa

The effective mean stress =  $288.75 + 20 = 308.75$  MPa

Substituting in the Gerber equation 2.21 similarly to par 4.3.2.1 yields:

$S_n = 317$  MPa at the fatigue life of 61480 cycles to failure.

These values are substituted into equation 4.4 to establish a new constant for this process.

$$\text{Log } S_n = -0.1128 \text{ Log } N_f + C$$

$$\text{Log } 317 = -0.1128 \text{ Log } 61480 + C$$

$$C = 3.0412$$

The life prediction equation then becomes:

$$\text{Log } S_n = -0.1128 \text{ Log } N_f + 3.0412 \quad \text{Equation 4.9}$$

The  $S_n$  value for DP 41, with 63420 cycles to failure, may be found by substituting into equation 4.8:

$$\begin{aligned} \text{Log } S_n &= -0.1128 \text{ Log } 63420 + 3.0412 \\ S_n &= 316 \text{ MPa} \end{aligned}$$

The difference in the stresses (and cycles to failure) with little difference in plastic strain is so small that they would almost appear as the same point on a Log  $S_n$ -Log  $N_f$  diagram, shown in Figure 119 for the sake of completeness.

Whether it is sufficiently representative of other similar specimens with comparative tests is uncertain.

At  $10^8$  cycles the endurance limit stress can be found:

$$\begin{aligned} \text{Log } S_n &= -0.1128 \text{ Log } 10^8 + 3.0412 = 2.1388 \\ S_n &= 138 \text{ MPa} \end{aligned}$$

The stress at  $10^3$  cycles becomes:

$$\begin{aligned} \text{Log } S_n &= -0.1128 \text{ Log } 10^3 + 3.0412 = 2.7028 \\ S_{1000} &= 504 \text{ MPa} \end{aligned}$$

Table 29 S-N and log-log values for group 6: shot peening CT and plastic strain

Nf (cycles)	Log Nf	Log Sn SP <sub>ct</sub> R = -1 Equation	Sn (MPa) SP <sub>ct</sub> R = -1 Equation
1000	3.00	2.70	504
10000	4.00	2.59	389
61480	4.79	2.50	317
63420	4.80	2.50	316
100000	5.00	2.48	300
1000000	6.00	2.36	231
100000000	8.00	2.14	138

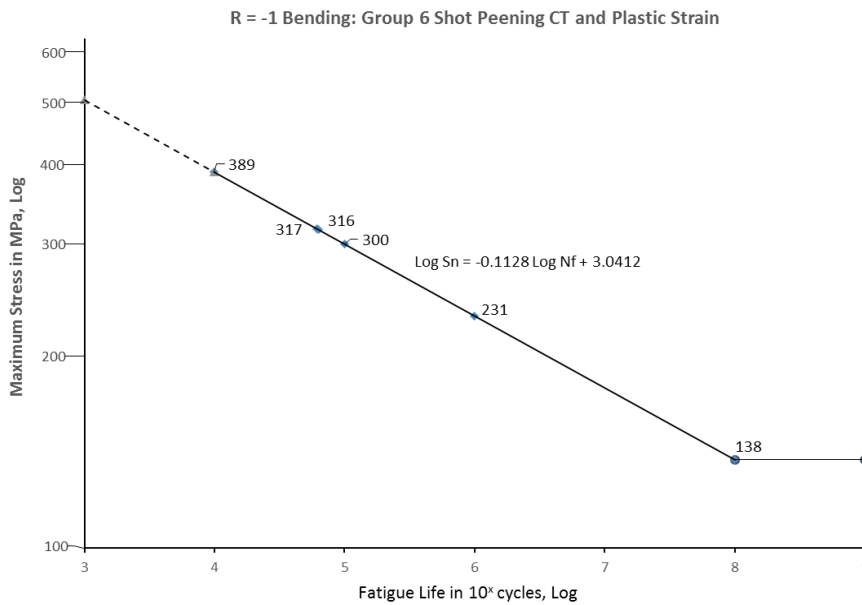


Figure 119 Log S-Log N of Group 6 for shot peening at CT and plastic strain for R = -1

#### 4.3.2.4 Groups 8: Specimens Shotpeened, Plastically Strained at CPUT and Skimmed

Group 8 consisted of 6 specimens of which one specimen, DP 25, underwent a residual stress-depth test at NMMU.

As shown in par 4.2.3 Test 6: Group 8, and par 4.2.4.1 for Groups 6, 7, 8 and 11, with their associated residual stress-depth diagrams, this is the most intriguing group in illustrating the important role of the microstructure in strain hardening and dislocation density. It combines the effects of a reduced residual stress and increasing strain hardening.

As previously only the effective mean stress is to be calculated for the Gerber equation with respect to DP 25.

The residual tensile stress = 21 MPa

The effective mean stress =  $288.75 + 22 = 310.75$  MPa

Substituting in the Gerber equation 2.21 similarly to par 4.3.2.2 yields:

$S_n = 318$  MPa at the fatigue life of 57840 cycles to failure.

These values are substituted into equation 4.4 to establish a new constant for this process.

$$\text{Log } S_n = -0.1128 \text{ Log } N_f + C$$

$$\text{Log } 318 = -0.1128 \text{ Log } 57840 + C$$

$$C = 3.0396$$

The life prediction equation then becomes:

$$\text{Log } S_n = -0.1128 \text{ Log } N_f + 3.0396$$

**Equation 4.10**

At  $10^8$  cycles the endurance limit stress can be found:

$$\text{Log } S_n = -0.1128 \text{ Log } 10^8 + 3.0396 = 2.1372$$

$$S_n = 137 \text{ MPa}$$

The stress at  $10^3$  cycles becomes:

$$\text{Log } S_n = -0.1128 \text{ Log } 10^3 + 3.0396 = 2.7012$$

$$S_{1000} = 503 \text{ MPa}$$

Table 30 and Figure 120 show the Log  $S_n$ –Log  $N_f$  values and lines, as shown below:

Table 30 S-N and log-log values for group 8: shot peening CPUT, plastic strain and skim

Group 8 Specimen Number DP	Nf (cycles) Actual	Log Nf Actual	Log Sn SP <sub>ct</sub> R = -1 Equation	Sn (MPa) SP <sub>ct</sub> R = -1 Equation	% PS	Nf (cycles) % PS Equation	Log Nf % PS Equation	Log Sn %PS Equation	Sn MPa %PS Equation
	1000	3.00	2.70	503					
	10000	4.00	2.59	388					
34	34180	4.53	2.53	337	0.6000	42911	4.63	2.52	329
26	38740	4.59	2.52	333	0.5960	42792	4.63	2.52	329
42	40890	4.61	2.52	331	0.3506	35491	4.55	2.53	336
43	41130	4.61	2.52	330	0.4617	38796	4.59	2.52	333
27	51890	4.72	2.51	322	0.8265	49650	4.70	2.51	324
25	57840	4.76	2.50	318	1.0072	55026	4.74	2.50	320
	100000	5.00	2.48	299					
	1000000	6.00	2.36	231					
	100000000	8.00	2.14	137					

Table 30 also includes, from columns 6 to 10, the number of cycles to failure and the estimated stress using the trendline equation in Figure 73 for Group 8:

$$N_f = 29752 (\%PS) + 25060 \quad \text{Equation 4.11}$$

Comparing the results between the life prediction equation 4.10 and the % plastic strain equation 4.11, there is a reasonably close correlation with the stresses in columns 5 and 10, with equation 4.11 yielding higher stresses.

The number of cycles to failure in columns 2 (actual) and 7 are higher for the % plastic strain equation 4.11 with specimens DP 26 and 34 which have almost the same % plastic strain around 0.6, with the remainder of the specimens having a lower estimated fatigue life.

The life prediction model represented by equation 4.10 is preferred as it is more directly aligned with the actual cycles.

Figure 120 shows the Log Sn–Log Nf line below according to equation 4.10:

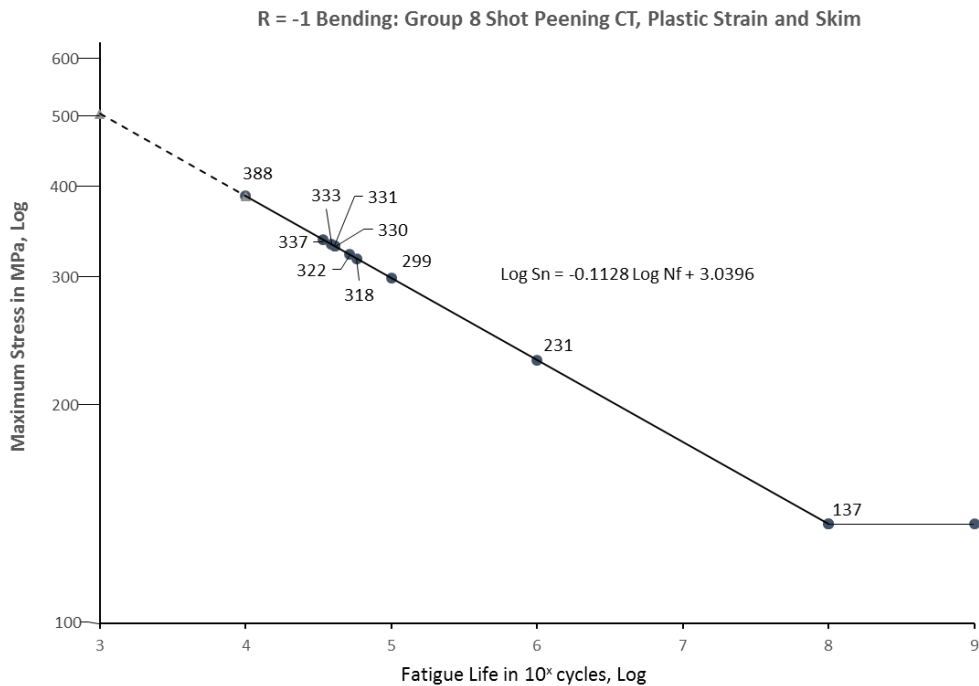


Figure 120 Log S-Log N of Group 8 for shot peening at CPUT, plastic strain and skim for R = -1

#### 4.3.2.5 Group 3: Specimens Unpeened, Pre-fatigued and Shot Peened at SAA

In par 4.2.2, Test 2 Group 3, concerns were raised about the validity of reliability of DP 15, the only specimen to undergo a residual stress test, as its fatigue life fell disproportionately short of the other two specimens.

This raises sufficient doubt in the validity of any life prediction modelling, even when taking into account the suggested motivations of the differences in the maximum fatigue test bending stresses to fatigue life discrepancies, as shown in par 4.2.3 test 2 Group 3.

With these factors in mind, there will be no attempt made to find a life prediction model for Group 3.

## 4.4 SUMMARY

The parameters for analysis covered in this chapter were arranged topically, as mentioned in the introduction in par 4.1, concluding with finding life prediction models in par 4.3.

All the specimens were arranged into groups with common treatment criteria so that comparisons could be made to analyse the contribution of the uniformity of each type of treatment to fatigue life.

### 4.4.1 Fatigue Analysis Profiles

This refers to par 4.2 which was arranged groupwise into four main topics, specimen list and groupings, fatigue tests, and residual stress-depth tests.

#### 4.4.1.1 Specimen List and Groupings

Table 10 gives a summary list of all the specimens of, and the treatments common to, each group, as well as relevant information required for the analysis. 11 groups are shown with their member specimens, descriptions of each treatment and testing process per group, as well as final results of fatigue life, degrees of plastic straining, residual tensile stresses, maximum bending stresses, as well as explanatory details for each group.

#### 4.4.1.2 Fatigue Tests: Groupwise

Five tests, some with a combination of groups depending on levels of commonality, were analysed, where the fatigue lives of the specimens were linked to plastic strain to demonstrate the role of the microstructure.

**Test 1** compared the fatigue lives of unpeened specimens to those which were also plastically strained of which one was then shot peened at SAA.

Unpeened specimens had an average fatigue life of 32167 cycles which decreased by 21 % for plastically strained specimens.

The specimen which was initially plastically strained and then shot peened at SAA fatigued at 250650 cycles, showed an impressive 682 % increase in fatigue life, or a 7.82 ratio to unpeened specimens, demonstrating the remarkable effect of shot peening in extending fatigue life. It was even better than the standard specimen shot peened by SAA by 92070

cycles! This is probably due to work hardening through the plastic straining, giving the specimen a higher yield stress, in combination with the residual compressive stress from the shot peening. The benefits of this treatment process are worthwhile.

**Test 2** attempted to demonstrate the effect of pre-fatiguing unpeened specimens to around 60 % of their fatigue life and then shot peening them at SAA to find out any effects. Besides a problem with one specimen, the other two showed an average 138665 cycles or 331 % increase in fatigue life, or 4.31 ratio. There was improvement almost comparative to the standard shot peened specimen.

**Test 3** compared two specimens, both shot peened at SAA, plastically strained by slightly different amounts, and with different maximum bending stresses of 480 and 525 MPa, with indifferent results. It seemed, inconclusively, that plastic straining reduced the fatigue life to an average of 44120 cycles from an expected 150000 cycles.

**Test 4** attempted to demonstrate the effects of increasing plastic strain on specimens shot peened at SAA. Unfortunately, the significantly wide scatter of results showed an average of 94650 cycles with an average 28875 cycles discrepancy, although still a minimum 81 % improvement over unpeened specimens. Any steady trend in the effects of increasing plastic strain, the main purpose of this test, however, could not be established.

**Test 5** demonstrated the effects of no strain to increasing plastic strain on specimens shot peened at CPUT and given a 200  $\mu\text{m}$  radial skim. The hoped for purpose was to try eliminate the shot peened layer that compressed and deformed the surface crystalline structure to make the surface like an unpeened specimen, but with a limited residual compressive stress at the surface.

This proved to be one of the more successful tests, showing an unexpectedly direct relationship between increasing plastic strain and increasing, instead of the expected decreasing, fatigue life. The plastic strain seemed to be responsible for the general decrease in fatigue life over specimens not plastically strained, but the localised modest increase in fatigue life of the group of specimens with an increase in plastic strain, indicated some role of strain hardening in fatigue life. The average improvement in fatigue life over the standard unpeened specimen was a modest 37 %.

The standard specimen shot peened and skimmed, but not plastically strained, showed the highest fatigue life of all the specimens in this research with an average 295725 cycles to failure and a 9.19 ratio or 819 % increase of fatigue life over standard unpeened specimens and a 22 % increase over the standard specimen shot peened at CPUT.

The dramatically high fatigue life of specimens in this test that were not plastically strained over those that were, indicates the dual role that microstructural altering plays in fatigue life. It will significantly reduce fatigue life over specimens plastically strained on the one hand, and provide strain hardening to modestly increase fatigue life with increasing increments of plastic strain.

#### 4.4.1.3 Residual Stress-Depth Tests

Only nine specimens were tested at NMMU laboratories to limit costs. The set of 3 specimens tested by the final year BSc student at UCT referred to in par 3.3.3, called DP 50, was required to obtain results for standard specimens shot peened at SAA, due to damage done to the specimens outside the control of the author.

The residual stress-depth test results needed further calibration, as detailed in par 3.3.3, to reduce their magnitude to more realistic values. This meant that the calibrations may have been up to 5 % out, but which was not expected to detrimentally affect the results overall.

The tested specimens were to represent the more important treatment processes. This resulted in 7 test groups to be analysed, primarily to find out (or confirm) the role of surface residual compressive stress in improving fatigue life.

The sought criteria were the residual stress amplitudes, tensile and compressive, as well as their average values. Their depth profiles were also important, especially with the potentially risky radial skimming of the shot peened surface, as discussed in par 2.6.1, and still hoping for a remnant of residual stress, which fortunately worked. The average residual tensile stress was required for the effective mean stress calculation in the Gerber equation.

**Test 1** was to represent the unpeened group and showed an expected relatively low residual stress profile, serving as a comparative reference for other tests.

**Test 2** was for Group 3 where unpeened specimens were pre-fatigued to 20000 cycles, sent for shot peening at SAA, and fatigued to failure. Stress-depth profiles were well proportioned but could not assist in the analysis due to a much earlier fatigue failure, compared to the other two specimens which possibly had more representative fatigue life values closer to other shot peened specimens in group 9, suspected to be caused by a possible material flaw in the tested specimen for the group, DP 15.

No meaningful fatigue life result could be obtained from this test, although the stress-depth profile proved to assist in analysing remaining residual stress magnitudes at depths after the possibility of radial skimming.

**Test 3** was for Group 4 with both specimens being tested for residual stress vs depth, which had good profiles. They were shot peened at SAA and were plastically strained.

The plastic straining demonstrated its ability to lower residual compressive stresses to about 30 % of unstrained specimens, probably explaining their decreased 44120 average cycles to failure, only 37 % higher than unpeened specimens, and 29 % of specimens shot peened at SAA.

A fatigue result profile was illustrative but not too conclusive. DP 13 with 0.4103 % plastic strain and fatigued at a higher maximum bending stress of 525 MPa and fatigue life of 55940 cycles, outperformed DP 5 with a slightly higher 0.5 % plastic strain and lower maximum bending stress of 480 MPa and fatigue life of 32750 cycles, a 22740 cycles or 71 % difference!

**Test 4** representing specimens with increasing plastic strain on specimens shot peened at SAA, and fatigued at a maximum bending stress of 525 MPa.

The maximum residual compressive stresses averaged 64 % of the standard specimen shot peened at SAA and a shorter fatigue life was expected, and found, averaging around 60 %. Stress-depth profiles of the 2 specimens tested were good and showed the maximum combined tensile stress during bending just exceeded the yield stress of 560 MPa.

The comments made in par 4.4.1.2 test 4 regarding the inconsistency of fatigue life results with a wide scatter, still hold here, with 2 out of a total of 5 specimens being given residual stress-depth tests.

The stress-depth profile, as was the case with most of the other profiles, was of assistance to determine stress-depth values after radial skimming.

**Test 5** was on DP 35 in Group 6 with shot peening at CPUPT and plastic straining. The residual stress-depth profile was good and showed a small 3 % decline in fatigue life with an 88 % increase in low plastic strain values. The results, though, were not conclusive as there were only 2 specimens in the group.

The maximum residual compressive stress was a respectable 74 % of the unstrained shotpeened specimen with an average 39 % of the fatigue life. The average fatigue life was a noticeable 94 % higher than unpeened specimens.

The maximum combined tensile stress during bending reached the yield stress but still lasted well.

**Test 6** was on DP 25 in Group 8 with shot peening at CPUPT and incrementally increasing plastic strain, as well as undergoing a 200  $\mu\text{m}$  radial skim. Residual stress-depth profiling was somewhat erratic on DP 25, probably due to it receiving the maximum 1 % plastic strain of the research. The maximum residual tensile stress reached an 84 MPa spike resulting in the combined bending tensile stress of 601 MPa, almost at the 612 MPa UTS.

Average values were much lower, probably contributing to the useful 55780 cycles to failure, 73 % higher than the standard unpeened specimen, but 24 % of the standard shot peened specimen, and 20 % of its unstrained skimmed counterpart.

Test 5 in par 4.4.1.2 comments on the relative success of the performance of this group hold here as well.

**Test 7** was on Group 9 representing specimens that were shot peened only and operating as a key reference point for other tests.

DP 38 was shot peened at CPUPT and given the residual stress-depth test at NMMU. The profile was very good and served as one of the main points of reference to help establish the calibration ratio for the rest of the specimens in this research.

DP 4 was shot peened at SAA and tested at NMMU, showing good profiling. Its maximum residual compressive stress value was 355 MPa which was 94 % of the 380 MPa reference value, assessed in par 3.3.3, for this research.

DP 50 (set of 3 specimens) tested at UCT represented the shot peening at SAA and partnered DP 38 in finding a balance in finding the calibration ratio. The maximum residual compressive stress measured at UCT had an average 370 MPa, 97 % of the reference value for this research and complies well with DP4, also shot peened at SAA.

Stress-depth profiles were not established in the source documentation, but estimated to be similar to those found in this research, and estimated to be useful for representative profiling.

#### 4.4.2 Microstructural Effects

Microstructural effects were analysed through plastic straining, microhardness and fractography, by their role in fatigue life.

##### 4.4.2.1 Plastic Straining

The role of % plastic strain in determining fatigue life was investigated and a diagram, showing all the plastic strain related tests together, constructed to gain an overall perspective of their context in the bigger picture. Trendlines of each group were investigated to determine their role in microstructural behaviour.

**Group 2** where unpeened specimens were plastically strained and performed the worst, probably due to it creating more residual tensile stresses. The trendline gradient was too small to offer assistance.

The specimen shot peened *after* being plastically strained performed exceptionally well, as discussed in par 4.4.1.2 test 1. The higher shot peening intensity from CPUT was thought to have played a significant role in the fatigue life, especially with the plastic straining thought to increase the yield stress limit.

**Group 4a and 5** where specimens were shot peened by SAA and plastically increasingly strained from 0.1703 to 0.4885 %, showing a trendline with a positive gradient directly proportional to fatigue life, although with an unrealistically wide scatter.

This was described as partially unexpected because increased plastic straining was expected to reduce residual compressive stress essential to cope with tensile bending stresses.

It was also partially expected because plastic straining contributes to strain hardening which strengthens the yield stress and increased dislocation density restraining crack growth.

**Groups 6, 7, 8 and 11** where all specimens were shot peened at CPUT, most specimens increasingly plastically strained as well as finally skimmed. The skimmed specimens without

plastic straining had very high fatigue lives whereas those with plastic straining had severely reduced fatigue lives.

Skimmed specimens with plastic straining experienced a significant overall reduction in fatigue life but, localised within this group, an increase in fatigue life with an increase in plastic strain, with a representatively narrow scatter this time.

The specimens without skimming showed little variance with an increase in plastic strain although a reasonable drop in fatigue life.

The general depth of the residual compressive stress was about 130  $\mu\text{m}$  deeper than originally expected, although hoped for, meaning that after the 200  $\mu\text{m}$  skim to remove the shot peened surface, there would still be 130  $\mu\text{m}$  of reduced residual compressive stress with an average of around 70 MPa.

This residual stress layer was given the credit for the competitive increase in fatigue life even when plastic straining is present.

The combination of the increase of strain hardening, affecting the role of the microstructure, in the presence of residual compressive stress contributed to an increase in fatigue life.

#### **4.4.2.2 Microhardness**

Three specimens were tested for Vickers microhardness through their diameters to find whether there was a relationship between microhardness depth and tensile strength as is the case with steels, although not confirmed with all aluminium alloys.

Although the data was well scattered, a trend showed the microhardness generally decreased steadily through the depth. This indicated that the surface had higher strength values which was attributed to strain hardening, and softened with depth.

Some difficulty was found acquiring reliable comparative diagrams for aluminium, and those that were found had very wide bandwidths rendering them to approximations.

The other factor was the role of microhardness is an indicator of the contribution of the microstructure to fatigue life.

The conclusion was that the microhardness data showed trends but was too scattered to be sufficiently reliable to draw accurate predictions of material strength and the role of the microstructure in 7075-T6 aluminium alloy.

#### 4.4.2.3 Fractography

SEM fractographs proved useful to view the microstructure of the fractured surfaces of specimens and show specific characteristics relating texture, shear cleavage planes, harder impurities or inclusions to strengthen the material, ductility, crack propagation, microvoid coalescence that cause stress raisers to assist fatigue, persistent slip bands, etc.

Two groupings were selected with representative sample specimens and their comparative fractographs were shown side-by-side to inspect common characteristics.

The groups involved were:

**Groups 4a and 5** with specimens shot peened at SAA and various plastic strains.

**Groups 6, 7, 8, and 11** with specimens shot peened from CPUT and most specimens given a 200  $\mu\text{m}$  radial skim and varied plastic straining.

Sets of similar fractographs of specimens were shown in pairs for comparison and a high amplification picture to view dimples and associated cracks.

At and near the crack initiation sites were marked dimples showing the presence of plastic strain around harder impurities at their centres, typical shear cleavage planes at about 45 degrees to the surface. Also shown were ductile striations and high atomic steps.

Further away from the crack initiation site were some microvoid coalescence sites, often caused by groupings of dimples in fast fracture regions with associated stress raisers, and indicating transgranular cracking. The hard particles at the dimple centres try to resist fatiguing forces causing slip bands.

Of particular interest was the depth of the shot peened residual compressive stress layer, where the 300  $\mu\text{m}$  depth can be seen and the 130  $\mu\text{m}$  layer for skimmed specimens, confirming the residual stress-depth diagram profiles.

#### 4.4.3 Life Prediction Modelling

The life prediction modelling presented some challenges in finding reliable S-N diagrams and representative residual tensile stresses for calculating the effective mean stress required for the Gerber equation to convert the alternating stress amplitude from the tension-tension

stress ratio from  $R = 0.1$ , used in the fatigue testing for this research, to the fully reversible stress ratio  $R = -1$ , to make the analysis more compliant to standard S-N diagrams.

It was also clear that a separate life prediction model would need to be found for each treatment process, limited to where residual stress-depth testing had taken place.

It was decided to inspect two possible S-N diagrams, one from the US Navy MIL-HDBK-5J handbook and the Atlas of Fatigue Curves.

The MIL-HDBK-5J diagrams were for axial fatigue and required conversion factors to change them to bending fatigue testing, which was done.

The Atlas of Fatigue Curves was already set for bending fatigue.

Points on the graphs were carefully plotted from both the original S-N diagrams to convert them to Excel S-N diagrams and trendline equations were established.

Generalised conversion factors were taken from Jvinall and Marshek to convert the  $10^3$  and  $10^8$  cycle endurance points for the material used and conditions of fatigue testing.

The alternating stress for fully reversible bending fatigue

The S-N diagrams were aligned to the converted points, finally leading to a representative Log Sn-Log Nf diagram with the associated linear trendline equation for each S-N source.

Values were tested against the two linear trendline equations to check which one would be the most suitable one for this research. The one chosen was from the MIL-HDBK-5J handbook which was utilised throughout.

S-N diagrams depicting unpeened and shot peened specimen fatigue testing were inspected and it was found that the Log Sn-Log Nf diagrams were mainly parallel, especially at the range of values used for this research, so the principle of using linear equations with the same gradient was adopted for all the treatment processes to be used. This meant that only the constant for the straight line equation had to be found for each process.

Gradients of shot peened specimens tend to be slightly steeper, so maintaining the same gradient would tend to make the results more conservative which was desirable to the researcher.

The life prediction models for the various processes under consideration were as follows:

The basic equation structure was:  $\text{Log } S_n = m \text{ Log } N_f + C$ ,  
 where:  $m = -0.1128$  throughout.

The final equation becomes:

$$\text{Log } S_n = -0.0028 \text{ Log } N_f + C \quad \text{Equation 4.12}$$

The value of the constant per process is shown in Table 31.

Note that:

- The constant for shot peening at SAA and plastically strained specimens could not be determined due to data scatter (Group 4a and 5).
- Unpeened, prefatigued and shot peened specimens at SAA could not be determined due to data unreliability (Group 3).

Table 31 Life prediction model equation constants per process

Treatment Process	Value of C
Unpeened	2.9514
Shot peened at CPUT (24 Almen intensity)	3.1280
Shot peened at SAA (8-14 Almen intensity)	3.1035
Shot peened at SAA and plastically strained	N/A
Shot peened at CPUT and plastically strained	3.0412
Shot peened at CPUT, plastically strained and skimmed	3.0396
Unpeened, prefatigued and shot peened at SAA	N/A

## CHAPTER 5. CONCLUSION

### 5.1 SUMMARY

The intention of this research was to improve our understanding of the effectiveness of shot peening to extend the low cycle fatigue life of 7075-T6 aluminium alloy round bar, taking into consideration surface residual stress, microstructural and microhardness parameters.

A broader intention was that this research would appeal to those wanting applied engineering approaches to deal with sometimes highly theoretical issues without compromising on academic requirements.

The literature review in **Chapter 2** includes important prerequisite information to assist in understanding the background to the criteria required to find workable solutions.

Metal fatigue through cyclic pulsating loading leads to crack initiation and propagation to final failure. Well-known theories of crack development are explained to obtain knowledge that sometimes necessarily reaches slightly beyond need-to-know limitation principles to have an appreciation of how this research fits into the wider world of the fatigue life community.

The core issue of shot peening and its practicalities like its physical characteristics of shot properties, peening intensity, applications and limitations, was broadly covered. Its main purpose in this research was for shot peening to provide the all-important residual compressive stress layer of sufficient magnitude and depth to combat and neutralise, as much as possible, the high tensile bending stresses in low cycle fatigue.

The most suitable shot type and intensity used to avoid structural surface damage was S230 size cut wire shot with 8 to 30 Almen intensity and 150 % coverage.

This was expected to provide a residual compressive stress of 300 to 400 MPa (50 to 65 % of the UTS) at a depth of approximately 200  $\mu\text{m}$ .

Any study of the microstructure has its challenges, and to investigate its effects on fatigue life required some innovative methods. The most practical approach found to suit this research was through controlled, incrementally increasing small plastic straining of specimens up to 1 % to prevent structural damage to the material. This would reduce some of the surface residual compressive stresses, and intentionally, its effect on fatigue life, as

well as mechanically altering the microstructure incrementally to create increased strain hardening and dislocation density, to help test for progressive microstructural intervention. To assist in gauging the effects on strain hardening, Vickers microhardness tests were planned, in the hope that they would provide useful insight in quantifying the localised strength through the diametral depth. Aluminium is not always as compliant as steel here so it was expected to be at least partially informative.

Another approach was to view the nature of the fractured surfaces through SEM fractographs to check for tell-tale effects such as shear planes, dimples with hard impurities at the centre, and striation markings, etc.

Life prediction modelling has been the aim of many researchers and various (usually empirical) techniques have been devised to assist engineers to combat the cause of over 80 % of cyclic loading failures. One such method is the life prediction model by Juvinall and Marshek, based on S-N diagrams, which was used in this research. One drawback is that most S-N diagrams are for fully reversible cyclic loading which is not always the case in practice. To make these diagrams versatile enough to accommodate other types of cyclic loading ratios, mathematical methods like the Gerber equation were needed for the transformation. To adapt the published S-N diagrams to experimental and specimen conditions, generalised fatigue factors that calibrate the stresses at  $10^3$  cycles and endurance points, were required, and used in this research.

**Chapter 3** discusses the experimental details including, shot peening and plastic straining at CPUT, fatigue testing of specimens at UCT, residual stress-depth and microhardness testing as well as SEM fractography at NMMU.

The shot peening was initially done at SAA at 8 to 14 Almen intensity and then at CPUT at 20 to 36 Almen intensity (which turned out to be an acceptable 24 Almen intensity).

Plastic straining at CPUT proved not to be as easy as seemed until the lab technician and author became accustomed to the practical strain behaviour of the material. However incremental straining from 0.15 to 1.0072 % plastic strain proved mostly successful.

Fatigue testing for 3 point bending on the ESH universal servo hydraulic machine at UCT was very specifically detailed and was arduously lengthy work, but also very satisfying. A bending stress ratio of 0.1 was used throughout. Initially the request was to use a maximum

bending stress of 480 MPa but was soon changed to 525 MPa to align with other testing at UCT.

Specimens were given a predetermined selection of treatment options to test the resulting fatigue lives so that the effects of those options could be quantified. The main options were unpeened, shot peened, plastic straining, and 200  $\mu\text{m}$  radial skimming, which were sometimes combined to determine microstructural effects on fatigue life.

26 specimens were fatigue tested and their results categorised per treatment type which was the basis for grouping them. The specimens were dog-bone shaped round bar with the testing diameters at 14 mm for 22 specimens, 12 mm for 1 specimen, and 10 mm for 3 specimens. The 4 specimens not at 14 mm diameter were selected to find out whether the diameter made any significant difference, which was not the case.

The cycles to failure ranged from around 25000 for unpeened and plastically strained specimens to around 300000 cycles for shot peened and skimmed specimens.

Two specimens were given tensile tests giving an average UTS of 612 MPa and 0.2 % proof stress of 560 MPa. These values were an approximate average of very divergent UTS stresses from other sources and considered sufficiently accurate.

Residual stress-depth testing at the NMMU laboratories showed final maximum residual stress amplitudes at about 11 times their expected value, and contrary to all literature, which restricts it to well below the proof stress and especially the UTS. The profiles were very good though. The reasons for this difficulty were unknown and these tests were too expensive to be repeated. To manage this difficulty the author decided to apply the most typical stress values from literature, and a test on identical specimens at UCT, and divide their workable average into the average of two maximum residual stresses in the tests. The result was deemed to be a reasonably representative and usable residual stress profile.

Microhardness tests through the diameter were performed on 3 specimens using the Vickers hardness scale. They showed a general decrease in hardness with depth but with a wide scatter, which was partly expected.

SEM tests on 6 specimens with many fractographs from various positions were produced. The crack initiation and fast fracture sites revealed the sought after evidence mentioned in

the 3<sup>rd</sup> paragraph of the Chapter 3 summary above, and gave valuable insights into the types of fracture and the depth of the shot peened surface, etc.

**Chapter 4** dealt with a multi-faceted analysis of the results, mainly due to the number of varied treatment types. It was decided to manage the treatments topically and then let the results of these analyses converge to support the attempt to find a life prediction model. This was not because the treatment topics were individually inadequate because they were, and their analysis results instructive for each treatment type. Eleven groups were formed depending on their commonality and investigative purpose.

Fatigue analysis profiles involved investigating the fatigue life results in the light of the various treatments, sometimes grouped together depending on the tests.

Five fatigue test groupings were made with revealing results per type of treatment.

The unpeened specimen was the primary point of reference (par 1.7.8 and par 4.1) to judge the fatigue life performance of other groups, with the specimens shot peened only, as the top point of reference, although it did not have the highest fatigue life value.

The tests showed that shot peening increased the fatigue life to over 7 times that of unpeened specimens.

Plastic straining tended to reduce the fatigue life of shot peened specimens between 22 % and 50 %, depending on the amount of plastic straining, although still higher than the unpeened specimen by a factor of around 1.4 to 3 times.

Skimming of shot peened specimens was a little detrimental with plastically straining probably due to most of the residual stress machined away, and only about 40 % higher fatigue life than unpeened specimens.

The purpose of skimming was to remove the shot peened layer and the main part of the residual stress. It was found from the stress-depth diagrams that the shot peened layer was over 300  $\mu\text{m}$  deep while the SEM fractographs showed the shot peened layer to be about 200  $\mu\text{m}$  deep, resulting in a remaining residual compressive stress at around 100  $\mu\text{m}$ , which proved to have positive results. The skim was intended to create a simulated “unpeened” specimen with relatively low residual compressive stress referred to in par 1.8.2, which turned out to be the case.

What was of interest was that, within this group of specimens shot peening at CPUT, the fatigue life actually increased with an increase in plastic strain, when the opposite was expected. This was judged to be due to strain hardening, with a limited amount of help from the reduced residual compressive stress which averaged at about 70 MPa, well short of the 380 MPa with the standard shot peened specimens.

The residual stress-depth analysis was also done through 7 groupwise tests. Unpeened specimens had the expected low residual stresses and shot peened ones the highest. Plastic straining reduced the shot peened residual compressive stresses to about 60 to 74 % of their original value

Microstructural effects were analysed through plastic straining, microhardness and SEM fractography.

The approach for plastic straining was to graphically compare fatigue life with % plastic strain and set up linear equations by using Excel trendlines which assisted in determining the role of the microstructure in fatigue life. In general the fatigue life decreased with plastic straining. The specimen that was plastically strained and then shot peened afterwards performed exceptionally well to 250650 cycles, 7.8 times more than the unpeened specimens and on slightly better than standard shot peened specimens, ascribed to a combination of the higher shot peening from CPUT and the increased strain hardening increasing the yield stress.

Plastic straining and shot peening from SAA had wide scatter results with no proper trend demonstrated, although with reasonable fatigue lives.

The specimens shot peened at CPUT, incrementally increasing plastic strain, and a 200  $\mu\text{m}$  radial skim, typically had reduced fatigue lives. This was the group that had an increase in fatigue life with an increase in plastic strain with the graph points very close to the trendline, which had a positive gradient. This was the most significant indication of the role of plastic strain in fatigue life.

The two specimens previously mentioned with shot peening from CPUT and radial skimming performed the best in fatigue tests with an exceptional average fatigue life of around 300000 cycles, in spite of having the major part of their residual stresses machined away. Although the machining provided a surface comparable to unpeened specimens, it might be noteworthy that the absence of plastic straining probably prevented a further reduction to an already smaller residual compressive stress.

This indicates that the microstructure may play a role in increasing fatigue life when the residual compressive stress is significantly reduced.

The microhardness tests showed a general decrease with depth but the results were too scattered to offer accurate predictions of material strength with hardness. However, the trend was still noticeable. Some aluminium alloys are known not to be too compliant.

SEM fractography pictures confirmed the depth of the shot peened layer to be about 200  $\mu\text{m}$ , shear planes at about 45 °, ductile striations with high atomic steps. Further away from the crack initiation site were troughs of microvoid coalescence consisting of groups of dimples with hard impurities at the bottom trying to resist fatigue forces.

Life prediction modelling was based on finding a reliable S-N curve. Once this was achieved coordinate points were carefully found on the diagram and a Microsoft Excel generated curve produced. Through the application of generalised fatigue factors for the specific conditions of the fatigue testing were taken into account, a more representative S-N diagram could be found.

The Gerber equation assisted in converting the bending stress amplitude for the stress ratio of 0.1 used in this research, to the fully reversible bending stress amplitude at the stress ratio of -1. Once the fully reversible stress amplitudes were found for each type of treatment, then a Log Sn-Log Nf straight line with an associated linear equation was established.

Comparison with other Log Sn-Log Nf diagrams showed very similar gradients, so it was decided to make all the line gradients the same and only find the equation constant for each treatment type. This ensured that the gradient used was the same or less than those in other diagrams sourced, making the results for this research more conservative.

The final equation (4.12) was:  $\text{Log Sn} = -0.1128 \text{ Log Nf} + C$

The C values for each treatment type can be found in Table 31, where it will be seen that no reliable constant, or uniform equation for that matter, could be found for specimens shot peened at SAA and plastically strained, and unpeened specimens that were prefatigued to 20000 cycles and then shot peened at SAA.

It is gratifying that the life prediction model generated yielded very reasonable results for the rest of the specimen treatment types. Caution needs to be taken that the accuracy of this equation has only been shown for the stress ranges applicable to this research.

## 5.2 RECOMMENDATIONS FOR FUTURE WORK

Recommendations for possible future research out of this dissertation will need to overcome shortcomings in this research and possibilities that spring out from it.

- Less treatment types would allow more focus on specific problems experienced here and not dilute some of the research specifics detrimentally.
- Values that should be kept constant should remain so, otherwise there will be too many variables to cope with, sometimes confusing the analysis criteria that need to be isolated for clearer solutions. This was experienced beyond the author's control when the maximum bending stress was changed during the fatigue testing as well as the type and intensity of the shot peening.
- More research could extend from this dissertation with the same, or a similar high strength, aluminium alloy to gain more clarity on the role of the microstructure in fatigue life with the focus on the effects of plastic strain, microhardness and material strength, different intensities of shot peening.
- The pursuit of life prediction models has an almost unlimited potential because they typically have limited ranges of values or conditions for validity.

## References

### REFERENCES

1. Al-Obaid YF. A Rudimentary Analysis of Improving Fatigue Life of Metals by Shot Peening. *Journal of Applied Mechanics*. 1990 June; 57: p. 307-312.
2. Almen J. *Residual Stresses and Fatigue in Metals* New York: McGraw-Hill Book Company, Inc.; 1963.
3. Marsh K. *Shot Peening: Techniques and Application* Marsh K, editor. London: Engineering Materials Advisory Service Ltd., UK, Chameleon Press Ltd.; 1993.
4. Ferguson Perforating. 7075 Aluminium Alloy -Ferguson Perforating. [Online].; 2015 [cited 2015 January 20. Available from: [www.fergusonperf.com/the-perforating./aluminium-alloy\\_7075.asp](http://www.fergusonperf.com/the-perforating./aluminium-alloy_7075.asp).
5. McGrath P. *An Investigation of Residual Stress Induced by Forming Processes on the Fatigue Resistance of Automotive Wheels*. 2001. PhD Thesis at the University of Plymouth.
6. Buch A. *Fatigue Strength Calculation*. 6th ed. Switzerland-Germany-UK-USA: Trans Tech Publications; 1988.
7. Miller K, de los Rios E, editors. *Short Fatigue Cracks* London: ESIS (European Structural Integrity Society), MEP (Mechanical Engineering Publications) Ltd.; 1992.
8. Anderson T. *Fracture Mechanics, Fundamentals and Applications*. 2nd ed.: CRC Press, Inc., Florida; 1995.
9. Ewalds H, Wanhill R. *Fracture Mechanics*. 1st ed. London: Edward Arnold Ltd and Delftse Uitgevers Maatschappij b.v. Netherlands; 1984.
10. Miannay D. *Fracture Mechanics, Mechanical Engineering Series* New York: Springer-Verlag New York, Inc.; 1998.
11. Askeland D. *The Science and Engineering of Materials*. 3rd ed.: Chapman and Hall.; 1996.
12. Evans W, Millan J. Effect of Microstrains and Particle Size on the Fatigue Properties of Steel. *The Shot Peener*. 1997; 11(4).
13. Institute of Precision Mechanics. *Shot Peening Present & Future* Nakonieczny A, editor. Warsaw: Institute of Precision Mechanics; 1999.

## References

14. Metal Improvement Company. Shot Peening Applications. 7th ed. Paramus: Metal Improvement Company; 1999.
15. The Society of Materials Science, Japan. Databook on Fatigue Strength of Metallic Materials, Volumes 1, 2 & 3. 1996th ed. Sakai KS&T, editor. Oxford: Elsevier Science Ltd; 1996.
16. The ASM Committee on Shot Peening. 398-The Shot Peening & Blast Cleaning Universe. [Online]. [cited 2015 January 20. Available from: [www.shotpeener.com/learning/shotpeening101.pdf](http://www.shotpeener.com/learning/shotpeening101.pdf).
17. Wohlfahrt H. The Influence of Peening Conditions on the Resulting Distribution of Residual Stress. In The 2nd International Conference on Shot Peening; 1984; Chicago. p. 316-331.
18. Al-Hassani S. An Engineering Approach to Shot Peening Mechanics. In 2nd International Conference on Shot Peening; 1984; Chicago. p. 275-282.
19. OSK Kiefer. Shot peening Media / OSK Kiefer GmbH. [Online]. [cited 2014 October 9. Available from: [osk-kiefer.de/en/quality-assurance/shot-peening-media](http://osk-kiefer.de/en/quality-assurance/shot-peening-media).
20. Hughes D. Investigation of the Mechanism of Fatigue Life Improvement Resulting From Shot Peening. 1998. Final Year Project, BSc Eng at UCT.
21. Wohlfahrt H. Practical Aspects of Application of Shot Peening to Improve the Fatigue Behaviour of Metals and Structural Components. In The 3rd International Conference on Shot Peening; 1987; Garmisch-Partenkirchen. p. 563-584.
22. Snowman A, Schmidt R. The Improvement of Fatigue and Surface Characteristics of Alloy 7075-T6 By Secondary Peening With Glass Beads. In The 1st International Conference on Shot Peening; 1981; Paris. p. 313-322.
23. Wikipedia. Wikipedia The Free Encyclopaedia. [Online].; 2014 [cited 2014 November 15. Available from: [en.wikipedia.org/wiki/Residual\\_stress](http://en.wikipedia.org/wiki/Residual_stress).
24. Meininger J, Dickerson S, Gibeling J. Observations of Tension/Compression Asymmetry in Cyclic Deformation of Aluminium Alloys. Fatigue and Fracture of Engineering Materials and Structures. 1996; 19(1).
25. Davis J. Aluminium and Aluminium Alloys. 1993rd ed. Davis J, editor.: ASM International; 1993.

## References

26. Romero JS. Optimisation of the Shot Peening Process in Terms of Fatigue Resistance. In The 7th International Conference on Shot Peening; 1999; Warsaw. p. 117-126.
27. Purdue University. Purdue University - Scanning Electron Microscope. [Online].; 2014 [cited 2014 October. Available from: [www.purdue.edu/rem/rs/sem.htm](http://www.purdue.edu/rem/rs/sem.htm).
28. James MN. PPT-Examples of Aluminium Fractography. [Online].; 2009 [cited 2014 December 6. Available from: [www.powershow.com/view/1204c8-ZTE10/Examples\\_of\\_Aluminium\\_Fractography\\_powerpoint\\_ppt\\_presentation](http://www.powershow.com/view/1204c8-ZTE10/Examples_of_Aluminium_Fractography_powerpoint_ppt_presentation).
29. Browell R. Calculating and Displaying Fatigue Results. 2006. The ANSYS Fatigue Module.
30. Maddox S. Effect of Mean Stress on Fatigue Crack Propagation. International Journal of Fracture. 1975 June; 11(3).
31. Juvinall R, Marshek K. Fundamentals of Machine Component Design. 5th ed. Ratts L, editor. Hoboken: John Wiley & Sons; 2012.
32. Department of Defense, USA. Metallic Materials and Elements for Aerospace Vehicle Structures. 5th ed. Atlantic City: Department of Defense, USA; 2003.
33. Boyer H. Atlas of Fatigue Curves. Illustrated Edition ed. Boyer H, editor.: ASM International; 1986.
34. Rambocus O. An Experimental Study of the Stress Intensity Factors of Semi-Elliptical & Crescent Moon Surface Cracks in Round Bars. 2005. Thesis in Partial Fulfilment For MSc Eng at UCT.
35. Spectro Analytical labs Limited. [Online].; 2014 [cited 2014 November 27. Available from: <http://www.spectro.in/Hardness-Conversion-Chart-for-Aluminium.html>.
36. Stephens RI, Fatemi A, Stephens RR, Fuchs HO. Metal Fatigue in Engineering 2nd Edition. In. New York: John Wiley & Sons; 2001. p. 122-124.
37. Barnes WH. ENGR322 Homework - Oregon State University. [Online].; 2012 [cited 2014 November 7. Available from: <http://www.oregonstate.edu/instruct/engr322/Homework//S12/ENGR322HW7.html>.
38. Metallurgical Technologies, Inc. Metallurgical Technologies Inc Web site. [Online]. [cited 2014 November. Available from: [www.met-tech.com](http://www.met-tech.com).

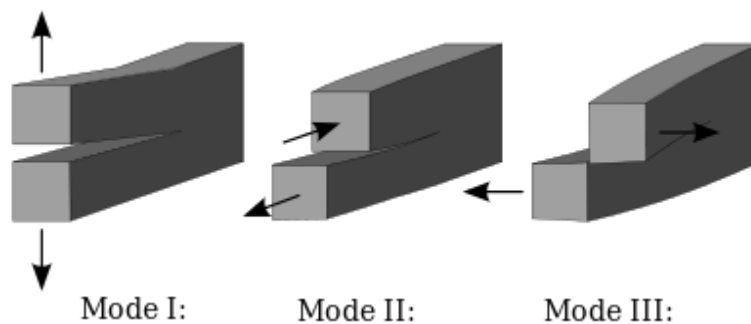
## References

39. Surface Engineering Forum. Brinell Hardness Vickers Hardness and Tensile Strength. [Online]. [cited 2014 November 5. Available from: [gordonengland.co.uk/hardness/vickers.htm](http://gordonengland.co.uk/hardness/vickers.htm).
40. Engineers Toolbox (ETBX). ETBX Stress-Life Fatigue Analysis Module. [Online].; 2010 [cited 2014 October 22. Available from: [www.fea-optimization.com/ETBX/stresslife\\_help.html](http://www.fea-optimization.com/ETBX/stresslife_help.html).

## APPENDICES

### APPENDIX A: THREE MODES OF CRACK PROPAGATION BY APPLIED FORCES

There are three modes by which a crack can extend as shown in the diagram below. Mode I is the tensile stress opening mode which is most common in fatigue, Mode II is the in-plane shearing stress or sliding mode, and Mode III is the tearing (torsional) stress or antiplane shear mode.



Mode I type cracks grow on the plane of maximum tensile stress and typical of crack extension for uniaxial loaded components.

Mixed-mode, with more than one mode present, is more present with microcrack initiation and tend to grow on the planes of maximum shear.

Mode III typically occurs in round notched bars loaded in torsion <sup>[36]</sup>.

Appendices

**APPENDIX B: PROPERTIES OF 7075-T6 ALUMINIUM ALLOY**

<b>Physical Properties</b>	<b>Metric</b>	<b>English</b>	<b>Comments</b>
Density	<u>2.81 g/cc</u>	0.102 lb/in <sup>3</sup>	AA; Typical
<b>Mechanical Properties</b>			
Hardness, Brinell	150	150	AA; Typical; 500 g load; 10 mm ball
Hardness, Knoop	191	191	Converted from Brinell Hardness Value
Hardness, Rockwell A	53.5	53.5	Converted from Brinell Hardness Value
Hardness, Rockwell B	87	87	Converted from Brinell Hardness Value
Hardness, Vickers	175	175	Converted from Brinell Hardness Value
Ultimate Tensile Strength	<u>572 MPa</u>	83000 psi	AA; Typical
Tensile Yield Strength	<u>503 MPa</u>	73000 psi	AA; Typical
Elongation at Break	<u>11 %</u>	11 %	AA; Typical; 1/16 in. (1.6 mm) Thickness
Elongation at Break	<u>11 %</u>	11 %	AA; Typical; 1/2 in. (12.7 mm) Diameter
Modulus of Elasticity	<u>71.7 GPa</u>	10400 ksi	AA; Typical; Average of tension and compression. Compression modulus is about 2% greater than tensile modulus.
Poisson's Ratio	0.33	0.33	
Fatigue Strength	<u>159 MPa</u>	23000 psi	AA; 500,000,000 cycles completely reversed stress; RR Moore machine/specimen

## Appendices

Fracture Toughness	<u>20 MPa-m<sup>1/2</sup></u>	18.2 ksi-in <sup>1/2</sup>	K(IC) in S-L Direction
Fracture Toughness	<u>25 MPa-m<sup>1/2</sup></u>	22.8 ksi-in <sup>1/2</sup>	K(IC) in T-L Direction
Fracture Toughness	<u>29 MPa-m<sup>1/2</sup></u>	26.4 ksi-in <sup>1/2</sup>	K(IC) in L-T Direction
Machinability	<u>70 %</u>	70 %	0-100 Scale of Aluminium Alloys
Shear Modulus	<u>26.9 GPa</u>	3900 ksi	
Shear Strength	<u>331 MPa</u>	48000 psi	AA; Typical
<b>Electrical Properties</b>			
Electrical Resistivity	<u>5.15e-006 ohm-cm</u>	5.15e-006 ohm-cm	AA; Typical at 68°F
<b>Thermal Properties</b>			
CTE, linear 68°F	<u>23.6 µm/m-°C</u>	13.1 µin/in-°F	AA; Typical; Average over 68-212°F range.
CTE, linear 250°C	<u>25.2 µm/m-°C</u>	14 µin/in-°F	Average over the range 20-300°C
Specific Heat Capacity	<u>0.96 J/g-°C</u>	0.229 BTU/lb-°F	
Thermal Conductivity	<u>130 W/m-K</u>	900 BTU-in/hr-ft <sup>2</sup> -°F	AA; Typical at 77°F
Melting Point	477 - 635 °C	890 - 1175 °F	AA; Typical range based on typical composition for wrought products 1/4 inch thickness or greater. Homogenization may raise eutectic melting temperature 20-40°F but usually does not eliminate eutectic melting.
Solidus	<u>477 °C</u>	890 °F	AA; Typical
Liquidus	<u>635 °C</u>	1175 °F	AA; Typical

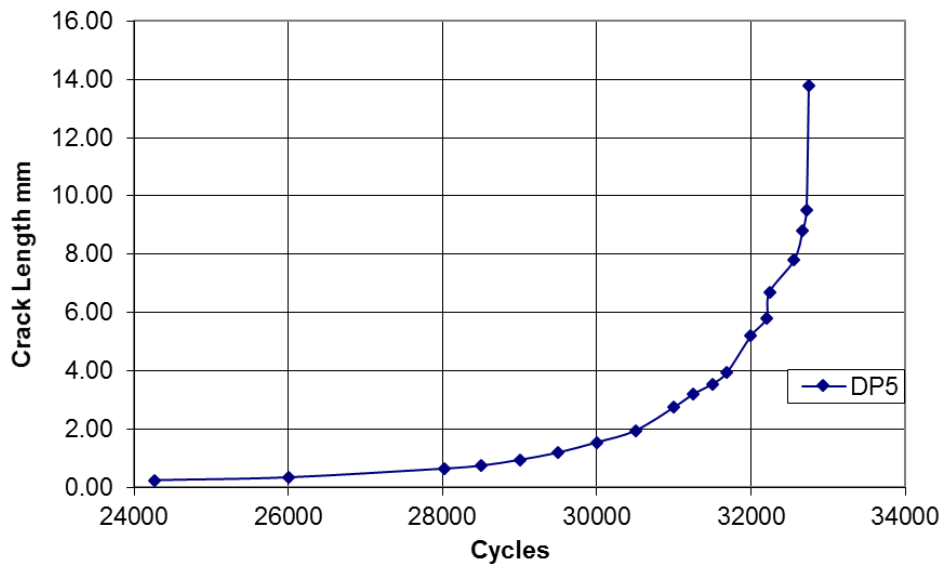
Appendices

<b>Processing Properties</b>			
Annealing Temperature	<u>413 °C</u>	775 °F	
Solution Temperature	466 - 482 °C	870 - 900 °F	
Aging Temperature	<u>121 °C</u>	250 °F	

**APPENDIX C: CRACK LENGTH VS CYCLES TO FAILURE DP 5**

Description	Value/No	Unit	Notes	No Cycles	Crack Length (mm)
Specimen	DP 5	Al 7075-T6	Mach from $\Phi 25$ mm Bar	24260	0.25
Peening	8 to 14	A		26000	0.35
$\epsilon_{pl}$	0.5	$\mu$ Strain		28030	0.65
R	0.1			28500	0.75
$\sigma_{bend\ min}$	48	MPa		29000	0.95
$\sigma_{Bend\ max}$	480	MPa		29500	1.20
$\sigma_{uts\ ave}$	612	MPa	Tests with $\Phi 8$ mm Bar	30000	1.55
$\sigma_{yield\ ave}$	560	MPa		30500	1.95
Diameter	13.8	mm		31000	2.75
$K_{1c}$	28.6	MPa.m <sup>1/2</sup>		31250	3.20
				31500	3.55
				31690	3.95
				32000	5.20
				32200	5.80
				32240	6.70
				32560	7.80
				32670	8.80
				32720	9.50
				32750	13.80

**DP5: Cycles to Failure vs Crack Length**



**APPENDIX D: FRACTOGRAPH OF DP 27 SHOT PEENED LAYER AFTER SKIM**

